Dipl.-Ing. Fabian Muralter, BSc

Vapor-Phase Synthesis of Smart Polymers

Thermoresponsive Films for Sensing, Actuating
and Pharmaceutical Applications

DOCTORAL THESIS

to achieve the university degree of

Doktor der technischen Wissenschaften

submitted to

Graz University of Technology

Supervisor

Assoc.Prof. Dr. Anna Maria Coclite

Institute of Solid State Physics

Graz, May 2020

Affidavit

I declare that I have authored this thesis independently, that I have not used other than the declared sources/resources and that I have explicitly indicated all material which has been quoted either literally or by content from the sources used. The text document uploaded to TUGRAZonline is identical to the present doctoral thesis.

_____ _____

Date Signature

Abstract EN

In this thesis, thermoresponsive hydrogel thin films and their applicability to device setups are explored. As many applications require the conformal thin-film deposition on delicate and nanostructured substrates (e.g., on pharmaceuticals, tissue), the solvent-free method of initiated chemical vapor deposition (iCVD) is adopted for polymer synthesis. With iCVD, such (co)polymer thin films with tailored properties can be readily prepared from chemicals delivered in the vapor phase. Two model systems of copolymers are synthesized: poly(*N*-isopropylacrylamide) (pNIPAAm) and poly(*N*-vinylcaprolactam) (pNVCL), both being cross-linked by di(ethylene glycol) divinyl ether (DEGDVE). While pNIPAAm-based systems are widely discussed in the literature, novel systems of cross-linked pNVCL thin films are developed, synthesized and characterized for the first time. A fundamental understanding of the linkage between material properties and deposition conditions and the materials' thermoresponsive behavior is generated. The thermoresponsiveness of such layers can be observed as a distinct transition in film thickness around their, so-called, lower critical solution temperature (LCST) in aqueous environment. This behavior is mainly investigated by monitoring the film thickness and optical properties of these systems by spectroscopic ellipsometry as a function of environmental parameters (e.g., relative humidity – RH, temperature – T). In iCVD, the material properties can be tuned via deposition conditions such as the deposited film thickness, concentration of cross-linker and initiator species being available during polymer synthesis, etc. In that way, smart polymers exhibiting strong thermoresponsive transitions with >200% change in film thickness upon ramping the temperature are achieved. Furthermore, the transition temperature can be tuned in the range 16-40 °C. Thermoresponsiveness was also demonstrated in high levels of RH for the first time. Interesting wettability and mechanical properties (modulus in the MPa range) are found, enabling the materials to be applied to various device setups. For instance, their tunable responsiveness to environmental stimuli (e.g., to T around human body temperature) together with being biocompatible allows for their applicability to biomedical setups; thus, a drug encapsulation layer based on thermoresponsive hydrogels is developed. Furthermore, the monotonous swelling in RH was utilized to test the applicability of such films to sensor setups. The kinetics were found to outperform a market-available device by the hydrogel responding to changes in RH twice as fast as this reference sensor. Furthermore, a humidity-driven and temperature-controlled actuator was developed, showcasing the great potential of these materials to be applied to purposes in soft robotics (e.g., soft gripping).

DE Kurzfassung

In dieser Arbeit werden thermoresponsive Hydrogel-Dünnschichten und die Möglichkeit ihrer technischen Anwendung untersucht. Da in vielen Fällen die konformelle Dünnschichtsynthese auf empfindlichen und nanostrukturierten Substraten (z.B. Pharmazeutika, Gewebe) gefordert ist, wird die lösungsmittelfreie Methode der initiierten chemischen Gasphasenabscheidung (iCVD) verwendet. Mit iCVD können solche (Co-)Polymer-Dünnschichten mit kontrollierbaren Eigenschaften hergestellt werden. Zwei Modellsysteme von Copolymeren werden untersucht: Poly(*N*-isopropylacrylamid) (pNIPAAm) und Poly(*N*-vinylcaprolactam) (pNVCL) – beide mit Di(ethylenglykol)divinylether (DEGDVE) vernetzt. Während pNIPAAm in der Literatur breit diskutiert ist, werden neue pNVCL-Dünnfilmsysteme erstmals entwickelt, synthetisiert und charakterisiert. Ein grundlegendes Verständnis des Zusammenhangs zwischen Materialeigenschaften, Abscheidungsbedingungen und thermoresponsivem Verhalten wird erarbeitet. Die Thermoresponsivität solcher Schichten zeigt sich als deutlicher Übergang in der Schichtdicke um ihre so genannte untere kritische Lösungstemperatur (LCST) in feuchter Umgebung. Dieses Verhalten wird hauptsächlich durch Bestimmung von Schichtdicke und optischen Eigenschaften dieser Systeme mittels spektroskopischer Ellipsometrie in Abhängigkeit von Umgebungsbedingungen (z.B. relative Feuchte – RH, Temperatur – T) untersucht. Mittels iCVD können die Materialeigenschaften über Parameter wie z.B. die Schichtdicke oder die Konzentration der bei der Polymersynthese verfügbaren Vernetzer- und Initiatorspezies beeinflusst werden. Auf diese Weise werden intelligente Polymere hergestellt, die stark thermoresponsives Verhalten mit >200% Änderung der Schichtdicke bei Temperaturerhöhung aufweisen. Darüber hinaus kann die LCST im Bereich 16-40 °C eingestellt werden. Thermoresponsivität wird zum ersten Mal auch in hoher RH demonstriert. Interessante Benetzbarkeit und mechanische Eigenschaften (Elasizitätsmodul im MPa-Bereich) unterstützen die Anwendbarkeit dieser Materialien. Da sie maßgeschneidert auf Umwelteinflüsse reagieren (z.B. auf T um die menschliche Körpertemperatur), können sie mit überprüfter Biokompatibilität z.B. in biomedizinischen Anwendungen eingesetzt werden. eine Medikamentenbeschichtung auf Basis derartiger Hydrogele wird entwickelt. Darüber hinaus zeigt das monotone Schwellungsverhalten der Filme in RH das Potenzial der Anwendbarkeit in Sensoren. Es wird festgestellt, dass ein Hydrogel kinetisch doppelt so schnell auf Änderungen der RH reagiert wie ein kommerzieller Sensor. Daneben wird ein feuchtigkeitsbasierter und temperaturgesteuerter Aktuator entwickelt, der das Potenzial einer Anwendung dieser Materialien in der Soft-Robotik (z.B. weiches Greifen) demonstriert.

Acknowledgements

Needless to say, the time in this doctoral program influenced the ways I think and live. From the people I met and interacted with to the ideas I encountered and developed, this is what shaped my thinking.

Prima di tutto, I want to express my sincere gratitude to my advisor Anna Maria Coclite. In addition to the superb supervision and the distinguished direct support during all my PhD studies, she provided an exceptional environment for developing diverse skills and applying them to research in an immensely interesting and seminal field. Furthermore, I am grateful to Oliver Werzer for being an excellent collaborator and continuously sharing with me his wealth of ideas. Moreover, I want to thank Kenneth K. S. Lau for enabling the opportunity to perform research at Drexel University in Philadelphia, PA, USA. He and his group supported me in and outside the lab and, in this way, made this stay in Philly an extraordinary experience.

I am grateful to former and current colleagues in the Coclite group, particularly to Richard Berger, Katrin Unger, Marianne Kräuter (Herbs) and Taher Abu Ali; especially, I want to thank Paul Christian for profoundly shaping my thinking. I am thankful for having met, worked and, consequently, spending time with Alberto Perrotta, former postdoc in our group, who provided sustained support throughout our collaboration and inspired an immense amount of thoughts on cuisine and other existential subject matters. Moreover, I am grateful for having a dear friend in fellow student, PhD candidate, group member and Kollege Julian Pilz (Mushroom). Not only do we climb multi-pitch routes together, we also worked, travel, spend time together and share a certain type of humor not everyone understands.

I want to express my gratitude to my brother Florian, who never ceases to create opportunities to meet, travel, surf, ski, climb and develop ideas together, in spite of the distance between the places we live in. Thanks for reading and giving valuable comments on this thesis and, in general, for coping with me not responding immediately (almost all of the time)!

Certainly, I am extremely grateful to my parents, for caring and for supporting me throughout my whole life. Without you, I definitely would not be where I am at right now in all aspects of life.

Ultimately, I am utterly thankful for being able to spend my time and life with Lisbetho, who always thinks about the questions I want to think about, laughs about the stuff I want to laugh about and cares about the things I want to care about. Thank you for iteratively rolling this immense but sometimes weightless boulder up the hill of absurdity together with me. See you on top of the hill again soon!

Contents

Acronyms

iCVD/oCVD initiated/oxidative chemical vapor deposition

pNIPAAm poly(*N*-isopropylacrylamide)

pNVCL poly(*N*-vinylcaprolactam)

DEGDVE di(ethylene glycol) divinyl ether

PE polyethylene

PP polypropylene

PVC poly(vinyl chloride)

PET polyethylene terephthalate

pHEMA poly(2-hydroxyethyl methacrylate)

PS(S) polystyrene (sulfonate)

PEN polyethylene naphthalate

PEDOT poly(3,4-ethylenedioxythiophene)

TBPO tert-butyl peroxide

EUD Eudragit

IR/UVR infrared/ultraviolet radiation

FTIR Fourier-transform infrared spectroscopy

SE spectroscopic ellipsometry

XRR X-ray reflectivity

WCA water contact angle

AFM atomic force microscopy

RH relative humidity

LCST lower critical solution temperature

DMM distribution of relative molecular masses

IUPAC International Union of Pure and Applied Chemistry

ACS American Chemical Society

ERC European Research Council

1

I Introductory Overview

This chapter provides a short introductory overview of the topics covered in this thesis. It should present a compilation of thoughts that allows to view the remainder of this thesis in the context of relevant historical, societal, industrial as well as scientific developments and frameworks.

I.1 Polymers and their Potentials/Problems

Polymers are essential parts of the world; for instance, naturally occurring polymeric substances such as DNA,[*] proteins and various forms of complex carbohydrates are central in all known forms of life. Cellulose,[†] cotton and rubber are further examples of polymers occurring in nature. They have been utilized by humans ever since civilizations formed; for example, already the early humans are known to have used fibers of silk, wool, flax and cotton for textile applications and to have processed natural rubber for waterproofing or for purposes, where elastic materials were required.[1]

Today, next to these naturally occurring substances, synthetic polymers and, specifically, plastics are ubiquitous in science & technology as well as in everyday life. Already in the late 1980s, the global annual plastics production surpassed the one of steel and is on the rise ever since.[2] In total, researchers estimate that approximately 8300 Mt of primary plastics (from virgin materials) have been produced to date (data of 2017).[3] Within the last 100 years, various kinds of such materials were developed to fulfill a plethora of tasks and functions. Applications in which essential parts are polymers include but are not limited to medical devices, sports equipment, domestic appliances, electronic devices, paint, pipes and packaging.[2] This broad range in feasible functionalities originates in the unique and versatile material properties, which, in turn, emanate from the specific chemical nature of polymers. Material scientists and engineers have found numerous ways of tailoring and tuning them in a continuum of properties via the chemical and physical nature and composition of the structures involved and their constitution/arrangement.[4] This allows to attain almost any required feature an application might demand. Some fundamentals on polymers with characteristics being linked to material properties and functionalities are provided in section II.1 of this thesis. Advantageous properties of plastics enabling the discussed versatile applicability include their strength and stiffness, despite their lightweight, their bio-inertness, ease in fabrication and low cost.[5] As such, plastics have contributed to significantly reducing energy consumption, (food) waste and maintenance efforts of, e.g., the products and devices mentioned above.[5]

Further features allowing for the applicability of these materials to the abovementioned purposes are their durability and resistance to degradation.[3] However, exactly these properties bring about major problems for societies and nature to deal with polymers as end-of-life materials and waste.

---

[*] deoxyribonucleic acid, carrying genetic information for the development, functioning, growth and reproduction of living organisms
[†] primary substance in wood and paper

Researchers estimate that ~6300 Mt of waste were cumulatively generated from plastics (between 1950 and 2015); of all this plastic waste, 12% (i.e., 800 Mt) have been incinerated and only 10% (i.e., 600 Mt) have been recycled, most of which only once.[3] While only ~30% (i.e., 2500 Mt) of all plastics ever produced are actually in use (data of 2017), the majority (~60%; 4900 Mt) are currently accumulating in landfills, in open dumps or in the natural environment.[3] As significant degradation of most of the mass-produced plastics is limited to solar ultraviolet radiation (UVR) fragmenting them into particles of ≤20 mm in size,[6] their impact on biological organisms and ecosystems needs to be examined. Such research is accelerating but predominantly concentrated on marine debris.[7] As such, plastics were shown to alter and, eventually, interfere with and harm life on every organizational level of biological systems (e.g., DNA damage, lesions in organs, death of organisms, etc.).[7] Thus, besides their great potentials, polymeric materials also represent major ecological concerns for the environment and pose challenges to waste management and recycling for societies throughout the world.

I.2 Biodegradability/-compatibility

One approach to tackle part of these problems is the usage and development of biodegradable[*] and biocompatible[†] polymers.[8] Since polymers are widely utilized in all sorts of industrial sectors such as packaging, building & construction, textiles, transportation, electrical/electronic and many more,[3] the potential for applications of bio-alternatives is extensive.

As mentioned above, in a first step, degradation of common plastics is, basically, limited to fragmentation by UVR.[6] In a second step, microorganisms can attach to the fragments and secrete exo-enzymes to break the polymer down to non-toxic products (e.g., minerals, water, volatile species).[6] Factors facilitating such biodegradation processes are, inter alia, low molar mass, low degree of crystallinity, low melting point and lack of side chains in the polymer's structure;[‡] furthermore, additives that enhance biodegradation can be included.[6] Prominent examples of such polymers are the naturally occurring cellulose and chitin and the synthetic polycaprolactone (PCL); all of them can be degraded at rates (e.g., PCL to 100% in 30 days) that are several orders of magnitude higher than the ones of conventional polymers such as polyethylene (PE) and polypropylene (PP).[6]

Besides biodegradability, biocompatibility can be an important asset of polymeric materials. On the one hand, utilizing biocompatible polymers

---

[*] Biodegradability: "Capability of being degraded by biological activity." (p. 382)[8]
[†] Biocompatibility: "Ability to be in contact with a living system without producing an adverse effect." (p. 382)[8]
[‡] These relevant properties are introduced in section II.1.

4

reduces the ecological impact of these substances; on the other hand, such materials can be employed in biological environments, which is crucial for their applicability to medical devices or other biotechnological setups (e.g., implants, drug delivery).

I.3 Vapor-Phase Synthesis

A critical aspect is the synthesis of biodegradable and biocompatible polymers for bio-applications. Besides being themselves fragile substances, they are demanded to be in contact with or attached to delicate surfaces, materials and setups (e.g., tissue, pharmaceuticals). Thus, mild processing conditions need to be employed. Instead of utilizing conventional solution-based methods, a promising approach is the synthesis of polymers from chemicals delivered in the vapor phase (e.g., chemical vapor deposition, CVD). In doing so, solvent-related inconveniencies such as the dissolution of constituents/the substrate, intermixing of components and surface tension can be avoided.[9] In copolymerizations, the need for a chemical in which all monomers are soluble can also be avoided. By changing the ratio of gases introduced to such a vapor-phase synthesis process, the composition of the resulting (co)polymer can be precisely controlled with the further possibility of grading and layering.[10] Thereby, properties such as the wettability, adhesion, chemical inertness, corrosion resistance, environmental and mechanical stability, permeability to gases, conductivity, biostability and biocompatibility can be controlled.[10]

As a variant of CVD, initiated chemical vapor deposition (iCVD) is a seminal technique for the synthesis/deposition of polymer thin films exhibiting distinct functionalities. A wide variety of possible chemistries are being successfully applied to iCVD for thin-film synthesis of dozens of polymers. The mild conditions employed in iCVD allow for the inclusion of specific units enabling the polymers to be, e.g., responsive to temperature, pH or specific chemical/biological molecules.[10] Furthermore, the polymer synthesis from chemicals delivered in the vapor phase facilitates the preparation of highly conformal and uniform layers.[10]

Basic principles of polymer synthesis are introduced in section II.2 of this thesis. In the subsection II.2.3, these fundamentals are applied to iCVD, consequently, focusing on specifics of the process in section II.2.3.3. In section III.1 and III.2, scientific articles are presented, focusing on material properties being directly linked to deposition conditions in polymer thin films synthesized by iCVD.

I.4 Smart Polymer Thin Films

Polymers exhibiting multiple functionalities are, commonly, termed smart or stimuli-responsive polymers.[*] Such materials can be utilized, inter alia, in the auspicious field of soft robotics, where sophisticated interfaces between robots and humans need to be developed. Furthermore, their inherently responsive behavior makes them particularly interesting for sensing and actuating applications in general.

Next to materials of macroscopic physical dimensions, thin films are being progressively utilized in such 'smart' setups for miniaturization and optimization purposes. Especially in diffusion-driven processes, the size of the structures involved plays a critical role, particularly when kinetics are relevant; hydrogels as polymeric systems, able to take up significant amounts of water, are a prominent example for that.[11] Given their hydrophilicity, hydrogel materials can serve as a distinct biocompatible, aqueous environment in biological/-medical applications, e.g., in contact lenses, wound care coverings, controlled/on-demand drug release and as matrices for cell encapsulation.[12-14] In section II.1.1, an introduction to hydrogels with a focus on their thermoresponsive variant is given. Section III.3 presents original scientific work on vapor-phase-synthesized hydrogels in drug coatings.

Besides yielding an aqueous matrix for certain applications, a further asset of stimuli-responsive hydrogel materials is their ability to respond to the environment by changing properties, the most obvious of which are their physical dimensions. This behavior can directly be utilized to apply hydrogels as the active material in sensor as well as actuator setups. Section II.1.3 provides an introduction to polymeric materials for such applications. Furthermore, in section III.4, a scientific contribution is presented evaluating and demonstrating the applicability of vapor-phase-synthesized hydrogel thin films to sensor and actuator setups.

---

[*] A more detailed introduction to these terms is given in section II.1.2.

I.5 Structure of this Thesis

The further part of this thesis is divided into three chapters: relevant basics and fundamentals (chapter II), original scientific contributions (chapter III) and conclusions (chapter IV).

Chapter II is structured as to introduce the basic terms and concepts (section II.1) about polymers and the materials relevant to the understanding of chapter III; subsequently, fundamentals about polymer synthesis and the methods applied for thin film deposition in the work presented in chapter III are discussed (section II.2); section II.3 provides a short introduction to the techniques employed for the characterization and investigation of the synthesized structures.

Chapter III presents four original scientific contributions that were reproduced from articles published in peer-reviewed journals. The articles in III.1 and III.2 discuss the linkage between material properties of vapor-phase-synthesized polymers to the applied deposition conditions. In section III.3, the work of a scientific contribution is presented that examines the potential of thermoresponsive hydrogel thin films to be applied in drug coatings. Within the article in section III.4, the applicability of smart polymer thin films to sensor and actuator setups is discussed and, ultimately, demonstrated.

Chapter IV represents a short summary of conclusions that can be drawn from the articles presented in chapter III with respect to the context and concepts discussed in the earlier chapters of this thesis.

In the Appendix, a list of publications, oral and poster presentations of the author of this thesis is provided. Furthermore, a cover art published as a supplementary journal cover in volume 2, issue 3 of 'ACS Applied Polymer Materials' is depicted; it was designed by the author of this thesis. Moreover, a research paper, summarizing work performed during a research stay at Drexel University in Philadelphia, PA, USA in the laboratory of Prof. Kenneth K. S. Lau, is appended. In the respective project funded by the Marshall Plan Foundation through a scholarship awarded to the author of this thesis, another CVD technique (oxidative chemical vapor deposition, oCVD) was successfully employed to deposit thin films of conducting polymers on flexible substrates to allow for piezo-resistive strain sensing.

I.6 References

(1)   Olatunji, O. Preface. In *Natural Polymers*; Olatunji, O., Ed.; Springer International Publishing: Cham, 2016; pp i–x. https://doi.org/10.1007/978-3-319-26414-1.

(2)   Abetz, V.; Chan, C. H.; Luscombe, C. K.; Matson, J. B.; Merna, J.; Nakano, T.; Raos, G.; Russell, G. T. Quo Vadis, Macromolecular Science? Reflections by the IUPAC Polymer Division on the Occasion of the Staudinger Centenary. *Isr. J. Chem.* **2020**, *60* (1–2), 9–19. https://doi.org/10.1002/ijch.201900182.

(3)   Geyer, R.; Jambeck, J. R.; Law, K. L. Production, Use, and Fate of All Plastics Ever Made. *Sci. Adv.* **2017**, *3* (7), e1700782. https://doi.org/10.1126/sciadv.1700782.

(4)   Su, W.-F. Chemical and Physical Properties of Polymers. In *Principles of Polymer Design and Synthesis*; Springer, Berlin, Heidelberg, 2013; pp 61–88. https://doi.org/10.1007/978-3-642-38730-2_4.

(5)   Andrady, A. L. Societal Benefits of Plastics. In *Plastics and Environmental Sustainability*; John Wiley & Sons, Inc: Hoboken, NJ, 2015; pp 121–144. https://doi.org/10.1002/9781119009405.

(6)   Andrady, A. L. Degradation of Plastics in the Environment. In *Plastics and Environmental Sustainability*; John Wiley & Sons, Inc: Hoboken, NJ, 2015; pp 145–184. https://doi.org/10.1002/9781119009405.

(7)   Rochman, C. M.; Browne, M. A.; Underwood, A. J.; van Franeker, J. A.; Thompson, R. C.; Amaral-Zettler, L. A. The Ecological Impacts of Marine Debris: Unraveling the Demonstrated Evidence from What Is Perceived. *Ecology* **2016**, *97* (2), 302–312. https://doi.org/10.1890/14-2070.1.

(8)   Vert, M.; Doi, Y.; Hellwich, K. H.; Hess, M.; Hodge, P.; Kubisa, P.; Rinaudo, M.; Schué, F. Terminology for Biorelated Polymers and Applications (IUPAC Recommendations 2012). *Pure Appl. Chem.* **2012**, *84* (2), 377–410. https://doi.org/10.1351/pac-rec-10-12-04.

(9)   Muralter, F.; Perrotta, A.; Coclite, A. M. Thickness-Dependent Swelling Behavior of Vapor-Deposited Smart Polymer Thin Films. *Macromolecules* **2018**, *51* (23), 9692–9699. https://doi.org/10.1021/acs.macromol.8b02120.

(10)   Gleason, K. K. Overview of Chemically Vapor Deposited (CVD) Polymers. In *CVD Polymers*; Wiley-VCH Verlag GmbH & Co. KGaA: Weinheim, Germany, 2015; pp 1–11. https://doi.org/10.1002/9783527690275.ch1.

(11)   Beebe, D. J.; Moore, J.; Bauer, J. M.; Yu, Q.; Liu, R. H.; Devadoss, C.; Jo, B. H. Functional Hydrogel Structures for Autonomous Flow Control inside Micro-Fluidic Channels. *Nature* **2000**, *404* (6778), 588–590. https://doi.org/10.1038/35007047.

(12)   Wei, M.; Gao, Y.; Li, X.; Serpe, M. J. Stimuli-Responsive Polymers and Their Applications. *Polym. Chem.* **2017**, *8* (1), 127–143. https://doi.org/10.1039/C6PY01585A.

(13)   Rosiak, J. M.; Yoshii, F. Hydrogels and Their Medical Applications. *Nucl. Instruments Methods Phys. Res. Sect. B Beam Interact. with Mater. Atoms* **1999**, *151* (1–4), 5. https://doi.org/10.1016/S0168-583X(99)00118-4.

(14)   Ullah, F.; Othman, M. B. H.; Javed, F.; Ahmad, Z.; Akil, H. M. Classification, Processing and Application of Hydrogels: A Review. *Mater. Sci. Eng. C* **2015**, *57*, 414–433. https://doi.org/10.1016/j.msec.2015.07.053.

2

II Fundamentals and Methods

The information gathered in this section provides background knowledge on polymers, their synthesis and ways of investigating them. All this should serve as a pool of information, definitions and terminology necessary and relevant for the understanding of the original, scientific work presented in the further chapters of this thesis.

II.1 Basics of Polymers

The term 'polymer' refers to a class of materials, whose manifold properties allow for their applicability to almost all areas of modern life. Generally, two types are distinguished, depending on their origin: *natural* and *synthetic polymers*. The former are naturally occurring substances such as DNA, wool, cellulose and proteins. The latter are synthesized by humans for specific purposes and are utilized in various sectors, e.g., packaging, textiles, building & construction and transportation. Synthetic polymers include materials such as polyethylene (PE), nylon, poly(vinyl chloride) (PVC), polyethylene terephthalate (PET) and polytetrafluoroethylene (PTFE). Overall, polymers can exhibit a plethora of properties ranging from rigid to soft, brittle to elastic, reactive to inert, from insulating to conducting, etc.

The International Union of Pure and Applied Chemistry (IUPAC)[*] defines a *polymer* as a "substance composed of macromolecules" (p. 2299).[1] To comprehend this definition, it is, thus, also essential to understand the concepts conveyed by the term 'macromolecule'. The prefix 'macro-' is derived from the Greek word 'makrós' (μακρός, *large/long*), denoting a *macromolecule* as a large/long molecule. Accordingly, the IUPAC define the term as follows:

> *Macromolecule (IUPAC definition, p. 2289)[1]*
> "A molecule of high relative molecular mass [IUPAC-defined[2]], the structure of which essentially comprises the multiple repetition of units derived, actually or conceptually, from molecules of low relative molecular mass."

Notably, the presence of repeated (constitutional) units, making up the macromolecular structure of a polymer, has defining status. Etymologically, the word 'polymer' is derived from the Greek words 'polús' (πολύς, *many*) and 'méros' (μέρος, *a share*), also referring to these repeated constitutional units. The precursor species reacting to form a macromolecule are termed *monomer molecules*. A single monomer molecule contributes a group of atoms (i.e., constitutional unit) to a macromolecule, the largest of which is referred to as a *monomeric unit*. The process, in which a monomer (i.e., "substance composed of monomer molecules", p. 2299)[1] or a mixture of them is converted into macromolecules, is called *polymerization*.[3] The underlying basic concepts reflected in these definitions were first adequately described by Staudinger in the 1920s, mainly following observations on isoprene and rubber.[4,5]

---

[*] The IUPAC recommendations are the most frequently used set of rules for unambiguous, uniform, and consistent nomenclature and terminology worldwide.

Concerning length, the IUPAC definition given above implies a certain relative molecular mass[*] compared to its constitutional units to be necessary for a molecule to be referred to as a macromolecule. Alternatively, this can be understood as a ('fuzzy') threshold in the number of repeated monomeric units (i.e., degree of polymerization)[1]. However, the IUPAC do not clearly specify how high this number must be. With a note added to the definition, they aim to clarify this point; they state that such "a molecule can be regarded as having a high relative molecular mass if the addition or removal of one or a few of the units has a negligible effect on the molecular properties" (p. 2289).[1] Although there might be exceptions, these IUPAC statements provide a suitable basic picture of what these very specific terms stand for. To categorize the corresponding molecules in terms of length even more specifically, molecules of intermediate relative molecular mass (i.e., number of repeated monomeric units between a monomer molecule – 1 – and a macromolecule – many) are referred to as *oligomer molecules*. Analogous to the definition of the term 'macromolecule' (cf. above), an additional note to the IUPAC definition of the term 'oligomer molecule' states that a "molecule is regarded as having an intermediate relative molecular mass if it has properties which do vary significantly with the removal of one or a few of the units" (p. 2289).[1] Correspondingly, the conversion of a monomer into an oligomer is termed oligomerization (cf. polymerization). Depending on the degree of polymerization, we speak of monomer molecules, oligomer molecules and macromolecules. The corresponding substances composed of the respective molecules are termed monomer, oligomer and polymer. For sake of clarity, these classifications are summarized and sketched in Figure II.1-1.

repeated units	individual molecule	substance
1	monomer molecule	monomer
a few	oligomer molecule	oligomer
many	macromolecule	polymer

Figure II.1-1. Subset of classifications sketched as per IUPAC definitions[1] of basic terms in polymer chemistry.

Besides being decisive for nomenclature, the relative molecular masses of the macromolecules within a polymer also determine, inter alia, the

---

[*] also termed molar mass or molecular weight[2]

polymer's properties. As mentioned above, the molar mass is a measure for the size of a molecule. For a macromolecule, it is also an indirect quantification of its length. To directly refer to the structure of a macromolecule, we speak of macromolecular or *polymer chains*. A direct measure for the length of a macromolecule is, thus, its chain length, i.e., the number of monomer molecules incorporated (actually or conceptually) into the macromolecule. Most real polymers contain macromolecules of various chain lengths. This can be described in a distribution of relative molecular masses (DMM), whose shape depends, inter alia, on the polymerization process. Thus, the molar mass in polymers is commonly expressed in weighted averages, such as the number-average M_n and mass-average molar mass M_w,

$$M_n = \frac{\sum_i n_i M_i}{\sum_i n_i}, \qquad M_w = \frac{\sum_i n_i M_i^2}{\sum_i n_i M_i}, \qquad \text{(II.1-1)}$$

where n_i represents the number of molecules with relative molecular mass M_i. The sum includes all molecules within the substance. Both numbers (M_n and M_w) are representative measures for the DMM. However, already from the equations, it is evident that distinct DMMs will be reflected differently in the values of M_n and M_w. The molar-mass dispersity $Đ_M = M_w/M_n$ is used to quantify this difference and, in turn, to give a measure for the broadness of the DMM of a polymer. If all chains (i.e., macromolecules) are equally long, $M_n = M_w$ and $Đ_M = 1$. In this case, the polymer is referred to as being *monodisperse*. The larger $Đ_M$ is, the broader the distribution and the more *polydisperse* the polymer.

In addition to the distribution of relative molecular masses within a polymer, the properties of the polymer also strongly depend on the specific chemical structure of the monomer molecules (more specifically, the monomeric units) and on how many different species of units are incorporated into the macromolecular chains. If the entire structure of a polymer is derived from one type of monomer, the substance is called *homopolymer*. For homopolymers, the IUPAC recommends to make the polymer's name directly by combining the name of the corresponding monomer with the prefix 'poly-' (e.g., polypropylene).[6*] The addition of a second species of monomer molecules can alter the polymer's properties significantly. In case of two or more species of monomeric units being involved, the resulting substance is referred to as a *copolymer*. For copolymers derived from two types of monomers, four main classes are differentiated, depending on the sequence arrangement of the two monomeric units within the polymer chains: *alternating*, *block*, *graft* and *random copolymers* (see Figure II.1-2). The chemical structure of the individual monomer molecules and the polymerization

---

[*] The name of the monomer is parenthesized in cases where ambiguities could arise (e.g., monomer's name consists of two words).[6]

process determine what type of class the resulting polymer will belong to. The IUPAC recommends deriving the name of the copolymer from the names of the respective monomers by adding the prefix 'poly-' and an italicized connective '-co-' between the monomers' names.[*] To specify the kind of sequence arrangement (e.g., alternating or random), the qualifier '-co-' can be replaced by the corresponding one (e.g., '-alt-' or '-ran-', respectively).[7] In non-linear (co)polymers (e.g., graft copolymers), the continuous "chain to which all other chains, long or short or both, may be regarded as being pendant" is referred to as the (polymer) backbone.[1]

alternating copolymer

block copolymer

graft copolymer

random copolymer
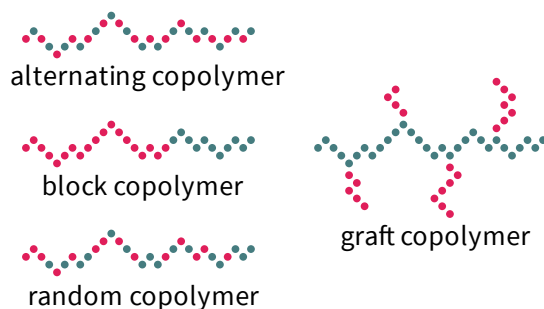
Figure II.1-2. Sketch of classes of copolymers differentiated depending on the sequence arrangement of the two types of monomeric units included (represented by dots in red and mint).

In its logical form, the IUPAC definition of the term 'polymer' (cf. above)[1] lacks a clear specification of the amount of macromolecules necessary for a substance to be regarded as a polymer. In practice, such terms are not always used perfectly according to their definitions but in doing so sometimes more intuitively. Thus, the term 'polymer', in general, denotes substances or materials of macromolecular nature[†].[3] However, the length scales, on which polymers exist, are diverse (from nanometers to the macroscale). Especially when industrially utilized on the macroscale, such materials are also commonly referred to as *plastics*. In addition to macromolecules, plastics "may contain other substances to improve performance and/or reduce costs".[3]

Another aspect influencing a polymer's properties is the arrangement of its macromolecules (or parts of them) with respect to one another (i.e., order). In the liquid state, no order is present (also in polymers). Interestingly, the boundary to the solid state is not as sharp as for most other materials (e.g., (inorganic) materials composed of small molecules, metals). In rigid 'solid-state' polymers, we distinguish between ordered semi-crystalline states and amorphous glassy states, formed depending on the chemical structure and

---

[*] E.g., the monomers styrene and isoprene can be copolymerized to form a copolymer (unspecified sequence arrangement) called poly(styrene-*co*-isoprene).
[†] e.g., including cross-linked polymer networks, cf. section II.1.1

14

molar mass of the polymer. At elevated temperatures, polymers can also form so-called rubbery phases. Phase transitions between these states are complex, whereas all of the mentioned phases in 'solid' polymers are thermodynamically metastable.[8] While all properties depend on the state the polymer is in, their mechanical behavior (rigid, glassy and rubbery) is specifically affected by and, in turn, quasi representative of the different phases.

As discussed before, the chemical structure of the monomer molecules is, inter alia, a decisive factor for the properties of the corresponding polymer. In many cases, this relationship is the basis for the polymer exhibiting intriguing functionalities. One such group of polymers with a distinct functionality due to a specific chemistry of monomer molecules are *hydrogels*. This class of materials is discussed in the following.

II.1.1 Hydrogels

Hydrogels are polymers that are able to take up significant amounts of water from their environment into their structure due to the specific chemistry of their monomer molecules. This water uptake behavior stems from the macromolecular chains exhibiting functional groups such as $-NH_2$, $-COOH$, $-CONH_2$, $-CONH-$, the capillary effect and osmotic pressure.[9] As a consequence, in the presence of H_2O, the material expands in size (i.e., swelling). To ensure mechanical integrity during swelling, the individual macromolecular chains need to be cross-linked. Two types are distinguished: *physical* and *chemical cross-linking* (cf. Figure II.1-3). Physical cross-links are, e.g., hydrogen bonds, ionic complexes or entangled macromolecular chains and depend strongly on the chemical structure of the polymer and the polymerization process. In chemical cross-linking, the individual macromolecular chains are connected via covalent bonds. Such (chemical) cross-links can be achieved, e.g., by copolymerizing a monomer able to connect/bind two separate macromolecular chains with the monomer exhibiting the desired functionalities. The resulting polymer can be viewed as a cross-linked network of macromolecular chains (i.e., polymer mesh/network).[*] The cross-links imply a confinement to (elastic) deformation the polymer can perform. Still, the hydrogel shows a certain solubility, originating in the hydrophilic units within its macromolecular chains. Both these properties result in the polymer network exhibiting a certain *mesh size (ξ)* connected to the maximum amount of water the hydrogel is able to take up in equilibrium (cf. Figure II.1-3).[10] Thus, the swelling behavior of hydrogels is altered by the chemical nature of the polymer and the degree of cross-linking.

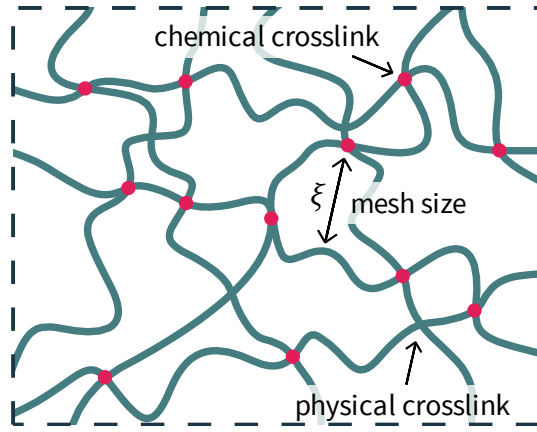[*] conceptually, in extremis, one (giant) macromolecule

Figure II.1-3. Sketched section of a polymer network with cross-linked macromolecular chains, indicating chemical and physical cross-links (mesh size ξ).

To describe equilibrium swelling in polymer networks, a theory developed by Flory & Rehner in the 1940s and 1950s is still one of the most widely used.[11,12] Thereby, the mesh size ξ of a polymer can be estimated from its equilibrium degree of (isotropic) swelling as

$$\xi = v_{p,s}^{-1/3}(\bar{r}_0^2)^{1/2} = \alpha(\bar{r}_0^2)^{1/2} = v_{p,s}^{-1/3}\left(\frac{2C_N\overline{M_C}}{M_r}\right)^{1/2}l, \quad \text{(II.1-2)}$$

where $v_{p,s}$ is the polymer volume fraction in the fully swollen state, $(\bar{r}_0^2)^{1/2}$ the unperturbed end-to-end distance of the polymer chains between cross-links, $\overline{M_C}$ the relative molecular mass between two cross-links, M_r the relative molecular mass of the monomeric units and l the length of the bond along the backbone of the macromolecular chain.[13] C_N is the Flory characteristic ratio and is a measure (experimentally determined) for the stiffness of a polymer chain (depending on its length N).

In addition to this theory on equilibrium swelling, a mathematical description of the kinetics during swelling of polymers (particularly in drug release) can be found in the works of Peppas & Colombo.[14] The kinetics are particularly interesting for the application of hydrogels to setups, in which fast responses are crucial (e.g., sensing). The details of this theory would go beyond the scope of the work presented in this thesis. Nevertheless, the applicability of polymers to sensing will be discussed in section II.1.3.

The development of the entire field of hydrogel materials was initiated in 1960, by Wichterle & Lím reporting on the polymerization of poly(2-hydroxyethyl methacrylate) (pHEMA) as a water swollen, elastic and clear gel.[15] Over the years, numerous chemical structures of polymers were found to exhibit similar functionalities. Together with properties such as biocompatibility, the materials' characteristics are deemed promising to present a suitable

basis for their usage in treating or replacing tissues and organs or, generally, in interacting with biological systems.[16] Up to date, hydrogels are used to provide an aqueous/wet matrix or environment in biological settings. The described properties enabled their application in contact lenses, wound care coverings, in setups for the controlled release of drugs, as matrices for cell encapsulation, etc.[9,16] A subclass of polymers that is particularly interesting and promising for broadening the range of possible applications in this context is referred to as *smart polymers*. What these materials are, is discussed in the following sections via outlining the basics of *smart materials* in general and describing the concepts applying to *thermo-responsive hydrogels*.

II.1.2 Smart Polymers

Already for several decades, the adjectives 'smart' and 'intelligent' are being broadly used in the fields of science, technology and engineering. These terms convey multi-faceted concepts, sometimes making it hard to grasp the real notion of their meanings in the actual contexts. In materials science, being *smart* or *intelligent* refers to properties of substances, structures or systems that are in a certain way sophisticated. In the foreword to their anthology 'Intelligent Materials', Shahinpur & Schneider state that "claiming to be intelligent is bold" and describe the materials addressed in their book rather as "respond[ing] in an interesting way to an external stimulus" (p. v).[17] They go on to arguing that *sensitive* may be more appropriate than intelligent. Nevertheless, 'smart' and 'intelligent' are common terms in materials science, the conceptions of which can be deduced from the contexts they are used in. Commonly, such as by Cao et al.[18], these concepts are captured with respect to functionality:

> *Smart Structures and Materials (p. 8330)*[18]
> "A smart structure is a system containing multifunctional parts that can perform sensing, control, and actuation; it is a primitive analogue of a biological body. Smart materials are used to construct these smart structures, which can perform both sensing and actuation functions."

Oftentimes, a comparison to a biological body is drawn (cf. above[18]), which might overstate the real smartness or intelligence of the synthetic substances or structures developed up to date (e.g., cognitively). However, the characteristics of responding to an external stimulus and being multifunctional are essential. Also, Shahinpur & Schneider define intelligent materials as "respond[ing] to external stimuli by a characteristic behaviour[sic]" and as being multifunctional, but add "due to their unique molecular structure" (p. xxi) to their definition.[17] In that way, a material's smartness or

intelligence originates in and is directly linked to fundamental molecular events. This leaves structures and "technical devices, which are engineered on the basis of intelligent materials," (p. xxi) out of the picture.[17] Regardless, this discrimination is not relevant to the work laid out in this thesis, as, herein, the focus is set specifically on smart materials.

The aim of the above discussion is to outline the complexity of a clear definition of the mentioned terms and their practical usage. What seems to be clear, is that smart materials are in close relation to their environment and react to it by changing their properties according to specific external stimuli. Based on these considerations, Cao et al.[18] specify the 'I.Q.' of smart materials as their *responsiveness* to environmental stimuli and their *agility*. The former criterion is connected to the magnitude of the response of the material (i.e., change in properties as a function of external stimulus). The latter assesses the kinetics of the response. A larger and faster response is associated with a higher 'I.Q.'. In conclusion, a smart material can be viewed as a (multi)functional substance, changing its properties in (direct) reaction to external stimuli in a fast and highly responsive manner.

Due to the specific nature of polymers, a plethora of functional units can be designed and incorporated into their macromolecular structure fairly easily (e.g., via copolymerization; cf. Aguilar & San Román[19]). Therefore, polymers are a class of materials that seem to be particularly promising in or, even, prone to being smart. Analogous to the above considerations, Aguilar & San Román describe *smart polymers* as "undergo[ing] large reversible changes, either physical or chemical, in their properties as a consequence of small environmental variations" (p. 1).[19] They use the term 'smart polymer' synonymously with 'stimuli-responsive polymer'. This specific class of materials is discussed in the following.

As mentioned above, *stimuli-responsive polymers* (also referred to as smart polymers) are polymeric substances that react to environmental stimuli such as temperature, pH, light intensity, electric or magnetic fields, enzymes or various other (bio)molecules.[19,20] Furthermore, these topics include and are in close connection to the scientific fields of shape memory polymers and self-healing, which also attracted particular interest in recent years.[19] Stimuli-responsive polymers are used, e.g., in systems for on-demand drug delivery, tissue generation/repair, biosensing, in smart coatings and artificial muscles.[20] In addition, hybrid structures of synthetic stimuli-responsive polymers with biomacromolecules were reported to enhance and widen the range of possible applications even further.[21]

A specific family of stimuli-responsive polymers relevant to the work presented in this thesis, namely *thermoresponsive hydrogels*, is addressed in the following section.

Thermoresponsive Hydrogels

A large part of the functionalities of smart polymers described above is based on the distinct solubility of hydrogels in solvents under specific environmental conditions. As indicated above, these materials respond to external stimuli via conformational transitions in their macromolecular structure (e.g., so-called coil-globule transitions).[22] Such coil-globule transitions were also reported to occur in natural, biological systems such as (small) proteins[23] or DNA.[24] The behavior of these natural macromolecules is analogous to the one found in synthetic macromolecular structures like the hydrogel networks discussed in this thesis.

In the actual coil-globule transition in hydrogels, the conformational arrangement of the individual macromolecular chains changes as a function of a specific external stimulus (see Figure II.1-4). Upon varying the environment, the polymer transitions from a good to a poor solvent behavior or vice versa. Thus, the change in polymeric conformation translates to a change in hydrophobicity/-philicity. The entropy of mixing and the attractive interactions of the macromolecular structure with itself are among the governing factors. Accordingly, the polymer chains transition between an expanded conformation (i.e., coil state) and a collapsed one (i.e., globule state[*]). This can be observed as a characteristic volumetric change of the material (i.e., swelling and deswelling) that can also be indirectly measured in a variety of material properties (e.g., refractive index, permeability, elastic modulus, interfacial tension, adhesion).[22]

In the specific case of thermoresponsive hydrogels, the external parameter yielding a change in their properties is the temperature. Among all the smart polymers, thermoresponsiveness is the most well-studied branch of stimuli-responsiveness.[20] Hydrogels exhibiting two general types of behavior are distinguished: The ones becoming miscible with the solvent and the ones becoming insoluble as the temperature is increased. The corresponding transition temperatures are termed *upper (UCST)* and *lower critical solution temperature (LCST)*. The most prominent example of a thermoresponsive hydrogel is poly(N-isopropylacrylamide) (pNIPAAm[†]). It is widely reported to exhibit an LCST of around ~32 °C in water.[25] Its thermoresponsiveness was shown by Heskins & Guillet[26] in 1968 and stems from two distinct functionalities: On the one hand, the polymer exhibits hydrophilic groups in its molecular structure (i.e., amide) yielding the possibility of forming hydrogen bonds to H_2O in aqueous environments, dominating at temperatures below the LCST. On the other hand, the polymer has hydrophobic groups (i.e., isopropyl) and shows a probability of attractive inter-segment interactions at

---

[*]also referred to as the shrunken state of the polymer
[a]Abbreviations also used for pNIPAAm include pNIPA, pNIPAM, pNIPAA, pNIPAm.

elevated temperatures.[27] The LCST of pNIPAAm can be tailored by modifying the polymer's internal structure (e.g., via copolymerization)[28] or by altering the solvent (e.g., via co-solvents,[29] salts[30]).
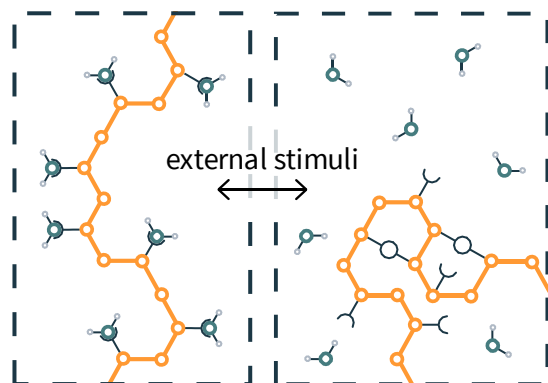

Figure II.1-4. Sections of the polymeric structure of a stimuli-responsive hydrogel sketched in its coil (left) and globule (right) sates; polymer backbone in orange, functional groups in dark blue.

In addition to pNIPAAm, various polymers exhibit similar functionalities. For this thesis, besides pNIPAAm, poly(*N*-vinylcaprolactam) (pNVCL) is of particular relevance. This polymer is reported to exhibit an LCST similar to pNIPAAm and was examined and shown to be biocompatible and not cyto-toxic in various studies.[31] In contrast to pNIPAAm, pNVCL behaves accord-ing to a typical Flory-Huggins miscibility behavior with H_2O, for which an increased polymer chain length leads to a downward shift of the LCST; the values of the transition temperature for samples of different molar mass were reported to lie in the range of ~30-40°C.[32] The hydrophilic swollen state in pNVCL is assumed to stem from attractive interactions of water molecules and polar groups in the polymer (i.e., hydrogen bonds with amide groups), but also contacts of hydrophobic groups of the polymer (i.e., methylene in the caprolactam ring) with water. Analogous to the behavior of pNIPAAm, these contacts become thermodynamically less favorable and are dominated by contacts between the hydrophobic groups themselves as the temperature is increased, resulting in the hydrophobic collapsed state of the polymer.[33]

Overall, both polymers (pNIPAAm and pNVCL) show a transition between a swollen and a shrunken state upon changing the external stimulus of tem-perature. Their LCST can be tuned in a range around human body tempera-ture, enabling the polymers to be particularly interesting for numerous bio-applications. One of the many conceivable options of applying these materi-als to device setups is their potential for sensing/actuating. The following sections give a short introduction into the field of (polymeric) sensors and actuators with a distinct focus on humidity sensing.

II.1.3 Polymeric Sensors/Actuators

*Sensors (*and *actuators)* are ubiquitous in the rise of an information society. Already from looking into everyday life (e.g., smart homes), there seems to be a commitment to quantifying and using almost all the data around us in order to facilitate our living. Within such functional systems, a sensor is an essential device. According to its etymological origin (e.g., Latin 'sensus', *sensation, feeling, meaning*) and in the manner of sensory organs, a sensor is a device that gets some 'meaning' (i.e., a piece of information) out of a 'feeling' (i.e., a datum). Comparable but in an adequate form, the IUPAC defines a *chemical sensor* as follows:

> *Chemical Sensor (IUPAC definition, p. 1248)[34]*
> "A chemical sensor is a device that transforms chemical information […] into an analytically useful signal. […] Chemical sensors contain two basic functional units: a receptor part and a transducer part. In the receptor part of a sensor the chemical information is transformed into a form of energy which may be measured by the transducer. The transducer part is a device capable of transforming the energy carrying the chemical information about the sample into a useful analytical signal."

Analogous, the IUPAC defines a *physical sensor* as "a device that provides information about a physical property of the system" (p. 1248).[34] The concepts of receptors and transducers and their relationship to the sensor can be used accordingly. Independent of the type of information, a sensor responds to a datum that is of interest (i.e., an external stimulus) by a change in properties, which is then translated into a signal that can be analyzed, processed and read out.

As mentioned above, integrated systems (e.g., Internet of Things) emerge and grow. Besides sensors, also actuators are vital components and crucial parts of them. Furthermore, both are essential in the broader field of robotics. The IUPAC recommends to use the term 'actuator' (specifically in the context of robotics and automation) for referring to "a power mechanism used to effect motion of the robot" or "a motor or transducer that converts electrical, hydraulic, or pneumatic energy into motion" (p. 611).[35] These statements address the field of conventional (hard) robotics but can be readily extrapolated into the upcoming field of soft robotics by leaving the forms of energy that are converted into motion open. As summarized by Whitesides,[36] hard robotics is a highly advanced and technologically sophisticated field, developing machines (consisting of rigid structural materials plus corresponding actuators) that can be and are used to precisely control (complex) mechanical motions. However, Whitesides claims that such robots are

(mostly) ineffective and built of non-compliant materials, making them unsuitable for specific types of applications (e.g., soft gripping).[36] Hard robots are heavy, mostly very expensive, require complex motion-control systems and are what is termed 'non-collaborative'[*].[36] Initial applications of soft robots include 'soft gripping', aiming to circumvent shortcomings of hard robots in working collaboratively with people and soft objects. In contrast to the hard robotics' focus on electronics and control units, soft robotics is seeking to utilize (smart) materials to perform complex functions with less/more efficient components and, thereby, reducing cost and effort (e.g., complex systems of electronic controllers, actuators and computers). Soft materials can be used to complement and, in some cases, outperform hard robotic systems. Therefore, soft robotics is strongly intertwined with the field of materials science and the specific material properties that are required to fulfill the tasks expected from the robots. This yields an enormous and interesting chance for materials science and engineering to (co)develop a highly seminal field, even if it is still in a very early stage of technological evolution.[36] As evident from the required material properties (e.g., soft, (super)elastic, functional), polymers are among the central building blocks of this development. Analogous to the (potentially inherent) smartness of polymeric materials (cf. section II.1.2), they present a highly versatile class of materials, suitable to tackle the challenges posed in such novel approaches.

For the applications mentioned above, sensors and actuators that are able to gather and respond to almost all pieces of information and data in our environments are required. At the same time, these systems are demanded to exhibit manifold properties as devices themselves determined by the specific application they ought to be used in. These developments open up a variety of new possibilities but also require the access to new materials and functions. As mentioned above, polymers with their specific but versatile material properties (e.g., softness, elasticity and functionality) are particularly interesting and promising for such applications.

Overall, polymers are functional materials that are easily processable and the properties of which may be tailored in a wide range of possibilities. Besides their manifold spectacular functions, e.g., in environments where required (e.g., with an analyte), they can also be readily selected to be inert.[37] Therefore, polymers are indispensable to modern sensor and actuator setups. In many such systems, such materials are applied, performing specific tasks, either directly in sensing/actuating, as structural components or having other assistive functions (e.g., immobilizing distinct species).[37] Depending on the piece of information a sensor is required to detect or an actuator

---

[*] Describing hard robots as 'non-collaborative' refers to their lack of safety in working "in close contact with (or proximity to) people or other fragile objects".[36]

is designed to react to, an almost infinite number of polymeric setups and materials have been and will be proposed. For the work presented in the later parts of this thesis, concepts for sensing and responding to a parameter termed 'relative humidity' need to be addressed. Thus, the following section gives an overview of relevant information on humidity and humidity sensing with a focus on materials used for such applications.

(Materials for) Humidity Sensing

The *humidity* is a measure for the concentration of water vapor (i.e., moisture) in mixed (e.g., air) or pure gases (e.g., nitrogen or argon). The importance of this parameter goes beyond its obvious implications and expands into various fields such as meteorology, biology and industry/technology. In meteorology, e.g., the humidity is known to be intimately linked to the likelihood for precipitation. In biology, humidity is, clearly, among the most important abiotic factors,[*] influencing life in an ecosystem in manifold ways. In technology, humidity, inter alia, alters the lifespan and functioning of numerous components in industrial systems.

Overall, various specific measures are used to quantify the humidity, two of which are particularly useful: *absolute* and *relative humidity*. The absolute humidity (*AH*) denotes the absolute amount of water vapor in the gas and can be measured in parts-per-million (ppm). The *AH* finds extensive application in industry and is, specifically in ppm, especially relevant for trace moisture measurements. It can be expressed in ppm_v (by volume) or via multiplying ppm_v by the ratio of the molar masses of water and air in ppm_w (by mass).[38] On the contrary, the relative humidity (*RH*)[†] is the ratio of the partial pressure of water vapor present in a gas (p_{H_2O}) to the saturation vapor pressure of the gas at a given temperature ($p^*_{H_2O}$):

$$RH = \frac{p_{H_2O}}{p^*_{H_2O}} \qquad\qquad (\text{II.1-3})$$

The *RH* is commonly expressed in percent (%) and is a function of temperature (thus, relative). It is easily comprehensible and, therefore, used in everyday life. Also, meteorology and numerous technical/industrial applications (e.g., various processes require specific levels of humidity) utilize the *RH*, as it also specifically covers a range of higher humidity than the *AH* (given in ppm). As the work presented in this thesis focuses on sensing of the relative humidity, the further part of this section introduces materials that can be employed for such an application.

---

[*] In biology and ecology, chemical and physical (non-living) environmental properties affecting organisms and the ecosystem are termed abiotic factors.
[†] The Greek letter ϕ (phi) may also be used to refer to this ratio.

In general, three different classes of materials are used for sensing of the relative humidity: ceramics (e.g., Al_2O_3), semiconductors (e.g., SnO_2) and polymers.[38] Usually, independent of the material applied, a porous system is utilized to take up a specific amount of water vapor from its environment. This causes a change in electrical properties of the material (e.g., conductivity), which is, subsequently, read out as a signal proportional to the relative humidity of the environmental gas. In such conventional humidity sensors, two categories of devices are distinguished: resistive-type, changing their resistance as a function of water vapor in the environment, and capacitive-type, responding to moisture by varying their dielectric constant.[39]

In polymers, besides utilizing a porous structure, the material's hydrophobicity/-philicity can be tuned by including/altering distinct functional units. Specifically, hydrogels offer the opportunity to sense the relative humidity in their environment via inherent volumetric changes resulting from water uptake (cf. section II.1.1). The most obvious and pursued way of detecting these characteristic changes upon swelling and deswelling are optical methods (e.g., photonic crystal hydrogels).[13] However, also other methods of detection are conceivable (e.g., combination with piezoelectric/piezo-resistive materials). As the water exchange with the environment is linked to a proportional volumetric change of the hydrogel material, a mechanical motion is inherent. This is exactly the function of an actuator (as described in section II.1.3), with the external stimulus of relative humidity actively effecting motion. For instance, such hydrogel-based actuators were shown to be applicable for autonomous flow control in micro-fluidic devices.[40]

Besides utilizing conventional hydrogel materials (e.g., pHEMA), stimuli-responsive polymers (as described in II.1.1 and II.1.2) yield the great potential of responding to two stimuli (RH and temperature T) simultaneously. Since the relative humidity is a temperature-dependent parameter, T needs to be measured independently or kept constant in setups applying conventional hydrogel materials. Via thermoresponsive hydrogels (e.g., pNIPAAm), the temperature can be directly evaluated from (de)swelling in a (fully) hydrated system.[13] Moreover, in such hydrated systems, a (photo)thermally programmable motion of a stimuli-responsive hydrogel was successfully reported.[41] Furthermore, pNIPAAm has already been shown to be applicable to humidity sensing.[42] In thermoresponsive hydrogels, only both the knowledge of T and RH define the state (i.e., degree of swelling) the material is in. A clever setup, achievable via the implementation of several polymers in close proximity to one another, exhibiting (slightly) different, strong LCST transitions, (theoretically) allows for the direct and simultaneous evaluation of both parameters (T and RH). Our group works on a clear demonstration/proof for the feasibility of this idea. Furthermore, the properties of thermoresponsive

polymers (response to *RH* and *T*) allow for their direct application as hygro-morphic[*] actuators (as demonstrated by our group; see section III.4).

Overall, hydrogels and, specifically, stimuli-responsive hydrogels show the great opportunity of fulfilling a multitude of the functions required of actuators and sensors within a single (smart) material. As indicated above, such materials can perform parts of the tasks of receptors and transducers simultaneously. Regardless, a strong response to the respective external stimuli (e.g., in swelling) is essential for their applicability to device setups. Additionally, as the swelling processes in hydrogels are rate-limited by water-diffusivity,[40] reducing/minimizing the materials' physical dimensions is crucial for achieving fast response times.[†] Not only for polymers, the synthesis and application of thin films and nanostructures has paved the way for miniaturization and optimization over the last decades. The synthesis of polymers, in general, and of polymeric thin films, in particular, is crucial for the work presented in this thesis and will be addressed in section II.2.

---

[*] changing shape as a function of humidity

[†] As evident from these considerations, the 'I.Q.' of a smart polymer (as described in section II.1.2) is also a measure of the quality of an actuator or a sensor.

II.1.4 References

(1)   Jenkins, A. D.; Kratochvíl, P.; Stepto, R. F. T.; Suter, U. W. Glossary of Basic Terms in Polymer Science (IUPAC Recommendations 1996). *Pure Appl. Chem.* **1996**, *68* (12), 2287–2311. https://doi.org/10.1351/pac199668122287.

(2)   Lehmann, H. P.; Fuentes-Arderiu, X.; Bertello, L. F. Glossary of Terms in Quantities and Units in Clinical Chemistry (IUPAC-IFCC Recommendations 1996). *Pure Appl. Chem.* **1996**, *68* (4), 957–1000. https://doi.org/10.1351/pac199668040957.

(3)   Vert, M.; Doi, Y.; Hellwich, K. H.; Hess, M.; Hodge, P.; Kubisa, P.; Rinaudo, M.; Schué, F. Terminology for Biorelated Polymers and Applications (IUPAC Recommendations 2012). *Pure Appl. Chem.* **2012**, *84* (2), 377–410. https://doi.org/10.1351/pac-rec-10-12-04.

(4)   Staudinger, H. Über Polymerisation. *Berichte der Dtsch. Chem. Gesellschaft (A B Ser.* **1920**, *53* (6), 1073–1085. https://doi.org/10.1002/cber.19200530627.

(5)   Staudinger, H.; Fritschi, J. Über Isopren Und Kautschuk. 5. Mitteilung. Über Die Hydrierung Des Kautschuks Und Über Seine Konstitution. *Helv. Chim. Acta* **1922**, *5* (5), 785–806. https://doi.org/10.1002/hlca.19220050517.

(6)   Maréchal, E.; Wilks, E. S. Generic Source-Based Nomenclature for Polymers(IUPAC Recommendations 2001). *Pure Appl. Chem.* **2001**, *73* (9), 1511–1519. https://doi.org/10.1351/pac200173091511.

(7)   Ring, W.; Mita, I.; Jenkins, A. D.; Bikales, N. M. Source-Based Nomenclature for Copolymers (Recommendations 1985). *Pure Appl. Chem.* **1985**, *57* (10), 1427–1440. https://doi.org/10.1351/pac198557101427.

(8)   Van Krevelen, D. W.; Te Nijenhuis, K. Typology of Polymers. In *Properties of Polymers*; Elsevier, 2009; pp 7–47. https://doi.org/10.1016/B978-0-08-054819-7.00002-9.

(9)   Ullah, F.; Othman, M. B. H.; Javed, F.; Ahmad, Z.; Akil, H. M. Classification, Processing and Application of Hydrogels: A Review. *Mater. Sci. Eng. C* **2015**, *57*, 414–433. https://doi.org/10.1016/j.msec.2015.07.053.

(10)   Canal, T.; Peppas, N. A. Correlation between Mesh Size and Equilibrium Degree of Swelling of Polymeric Networks. *J. Biomed. Mater. Res.* **1989**, *23* (10), 1183–1193. https://doi.org/10.1002/jbm.820231007.

(11)   Flory, P. J.; Rehner, J. Statistical Mechanics of Cross-Linked Polymer Networks II. Swelling. *J. Chem. Phys.* **1943**, *11*, 521–526. https://doi.org/10.1063/1.1723792.

(12)   Flory, P. J. Statistical Mechanics of Swelling of Network Structures. *J. Chem. Phys.* **1950**, *18*, 108–111. https://doi.org/10.1063/1.1747424.

(13)   Buenger, D.; Topuz, F.; Groll, J. Hydrogels in Sensing Applications. *Prog. Polym. Sci.* **2012**, *37* (12), 1678–1719. https://doi.org/10.1016/j.progpolymsci.2012.09.001.

(14)   Peppas, N. A.; Colombo, P. Analysis of Drug Release Behavior from Swellable Polymer Carriers Using the Dimensionality Index. *J. Control. Release* **1997**, *45* (1), 35–40. https://doi.org/10.1016/S0168-3659(96)01542-8.

(15)   Wichterle, O.; Lím, D. Hydrophilic Gels for Biological Use. *Nature* **1960**, *185*, 117–118. https://doi.org/10.1038/185117a0.

(16)   Rosiak, J. M.; Yoshii, F. Hydrogels and Their Medical Applications. *Nucl. Instruments Methods Phys. Res. Sect. B Beam Interact. with Mater. Atoms* **1999**, *151* (1–4), 5. https://doi.org/10.1016/S0168-583X(99)00118-4.

(17)   Shahinpoor, M.; Schneider, H.-J. Preliminary Content. In *Intelligent Materials*; Shahinpoor, M., Schneider, H.-J., Eds.; Royal Society of Chemistry: Cambridge, 2007; pp v–xxi. https://doi.org/10.1039/9781847558008.

(18)   Cao, W.; Cudney, H. H.; Waser, R. Smart Materials and Structures. *Proc. Natl. Acad. Sci.* **1999**, *96* (15), 8330–8331. https://doi.org/10.1073/pnas.96.15.8330.

(19)   Aguilar, M. R.; San Román, J. Introduction to Smart Polymers and Their Applications. In *Smart Polymers and their Applications*; Elsevier, 2014; pp 1–11. https://doi.org/10.1533/9780857097026.1.

(20)   Wei, M.; Gao, Y.; Li, X.; Serpe, M. J. Stimuli-Responsive Polymers and Their Applications. *Polym. Chem.* **2017**, *8* (1), 127–143. https://doi.org/10.1039/C6PY01585A.

(21)   Cobo, I.; Li, M.; Sumerlin, B. S.; Perrier, S. Smart Hybrid Materials by Conjugation of Responsive Polymers to Biomacromolecules. *Nat. Mater.* **2015**, *14* (2), 143–159. https://doi.org/10.1038/nmat4106.

(22)   Tokarev, I.; Minko, S. Stimuli-Responsive Hydrogel Thin Films. *Soft Matter* **2009**, *5* (3), 511–524. https://doi.org/10.1039/B813827C.

(23)   Sherman, E.; Haran, G. Coil-Globule Transition in the Denatured State of a Small Protein. *Proc. Natl. Acad. Sci.* **2006**, *103* (31), 11539–11543. https://doi.org/10.1073/pnas.0601395103.

(24)   Vasilevskaya, V. V.; Khokhlov, A. R.; Matsuzawa, Y.; Yoshikawa, K. Collapse of Single DNA Molecule in Poly(Ethylene Glycol) Solutions. *J. Chem. Phys.* **1995**, *102* (16), 6595–6602. https://doi.org/10.1063/1.469375.

(25)   Schild, H. G. Poly(N-Isopropylacrylamide): Experiment, Theory and Application. *Prog. Polym. Sci.* **1992**, *17* (2), 163–249. https://doi.org/10.1016/0079-6700(92)90023-R.

(26)   Heskins, M.; Guillet, J. E. Solution Properties of Poly(N-Isopropylacrylamide). *J. Macromol. Sci. Part A - Chem.* **1968**, *2* (8), 1441–1455. https://doi.org/10.1080/10601326808051910.

(27)   Liu, R.; Fraylich, M.; Saunders, B. R. Thermoresponsive Copolymers: From Fundamental Studies to Applications. *Colloid Polym. Sci.* **2009**, *287* (6), 627–643. https://doi.org/10.1007/s00396-009-2028-x.

(28)   Pena-Francesch, A.; Montero, L.; Borrós, S. Tailoring the LCST of Thermosensitive Hydrogel Thin Films Deposited by ICVD. *Langmuir* **2014**, *30* (24), 7162–7167. https://doi.org/10.1021/la5003594.

(29)   Schild, H. G.; Muthukumar, M.; Tirrell, D. A. Cononsolvency in Mixed Aqueous Solutions of Poly(N- Isopropylacrylamide). *Macromolecules* **1991**. https://doi.org/10.1021/ma00004a022.

(30)   Zhang, Y.; Furyk, S.; Bergbreiter, D. E.; Cremer, P. S. Specific Ion Effects on the Water Solubility of Macromolecules: PNIPAM and the Hofmeister Series. *J. Am. Chem. Soc.* **2005**, *127* (41), 14505–14510. https://doi.org/10.1021/ja0546424.

(31)   Cortez-Lemus, N. A.; Licea-Claverie, A. Poly(N-Vinylcaprolactam), a Comprehensive Review on a Thermoresponsive Polymer Becoming Popular. *Prog. Polym. Sci.* **2016**, *53*, 1–51. https://doi.org/10.1016/j.progpolymsci.2015.08.001.

(32)   Meeussen, F.; Nies, E.; Berghmans, H.; Verbrugghe, S.; Goethals, E.; Du Prez, F. Phase Behaviour of Poly(N-Vinyl Caprolactam) in Water. *Polymer (Guildf).* **2000**, *41* (24), 8597–8602. https://doi.org/10.1016/S0032-3861(00)00255-X.

(33)   Laukkanen, A.; Valtola, L.; Winnik, F. M.; Tenhu, H. Formation of Colloidally Stable Phase Separated Poly(N-Vinylcaprolactam) in Water: A Study by Dynamic Light Scattering, Microcalorimetry, and Pressure Perturbation Calorimetry. *Macromolecules* **2004**, *37* (6), 2268–2274. https://doi.org/10.1021/ma035124l.

(34)   Hulanicki, A.; Glab, S.; Ingman, F. Chemical Sensors: Definitions and Classification. *Pure Appl. Chem.* **1991**, *63* (9), 1247–1250. https://doi.org/10.1351/pac199163091247.

(35)   Kingston, H. M.; Kingston, M. L. Recommendations for Nomenclature in Laboratory Robotics and Automation (IUPAC Recommendations 1994). *Pure Appl. Chem.* **1994**, *66* (3), 609–630. https://doi.org/10.1351/pac199466030609.

(36)   Whitesides, G. M. Soft Robotics. *Angew. Chemie Int. Ed.* **2018**, *57* (16), 4258–4273. https://doi.org/10.1002/anie.201800907.

(37)   Adhikari, B.; Majumdar, S. Polymers in Sensor Applications. *Prog. Polym. Sci.* **2004**, *29* (7), 699–766. https://doi.org/10.1016/j.progpolymsci.2004.03.002.

(38)   Chen, Z.; Lu, C. Humidity Sensors: A Review of Materials and Mechanisms. *Sens. Lett.* **2005**, *3* (4), 274–295. https://doi.org/10.1166/sl.2005.045.

(39)   Sakai, Y.; Sadaoka, Y.; Matsuguchi, M. Humidity Sensors Based on Polymer Thin Films. *Sensors Actuators B Chem.* **1996**, *35* (1–3), 85–90. https://doi.org/10.1016/S0925-4005(96)02019-9.

(40)   Beebe, D. J.; Moore, J.; Bauer, J. M.; Yu, Q.; Liu, R. H.; Devadoss, C.; Jo, B. H. Functional Hydrogel Structures for Autonomous Flow Control inside Micro-Fluidic Channels. *Nature* **2000**, *404* (6778), 588–590. https://doi.org/10.1038/35007047.

(41)   Hauser, A. W.; Evans, A. A.; Na, J.-H.; Hayward, R. C. Photothermally Reprogrammable Buckling of Nanocomposite Gel Sheets. *Angew. Chemie Int. Ed.* **2015**, *54* (18), 5434–5437. https://doi.org/10.1002/anie.201412160.

(42)   Ramakrishnan, N.; Vamsi, T.; Khan, A.; Nemade, H. B.; Palathinkal, R. P. Humidity Sensor Using NIPAAm Nanogel as Sensing Medium in SAW Devices. *Int. J. Nanosci.* **2011**, *10* (01n02), 259–262. https://doi.org/10.1142/S0219581X11007880.

II.2 Synthesis of Polymers

Polymeric materials can be synthesized by numerous methods via various mechanisms. As introduced in section II.1, the process in which a polymer is formed from a monomer is called polymerization. The chemical nature of the monomer(s), the desired result of a polymeric structure and the applied conditions determine what type of reactions are possible and what kind of polymers can be achieved. Over the years, different ways of categorizing polymers according to the reactions and mechanisms employed for their synthesis have been proposed (cf. Carothers,[1] IUPAC,[2,3] etc.). Depending on the reactivities of the involved molecules with one another and how polymerization proceeds, two basic schemes of reactions can be distinguished: *chain polymerization* and *polyaddition*.[*] Resting on this distinction, the basics of polymerization mechanisms with a focus on the topics related to the work presented in the later parts of this thesis are summarized in the following sections.

II.2.1 Basics of Polymerization Mechanisms

As mentioned above, two basic types of polymerization reactions can be differentiated. For the sake of comprehensibility, chain polymerization is introduced first. A more detailed discussion of this reaction type is given in section II.2.2, with a particular focus on the reaction mechanisms relevant to this thesis' work. The IUPAC defines chain polymerization as follows:

> *Chain Polymerization (IUPAC definition, p. 2169)[3]*
> "Chain reaction in which the growth of a polymer chain proceeds exclusively by reaction(s) between monomer(s) and active site(s) on the polymer chain with regeneration of the active site(s) at the end of each growth step."

The individual growth steps in chain polymerization reactions can, thus, be expressed as

$$C_x + M \rightarrow C_{x+1}, \qquad \text{with } x \in \{1,2,\dots \infty\}, \qquad \text{(II.2-1)}$$

where C_x denotes a growing chain of degree of polymerization x and M a monomer molecule.[3]

A second class of basic mechanisms in polymerization reactions are termed polyaddition. Contrary to chain polymerization reactions, in polyaddition,

---

[*] The IUPAC recommend avoiding the popular discrimination of *step-growth* and *chain-growth* polymerizations commonly used in textbooks.[2]

the (growing) polymer chain(s) can not only react with monomer molecules but with molecules of all degrees of polymerization (e.g., oligomer molecules, other (growing) polymer chains). Accordingly, the IUPAC define these types of reactions as follows:

Polyaddition (IUPAC definitions, p. 2181)[3]
"Polymerization in which the growth of polymer chains proceeds by addition reactions between molecules of all degrees of polymerization."

The individual growth steps in polyaddition reactions can be expressed as

$$C_x + C_y \rightarrow C_{x+y}, \qquad \text{with } x, y \in \{1, 2, \dots \infty\}, \qquad \text{(II.2-2)}$$

where C_x and C_y denote growing chains of degrees of polymerization x and y, respectively.[3]

In general, chain polymerization and polyaddition can also occur as condensative reactions, where a low-molar-mass by-product is formed (e.g., water).[*] The corresponding reactions are termed *condensative chain polymerization* and *polycondensation*, respectively.[3]

Some of the most prominent polymers commonly synthesized by reactions in the schemes of polyaddition or polycondensation include polyurethanes (mechanism according to the former), polyesters and polyamides (processes in the scheme of the latter).[4,5] For instance, the most important polyester, poly(ethylene terephthalate) (PET), is used for water bottles, bottles for soft drinks, juices, cleaners, etc. as a resin, which accounts for approximately 10% of the global polymer resin production (data covering the period 2002-2014); polyester, polyamide and acrylic fibers (PP&A fibers), most of which are also PET (~70%), are widely used in the textile industry and make up approximately 15% (i.e., ~59 Mt) of the global primary polymer (resin and fiber) production (data from 2015).[6] However, for this work as well as industrially, chain polymerization is the more relevant reaction mechanism. The underlying concepts are introduced in the following sections.

II.2.2 Chain Polymerization

A list of the most relevant polymers commonly synthesized via chain polymerization mechanisms includes polyethylene (PE), polypropylene (PP) and poly(vinyl chloride) (PVC).[7] The importance of these materials becomes evident when reviewing the types of polymeric materials actually making for a total of 7300 Mt of overall (non-fiber) plastics production (1950-2015);

---

[*] The reaction equations need to be adjusted by adding a term denoting the low-molar-mass by-product to the right side of the Equations II.2-1 and II.2-2, respectively.

together, PE, PP and PVC account for more than two thirds of this number: PE - 36%, PP - 21%, and PVC - 12%.[6] PE and PP are the most common polymer resins used in packaging (industry sector, where most plastics are utilized), whereas PVC is used predominantly in building & construction.[6]

As evidenced in the examples listed above, specific types of polymers corresponding to monomer precursors containing unsaturated bonds (e.g., ethylene, propylene, etc.) are attainable via chain polymerization reactions. This is due to such reactions proceeding via unsaturated bonds, e.g., carbon-carbon double bonds in vinyl monomers or carbon-oxygen double bonds in aldehydes and ketones; polymerization via the former represents by far the most important scheme.[7] In addition to the monomer being required to exhibit specific chemistries, an *active site* needs to be present at the end of the growing chain for every step in the polymerization process (cf. IUPAC definition 'chain polymerization').[3] In a first step, the active site on a monomer molecule must be initiated. For its 'activation', specific chemicals, termed 'initiators', are added and used. The *initiator* provides active species (commonly either radicals or ions) that react with the monomer molecules, yielding an active site. The reactivities of this active site and the unsaturated bonds in the monomer molecules must be such that they prevalently react with one another. Reactions with other molecules of different degrees of polymerization (i.e., other (growing) polymer chains) need to be highly improbable. Thus, the chain grows by repeatedly appending a single monomeric unit to its active site and thereby regenerating the active site at the chain's end. Multiple repetition of these two processes yields a macromolecular structure. Accordingly, in a note added to the definition, the IUPAC categorizes chain polymerization as consisting of several (sub)processes: *chain initiation* and *chain propagation* reactions. It "may also include *chain deactivation* [i.e., *termination*] or chain transfer reactions, or both" (emphasis F.M., p. 2169).[3] These sub-steps are discussed in the following based on the example of *radical chain polymerization*.

II.2.2.1 Radical Chain Polymerization

In chain polymerization reactions, a specific chemical (initiator) is used to provide active species initiating the polymerization process. If these species are radicals and, thus, the polymerization proceeds via radicals as the active sites, we speak of radical chain polymerization. Based on a detailed description of the underlying assumptions and derivations in the book 'Principles of Polymerization' by Odian,[7] the individual steps in the polymerization process can be described as follows:

Initiation

Two individual reactions make up the initiation step. First, (free) radicals $R\bullet$, termed 'initiator radicals', are generated from an initiator species I, usually, by homolytic dissociation (producing two identical radicals),

$$I \xrightarrow{k_d} 2R\bullet, \qquad\qquad (\text{II.2-3})$$

with k_d being the rate constant for dissociation.[*] The most common type of compounds used as initiators are peroxides, as they exhibit labile O-O bonds that dissociate at energies in the range 100-170 kJ mol^{-1}; providing moderate amounts of thermal energy (in the range 50-200 °C) is the most widely used mode of generating initiator radicals.[7]

Second, a radical generated in such a way is appended to a monomer molecule M, producing the chain-initiating radical $C_1\bullet$,

$$R\bullet + M \xrightarrow{k_i} C_1\bullet, \qquad\qquad (\text{II.2-4})$$

where k_i denotes the corresponding rate constant of radical initiation.

Propagation

During propagation, $C_1\bullet$ grows by the repetitive addition of hundreds to thousands of monomer molecules. Upon each step, a new (longer) radical is formed, again, being similarly prone to appending another monomer molecule as the previous one. In general terms, these individual steps can be expressed as

$$C_n\bullet + M \xrightarrow{k_p} C_{n+1}\bullet, \qquad\qquad (\text{II.2-5})$$
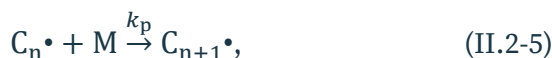
where the radical $C_n\bullet$ of chain length n is converted into a longer radical $C_{n+1}\bullet$ (cf. 'degree of polymerization') by appending a monomer molecule M at a rate represented by the rate constant of propagation k_p.

Termination

At some point, the radical is annihilated (e.g., by another radical) and the propagating chain stops growing (i.e., termination). This reaction of two radicals can proceed by *combination (coupling)* or, less frequently, by *disproportionation.*, yielding a terminated polymer chain. Coupling of two radicals $C_n\bullet$ and $C_m\bullet$ results in a macromolecular chain with length m+n, disproportionation yields two species of length m and n, respectively (one saturated, one unsaturated). In general, the result is one terminated macromolecular chain P, with which no growth can proceed, expressible as

---

[*] From rate constants, the corresponding rates can be calculated by multiplication with the concentrations of the reacted/required species, respectively.

$$C_n \bullet + C_m \bullet \xrightarrow{k_t} P, \qquad \text{(II.2-6)}$$

where k_t is the (total) rate constant of termination.

All the individual rate constants depend on the chemistries of the involved components and the applied conditions (e.g., temperature, pressure). Generally and for the notation above to be adequate, it is assumed that k_p and k_t are independent of the radicals' sizes.[7]

Kinetic Model for Radical Chain Polymerization

To describe chain polymerizations mathematically, a kinetic model can be developed by considering the rates at which the respective molecules react in the individual steps. In a typical polymerization process, far less molecules are reacted for initiation than for propagation. Thus, the polymerization rate, as the rate at which the concentration of monomer molecules[*] decreases over time, can be expressed solely by the rate of propagation R_p as

$$-\frac{d[M]}{dt} = R_p. \qquad \text{(II.2-7)}$$

As mentioned above, the rate constants are assumed to remain constant throughout all the individual propagation steps. Therefore, the rate of polymerization can be expressed as

$$R_p = k_p[C\bullet][M]. \qquad \text{(II.2-8)}$$

$[C\bullet]$ is the overall concentration of chain radicals of all degrees of polymerization. This number is low and, therefore, difficult to quantify, but it is assumed to attain a constant, steady-state value; typical radical chain polymerization reactions reach such a steady-state rather quickly (after a minute, at most).[7] In this case, the rate of change of $[C\bullet]$ is zero, ergo, the rates of initiation R_i and termination R_t need to be identical. Analogous to Equation II.2-8, R_t and R_i can be expressed as

$$R_i = 2f k_d[I] = R_t = 2k_t[C\bullet]^2, {}^{\dagger} \qquad \text{(II.2-9)}$$

where, f is the *initiator efficiency*, i.e., the fraction of initiator radicals produced that, actually, initiate polymer chains.[7] With II.2-8, this yields

$$R_p = k_p[M] \left(\frac{R_t}{2k_t}\right)^{1/2} = k_p[M] \left(\frac{f k_d[I]}{k_t}\right)^{1/2}. \qquad \text{(II.2-10)}$$

Notably, in this approximation, the polymerization rate shows a square-root dependence on R_i, R_t and, consequently, the concentration of initiator molecules $[I]$.

---

[*] The concentration of a species A is expressed by using square brackets, i.e., [A].

[†] The factor 2 is used by convention for termination/initiation (2 radicals involved).[7]

Additionally, this kinetic model can be used to derive an expression for the (kinetic) chain length and the number-average molar mass of the resulting polymer. In a radical chain polymerization, the *kinetic chain length ν* is defined as the number of monomer molecules incorporated into a polymer chain on average per radical that initiates a chain.[7] It can, thus, be expressed as the ratio of R_p and R_i or R_t. Combined with II.2-8 and II.2-9, this yields

$$\nu = \frac{R_p}{R_i} = \frac{R_p}{R_t} = \frac{k_p[M]}{2k_t[C\bullet]} = \frac{(k_p[M])^2}{2k_t R_p}. \qquad \text{(II.2-11)}$$

Assuming a steady-state (inserting II.2-10) and combined with II.2-9, ν reads

$$\nu = \frac{k_p[M]}{(2k_t R_i)^{1/2}} = \frac{k_p[M]}{2(f k_t k_d[I])^{1/2}}. \qquad \text{(II.2-12)}$$

The number-average molar mass M_n of a polymer, as introduced in section II.1 (cf. Equation II.1-1), is directly related to the kinetic chain length ν and how the (kinetic) chains are terminated. If termination occurs via combination of two chain radicals (coupling), two kinetic chain lengths form the macromolecule. In case of disproportionation, the terminated macromolecule is equally as long as a single kinetic chain (length). In most polymerization processes, both mechanisms will occur at specific rates; this can be accounted for by a factor describing the average number of initiator fragments per polymer molecule (b). Thus, the number-average molar mass M_n reads

$$M_n = b\nu M_{\text{mon}}, \qquad \text{(II.2-13)}$$

where M_{mon} is the molar mass of the respective monomeric unit.[7,8]

All the rate constants and concentrations relevant to the model introduced above depend on the specifics of the synthesis method, including the actual mechanisms taking place, the chemicals used and the reaction conditions employed. One such method is described in the following section.

II.2.3 Initiated Chemical Vapor Deposition (iCVD)

Initiated chemical vapor deposition (iCVD) is an example of a technique utilizing reactions in the scheme of radical chain polymerization for the deposition of polymer thin films. The process was developed and first extensively described in the 2000s by Gleason's group at MIT.[8–10] Up to that point, the mechanisms of radical polymerization were already well-advanced and widely employed in solution-based polymerization methods. For instance, ATRP[11,12] and RAFT[13] were discovered in the 1990s,[*] enabling the production

---

[*] ATRP stands for *atom transfer radical polymerization*, RAFT for *reversible addition-fragmentation chain transfer polymerization*, both being types of *reversible deactivation radical polymerizations*.

of polymers with a more precise control over architecture and composition than ever before.[14] Moreover, more than 18 out of the 50 Mt of polymers produced in the USA in 2001 were synthesized by radical chain polymerization.[7] Thus, the state-of-the-art knowledge available on radical chain polymerization was adopted and applied to develop iCVD as a method for the deposition of polymer thin films from the vapor phase "using monomer-initiator chemistries that are analogous to liquid-phase free radical polymerization" (p. 3688).[9]

As mentioned before, the fabrication of polymer thin films becomes more and more essential with the growing demand for miniaturized setups and devices. In a typical, conventional solution-based process for the synthesis of polymer thin films (e.g., spin-coating, ink-jet printing), three steps are necessary: First, the bulk polymer needs to be polymerized from its monomer(s). Second, the thin film is formed from the bulk polymer. Third, the resulting film must be cured (i.e., post-treated).[15] In iCVD, polymerization proceeds in the course of thin film growth and, typically, no curing is required post-deposition, as no solvents are employed. Thus, the number of processing steps that are required is reduced significantly. The basics and underlying concepts of iCVD, as a state-of-the-art synthesis method for polymer thin films, are introduced in the following sections.

II.2.3.1 Experimental Setup

As iCVD is designed to run on chemicals delivered from the vapor phase, a specific setup of a (vacuum) reaction chamber is necessary. A schematic of such a reactor is depicted in Figure II.2-5.

Typical iCVD reactors are cylindrically or cuboid-shaped, commonly being wider than tall[*] (few liters in volume). The bottom of the reactor serves as a sample stage, whereon the substrates are placed for deposition (typically, held at 10-50 °C). In a paradigmatic iCVD process, the employed monomers are liquid chemicals that need to be heated in individual (glass) jars to facilitate evaporation (typically, to 50-90 °C). The monomer molecules enter the vacuum chamber through heated gas (mixing) lines. Flow control valves (e.g., needle valves) are used to adjust the desired flow rates. Usually, also the initiators are liquid substances; most of them are volatile enough in the applied reaction conditions to ensure sufficient flow into the reaction chamber without heating. In the majority of iCVD processes reported, thermal energy is employed to produce initiator radicals in the reactor.[10] Therefore, a (metallic) filament array that can be resistively heated (typically to filament temperatures, T_{fil}, of 200-350 °C) is suspended within the vacuum chamber a few cm above the growth surface. The pressure is, usually, controlled by a

---

[*] also referred to as pancake shaped

feedback-loop between a pressure sensor, a downstream throttle valve and a pump system (e.g., roughening pump, filters); the working pressure is held constant during deposition (typically, at a value in the range 100-400 mTorr).
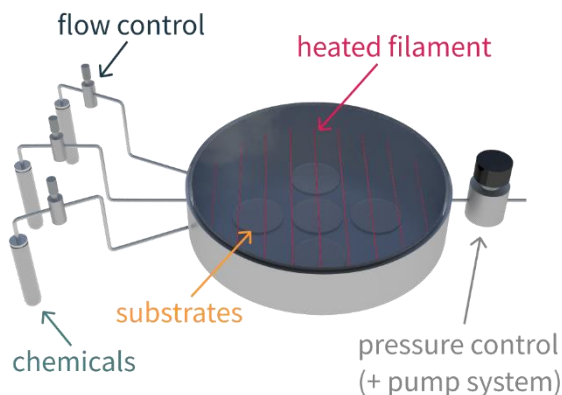

Figure II.2-5. Schematic of a typical iCVD reactor (key parts are labelled).

II.2.3.2 Method

The technique of iCVD is used for the deposition of polymer thin films from chemicals delivered in the vapor phase in the scheme of radical chain polymerization. As such, iCVD is compatible with numerous vinyl monomer precursors (e.g., acrylates, styrenes, methacrylates, acrylamides, etc.).[15] Initiator and monomer(s) are introduced into the reaction chamber in the vapor phase. Commonly, tert-butyl peroxide (TBPO) is used as the initiator. In the vicinity of the heated filament wires, the initiator molecules entering the reactor are thermally decomposed into (initiator) radicals. This is a selective process, as the monomer precursors employed are structurally stable at the temperatures the filament is heated to (cf. above).[16] The initiator radicals diffuse through the gas phase, eventually, adsorb at (substrate) surfaces and carry out surface reactions with other species being adsorbed there. Volatile products need to desorb again and diffuse away.[15] The monomer molecules are also delivered to the reactor in the vapor phase at a sufficient flow rate, so that an equilibrium amount is adsorbed on the (substrate) surface at all times during synthesis.[8] There, the steps of chain initiation, propagation and termination can proceed as surface reactions in the manner described in section II.2.2.1, "analogous to liquid-phase free radical polymerization"; they are "identical to the […] steps in the bulk phase, albeit on a surface" (p. 3696).[8] A typical iCVD process involves the initiator radicals attacking the unsaturated vinyl bond(s) in the adsorbed monomer molecules and, thus, initiating polymerization. The resulting chain-initiating radical is then available for the addition of a monomer molecule, consequently, forming a longer chain radical. By iteratively repeating this reaction, the polymer chains grow over time on available (substrate) surfaces, making for the formation of a

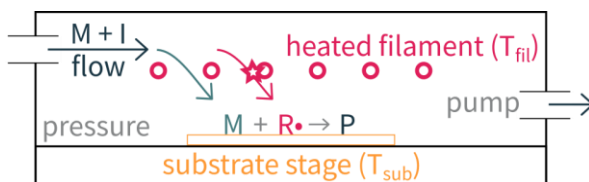uniform and conformal (cf. below) polymer thin film. The described process is sketched in Figure II.2-6.

Figure II.2-6. Schematic of the steps within an iCVD process leading to the formation of a polymer P thin film; monomer M, initiator I, initiator radical R•.

A Kinetic Model for the iCVD Process

A kinetic model for iCVD polymerization has been developed by Lau & Gleason[8] on the basis of the well-established model introduced in section II.2.2.1, applying to radical chain polymerization in general. It assumes that the initiator is decomposed into radicals at T_{fil}, whereas the rest of the polymerization reactions proceed at T_{sub}. Based on a model system of depositions of poly(butyl acrylate), this kinetic model presents an exceptional quantitative description of the iCVD process (e.g., growth rate, molar mass of the resulting polymer).

According to the model,[8] the synthesis of a polymer thin film by iCVD includes three specific types of processes: (i) reactions in the vapor phase, (ii) gas-to-surface processes and (iii) surface reactions. In the gas phase (i), the initiator molecules decompose into radicals in the vicinity of the heated filament at a rate described by the rate constant k_d (cf. Equation II.2-3). Monomer molecules and initiator radicals adsorb on the surface (ii) at rates represented by the rate constants $k_{ad,M}$ and $k_{ad,R•}$, respectively. On the surface (iii), reactions of initiation, propagation and termination of the polymer chains proceed as introduced in section II.2.2.1 (cf. Equations II.2-4, II.2-5 and II.2-6 with the corresponding rate constants k_i, k_p and k_t, respectively). Additionally, the model includes the possibility of two further surface reactions: termination events occurring via initiator radicals and recombination of initiator radicals, represented by the rate constants k_t' and k_t'', respectively. The model also includes an estimation about how the macromolecular chains are terminated (cf. b in Equation II.2-13). A further parameter (r) is introduced to represent the rate of initiator radicals adsorbed that eventually participate in the surface reactions described above. In a later study, the sticking probability of initiator radicals was reported to vary with the concentration of adsorbed monomer molecules; these results indicate that the initiation step in iCVD proceeds via reactions of vapor-phase initiator radicals with monomer molecules adsorbed on the surface.[17] Such surface

reactions are known as occurring by the *Eley-Rideal* mechanism.[*] This be-havior is especially relevant for understanding specific features of the iCVD process (e.g., employing distinct conditions, cf. section II.2.3.3) but does not alter the basic implications of the kinetic model developed by Lau & Gleason.[8]

It was found experimentally that the iCVD process is predominantly adsorp-tion-limited and, thus, primarily surface-driven, where deposition rate and molar mass of the resulting polymer depend on the concentration of mono-mer molecules adsorbed at the surface; the kinetics of the process were shown to strongly depend on the substrate temperature.[8,9] These findings made it possible to also limit the parameters in the mathematical model for iCVD reactions to the ones describing surface reactions. Considering all the (sub)processes occurring on the (substrate) surface described above, the model's sensitivity to variations in the individual rate constants/parameters could be ranked as follows: $k_p > k_i \sim k_t' \sim r > k_t > b > k_t''$.[8] The model is, thus, in accordance with the fact that the rate of propagation can be viewed as "the fundamental parameter in iCVD kinetics" (p. 3701) determining both rate of polymerization and molar mass of the resulting polymer; thus, monomers need to exhibit high kinetic coefficients of propagation to allow for appre-ciable deposition rates.[8] Interestingly, the ranking also sheds light on the im-portance of primary radical termination and the concentration of initiator radicals adsorbed, eventually taking part in surface reactions. Ultimately, the model relates the polymerization rate and the kinetic chain length to the surface concentration of monomer molecules. Thus, mathematically as well as experimentally, the iCVD process can, essentially, be broken down to one single, central aspect: the amount(s) of monomer molecules adsorbed at the (substrate) surface. This parameter can be described by the ratio of the (re-spective) monomer's vapor pressure to its saturation vapor pressure (p_M/p_{sat}) in the applied conditions (pressure and T_{sub}) in the framework of the *Brunauer-Emmett-Teller (BET)* theory.[18] Experimentally, p_M can be de-rived from the ratio of the monomer's (volumetric) flow rate Q_M to the total flow rate into the reactor Q_{tot} (including, e.g., other monomers, carrier gases) and the applied (working) pressure p_w as

$$p_M = \frac{Q_M}{Q_{tot}} p_w. \tag{II.2-14}$$

The saturation vapor pressure p_{sat} of a monomer is temperature-dependent and is, commonly, estimated via the *Clausius-Clapeyron* equation and two arbitrary pairs of vapor pressure and temperature (p_1, T_1 and p_2, T_2) known for the respective monomer (literature data of, e.g., the boiling point, i.e.,

---

[*] *Eley-Rideal* mechanism: an adsorbed species reacts with a vapor-phase species.

where the vapor pressure equals ambient pressure, and the vapor pressure at room temperature, i.e., at 25 °C). At T_{sub}, p_{sat} reads

$$p_{sat} = p_1 e^{\frac{\ln(p_2/p_1)}{1/T_1 - 1/T_2}\left(\frac{1}{T_1} - \frac{1}{T_{sub}}\right)}. \tag{II.2-15}$$

Since first introduced by Lau & Gleason in the fundamental kinetic model and experimental study of iCVD polymerizations,[8,9] the parameter p_M/p_{sat} is widely used to assess the volume and, consequently, the concentration of monomer molecules adsorbed on the (substrate) surface. Furthermore, in copolymerization reactions (employing/adsorbing multiple monomers), the p_M/p_{sat} values can be utilized to assess the surface fractions of the respective monomers f_i. In that way, the composition of the resulting copolymer can be estimated (as done in the scientific contributions presented in chapter III, cf. III.1.5, III.2.5), with i summing over all the present components, as

$$f_i = \frac{(p_M/p_{sat})_i}{\sum_i (p_M/p_{sat})_i}. \tag{II.2-16}$$

Overall, the model and experimental framework of the iCVD method introduced by Lau & Gleason[8,9] yields that a lower p_{sat} (i.e., more adsorbing monomer molecules) corresponds to a faster deposition rate. Moreover, there is a need to sufficiently deliver monomer molecules into the reactor (i.e., vapor pressure must be high enough). In addition to the choice of the monomer, typically, lower substrate temperatures enhance adsorption of the monomer, resulting in an increased deposition rate. To avoid an excess of monomer molecules to arrive at the surface (e.g., condensation leading to nonuniform depositions), T_{sub} should be sufficiently high (so that $p_M/p_{sat}<1$). Accordingly, Lau & Gleason recommended to employ deposition conditions (p_M/p_{sat}) that correspond to 1-3 monolayers of monomer molecules being present at the surface (in case of ethyl acrylate, i.e., $0.4<p_M/p_{sat}<0.7$).[9]

II.2.3.3 Specifics of iCVD

Due to certain specifics of the iCVD process, a number of interesting features are attainable in the resulting polymer thin films. How these prospects are linked to the deposition method and the reaction conditions is described in the following.

Possible Chemistries
Up to date, numerous chemistries were employed to successfully deposit thin films of dozens of distinct (free radical) homopolymers, random copolymers and alternating copolymers by iCVD. As described above, the process allows for the deposition of polymers from numerous precursors (typically, vinyl monomers). A list of chemistries that were successfully employed in iCVD and reported in scientific journals with the corresponding references (data and status as of 2015) can be found in the book 'CVD Polymers' edited

by Gleason;[19] polymers synthesized by iCVD include fluorocarbons, organo-silicons, acrylates, methacrylates, styrenes, vinyls, with the further possibilities of preparing cross-linked systems and ring-opened polymers.[16] Copolymerization with monomers exhibiting multiple vinyl groups was demonstrated to present a platform for controllably cross-linking films in order to make them resistant to solvent damage.[20]

Uniformity and Conformality

The iCVD process has been shown to readily yield a method for the deposition of high-quality, pin-hole free polymer thin films over large areas (e.g., as shown by Chen et al.[21]). A smart but simple reactor design, ensuring uniform gas flow, allows for depositions exhibiting excellent *uniformity* in film thickness.[22] Additionally, *conformality* denotes the uniform thickness of a film deposited over (complex) contours of geometric features.[15] Such uniform/conformal coatings over micro- and/or nano-scale 3D-structures are essential in various kinds of applications. Setups, where uniformity and conformality are required, include integrated circuitry, membranes, microfluidic devices and micro-electromechanical systems (MEMS).[23]

In iCVD, the specific delivery of chemicals in the vapor phase allows for the molecules to diffuse "into very small geometries such as pores, trenches, and even the spaces between woven fibers" (p. 87) during polymer synthesis.[23] As mentioned above, an inverse relationship between the sticking probability of the initiator radicals to the concentration of adsorbed monomer molecules was reported; correspondingly, improved step coverage and, thus, conformality were observed when employing low p_M/p_{sat} values, whereas excellent conformality was reported (on trenches exhibiting aspect ratios of up to 8.4) for various different polymer thin films.[17,24] In addition to trenches, particles and wires of different sizes (nm-μm) were coated successfully and conformally by iCVD with polymer films exhibiting various functionalities (e.g., as reported by Lau & Gleason[25,26]).

Furthermore, this shows that, in addition to the commonly applied deposition conditions recommended above, the processing parameters can be tailored so that other aspects of the polymerization process (e.g., initiation, termination) become more relevant and, in extremis, even rate-limiting. This yields a further possibility of altering the process in order to achieve specific material properties that are not accessible by other means.

Functional Polymers/Groups

Functional polymer films are highly desirable in various steps of product development. As discussed above, the iCVD process yields an intriguing platform for the synthesis of a plethora of possible chemistries. Besides depositing films that can be functionalized post-deposition through facile, one-step modification reactions (e.g., through simple nucleophilic

addition/substitution reactions), functional moieties can be directly incorporated into the polymer's structure via the monomer(s) that are fed into the reactor for polymerization.[27] As, mostly, vinyl monomers are employed in iCVD, the functionality of the resulting polymer thin films arises, chiefly, from specific pendant functional groups. The mild processing conditions (e.g., low T_{sub}, no solvent) enable such groups, including epoxy, amine or carboxylic acid moieties, to be fully retained in the iCVD films.[15] In addition to the choice and design of specific monomers, the precise control over the deposition conditions allows for versatile tailoring and tuning of the resulting polymer films' properties. Thus, as film composition and structure also govern the physicochemical behavior of functional polymers, iCVD yields an excellent platform for the synthesis of functional polymer thin films for device fabrication.[27] Specific chemical functionalities of iCVD films were demonstrated to be useful for subsequent surface attachment of, e.g., fluorescent dyes,[28] bioactive molecules[20] and inorganic nanoparticles.[29] Moreover, properties such as wettability,[30] adhesion,[31] biocompatibility,[32] functional cell adhesion[33] and anti-biofouling[34] were shown to be systematically controllable via the synthesis of polymer thin films by iCVD. This tunability allows for the films' applicability to setups for, e.g., biosensing,[35] controlled drug delivery,[36,37] implantable medical devices,[38] etc. The basis for most of these applications are functional units that behave in a certain way when exposed to distinct environmental conditions. As described in section II.1.1, stimuli-responsive hydrogels are among the polymers applicable to such smart structures. In a thin film setup (i.e., as synthesized by iCVD), stimuli-responsive swelling is observable as a change in film thickness in response to a change in temperature, external field (magnetic/electric) or pH.[22] Thus, these layers transduce physical, chemical or biological events into mechanical, electrical or optical signals. Several such hydrogel thin films are attainable via iCVD. Our group also contributed a number of articles reporting on the development and applicability of such films as light-responsive materials,[39] in drug encapsulations,[40] drug delivery[41] and sensing.[42]

Miscellaneous

The iCVD method was demonstrated to be successfully up-scalable to batch reactors (more than 100-fold larger than lab systems)[22] or even to roll-to-roll processing.[43] Furthermore, the mild processing conditions (e.g., low T_{sub}, no solvent) allow for the coating of delicate or flexible substrates like plastics, papers, textiles, and membranes; as an all-dry synthesis technique, iCVD also shows the potential of reducing solvent-related environmental, health and safety implications as well as costs for solvent disposal.[22]

II.2.4 References

(1)   Carothers, W. H. Polymerization. *Chem. Rev.* **1931**, *8* (3), 353–426. https://doi.org/10.1021/cr60031a001.

(2)   Mita, I.; Stepto, R. F. T.; Suter, U. W. Basic Classification and Definitions of Polymerization Reactions (IUPAC Recommendations 1994). *Pure Appl. Chem.* **1994**, *66* (12), 2483–2486. https://doi.org/10.1351/pac199466122483.

(3)   Penczek, S.; Moad, G. Glossary of Terms Related to Kinetics, Thermodynamics, and Mechanisms of Polymerization (IUPAC Recommendations 2008). *Pure Appl. Chem.* **2008**, *80* (10), 2163–2193. https://doi.org/10.1351/pac200880102163.

(4)   Saldívar-Guerra, E.; Vivaldo-Lima, E. Introduction to Polymers and Polymer Types. In *Handbook of Polymer Synthesis, Characterization, and Processing*; John Wiley & Sons, Inc.: Hoboken, NJ, USA, 2013; pp 1–14. https://doi.org/10.1002/9781118480793.ch1.

(5)   Odian, G. Introduction. In *Principles of Polymerization*; John Wiley & Sons, Inc.: Hoboken, NJ, USA, 2004; pp 1–38. https://doi.org/10.1002/047147875X.ch1.

(6)   Geyer, R.; Jambeck, J. R.; Law, K. L. Production, Use, and Fate of All Plastics Ever Made. *Sci. Adv.* **2017**, *3* (7), e1700782. https://doi.org/10.1126/sciadv.1700782.

(7)   Odian, G. Radical Chain Polymerization. In *Principles of Polymerization*; John Wiley & Sons, Inc.: Hoboken, NJ, USA, 2004; pp 198–349. https://doi.org/10.1002/047147875X.ch3.

(8)   Lau, K. K. S.; Gleason, K. K. Initiated Chemical Vapor Deposition (ICVD) of Poly(Alkyl Acrylates): A Kinetic Model. *Macromolecules* **2006**, *39* (10), 3695–3703. https://doi.org/10.1021/ma0601621.

(9)   Lau, K. K. S.; Gleason, K. K. Initiated Chemical Vapor Deposition (ICVD) of Poly(Alkyl Acrylates): An Experimental Study. *Macromolecules* **2006**, *39* (10), 3688–3694. https://doi.org/10.1021/ma0601619.

(10)   Tenhaeff, W. E.; Gleason, K. K. Initiated and Oxidative Chemical Vapor Deposition of Polymeric Thin Films: ICVD and OCVD. *Adv. Funct. Mater.* **2008**, *18* (7), 979–992. https://doi.org/10.1002/adfm.200701479.

(11)   Wang, J.-S.; Matyjaszewski, K. Controlled/"living" Radical Polymerization. Atom Transfer Radical Polymerization in the Presence of Transition-Metal Complexes. *J. Am. Chem. Soc.* **1995**, *117* (20), 5614–5615. https://doi.org/10.1021/ja00125a035.

(12)   Kato, M.; Kamigaito, M.; Sawamoto, M.; Higashimura, T. Polymerization of Methyl Methacrylate with the Carbon Tetrachloride/Dichlorotris-(Triphenylphosphine)Ruthenium(II)/Methylaluminum Bis(2,6-Di-Tert-Butylphenoxide) Initiating System: Possibility of Living Radical Polymerization. *Macromolecules* **1995**, *28* (5), 1721–1723. https://doi.org/10.1021/ma00109a056.

(13)   Chiefari, J.; Chong, Y. K. (Bill); Ercole, F.; Krstina, J.; Jeffery, J.; Le, T. P. T.; Mayadunne, R. T. A.; Meijs, G. F.; Moad, C. L.; Moad, G.; Rizzardo, E.; Thang, S. H. Living Free-Radical Polymerization by Reversible Addition−Fragmentation Chain Transfer: The RAFT Process. *Macromolecules* **1998**, *31* (16), 5559–5562. https://doi.org/10.1021/ma9804951.

(14)   Guerrero-Santos, R.; Saldívar-Guerra, E.; Bonilla-Cruz, J. Free Radical Polymerization. In *Handbook of Polymer Synthesis, Characterization, and Processing*; John Wiley & Sons, Inc.: Hoboken, NJ, USA, 2013; pp 65–83. https://doi.org/10.1002/9781118480793.ch4.

(15)   Gleason, K. K. Overview of Chemically Vapor Deposited (CVD) Polymers. In *CVD Polymers*; Wiley-VCH Verlag GmbH & Co. KGaA: Weinheim, Germany, 2015; pp 1–11.

https://doi.org/10.1002/9783527690275.ch1.

(16) Lau, K. K. S. Growth Mechanism, Kinetics, and Molecular Weight. In *CVD Polymers*; Wiley-VCH Verlag GmbH & Co. KGaA: Weinheim, Germany, 2015; pp 13–44. https://doi.org/10.1002/9783527690275.ch2.

(17) Baxamusa, S. H.; Gleason, K. K. Thin Polymer Films with High Step Coverage in Microtrenches by Initiated CVD. *Chem. Vap. Depos.* **2008**, *14* (9–10), 313–318. https://doi.org/10.1002/cvde.200806713.

(18) Brunauer, S.; Emmett, P. H.; Teller, E. Adsorption of Gases in Multimolecular Layers. *J. Am. Chem. Soc.* **1938**, *60* (2), 309–319. https://doi.org/10.1021/ja01269a023.

(19) *CVD Polymers*; Gleason, K. K., Ed.; Wiley-VCH Verlag GmbH & Co. KGaA: Weinheim, Germany, 2015. https://doi.org/10.1002/9783527690275.

(20) O'Shaughnessy, W. S.; Marí-Buyé, N.; Borrós, S.; Gleason, K. K. Initiated Chemical Vapor Deposition of a Surface-Modifiable Copolymer for Covalent Attachment and Patterning of Nucleophilic Ligands. *Macromol. Rapid Commun.* **2007**, *28* (18–19), 1877–1882. https://doi.org/10.1002/marc.200700333.

(21) Chen, N.; Reeja-Jayan, B.; Liu, A.; Lau, J.; Dunn, B.; Gleason, K. K. ICVD Cyclic Polysiloxane and Polysilazane as Nanoscale Thin-Film Electrolyte: Synthesis and Properties. *Macromol. Rapid Commun.* **2016**, *37* (5), 446–452. https://doi.org/10.1002/marc.201500649.

(22) Asatekin, A.; Barr, M. C.; Baxamusa, S. H.; Lau, K. K. S.; Tenhaeff, W.; Xu, J.; Gleason, K. K. Designing Polymer Surfaces via Vapor Deposition. *Mater. Today* **2010**, *13* (5), 26–33. https://doi.org/10.1016/S1369-7021(10)70081-X.

(23) Baxamusa, S. Conformal Polymer CVD. In *CVD Polymers*; Wiley-VCH Verlag GmbH & Co. KGaA: Weinheim, Germany, 2015; pp 87–109. https://doi.org/10.1002/9783527690275.ch5.

(24) Ozaydin-Ince, G.; Gleason, K. K. Tunable Conformality of Polymer Coatings on High Aspect Ratio Features. *Chem. Vap. Depos.* **2010**, *16* (1–3), 100–105. https://doi.org/10.1002/cvde.200906821.

(25) Lau, K. K. S.; Gleason, K. K. Particle Surface Design Using an All-Dry Encapsulation Method. *Adv. Mater.* **2006**, *18* (15), 1972–1977. https://doi.org/10.1002/adma.200600896.

(26) Lau, K. K. S.; Gleason, K. K. All-Dry Synthesis and Coating of Methacrylic Acid Copolymers for Controlled Release. *Macromol. Biosci.* **2007**, *7* (4), 429–434. https://doi.org/10.1002/mabi.200700017.

(27) Tenhaeff, W. E. Reactive and Stimuli-Responsive Polymer Thin Films. In *CVD Polymers*; Gleason, K. K., Ed.; Wiley-VCH Verlag GmbH & Co. KGaA: Weinheim, Germany, 2015; pp 171–198. https://doi.org/10.1002/9783527690275.ch8.

(28) Im, S. G.; Bong, K. W.; Kim, B.-S.; Baxamusa, S. H.; Hammond, P. T.; Doyle, P. S.; Gleason, K. K. Patterning Nanodomains with Orthogonal Functionalities: Solventless Synthesis of Self-Sorting Surfaces. *J. Am. Chem. Soc.* **2008**, *130* (44), 14424–14425. https://doi.org/10.1021/ja806030z.

(29) Vaddiraju, S.; Seneca, K.; Gleason, K. K. Novel Strategies for the Deposition of ⎯COOH Functionalized Conducting Copolymer Films and the Assembly of Inorganic Nanoparticles on Conducting Polymer Platforms. *Adv. Funct. Mater.* **2008**, *18* (13), 1929–1938. https://doi.org/10.1002/adfm.200800196.

(30) Ma, M.; Mao, Y.; Gupta, M.; Gleason, K. K.; Rutledge, G. C. Superhydrophobic Fabrics Produced by Electrospinning and Chemical Vapor Deposition. *Macromolecules* **2005**, *38* (23), 9742–9748. https://doi.org/10.1021/ma0511189.

(31) Im, S. G.; Bong, K. W.; Lee, C.-H.; Doyle, P. S.; Gleason, K. K. A Conformal Nano-Adhesive via Initiated Chemical Vapor Deposition for Microfluidic Devices. *Lab Chip* **2009**, *9* (3), 411–416. https://doi.org/10.1039/B812121D.

(32) Achyuta, A. K. H.; Polikov, V. S.; White, A. J.; Lewis, H. G. P.; Murthy, S. K. Biocompatibility Assessment of Insulating Silicone Polymer Coatings Using an in Vitro Glial Scar Assay. *Macromol. Biosci.* **2010**, *10* (8), 872–880. https://doi.org/10.1002/mabi.200900451.

(33) Bose, R. K.; Lau, K. K. S. Initiated CVD of Poly(2-Hydroxyethyl Methacrylate) Hydrogels: Synthesis, Characterization and In-Vitro Biocompatibility. *Chem. Vap. Depos.* **2009**, *15* (4–6), 150–155. https://doi.org/10.1002/cvde.200806748.

(34) Yang, R.; Jang, H.; Stocker, R.; Gleason, K. K. Synergistic Prevention of Biofouling in Seawater Desalination by Zwitterionic Surfaces and Low-Level Chlorination. *Adv. Mater.* **2014**, *26* (11), 1711–1718. https://doi.org/10.1002/adma.201304386.

(35) Montero, L.; Gabriel, G.; Guimerà, A.; Villa, R.; Gleason, K. K.; Borrós, S. Increasing Biosensor Response through Hydrogel Thin Film Deposition: Influence of Hydrogel Thickness. *Vacuum* **2012**, *86* (12), 2102–2104. https://doi.org/10.1016/j.vacuum.2012.06.002.

(36) McInnes, S. J. P.; Szili, E. J.; Al-Bataineh, S. A.; Xu, J.; Alf, M. E.; Gleason, K. K.; Short, R. D.; Voelcker, N. H. Combination of ICVD and Porous Silicon for the Development of a Controlled Drug Delivery System. *ACS Appl. Mater. Interfaces* **2012**, *4* (7), 3566–3574. https://doi.org/10.1021/am300621k.

(37) McInnes, S. J. P.; Szili, E. J.; Al-Bataineh, S. A.; Vasani, R. B.; Xu, J.; Alf, M. E.; Gleason, K. K.; Short, R. D.; Voelcker, N. H. Fabrication and Characterization of a Porous Silicon Drug Delivery System with an Initiated Chemical Vapor Deposition Temperature-Responsive Coating. *Langmuir* **2016**, *32* (1), 301–308. https://doi.org/10.1021/acs.langmuir.5b03794.

(38) Park, S. W.; Lee, D.; Lee, H. R.; Moon, H.-J.; Lee, B. R.; Ko, W.-K.; Song, S.-J.; Lee, S. J.; Shin, K.; Jang, W.; Yi, J.-K.; Im, S. G.; Kwon, I. K. Generation of Functionalized Polymer Nanolayer on Implant Surface via Initiated Chemical Vapor Deposition (ICVD). *J. Colloid Interface Sci.* **2015**, *439*, 34–41. https://doi.org/10.1016/j.jcis.2014.10.018.

(39) Unger, K.; Salzmann, P.; Masciullo, C.; Cecchini, M.; Koller, G.; Coclite, A. M. Novel Light-Responsive Biocompatible Hydrogels Produced by Initiated Chemical Vapor Deposition. *ACS Appl. Mater. Interfaces* **2017**, *9* (20), 17408–17416. https://doi.org/10.1021/acsami.7b01527.

(40) Christian, P.; Ehmann, H. M. A.; Coclite, A. M.; Werzer, O. Polymer Encapsulation of an Amorphous Pharmaceutical by Initiated Chemical Vapor Deposition for Enhanced Stability. *ACS Appl. Mater. Interfaces* **2016**, *8* (33), 21177–21184. https://doi.org/10.1021/acsami.6b06015.

(41) Christian, P.; Tumphart, S.; Ehmann, H. M. A.; Riegler, H.; Coclite, A. M.; Werzer, O. Controlling Indomethacin Release through Vapor-Phase Deposited Hydrogel Films by Adjusting the Cross-Linker Density. *Sci. Rep.* **2018**, *8* (1), 7134. https://doi.org/10.1038/s41598-018-24238-w.

(42) Buchberger, A.; Peterka, S.; Coclite, A.; Bergmann, A. Fast Optical Humidity Sensor Based on Hydrogel Thin Film Expansion for Harsh Environment. *Sensors* **2019**, *19* (5), 999. https://doi.org/10.3390/s19050999.

(43) Gupta, M.; Gleason, K. K. Large-Scale Initiated Chemical Vapor Deposition of Poly(Glycidyl Methacrylate) Thin Films. *Thin Solid Films* **2006**, *515* (4), 1579–1584. https://doi.org/10.1016/j.tsf.2006.05.021.

II.3 Analysis of Polymer Thin Films

Due to the wide variety of structures and shapes polymers can adopt and exist in, there are similarly many techniques with which this class of materials can be investigated and analyzed. This section provides a short introduction to the experimental techniques mainly employed within the work summarized in this thesis. The description evolves around the application of these methods to the specific case of (thermoresponsive) hydrogel thin films. First, a short introduction to the technique of *Fourier-transform infrared spectroscopy (FTIR)* for the analysis of the (macro)molecular nature of the respective samples will be given. Second, this section includes a more extensive description of the method of *spectroscopic ellipsometry (SE)*. This experimental technique allows for analyzing the optical properties as well as precisely determining and monitoring the thickness of (polymeric) thin films. Consequently, spectroscopic ellipsometry was also the method that was primarily employed within the framework of this thesis. The following discussion will be, mostly, limited to the aspects of the two techniques relevant to the work presented herein.

II.3.1 Molecular Analysis by FTIR

Infrared spectroscopy is a technique in which electromagnetic radiation exhibiting a wavelength/energy in the infrared (IR) part of the spectrum is shone onto a sample; upon irradiation, certain parts of this light are reflected, absorbed or transmitted by the specimen (cf. Figure II.3-1). Consequently, an infrared spectrum measures the response (in absorbance or transmittance) of a system to IR radiation as a function of energy. In dispersive spectrometry, monochromatic light is used to examine the response to every single wavelength in the spectrum probed individually. On the contrary, in Fourier-transform infrared spectroscopy (FTIR), the infrared light used to shine onto the sample is polychromatic, usually consisting of a broad spectrum of wavelengths (in the IR). The distribution (in intensity) of this radiation is, commonly, regulated by a Michelson interferometer containing a moving mirror, whose position is precisely controllable. The abovementioned response of the sample is, thus, measured as a function of the mirror position (raw data). Knowing the relation between the mirror position and the distribution of intensities, subsequently, the raw data needs to be converted into the sample's spectrum by applying a Fourier transform.

Infrared radiation shining onto a specimen can induce molecular vibrations and rotations in the sample material, i.e., arbitrarily complex (repetitive) motions of atoms with respect to one another in a molecular system. These molecular vibrations and rotations can be understood as transitions between

(quantized) energy states (cf. Figure II.3-1). Thus, we can define corresponding vibrational and rotational frequencies, at which such molecular motions are induced. These frequencies are, usually, expressed in the units of wavenumber, i.e., the number of waves per unit length (commonly, cm⁻¹). The applied energy of the IR radiation determines what type of transitions the atoms in the material will undergo. Usually, energies resembling radiation in the mid-infrared spectrum (4000-400 cm⁻¹) are employed; such frequencies correspond to the energy difference for transitions between the ground state and the first excited state of most molecular vibrations.[1] In turn, the IR spectrum yields information about the molecular structure of the sample.

To specifically investigate thin films with FTIR, several measurement modes are possible. The simplest one (see Figure II.3-1) is to deposit the thin film to be characterized onto a substrate that is transparent to the IR radiation employed (e.g., silicon)[2]. The recorded sample spectrum (i.e., thin film + substrate in transmission) can, subsequently, be normalized by a spectrum measured accordingly on the pristine substrate.
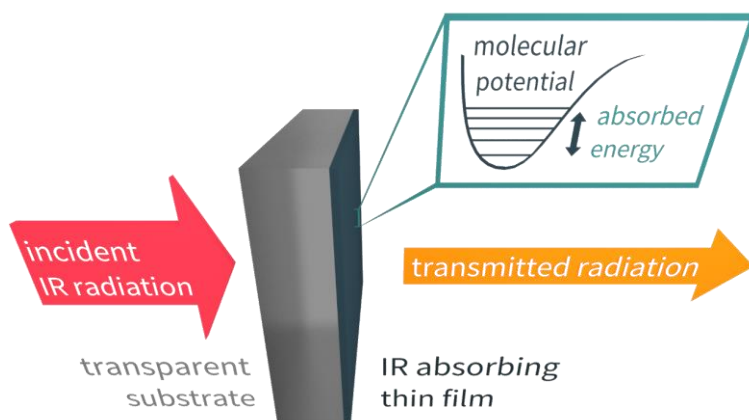

Figure II.3-1. Schematic of an FTIR measurement of a thin film on a transparent substrate in transmission, absorbing infrared (IR) radiation of specific energies due to molecular vibrations.

A further possibility to examine thin films with FTIR is to record spectra in a mode termed attenuated total reflection (ATR). In ATR, the sample is placed in (good) contact with a surface of a medium (e.g., a crystal), onto which the incident IR beam is shone at an angle below its critical angle of total reflection. Upon internal reflection, an evanescent wave forms, penetrating a few dozens of nm to several µm into the sample. This wave is altered by the abovementioned molecular vibrations and rotations, through which the IR response of the specimen is measured.[3] In addition to its applicability to thin films (low penetration depth), ATR enables samples to be examined with little preparation being necessary due to the simplicity of the measurement principle.[3]

The molecular vibrations and rotations resulting from IR irradiation of a sample yield a spectrum consisting of absorption peaks at distinct energies (wavenumbers). The energy bands these peaks are observed in can, thus, be assigned to certain arrangements of atoms (e.g., groups, bonds) within the molecular structure of a sample being excited in specific manners (modes). In many such modes, few atoms move heavily, while most of the molecule remains (almost) quiescent. For these modes, the (observed) energy is characteristic of the functional group or, more specifically, even the bond the movement is localized at. Their position in energy is practically independent of the constitution of the rest of the molecule. Therefore, the observation of certain such bands in an FTIR spectrum can be indicative of specific functional groups or bonds being present in the molecular structure of the sample material.[1] Typically, these bands occur in the spectral region above ~1400 cm^{-1}, for which correlation charts can be used to list the assignment of distinct infrared absorptions to specific functional groups.[4] On the contrary, for other bands, the (observed) frequency can also be related to the motion of a few atoms within the molecule, but their exact position in energy varies depending on the surrounding atoms or molecular structure. That makes the resulting spectrum more complex but can prove useful for the precise discrimination of individual molecular arrangements in systems containing similar functional groups.[1] Such bands, typically, occur below ~1400 cm^{-1} and show a unique characteristic pattern for each molecule. That is why this part of the spectrum is also referred to as the *fingerprint region*.[4]

The above description already indicates that FTIR is an extremely powerful method with respect to analyzing the complex (macro)molecular structure of polymers and polymer thin films. Besides determining the presence of specific functional units and, thus, functionalities within the polymer, FTIR can also be used, in turn, to identify monomeric units (exhibiting distinct functional groups) within a sample material from the corresponding bands observed in the spectrum. By comparing peak heights/areas of individual spectra, even a quantitative analysis of the composition of polymers can be realized; for instance, a recent article authored by several group colleagues of mine reports on the successful development of a method for the simple and quantitative compositional analysis of copolymer thin films by FTIR.[5]

II.3.2 Spectroscopic Ellipsometry

Spectroscopic ellipsometry (SE) is a powerful optical technique, in which the change in polarization of a light beam, e.g., upon reflection from a sample is measured as a function of wavelength. Commonly, the ultraviolet/visible region of the electromagnetic spectrum[*] is probed.[6] The incident light (typically, linearly polarized) interacts with the sample, causing its polarization state to change. Generally, the reflected light is elliptically polarized, thus, yielding the name of the technique. From that change in polarization, information on the sample's thickness, roughness or other optical properties can be deduced.

II.3.2.1 Optical Basics and Measurement Principle

In SE, the reflection of linearly polarized light from a sample is examined. Correspondingly, the measurement principle relies on the description of different polarization states of light and their interaction with (sample) matter.

According to the Maxwell's equations, light is an electromagnetic wave, whose propagation (in time t and space) can either be represented by its electric field $\boldsymbol{E}$ or the perpendicular magnetic induction component $\boldsymbol{B}$. In general, a time-varying $\boldsymbol{E}$ induces $\boldsymbol{B}$ (Ampère's law) and vice versa (Faraday's law of induction). The direction of propagation is perpendicular to both $\boldsymbol{E}$ and $\boldsymbol{B}$, whereas the speed of light is independent of the wavelength, $c_0 = 2.99792\times10^8$ m/s (in vacuum). Due to these strict relationships, in most mathematical treatments, it suffices to only use one component (e.g., E). In such a simple model, light can be represented by a one-dimensional wave of E travelling in z-direction as

$$E = E_0 \exp[i(\omega t - Kz + \delta)], \qquad \text{(II.3-1a)}$$
$$\text{with } K = 2\pi n/\lambda. \qquad \text{(II.3-1b)}$$

Herein, E_0 denotes the wave amplitude, i the complex unit, ω the angular frequency, K the propagation number with wavelength λ and refractive index n (introduced below); δ represents a phase shift useful to interpret polarization and interference effects (cf. below). The above model can be used to describe light within a certain medium. At an interface, however, parts get reflected[†] and others will be transmitted into the second material. In general, light interacts with matter. Various phenomena can occur that are

---

[*] IR radiation is also widely used to investigate different aspects/gather complementary information (e.g., on phonons) to the one gained by SE as described herein.[6]
[†] *Law of reflection:* surface normal, incident and reflected beam all lie in the same plane; angle of incidence and reflection are equal (relative to the surface normal).

relevant to the measurement principle of SE, the most important of which are described in the following.

Refraction

The value of c_0 given above represents the speed of light in vacuum. When light moves into a different medium, the speed of wave propagation changes according to the material of this object. This change can, classically, be represented by the refractive index n as

$$n = c_0/c, \tag{II.3-2}$$

where c denotes the speed of light in the respective material. In air, $n = 1.0003$, and, thus, light behaves almost identical as in vacuum ($n = 1$); in other materials, n can be significantly larger (e.g., 3.41 for silicon).[7] In transparent media (i.e., no absorption), light propagation is described by the Equations II.3-1. Thus, the wavelength of light is reduced in materials exhibiting larger n.[*] According to the Huygens' principle, each point on a wave front is itself a source for a (spherical) wave; these sub-waves interact to form, again, the wave front. Consequently, when light moves past an interface between two (different) materials at oblique incidence, the change in speed of light leads to a change in propagation direction (cf. Figure II.3-2). Such behavior is termed *refraction* and can be described by Snell's law as

$$n_i \sin(\vartheta_i) = n_t \sin(\vartheta_t), \tag{II.3-3}$$

where ϑ_i and ϑ_t denote the angles of incidence and transmission, respectively, and n_i and n_t are the refractive indices of the respective materials.

Light Absorption

Many materials are not transparent and, thus, absorb light. To describe such behavior, n can be modified by introducing the extinction coefficient k, describing the light absorption in a certain material. This yields the complex refractive index N as

$$N = n - ik. \tag{II.3-4}$$

Accordingly, n can be replaced by N in Equation II.3-1b and included into the description of a light wave in Equation II.3-1a. While the wavelength (imaginary part of the exponential function) remains unaltered by including k, a (real) exponential factor $\exp(-2\pi k z/\lambda)$ is generated. This can be understood as an exponential decay in wave amplitude along the spatial coordinate of propagation z in absorbing media.

---

[*] As light reflection occurs at interfaces, the wave's amplitude in a medium will also be smaller upon transmission through an interface.

Polarization Effects and Interfaces

When reviewing the behavior of electromagnetic waves at interfaces, the *polarization* of light as the oscillatory direction of its electric field can be highly relevant.[7] To understand the polarization state of light, two waves with electric fields, oscillating in orthogonal directions with respect to one another and the direction of propagation, can be considered. For waves travelling along the z-axis (analogous to Equation II.3-1), their superposition yields

$$\boldsymbol{E}(z,t) = \boldsymbol{E}_x(z,t) + \boldsymbol{E}_y(z,t) \qquad\qquad (\text{II.3-5})$$
$$= \{E_{x0}\exp[i(\omega t - Kz + \delta_x)]\}\boldsymbol{x} + \{E_{y0}\exp[i(\omega t - Kz + \delta_y)]\}\boldsymbol{y},$$

where the indices x and y denote the parameters (analogous to Equation II.3-1) of the corresponding waves oscillating in the x- and y-directions, respectively. Additionally, $\boldsymbol{x}$ and $\boldsymbol{y}$ represent unit vectors in the respective axis directions. Consequently, the polarization state of light can be described by the phase difference $\delta_y - \delta_x$ between the two superimposed (orthogonal) waves. Specific cases can be distinguished, for the sake of comprehensibility, assuming $E_{x0} = E_{y0}$ and $K = 1$. If the phase difference is zero, the orientation of the superimposed $\boldsymbol{E}$ is constant in the x-y plane. The corresponding light is termed linearly polarized. If $\delta_y - \delta_x = 90°$, the resulting $\boldsymbol{E}$ rotates on a circle in the x-y plane and, thus, is called circularly polarized. In an intermediate case (e.g., $\delta_y - \delta_x = 45°$), correspondingly, the light is referred to as being elliptically polarized.

Upon reflection from an interface at oblique incidence, light can be classified as exhibiting p- or s-polarization, when looking at the polarization state relative to the plane of incidence[*]. For p-polarized light, the electric field oscillates within this particular plane, for s-polarized light, perpendicular to it. Analogous to Equation II.3-5 considering x and y-components, an arbitrary polarization state can also be described via s- and p-polarization.

The boundary conditions of electromagnetic waves at interfaces require that the components of the fields (E as well as B) parallel to the surface are continuous upon transmission.[7] Together with applying the relations between E and B, trigonometric considerations, Snell's law (Equation II.3-3) and the law of reflection,[†] the amplitude reflection r and transmission t coefficients for s- and p-polarized light can, thus, be written as

$$r_{\text{p}} = \frac{E_{\text{r,p}}}{E_{\text{i,p}}} = \frac{n_\text{t}\cos(\vartheta_\text{i}) - n_\text{i}\cos(\vartheta_\text{t})}{n_\text{t}\cos(\vartheta_\text{i}) + n_\text{i}\cos(\vartheta_\text{t})}, \qquad\qquad (\text{II.3-6a})$$

$$t_{\text{p}} = \frac{E_{\text{t,p}}}{E_{\text{i,p}}} = \frac{2n_\text{i}\cos(\vartheta_\text{i})}{n_\text{t}\cos(\vartheta_\text{i}) + n_\text{i}\cos(\vartheta_\text{t})}, \qquad\qquad (\text{II.3-6b})$$

---

[*] plane of the incident and reflected beam (perpendicular to the sur-/interface)
[†] A detailed derivation can be found in Fujiwara's 'Spectroscopic Ellipsometry'.[7]

$$r_{\mathrm{s}} = \frac{E_{\mathrm{r,s}}}{E_{\mathrm{i,s}}} = \frac{n_{\mathrm{i}}\cos(\vartheta_{\mathrm{i}}) - n_{\mathrm{t}}\cos(\vartheta_{\mathrm{t}})}{n_{\mathrm{i}}\cos(\vartheta_{\mathrm{i}}) + n_{\mathrm{t}}\cos(\vartheta_{\mathrm{t}})}, \qquad \text{(II.3-6c)}$$

$$t_{\mathrm{s}} = \frac{E_{\mathrm{r,s}}}{E_{\mathrm{i,s}}} = \frac{2n_{\mathrm{i}}\cos(\vartheta_{\mathrm{i}})}{n_{\mathrm{i}}\cos(\vartheta_{\mathrm{i}}) + n_{\mathrm{t}}\cos(\vartheta_{\mathrm{t}})}. \qquad \text{(II.3-6d)}$$

The indices p and s denote the respective polarization; i, r and t represent the incident, reflected and transmitted components/values of the corresponding parameters, respectively. The above relations are also, commonly, known as the Fresnel equations. Overall, these relations describe what parts of the electric field (of light) are transmitted and reflected at an interface, depending on their polarization state. For absorbing media, the refractive indices can, again, be replaced by their complex counterparts (cf. Equation II.3-4).

Optical Interference

As already indicated in the Huygens' principle mentioned above, if multiple light waves overlap locally, they can superimpose, creating different amplitude patterns. This phenomenon is called *optical interference*.

Besides in refraction, such behavior can, specifically, be relevant when the optical response of layered structures (e.g., thin film(s) on a substrate) needs to be interpreted (cf. Figure II.3-2). As described by the Fresnel equations (Equations II.3-6), certain parts of light are reflected at an interface between two materials, others are transmitted. The difference in refractive indices results in refraction, as described above. Beyond that, in a layered structure, a part of the light transmitted through the first interface is reflected at the second one (secondary reflection). Such light waves travel back towards the first interface and are, eventually, transmitted into the medium, in which the incident light strikes the interface. As they travel in the same direction as directly reflected light waves (as follows from Snell's law and the law of reflection), these individual light waves can superimpose (cf. Figure II.3-2). Due to the difference in paths these light waves have travelled, they will exhibit a phase difference with respect to one another (phase shift δ, cf. Equation II.3-1). In turn, the corresponding superimposed wave will exhibit a distinct amplitude, depending on the path difference and, thus, the thickness of the layer d. The phase difference α of a directly reflected to a secondarily reflected beam can be derived from geometrical considerations, K in the medium (Equation II.3-1b) and Snell's law (Equation II.3-3) to yield

$$\alpha = \frac{4\pi d}{\lambda} n_{\mathrm{t}}\cos\vartheta_{\mathrm{t}} = \frac{4\pi d}{\lambda}(n_{\mathrm{t}}^{2} - n_{\mathrm{i}}^{2}\cos\vartheta_{\mathrm{i}})^{1/2}.^{*} \quad \text{(II.3-7)}$$

If the phase difference is 0 (or multiples of 2π), there will be constructive interference resulting in a maximum of the combined (reflected) field; for

---

[*] for details, cf. the respective section in Fujiwara's 'Spectroscopic Ellipsometry'[7]

$\alpha = \pi$ (or odd multiples of it), destructive interference will minimize the (reflected) field. Accordingly, the maxima are given by the condition

$$\frac{\alpha}{2} = \frac{2\pi d}{\lambda} n_t \cos \vartheta_t = m, \quad \text{with } m \in \mathbb{N}. \qquad \text{(II.3-8)}$$

Multiple transmissions and reflections at every interface and the corresponding interferences can add numerous components to the overall reflected and transmitted amplitudes. This can be described as a sum of reflection and transmission coefficients with the corresponding path lengths analogous to the Equations II.3-6 (cf. Figure II.3-2). When considering multilayered structures (>1 layer), the situation gets even more complex but can be treated analogously.

II.3.2.2 The Actual Measurement and (Model) Analysis

In conventional SE, the change in polarization is measured upon reflection of light from a sample at oblique incidence as a function of wavelength (see Figure II.3-2). Usually, a light source and a polarizer are used on the incident side, whereas an analyzer and a detector are employed on the reflection side. To enable fast measurements (e.g., for real-time monitoring of deposition processes), white light is used for illumination and the response is detected by a photodiode array or a high-speed CCD[*] detector combined with a rotating compensator[†].[8]
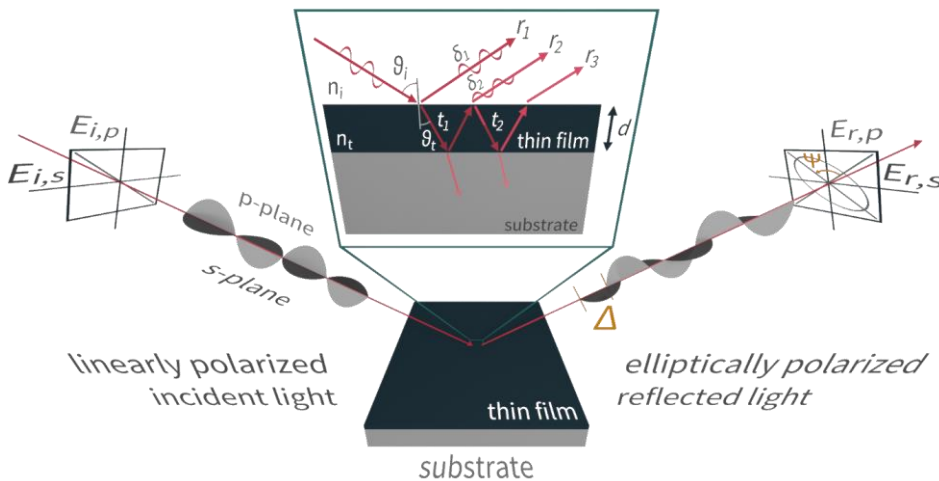
Figure II.3-2. Schematic of an ellipsometry measurement on a specimen (thin film on a substrate); interaction mechanisms of light with the sample sketched as discussed in the text, parameters Ψ and Δ are marked accordingly

---

[*] charge-coupled device, first described by Boyle & Smith in 1970[10]
[†] rotating birefringent element for modulation of the polarization state

The measured change in polarization can be expressed with respect to s- and p-polarization (cf. above). Thus, the signal gained in SE represents the ratio of reflection coefficients of the respectively polarized components

$$\rho = \left(\frac{E_{r,p}}{E_{i,p}}\right) \bigg/ \left(\frac{E_{r,s}}{E_{i,s}}\right) = \frac{r_p}{r_s} = \tan\Psi \exp(i\Delta). \qquad \text{(II.3-9)}$$

This signal can, thus, be divided into two parameters: Ψ, which denotes the amplitude ratio, and Δ representing the phase difference between p- and s-polarization, respectively. They are measured as a function of wavelength.

As given by the Fresnel equations (Equations II.3-6) and indicated in the sections discussing the phenomena of the interaction of light with matter relevant to SE, various parameters can be deduced from the measured signal. However, as discussed in the following, optical models according to pre-accessible information available on the investigated systems are necessary.

In the simplest case, the measured setup can be characterized by a single flat air/sample interface. This approximation holds for model systems consisting of materials with infinite thickness or materials that absorb light sufficiently so that only direct reflections from the air/sample interface are detected. Consequently, Equations II.3-6a and c (also with complex refractive indices) can be inserted into Equation II.3-9. As the incident angle ϑ_i and the refractive index of air n_i are known and the transmission angle ϑ_t can be calculated using Snell's law (Equation II.3-3), the refractive index of the sample material n_t can be directly evaluated from the measured data.

In thin film geometries, optical interference can be considered by including the adequate sums of reflection and transmission coefficients according to the respective phase differences connected to the film thickness (cf. Equation II.3-7, Figure II.3-2). At distinct wavelengths, constructive (cf. Equation II.3-8) and destructive interference can be observed as maxima and minima in the measured amplitude signal ($\Psi(\lambda)$). In case the refractive indices of the materials (thin film(s) and substrate) are known, the film thickness(es) can be (directly) evaluated from the measured signal. If no such information is accessible, optical models are employed, in which, inter alia, the effects described in the previous sections are included. Such models are developed based on specific pieces of information (e.g., transparency, layered structure, etc.) being available for the measured specimen prior to parameter extraction. Subsequently, certain variable parameters can be fitted to the measured signal. For transparent media ($k = 0$), commonly, the Cauchy model (with three parameters) is applied to describe n as a function of λ:

$$n(\lambda) = A + \frac{B}{\lambda^2} + \frac{C}{\lambda^4}. \qquad \text{(II.3-10)}$$

The parameters A, B and C can be fitted to the measurement data. Minor absorptions (small k) can be included by an Urbach tail expressible as

$$k(\lambda) = k_0 \exp\left(\frac{hc}{\lambda E_U} - \frac{E_g}{E_U}\right), \qquad \text{(II.3-11)}$$

where k_0 is the absorption amplitude and E_U the Urbach energy, which describes light absorption by a tail state near a band gap E_g.[9] These parameters can also be varied to fit the measurement data. Further models (e.g., Tauc-Lorentz, Drude) can be employed depending on the optical properties of the materials that are investigated. Regardless, for the purposes of the work presented in this thesis (mostly transparent polymers), Cauchy models with Urbach tails were found to yield adequate and meaningful results.

Due to the effects described in section II.3.2.1, SE is particularly sensitive to surfaces and interfaces. To analyze such structures, the effective medium approximation (EMA) can be adopted. Through it, the complex refractive indices of surface roughness, interface layers and composite materials can be calculated fairly easily.[9] This also enables the determination of volume fractions of components in a composite system, e.g., a swollen hydrogel (components: polymer, water, air). The complex refractive index N of a system (composed of n components) can, thus, be calculated from its components i as

$$\sum_{i=1}^{n} f_i \frac{N_i{}^2 - N^2}{N_i{}^2 + 2N^2} = 0.[9] \qquad \text{(II.3-12)}$$

Herein, f_i denotes the respective volume fractions. This approximation can also be used to describe surface roughness (components: material, ambient medium) or interfaces between two materials (components: material 1 and 2). Even though employing this approximation is a potent means, there are limitations to its application regarding the sizes of the structures that are investigated.[*]

Overall, even though spectroscopic ellipsometry requires the careful interpretation and analysis of the measured data, it is an extremely powerful technique for the investigation of optical properties of materials and the precise determination of film thicknesses in layered structures. Extraordinary sensitivity to thickness (~0.1 Å) can be obtained.[6] With commercializing SE instruments, the application of this technique (e.g., to research) has risen significantly from the early 1990s on.[6] Especially the fast acquisition of measurement data in modern instruments (below 1 s) allows for real-time and in-situ monitoring of growth and other dynamic processes such as swelling (in water or different media, e.g., humidity).

---

[*] More details can be found in the section on EMAs in 'Spectroscopic Ellipsometry'.[9]

II.3.3 References

(1) Griffiths, P. R.; de Haseth, J. A. Introduction to Vibrational Spectroscopy. In *Fourier Transform Infrared Spectrometry*; John Wiley & Sons, Inc.: Hoboken, NJ, USA, 2007; pp 1–18. https://doi.org/10.1002/9780470106310.ch1.

(2) Griffiths, P. R.; de Haseth, J. A. Conventional Transmission Spectrometry. In *Fourier Transform Infrared Spectrometry*; John Wiley & Sons, Inc.: Hoboken, NJ, USA, 2007; pp 251–260. https://doi.org/10.1002/9780470106310.ch11.

(3) Griffiths, P. R.; de Haseth, J. A. Attenuated Total Reflection. In *Fourier Transform Infrared Spectrometry*; John Wiley & Sons, Inc.: Hoboken, NJ, USA, 2007; pp 321–348. https://doi.org/10.1002/9780470106310.ch15.

(4) Kemp, W. Infrared Spectroscopy. In *Organic Spectroscopy*; Macmillan Education UK: London, 1991; pp 19–99. https://doi.org/10.1007/978-1-349-15203-2_2.

(5) Tazreiter, M.; Christian, P.; Schennach, R.; Grießer, T.; Coclite, A. M. Simple Method for the Quantitative Analysis of Thin Copolymer Films on Substrates by Infrared Spectroscopy Using Direct Calibration. *Anal. Methods* **2017**, *9* (36), 5266–5273. https://doi.org/10.1039/C7AY01748K.

(6) Fujiwara, H. Introduction to Spectroscopic Ellipsometry. In *Spectroscopic Ellipsometry*; John Wiley & Sons, Ltd: Chichester, UK, 2007; pp 1–11. https://doi.org/10.1002/9780470060193.ch1.

(7) Fujiwara, H. Principles of Optics. In *Spectroscopic Ellipsometry*; John Wiley & Sons, Ltd: Chichester, UK, 2007; pp 13–48. https://doi.org/10.1002/9780470060193.ch2.

(8) Fujiwara, H. Principles of Spectroscopic Ellipsometry. In *Spectroscopic Ellipsometry*; John Wiley & Sons, Ltd: Chichester, UK, 2007; pp 81–146. https://doi.org/10.1002/9780470060193.ch4.

(9) Fujiwara, H. Data Analysis. In *Spectroscopic Ellipsometry*; John Wiley & Sons, Ltd: Chichester, UK, 2007; pp 147–207. https://doi.org/10.1002/9780470060193.ch5.

(10) Boyle, W. S.; Smith, G. E. Charge Coupled Semiconductor Devices. *Bell Syst. Tech. J.* **1970**, *49* (4), 587–593. https://doi.org/10.1002/j.1538-7305.1970.tb01790.x.

3

III Scientific Publications

This section provides information on original scientific work on thermoresponsive hydrogel thin films. The results are reproduced from peer-reviewed open access publications and were reformatted/edited to fit the style of this thesis with permission from the publisher. Further permissions related to the material excerpted should be directed to the publisher.

The direct links to the articles are

https://pubs.acs.org/doi/abs/10.1021/acs.macromol.8b02120,

https://pubs.acs.org/doi/abs/10.1021/acs.macromol.9b01364,

https://pubs.acs.org/doi/abs/10.1021/acs.jpcc.9b07340,

https://pubs.acs.org/doi/abs/10.1021/acsapm.9b00957.

III.1 Thickness-Dependent Swelling Behavior of Vapor-Deposited Smart Polymer Thin Films

Thickness-Dependent Swelling Behavior of Vapor-Deposited Smart Polymer Thin Films

Fabian Muralter,[ORCID] Alberto Perrotta,[ORCID] and Anna Maria Coclite*[ORCID]

Institute of Solid State Physics, NAWI Graz, Graz University of Technology, Petersgasse 16, 8010 Graz, Austria

Macromolecules   Article

Corresponding Author
*E-mail: anna.coclite@tugraz.at.

III.1.1 Preface

The work, the results of which are published in this article, was conducted at the Graz University of Technology. The author of this thesis performed the sample preparation, characterization, data evaluation and wrote the manuscript. Alberto Perrotta provided support regarding data interpretation and in preparing the manuscript. Anna Maria Coclite supervised the project and supported the manuscript preparation process. The following sections, with their text and illustrations being identical to the published material, are reproduced with permission.

III.1.2 Abstract

In this contribution, the temperature-dependent swelling behavior of vapor-deposited smart polymer thin films is shown to depend on cross-linking and deposited film thickness. Smart polymers find application in sensor and actuator setups and are mostly fabricated on delicate substrates with complex nanostructures that need to be conformally coated. As initiated chemical vapor deposition (iCVD) meets these specific requirements, the present work concentrates on temperature-dependent swelling behavior of iCVD poly(N-isopropylacrylamide) thin films. The transition between swollen and shrunken state and the corresponding lower critical solution temperature (LCST) was investigated by spectroscopic ellipsometry in water. The films' density in the dry state evaluated from X-ray reflectivity could be successfully correlated to the position of the LCST in water and was found to vary between 1.1 and 1.3 g/cm^3 in the thickness range 30-330 nm. This work emphasizes the importance of insights in both the deposition process and mechanisms during swelling of smart polymeric structures.

III.1.3 Introduction

Hydrogels are networks of hydrophilic polymer chains. In a water environment, either in humidity or in liquid state, water molecules form hydrogen bonds with the hydrophilic groups in the polymeric structure, making the material rearrange and swell up to a multiple of its dry size. Upon changing the amount of water in contact with the polymeric network, the hydrogel reacts reversibly by taking up water into or repelling out water from its inherent structure. This reversible swelling behavior makes this class of materials interesting for a variety of different setups (e.g., in drug delivery,[1] contact lenses).

The kinetics of the water uptake are time-limited by water diffusivity.[2] Therefore, adopting thin polymeric films is crucial for achieving fast response times and, in turn, optimal device performance. However, often the water uptake processes and the corresponding rearrangement of polymer chains impose stress on the thin film and could result in poor adhesion or mechanical failure. Consequently, to ensure mechanical stability during swelling, a specific cross-linking co-monomer can be added. Cross-linking is achieved by adding a chemical species that allows for the binding of two separate polymer chains. This cross-linked hydrogel can, therefore, be seen as a polymer mesh, able to take up a specific amount of water into its structure.[3]

Monomer and cross-linker choice influence the responsiveness to water and to other external stimuli. Specific chemical functionalities in the monomer units can be utilized to fabricate stimuli-responsive hydrogels. A variety of

such smart polymers have been demonstrated to respond to temperature, pH, magnetic/electric fields, or different concentrations of specific chemical species (e.g., glucose).[4] In the current study, the most prominent temperature-responsive hydrogel, poly-*N*-isopropylacrylamide (pNIPAAm), has been investigated. Its temperature-responsiveness stems from the molecule exhibiting hydrophilic groups (i.e., amide), forming hydrogen bonds in the presence of water, and the probability for attractive intrachain interactions leading to polymer collapse, depending on the material's temperature.[5] The presence of both functionalities results in interesting thermoresponsive properties, namely, the lower critical solution temperature (LCST). At this temperature, pNIPAAm undergoes a phase transition from a hydrated swollen state to a dehydrated shrunken state, below and above the LCST, respectively. This reversible temperature-dependent swelling behavior attracts particular interest for using smart polymer thin films in sensor[6] and actuator setups.[7]

As in several applications delicate surfaces (e.g., drugs, flexible substrates) need to be coated, often with specific nanostructure, vapor-based techniques are more suitable for the purpose than solution processing due to the absence of solvent-related inconveniences: dissolution of the substrate, intermixing of components, surface tension. In this contribution, initiated chemical vapor deposition (iCVD) was adopted. In this solvent-free technique, monomer, cross-linker, and radical initiator molecules are flown into a vacuum chamber in the gas phase at set flow rates. The initiator (usually a peroxide) decomposes into radicals at a heated filament (200-350 °C) mounted above the sample stage. The monomer and cross-linker molecules adsorb on the low temperature substrate (held at 10-40 °C). The initiator radicals attack the unsaturated bonds in the monomer and cross-linker species and, hence, initiate polymerization on the substrate similar to free radical polymerization processes.[8] However, the mild processing conditions allow for full retention of delicate functionalities upon deposition such as thermoresponsive groups, enabling precise engineering of the material properties. With iCVD, accurate control on the film thickness can be achieved via deposition time and accurate tuning of the chemical composition can be achieved by setting the monomer/cross-linker/initiator ratio and by choosing their distinct chemical nature.

The cross-linker content is known to affect the mesh size and, therefore, the degree of swelling of a polymer.[3] Surface attached networks[9] and, in particular, thin films deposited by iCVD[10] have been shown to behave correspondingly. Furthermore, it has been previously reported that cross-linking and its amount within the polymeric structure affect the position of the LCST transition, with the hydrophobicity[11] or hydrophilicity[12] of the cross-linker determining the direction of the shift. However, next to the chemical

composition affecting the thermoresponsive properties of the polymer, thickness should also be a crucial parameter affecting the LCST position. In the literature, the LCST of solution-processed photo-cross-linked pNIPAAm-based thin films has been reported to change as a function of film thickness ranging from 20 nm up to 2 μm, with the amount of cross-linking defining the magnitude of this effect.[13] For pNIPAAm thin films with a low amount of cross-linking and film thicknesses up to 100 nm, stable values for the LCST have been reported. Above 100 nm, the films' transition temperature was shown to decrease linearly with increasing film thickness. The state in which the thin films are cross-linked (dry or partially swollen) has been deemed responsible for changes in shape and position of the LCST transition. Swelling is one-dimensional in thin films and introduces compression in the polymeric system in pNIPAAm films cross-linked in the dry state. As the magnitude of this compression changes with film thickness, this results in a thickness-dependent LCST.[13]

As this thickness-dependent swelling behavior is not very well documented for solution-processed polymers and not reported for vapor-deposited thin polymeric films, in this study, we aim at demonstrating the effect of cross-linking and film thickness on the thermoresponsive behavior also for pNIPAAm thin films deposited by initiated chemical vapor deposition. The film thickness range between 30 and 330 nm, most suitable for vapor-based techniques, is investigated, focusing on the low film thickness regime. Results on the applicability of the investigated polymeric system to humidity sensing have previously been reported by our group in Salzmann et al.[14] There, the temperature-dependent swelling behavior of two different polymeric systems in a humid environment has been analyzed and compared. In the present contribution, the iCVD synthesis of one of these systems, namely, p(NIPAAm-*co*-DEGDVE), as already reported by Alf et al.,[15] was used as a case study. Herein, the focus is on fundamental investigations of thin film properties and their connection to thickness-dependent swelling behavior of vapor-deposited systems in water. For this purpose, in the present work, the LCST together with optical properties of the thin films are determined by swelling experiments in water recorded in situ by spectroscopic ellipsometry (SE). X-ray reflectivity (XRR) measurements and SE measurements in a controlled environment (nitrogen/humidity) have been carried out, deepening the understanding of the investigated effects in terms of thin film properties.

III.1.4 Experimental Section

Hydrogel layers of thicknesses ranging between 30 and 330 nm have been deposited in a custom-built initiated chemical vapor deposition (iCVD)

reactor. The deposition processes were run in a cylindrical chamber (diameter 360 mm, height 55 mm), in which the pressure during deposition is controlled by a Duo 5M rotary vane pump (Pfeiffer Vacuum, Germany) and a throttle valve (MKS Instruments, USA). Single-sided polished silicon wafers with a native oxide of 1.5-2 nm thickness on top (Siegert Wafer, Germany) are used as substrates. The substrates are positioned on the bottom of the reaction chamber, where the temperature is set to 35 °C by an Accel 500 LC heater/chiller (Thermo Fisher Scientific, USA). The deposited film thickness is monitored in situ by laser interferometry with a He-Ne laser ($\lambda = 633$ nm; Thorlabs, USA) through a removable quartz glass lid. Di-tert-butyl peroxide (TBPO, 98%; Aldrich, Germany) is used as an initiator. TBPO is kept at room temperature in a glass jar connected to the reaction chamber via a needle valve (Swagelok, USA) to be able to set the desired flow rate of 1 sccm. Twenty-five mm above the substrates, a Ni-Cr wire wound in 12 parallel lines (20 mm wire separation) functions as a heated filament (200 °C) to cleave the initiator molecules entering the reaction chamber. *N*-isopropylacrylamide (NIPAAm, 99%; Aldrich, Germany) is used as monomer and di(ethylene glycol) divinyl ether (DEGDVE, 99%; Aldrich, Germany) as cross-linker. NIPAAm and DEGDVE are also kept in glass jars but heated to 85 and 70 °C, respectively. The monomer and cross-linker vapors are flown into the reaction chamber through a heated mixing line (90 °C). Needle valves (Swagelok, USA) are used to set flow rates and achieve controlled composition. Since the deposition rate depends on the individual flow rates, substrate temperature, and working pressure, the film thickness increase as monitored in situ by laser interferometry was used to stop the deposition at different deposition times when the desired thickness was achieved.

Spectroscopic ellipsometry (SE) in a wavelength range of 370-1000 nm (M-2000S, J.A. Woollam, USA) was used to determine the film thickness and optical properties of the thin films in a controlled environment (nitrogen, relative humidity, and water at set temperature). A temperature controlled liquid stage (J. A. Woollam, USA) was used for performing swelling experiments in deionized water. The recorded data were evaluated with an optical model consisting of a c-Si semi-infinite layer on the bottom (temperature-dependent), a 1.6 nm thick native SiO_2 layer in the middle, and the polymer film on top. The polymer layer was modeled with a Cauchy function, and an Urbach tail was adopted accounting for adsorption in the low wavelength region. The surrounding medium was set to H_2O with temperature-dependent optical properties. For the temperature-dependent swelling experiments, the liquid stage and the mounted sample (already exposed to deionized water) were precooled to 10 °C. The respective signal was then recorded while applying a temperature ramp from 10 to 50 °C at a heating rate of 0.5 °C/min. Directly after deposition, the thin film samples were rinsed for

30 s with deionized water for equilibration. Despite rinsing, the first and second heating experiments showed differences in shape and position of the transition. As equilibration has been earlier reported to be needed for the study of temperature-dependent behavior of iCVD thin films,[16] the third heating experiment was used for the determination of the LCST, as all of the further heating ramps give similar results. This effect was attributed to the removal of loosely attached material and the rearrangement of polymer chains in the first couple of heating cycles for which rinsing is not sufficient while heavier rearrangements during cooling/heating are (especially in films exhibiting a low amount of cross-linking). As described in detail later, the film thickness changes after rinsing, but together with the optical properties as recorded by SE, it has not been observed to change after the first two heating cycles applied for equilibration purposes. This hints to structural rearrangements occurring during equilibration that do not affect the amount of material present on the substrate. The ellipsometry measurements in relative humidity and N_2 atmosphere were performed in a THMS600 temperature stage (Linkam, UK) at room temperature (~25 °C), with the gases being supplied from a custom-built mixing setup. An SHT15 humidity sensor (Sensirion, Switzerland) was used to monitor the relative humidity (RH) in the sample stage in situ; the samples were measured after equilibration in the respective environment, so that the film thickness would not change more than 0.5 nm in 5 min. The recorded optical data have been evaluated using the same model as that in the liquid case but with the ambient material being set to air (n ≈ 1). Likewise, measurements to obtain information about the available free volume detectable with water have been carried out similar to Perrotta et al.[17,18] Therefore, the thin film samples have been kept under a nitrogen atmosphere at a constant temperature (25 °C), determining their optical properties. Subsequently, water vapor has been introduced into the system in 10% RH steps, to which the films respond by filling free volume with H_2O. Hence, the refractive index first increases due to water permeation, which can be understood as a measure for free volume of the respective thin film.

X-ray reflectivity (XRR) measurements were performed on a PANalytical Empyrean diffractometer. The diffractometer uses a copper sealed tube, a multilayer mirror for monochromatizing the beam (λ = 0.154 nm), a beam mask of 10 mm, and a 1/32° divergence slit on the incident beam side. On the diffracted beam side, a receiving slit of 0.1 mm and a 0.02 rad Soller slit were used in front of a PANalytical PIXcel 3D detector in point detector mode. The critical angle of total reflection was read out of the XRR patterns as the angle 2θ slightly above the maximum intensity where the intensity drops to half its maximum value.[19] All of the XRR measurements have been performed at room temperature (~25 °C) and at a relative humidity of ~40%.

Absorbance spectra of several samples were collected in transmission mode on a Bruker IFS 66 v/s Fourier transform infrared (FTIR) spectrometer. The measurements were run in the wavenumber range 1000-4000 cm^{-1} at a resolution of 4 cm^{-1} and a zero filling factor of 8.

III.1.5 Results and Discussion

A series of thin films of p(NIPAAm-*co*-DEGDVE) with varying amounts of cross-linking and film thickness have been successfully deposited by iCVD, as also previously reported.[14] The respective degree of cross-linking has been set by adjusting the ratio of the monomer, cross-linker, and initiator flow rates. From the flow rates, the nominal composition of the deposited thin films was calculated via the partial pressure of the chemicals compared to their saturation pressure (P_M/P_{sat}) in the applied temperature and pressure conditions. All of the flow rates have been chosen so that the P_M/P_{sat} values lie in the range 0.05-0.2, a regime where surface concentration is reported to depend linearly on the P_M/P_{sat} value.[20] Hence, the presented values of the nominal cross-linker amount correspond to the calculated amount of cross-linker species available on the surface during deposition and, therefore, are related to but do not represent the exact fraction of cross-linker molecules in the respective deposited polymeric system. The following formula has been used to calculate the nominal DEGDVE crosslinker amount from the P_M/P_{sat} values of the components of the deposited polymeric structure (NIPAAm and DEGDVE):

$$\text{crosslinker amount [\%]} = \frac{(P_M/P_{sat})_{\text{DEGDVE}}}{(P_M/P_{sat})_{\text{NIPAAm}} + (P_M/P_{sat})_{\text{DEGDVE}}} \times 100$$

For this investigation, two differently cross-linked polymers of p(NIPAAm-*co*-DEGDVE) were chosen as case models to investigate the effect of cross-linker concentration and overall thin film thickness on the LCST. For the less cross-linked series, the nominal percentage of cross-linking was set to 25%, whereas it was set to 40% for the more cross-linked samples. Additionally, a series of p(NIPAAm-*co*-DEGDVE) samples with a deposited film thickness of 70 nm has been prepared with cross-linker amounts varying between 25 and ~60%.

FTIR absorbance spectra were collected on the differently cross-linked samples with varying film thickness. The presence of the cross-linker could not be determined from FTIR due to DEGDVE lacking strong characteristic FTIR absorption bands, as reported earlier.[15] However, a representative spectrum is shown in Figure III.1-1 to illustrate successful polymerization with the absence of characteristic vinyl group vibrations at 3150, 1620, and 1400 cm^{-1} as labeled by Salzmann et al.[14] The recorded absorption bands compare well to

FTIR data of p(NIPAAm-*co*-DEGDVE) films deposited by iCVD in the literature,[15] and all recorded peaks could be successfully assigned to absorption bands within the chemical structure of pNIPAAm according to Sun et al.[21]
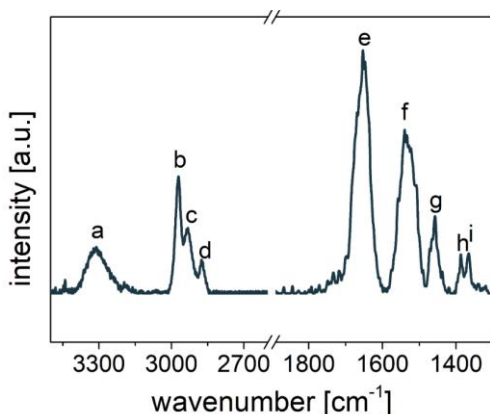
Label	Assignment	Position [cm^{-1}]
a	N-H stretch	3300
b	CH$_3$ asymm. stretch	2970
c	CH$_2$ asymm. stretch	2930
d	CH$_3$ symm. stretch	2870
e	amide I (C=O stretch)	1650
f	amide II (N-H)	1540
g	CH$_2$ asymm. bend	1460
h	CH$_3$ symm. bend	1390
i	CH$_2$ symm. bend	1370

Figure III.1-1. FTIR absorption spectrum of a 330 nm 25% cross-linked p(NIPAAm-*co*-DEGDVE) sample indicating successful polymerization by not exhibiting vinyl group absorption bands[14] at 3150, 1620, and 1400 cm^{-1}; peaks labeled and assigned according to Sun et al.[21]

As pure pNIPAAm films dissolve in water, the presence of the cross-linker has been successfully verified by the films' stability upon rinsing, down to a nominal DEGDVE content of 25%. As stated earlier, rinsing leads to the removal of loosely attached material. The amount of material removed decreases with increasing amount of cross-linking, from 7-8% of the deposited dry film thickness for 25%-cross-linked samples to 3-4% for samples with 40% DEGDVE cross-linker fraction, as evaluated from SE measurements. However, the investigated samples within a similarly cross-linked thickness series show similar percentages of material removal during rinsing. This points out that rinsing affects the entire thin film independently of the overall film thickness, instead of just removing material, e.g., from the surface of the sample. Furthermore, proving the presence of the cross-linker at different degrees, the films are able to take up significant amounts of water, in

a range going from ~10% (with a high amount of cross-linker) up to 120% of their dry film thickness (with a low amount of cross-linker) at 20 °C (see Figure III.1-2).
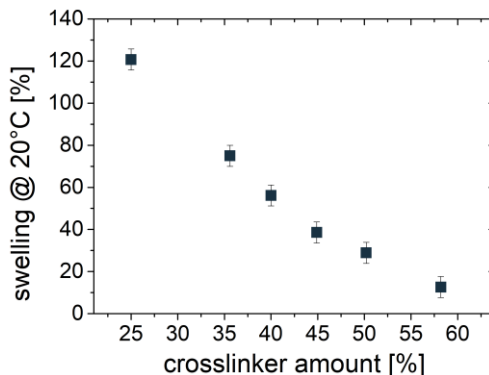

Figure III.1-2. Swelling at 20 °C (thickness in water compared to the dry thickness) as a function of the nominal cross-linker amount (DEGDVE fraction) of differently cross-linked 70 nm-thick p(NIPAAm-*co*-DEGDVE) samples.

The LCST values of the respective thermoresponsive thin film samples have been evaluated as the mean values of the points of inflection of thickness and refractive index (measured at 633 nm) curves derived from spectroscopic ellipsometry. The data were acquired in water as a function of temperature during heating from ~15 to 50 °C (see Figure III.1-3 for representative measurement data). The thickness is reported here normalized to the thickness measured at 50 °C, for clarity.

As the film thickness also affects the kinetics of the swelling/deswelling process,[2] several different heating rates between 0.25 and 4 °C/min have been adopted (see the Supporting Information). As a result, a heating rate of 0.5 °C/min has been used for all of the swelling experiments, because kinetic effects can be neglected: Heating ramps at this rate yield similar results as applying lower heating rates for the investigated film thickness regime, while still being sufficiently quick to achieve reasonably constant heating ramps in a room temperature environment.

As aforementioned and evident from the plots in Figure III.1-3, the cross-linking amount also affects the LCST transition.[12] Two effects have been deemed responsible: First, the mesh size is being reduced by introducing more cross-linker into the polymeric system. Therefore, the maximum amount of water the polymer thin film is able to take up is reduced by increasing the amount of cross-linker.[3] In the investigated systems, the maximum swelling at 20 °C for several differently cross-linked p(NIPAAm-*co*-DEGDVE) thin films (see Figure III.1-2) shows a clearly decreasing trend
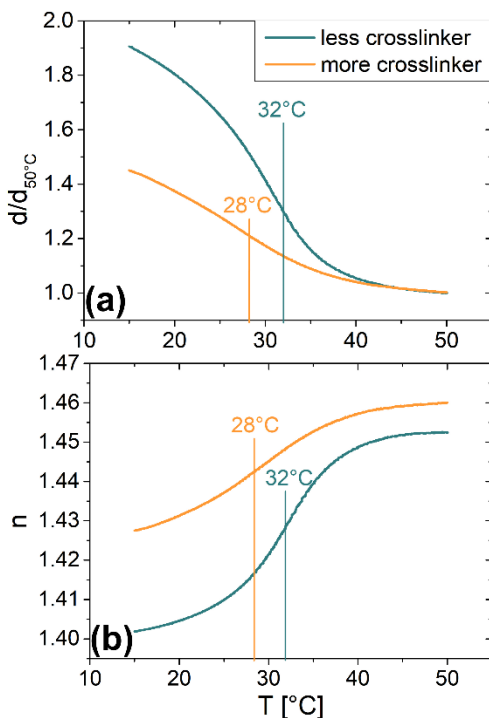
Figure III.1-3. (a) Thickness normalized to the value measured at 50 °C ($d/d_{50°C}$) and (b) refractive index n measured at 633 nm as a function of temperature during heating in water for the evaluation of the LCST as the mean value of the points of inflection of the respective curves plotted for two differently cross-linked 70 nm-thick samples.

from 120% for a cross-linking degree of 25% to swelling of approximately 10% for a cross-linking degree of ~60%. Second, the hydrophobic cross-linker DEGDVE makes it favorable for the thin film to repel out water, even at lower temperatures. This leads to a decreased LCST for more cross-linked thin films, whereas the LCST values of the pNIPAAm thin films with a low amount of cross-linking are comparable to pure bulk pNIPAAm hydrogels[22] or solution-processed pNIPAAm layers grafted onto surfaces,[23] exhibiting values of around 32 °C. The LCST values of the photo-cross-linked pNIPAAm thin films reported by Harmon et al.[13] also compare well to the values reported in this study. Also, the magnitude of LCST shifts due to the different amounts of cross-linking are comparable to literature values, as the LCST was reported to shift for ~5 °C when changing the amount of cross-linking from 10 to 30% in p(NIPAAm-*co*-EGDA) films deposited by iCVD.[12] In order to verify the effect of different thin film thickness values on the LCST, heating ramps upon water exposure were measured to obtain the LCST values for p(NIPAAm-*co*-DEGDVE) layers ranging from 30 to 330 nm. The LCST values for two thickness series with different amounts of cross-linking are reported in Figure III.1-4.
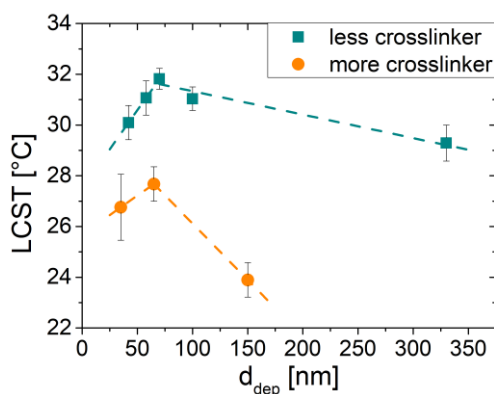
Figure III.1-4. LCST as a function of deposited film thickness (d_{dep}) for differently cross-linked p(NIPAAm-*co*-DEGDVE) thin films (dotted lines are for guidance of the eye).

Both series exhibit a maximum LCST value for a deposited film thickness of ~70 nm, at 27.7 and 31.8 °C for the more and less cross-linked polymers, respectively. Furthermore, the LCST decreases at higher film thickness, with the effect being more pronounced for the less cross-linked films. This is in agreement with what has been found for photo-cross-linked pNIPAAm films by Harmon et al.[13] and, as previously mentioned, explained by film thickness affecting the state of the polymer during swelling compared to the reference state as cross-linked (compression or elongation). The investigated iCVD thin films are deposited at a pressure of 250 mTorr and at a substrate temperature of 35 °C (dry and above the LCST), where Harmon et al. state that a gel that is cross-linked in dry state is always under compression upon swelling, with the compression being greater further from the substrate.[13] Therefore, two regimes have been identified, above and below a certain critical film thickness depending on the amount of cross-linking. Above the critical thickness, the LCST decreases linearly with film thickness. Harmon et al.[13] also report on the LCST being constant below this critical film thickness. However, in the present study, the LCST was found to decrease toward lower film thickness for both series of different amounts of cross-linking, which has not been reported before. Therefore, the present investigations show that the p(NIPAAm-*co*-DEGDVE) thin films deposited by iCVD exhibit a thickness- and cross-linker-dependent swelling behavior, possibly caused by thickness-dependent physical properties of the investigated polymeric systems, as described later.

In order to verify the expected relation between the variation in LCST values and the physical properties of the thin films, the refractive index (n) was recorded in different environments. Refractive index values are a measure for the optical density of thin film samples. Therefore, the index as measured in a nitrogen environment (dry) gives information about the density of the

polymeric matrix without the presence of water. These values of n measured at ~25 °C as a function of the film thickness and composition are reported in Figure III.1-5a. The trends for the individual thickness series show similarities to the LCST behavior as a function of deposited film thickness. Temperature-dependent measurements in a nitrogen atmosphere revealed that the polymer layers do not exhibit an LCST transition without the presence of water. Temperature only plays a minor role in a pure nitrogen environment, where the samples show thermal expansion of 0.6% of their film thickness between 20 and 50 °C, independent of the cross-linker amount and the deposited thickness. However, the refractive index values of the polymer layers in water at 50 °C give a measure for water being trapped in the system in the collapsed state (see Figure III.1-5b). Additionally, also the respective thickness values measured in water at 50 °C give evidence that water is retained in the system (in the collapsed state). The percentage of thickness difference compared to the dry state is at around +20% for all samples of both cross-linker series. At high deposited film thickness, the values of n at around 1.46 independent of the cross-linker amount are in agreement with what has been previously reported for this regime.[13] At low film thickness,
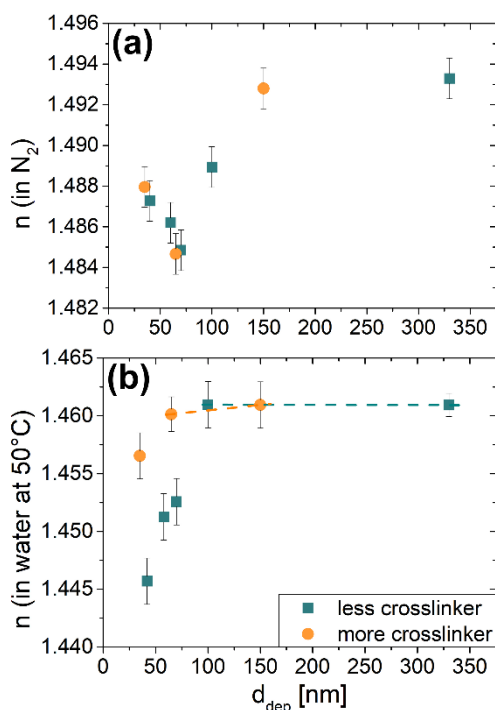
Figure III.1-5. Refractive index n (measured at 633 nm) (a) in nitrogen environment at 25 °C and (b) in water at 50 °C after heating (collapsed state) of the polymer layers plotted as a function of deposited film thickness (d_{dep}) as measured by spectroscopic ellipsometry (dotted lines are for guidance of the eye).

the refractive index at 50 °C is found to decrease, with the effect being more pronounced for the less cross-linked films. Presumably, higher hydrophobicity (water contact angle of 60-90°)[15] compared to the substrate (water contact angle of ~40°) induces differences in swelling behavior during diffusion for different distances from the substrate and hence film thickness regimes. During swelling, this would lead to a water-rich layer close to the substrate. However, this has not been confirmed from fitting the SE data. With the film thickness being large enough (at around 100 nm), these substrate-induced effects anyways seem negligible. As the mesh size also influences diffusivity, the cross-linker amount is found to determine the magnitude of the investigated effect.

As described previously, the free volume of the thin films accessible to water vapor has been investigated. The magnitude of the initial refractive index increase while introducing water vapor into the nitrogen filled system can display differences in the available free volume (see Figure III.1-6). The refractive index difference is found constant for both cross-linker series and shows just one smaller value for the lowest film thickness of the more cross-linked samples (see Figure III.1-6a). This hints no influence of the free volume accessible via this water uptake on the thickness dependence of the LCST. However, the refractive index difference is lower for the less cross-linked series. As mentioned previously, the less cross-linked films swell more than the more cross-linked ones. As swelling also occurs in humidity and causes the refractive index to decrease, it leads to a lower refractive index difference for the less cross-linked samples (see Figure III.1-6b). Hence, the free volume is only partially probed. The water molecules just adsorb up to a point where swelling is more prominently observed in refractive index behavior. Therefore, the shape and position of the LCST, swelling in humidity, and density are possibly influencing this measurement as well as just the adsorption of water molecules into the free volume of the investigated polymeric systems. However, the investigated films swell already by changing the environment from 0 to 10% RH (see the Supporting Information), which is promising for utilization in sensing applications.

To deepen the understanding of the results of the refractive index measurements in a nitrogen environment (see Figure III.1-5a), XRR measurements have been used to investigate the density of the thin films. The position of the critical angle of total reflection is proportional to the electron density of the investigated layers.[19] By assuming the nominal percentages of cross-linking and knowing the molecular weight and number of electrons of the respective monomers, an estimation of the mass density of the investigated thin films could be derived. For that, the average number of electrons of an individual polymeric structure can be assumed to be constant for films of the same composition in one series of similar cross-linking. Therefore, the
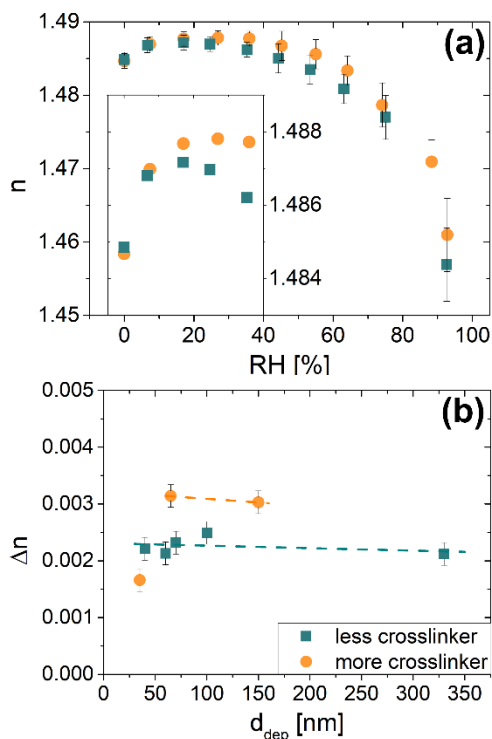
Figure III.1-6. (a) Refractive index n (at 633 nm) as measured via SE during relative humidity exposure of two differently cross-linked 70 nm-thick p(NIPAAm-*co*-DEGDVE) samples (the inset shows a zoom of the region below 40% relative humidity, where the increase in refractive index Δn was evaluated). (b) Refractive index difference Δn as a measure of the free volume of the thin films prone to uptake of water vapor plotted as a function of deposited film thickness d_{dep} (dotted lines are for guidance of the eye).

mass density evaluated from the XRR measurements has been plotted as a function of deposited film thickness for different amounts of cross-linking (see Figure III.1-7). The mass density values are found to lie in a range of 1.1-1.3 g/cm^3, which is in agreement with literature values. The mass density of emulsion polymerized pNIPAAm microgels cross-linked by 2.5 mol% *N,N'*-methylenbis(acrylamide) (BIS) has been reported to be around 1.15 g/cm^3.[24] The differences in cross-linking (amount and chemical nature) and different polymerization techniques account for the differences in density reported in the present work. In the thickness study, the density decreases in the low film thickness regime of up to ~70 nm for both cross-linker series. At higher film thickness, the density increases again, with values surpassing the ones at low film thickness. Overall, the mass density of the more cross-linked thin films has been evaluated to be higher than the one of the less cross-linked samples. Therefore, XRR results are found to be in agreement with the refractive index as measured with SE in a nitrogen

environment (see Figure III.1-5a) and mimic the trend of the LCST values as a function of deposited film thickness for both cross-linker series with inverse proportionality. Not knowing the exact compositions, the exact polymer molecular weight and, therefore, also the exact number of electrons of the polymeric structures results in large error bars of the mass density estimates. However, the measured critical angles of total reflection (see the Supporting Information) infer a correlation between the density of the polymeric matrix and the position of the LCST of the respective p(NIPAAm-*co*-DEGDVE) thin film samples.
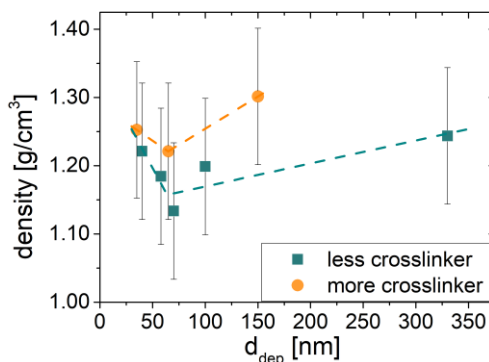
Figure III.1-7. Mass density as calculated from the critical angle of total reflection evaluated from XRR measurements as a function of deposited film thickness (d_{dep}) for differently cross-linked sample series (dotted lines are for guidance of the eye).

As aforementioned, by choosing a slow heating rate (0.5 °C/min), the chance of kinetic effects interfering with the evaluation of the LCST from the SE measurements in water has been minimized. Long-term kinetic effects cannot be ruled out, as it has been reported to take polyelectrolyte thin films several days to reach a constant film thickness during swelling in relative humidity.[25] In addition, a difference in density among thin films of different thicknesses is generally caused by a variation of the deposition conditions. However, similar deposition rates, in the range 1.6-2.0 nm/min, were measured for all of the investigated samples in the case studies, excluding fluctuations of this parameter having an effect on the molecular weight of the resulting thin films.[20] In the literature, Bonnet et al. reported two growth regimes in iCVD polymerization of p(neo-pentyl methacrylate) thin films, stating that the initial stages of a deposition exhibit a lower deposition rate and therefore yield lower molecular weight thin films.[26] In the present study, no significant variation of the deposition rate has been observed via in situ laser interferometry upon deposition. Overall, the deposition rate has not been noted to change more than 10% over time during a single deposition process. Bonnet et al. also did not report on changes in the density of the investigated thin films;[26] although the changes in density are delicate in the present work,

they lead to consistent and significant changes in swelling behavior. A possible explanation would be local depletion of monomer at the substrate level during one deposition with time, as higher cross-linking would lower the LCST, as described previously. This would lead to a gradient of cross-linking, with high film thickness samples exhibiting more cross-linking and therefore lower LCST values. However, the maximum swelling was comparable for the similarly cross-linked samples within a thickness series (120 and 60% swelling for the less and more cross-linked films at 20 °C, respectively), pointing out that a gradient in cross-linking in the layer can be excluded, as it would possibly also lead to an altered maximum swelling value. In the film thickness range up to ~70 nm, the opposite LCST behavior compared to the region above 70 nm has been observed. In particular, the LCST was found to decrease toward lower film thickness, but still, the maximum swelling of the corresponding films compared well to the ones of the films with higher LCSTs of similar cross-linking. In contrast to the photo-cross-linked thin films reported on by Harmon et al.,[13] the iCVD thin films grow steadily from the substrate with cross-linking happening during film growth. Hypothetically, the copolymerization of the two chemical species used in the present work, NIPAAm and DEGDVE, yields local differences in composition and morphology of the thin films, resulting in differences of the average mass density of the resulting thin films. These differences then lead to a variation of the swelling behavior and therefore of the LCST transition.

III.1.6 Conclusions

In this work, pNIPAAm-based thin films have been successfully prepared with different degrees of cross-linking and film thickness by iCVD. The understanding of the shape and position of their LCST transition has been deepened, as effects of both cross-linking and film thickness have been investigated. Increasing the DEGDVE cross-linker amount leads to a lower maximum swelling degree and a lower LCST. (Mass) density (as evaluated from SE and XRR) mimics the trends of the LCST as a function of cross-linking and deposited film thickness. Hence, an increase in the density of the polymeric matrix leads to a decrease in the transition temperature. The density in the dry state can be increased by adding more cross-linker. Both investigated thickness series exhibit a maximum density at a film thickness of about 70 nm, leading to a minimum in LCST for the respective similarly cross-linked thickness series. As deposition conditions within the thickness series have been carefully set constant, either local fluctuations in the reaction chamber or differences in the copolymerization procedure of NIPAAm and DEGDVE over time during one deposition process have been deemed responsible for the differences in density as a function of film thickness. When the polymer is cross-linked in the dry state, thickness-dependent

compression leads to a lower LCST at higher film thickness.[13] The present work provides a further understanding of the proposed hypothesis and adds to it the correlation to the mass density of the polymeric thin films. The role of gradients in water diffusivity due to the substrate-polymer interface altering the hydrophobicity within the investigated systems as a function of film thickness needs to be further addressed. However, these detailed insights should raise awareness about the influence of growth conditions as well as behavior on a plethora of material's properties.

III.1.7 Associated Content

Supporting Information
The Supporting Information is available free of charge on the ACS Publications website at DOI: 10.1021/acs.macromol.8b02120.

> Swelling in humidity of p(NIPAAm-*co*-DEGDVE) thin films of different cross-linker amount, several heating ramps in water of different p(NIPAAm-*co*-DEGDVE) samples, and critical angle of total reflection of p(NIPAAm-*co*-DEGDVE) thin film samples as read out from X-ray reflectivity measurements (PDF)
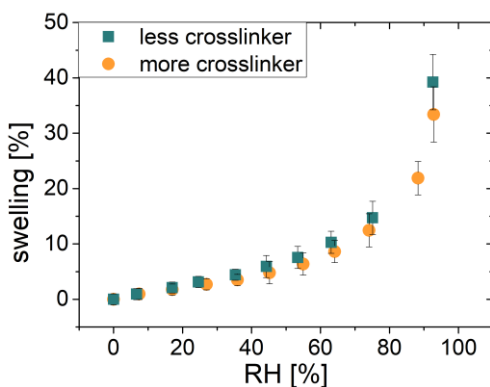
Figure III.1-S1. Swelling (thickness normalized to the value at 0% RH) as a function of relative humidity (RH) for two differently cross-linked 70-nm-thick p(NIPAAm-*co*-DEGDVE) thin film samples; swelling already occurring at low RH counteracting the filling of free volume of the thin films with water vapor, which interferes with the estimation of the free volume by evaluating the magnitude of the refractive index increase in the region below 40% RH.
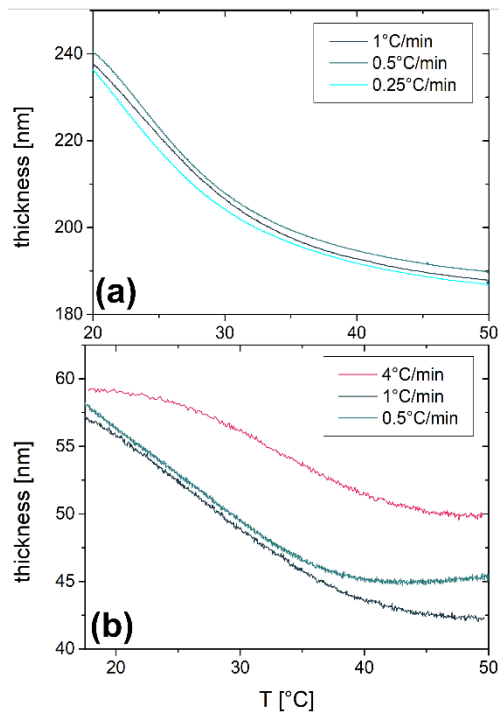
Figure III.1-S2. Film thickness recorded by spectroscopic ellipsometry during heating ramps in water of two differently thick p(NIPAAm-co-DEGDVE) samples recorded at heating rates of (a) 4.0, 1.0 and 0.5°C/min and (b) 1.0, 0.5, 0.25°C/min; kinetic effects influence the film thickness measurement above a heating rate of 1°C/min; the liquid in the cell used for the measurements needs to equilibrate at a certain temperature; also the thin films need to adjust to certain conditions, as swelling processes are time-limited by diffusivity. Applying a heating rate of 4°C/min yields a higher film thickness at elevated temperatures after starting off at a similar thickness as in the other cases (within uncertainty) at low temperatures.
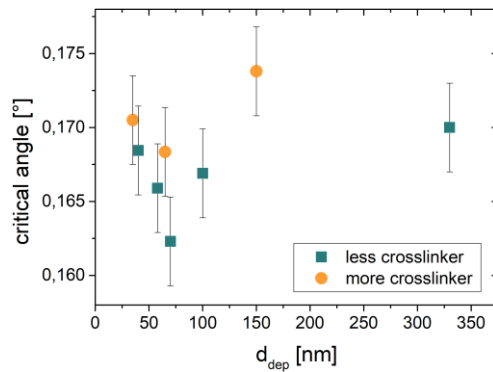
Figure III.1-S3. Critical angle of total reflection (as evaluated from XRR measurements) as a function of deposited film thickness for two differently crosslinked thickness series of p(NIPAAm-*co*-DEGDVE) thin films; the critical angle of total reflection translates directly to the electron density of the deposited polymeric systems. By knowing the molecular weight and the number of electrons of a respective polymeric structure, the mass density can be derived from the data shown. The errorbars arise from the beam width of the instrument and the uncertainty in reading out the values from the measurement curves.

III.1.8 Acknowledgments

III.1.9 References

(1)   Fusco, S.; Huang, H. W.; Peyer, K. E.; Peters, C.; Häberli, M.; Ulbers, A.; Spyrogianni, A.; Pellicer, E.; Sort, J.; Pratsinis, S. E.; Nelson, B. J.; Sakar, M. S.; Pané, S. Shape-Switching Microrobots for Medical Applications: The Influence of Shape in Drug Delivery and Locomotion. *ACS Appl. Mater. Interfaces* **2015**, *7* (12), 6803–6811. https://doi.org/10.1021/acsami.5b00181.

(2)   Beebe, D. J.; Moore, J.; Bauer, J. M.; Yu, Q.; Liu, R. H.; Devadoss, C.; Jo, B. H. Functional Hydrogel Structures for Autonomous Flow Control inside Micro-Fluidic Channels. *Nature* **2000**, *404* (6778), 588–590. https://doi.org/10.1038/35007047.

(3)   Canal, T.; Peppas, N. A. Correlation between Mesh Size and Equilibrium Degree of Swelling of Polymeric Networks. *J. Biomed. Mater. Res.* **1989**, *23* (10), 1183–1193. https://doi.org/10.1002/jbm.820231007.

(4)   Chu, L.-Y.; Xie, R.; Ju, X.-J.; Wang, W. Smart Hydrogel Functional Materials. In *Smart Hydrogel Functional Materials*; Springer-Verlag: Berlin, Heidelberg, 2013; pp V–VII. https://doi.org/10.1007/978-3-642-39538-3.

(5)   Liu, R.; Fraylich, M.; Saunders, B. R. Thermoresponsive Copolymers: From Fundamental Studies to Applications. *Colloid Polym. Sci.* **2009**, *287* (6), 627–643. https://doi.org/10.1007/s00396-009-2028-x.

(6)   Palagi, S.; Mark, A. G.; Reigh, S. Y.; Melde, K.; Qiu, T.; Zeng, H.; Parmeggiani, C.; Martella, D.; Sanchez-Castillo, A.; Kapernaum, N.; Giesselmann, F.; Wiersma, D. S.; Lauga, E.; Fischer, P. Structured Light Enables Biomimetic Swimming and Versatile Locomotion of Photoresponsive Soft Microrobots. *Nat. Mater.* **2016**, *15* (6), 647–653. https://doi.org/10.1038/nmat4569.

(7)   Ramakrishnan, N.; Vamsi, T.; Khan, A.; Nemade, H. B.; Palathinkal, R. P. Humidity Sensor Using NIPAAm Nanogel as Sensing Medium in SAW Devices. *Int. J. Nanosci.* **2011**, *10* (01n02), 259–262. https://doi.org/10.1142/S0219581X11007880.

(8)   Lau, K. K. S.; Gleason, K. K. Initiated Chemical Vapor Deposition (ICVD) of Poly(Alkyl Acrylates): An Experimental Study. *Macromolecules* **2006**, *39* (10), 3688–3694. https://doi.org/10.1021/ma0601619.

(9)   Toomey, R.; Freidank, D.; Rühe, J. Swelling Behavior of Thin, Surface-Attached Polymer Networks. *Macromolecules* **2004**, *37* (3), 882–887. https://doi.org/10.1021/ma034737v.

(10)   Chan, K.; Gleason, K. K. Initiated Chemical Vapor Deposition of Linear and Cross-Linked Poly(2-Hydroxyethyl Methacrylate) for Use as Thin-Film Hydrogels. *Langmuir* **2005**, *21* (19), 8930–8939. https://doi.org/10.1021/la051004q.

(11)   Alf, M. E.; Hatton, T. A.; Gleason, K. K. Novel N-Isopropylacrylamide Based Polymer Architecture for Faster LCST Transition Kinetics. *Polymer* **2011**, *52* (20), 4429–4434. https://doi.org/10.1016/j.polymer.2011.07.051.

(12)   Pena-Francesch, A.; Montero, L.; Borrós, S. Tailoring the LCST of Thermosensitive Hydrogel Thin Films Deposited by ICVD. *Langmuir* **2014**, *30* (24), 7162–7167. https://doi.org/10.1021/la5003594.

(13)   Harmon, M. E.; Kuckling, D.; Pareek, P.; Frank, C. W. Photo-Cross-Linkable PNIPAAm Copolymers. 4. Effects of Copolymerization and Cross-Linking on the Volume-Phase Transition in Constrained Hydrogel Layers. *Langmuir* **2003**, *19* (26), 10947–10956. https://doi.org/10.1021/la030217h.

(14)   Salzmann, P.; Perrotta, A.; Coclite, A. M. Different Response Kinetics to Temperature and Water Vapor of Acrylamide Polymers Obtained by Initiated Chemical Vapor Deposition. *ACS Appl. Mater. Interfaces* **2018**, *10* (7), 6636–6645. https://doi.org/10.1021/acsami.7b18878.

(15) Alf, M. E.; Hatton, T. A.; Gleason, K. K. Initiated Chemical Vapor Deposition of Responsive Polymeric Surfaces. *Thin Solid Films* **2011**, *519* (14), 4412–4414. https://doi.org/10.1016/j.tsf.2011.01.286.

(16) Christian, P.; Coclite, A. M. Vapor-Phase-Synthesized Fluoroacrylate Polymer Thin Films: Thermal Stability and Structural Properties. *Beilstein J. Nanotechnol.* **2017**, *8* (1), 933–942. https://doi.org/10.3762/bjnano.8.95.

(17) Perrotta, A.; Kessels, W. M. M.; Creatore, M. Dynamic Ellipsometric Porosimetry Investigation of Permeation Pathways in Moisture Barrier Layers on Polymers. *ACS Appl. Mater. Interfaces* **2016**, *8* (38), 25005–25009. https://doi.org/10.1021/acsami.6b08520.

(18) Perrotta, A.; Fuentes-Hernandez, C.; Khan, T. M.; Kippelen, B.; Creatore, M.; Graham, S. Near Room-Temperature Direct Encapsulation of Organic Photovoltaics by Plasma-Based Deposition Techniques. *J. Phys. D. Appl. Phys.* **2017**, *50* (2), 024003–024015. https://doi.org/10.1088/1361-6463/50/2/024003.

(19) Gibaud, A.; Vignaud, G. Specular Reflectivity from Smooth and Rough Surfaces. *Lect. Notes Phys.* **2009**, *770*, 85–131. https://doi.org/10.1007/978-3-540-88588-7_3.

(20) Lau, K. K. S.; Gleason, K. K. Initiated Chemical Vapor Deposition (ICVD) of Poly(Alkyl Acrylates): An Experimental Study. *Macromolecules* **2006**, *39* (10), 3688–3694. https://doi.org/10.1021/ma0601619.

(21) Sun, B.; Lin, Y.; Wu, P. Structure Analysis of Poly (N-Isopropylacrylamide) Using Near- Infrared Spectroscopy and Generalized Two-Dimensional Correlation Infrared Spectroscopy. *Appl. Spectrosc.* **2007**, *61* (7), 765–771. https://doi.org/10.1366/000370207781393271.

(22) Schild, H. G. Poly(N-Isopropylacrylamide): Experiment, Theory and Application. *Prog. Polym. Sci.* **1992**, *17* (2), 163–249. https://doi.org/10.1016/0079-6700(92)90023-R.

(23) Ishida, N.; Biggs, S. Direct Observation of the Phase Transition for a Poly(N-Isopropylacryamide) Layer Grafted onto a Solid Surface by AFM and QCM-D. *Langmuir* **2007**, *23* (22), 11083–11088. https://doi.org/10.1021/la701461b.

(24) Seelenmeyer, S.; Deike, I.; Rosenfeldt, S.; Norhausen, C.; Dingenouts, N.; Ballauff, M.; Narayanan, T.; Lindner, P. Small-Angle x-Ray and Neutron Scattering Studies of the Volume Phase Transition in Thermosensitive Core-Shell Colloids. *J. Chem. Phys.* **2001**, *114(23)* (23), 10471–10478. https://doi.org/10.1063/1.1374633.

(25) Secrist, K. E.; Nolte, A. J. Humidity Swelling/Deswelling Hysteresis in a Polyelectrolyte Multilayer Film. *Macromolecules* **2011**, *44* (8), 2859–2865. https://doi.org/10.1021/ma101983s.

(26) Bonnet, L.; Altemus, B.; Scarazzini, R.; Veillerot, M.; D'Agosto, F.; Faguet, J.; Jousseaume, V. Initiated-Chemical Vapor Deposition of Polymer Thin Films: Unexpected Two-Regime Growth. *Macromol. Mater. Eng.* **2017**, *302* (12), 1–9. https://doi.org/10.1002/mame.201700315.

III.2 Interlink between Tunable Material Properties and Thermoresponsiveness of Cross-Linked Poly(*N*-vinylcaprolactam) Thin Films Deposited by Initiated Chemical Vapor Deposition

Interlink between Tunable Material Properties and Thermoresponsiveness of Cross-Linked Poly(*N*-vinylcaprolactam) Thin Films Deposited by Initiated Chemical Vapor Deposition

Fabian Muralter,[†] Alberto Perrotta,[†] Oliver Werzer,[‡] and Anna Maria Coclite*[,†]

[†]Institute of Solid State Physics, NAWI Graz, Graz University of Technology, Petersgasse 16, 8010 Graz, Austria
[‡]Institute of Pharmaceutical Science, Department of Pharmaceutical Technology, University of Graz, Universitaetsplatz 1, 8010 Graz, Austria

Macromolecules — Article

Corresponding Author
*E-mail: anna.coclite@tugraz.at.
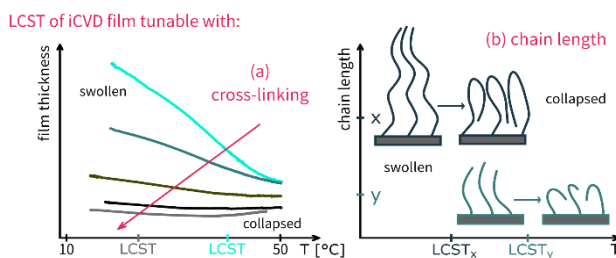
Reference: Muralter, F.; Perrotta, A.; Werzer, O.; Coclite, A. M. Interlink between Tunable Material Properties and Thermoresponsiveness of Cross-Linked Poly(*N*-vinylcaprolactam) Thin Films Deposited by Initiated Chemical Vapor Deposition. *Macromolecules* **2019**, *52* (18), 6817-6824. https://doi.org/10.1021/acs.macromol.9b01364.

III.2.1 Preface

The work for this publication was conducted mainly at the Graz University of Technology. Oliver Werzer performed nano-indentation measurements and the corresponding data evaluation at the University of Graz; he also provided support in preparing the manuscript. This thesis' author performed the sample preparation, the remaining characterization and data evaluation and wrote the manuscript. Alberto Perrotta helped in interpreting data and in preparing the manuscript. Anna Maria Coclite supervised the project and aided the manuscript preparation process. The published article is reproduced (text and illustrations identical) in the following with permission from ACS.

III.2.2 Abstract

In this contribution, we report on the thin-film synthesis of a novel thermoresponsive polymer, namely, poly(*N*-vinylcaprolactam) cross-linked by di(ethylene glycol) divinyl ether [p(NVCL-*co*-DEGDVE)] by initiated chemical vapor deposition (iCVD). Its transition between swollen and shrunken states in film thickness and the corresponding lower critical solution temperature (LCST) was investigated by spectroscopic ellipsometry in water. Water contact angle measurements and nano-indentation experiments reveal that the transition is accompanied by a change in wettability and elastic modulus. The amount of cross-linking was used to tune the thermoresponsive behavior of the thin films, resulting in higher swelling and LCST, increased surface rearrangement, and lower stiffness for less cross-linked polymers. For the first time, the filament temperature during iCVD synthesis was used to vary the chain length of the resulting polymeric systems and, thus, the position of their thermoresponsive transition. With that, swelling of up to 250% compared to the dry thickness and transition temperatures ranging from 16 to 40 °C could be achieved.

III.2.3 Introduction

Smart hydrogel materials can be used in a variety of sensor[1] and actuator[2] setups because of their ability to react to a number of external stimuli including temperature, pH, magnetic/electric fields, or concentrations of specific chemical species (e.g., glucose).[3] In an aqueous environment, such a hydrogel binds water molecules because of its network of hydrophilic polymer chains, making the material rearrange and swell to multiples of its dry size. Upon changing the environment, the smart polymer reversibly takes up water into or repels out water from its inherent structure.

Kinetically, the water exchange is time-limited by water diffusivity.[4] Thus, fast response times and, in turn, optimal device performance, can be achieved by employing thin polymeric films. However, the water exchange imposes stress on the film and could eventuate in delamination or mechanical failure. To ensure mechanical stability, a cross-linking agent can be co-polymerized with the monomer exhibiting the initially desired functionalities. The cross-linked hydrogel can be viewed as a polymer mesh (with a certain mesh size), which can take up a specific amount of water into its structure.[5]

The devices, where smart polymer thin films are usually applied, involve delicate surfaces (e.g., drugs and flexible substrates), oftentimes exhibiting sophisticated nanostructure, which need to be coated conformally. For these reasons, instead of ordinary solution processing, in this contribution,

initiated chemical vapor deposition (iCVD) was used. With this solvent-free technique, functional co-polymers of desired composition can be vapor-phase-synthesized similar to free radical polymerization processes.[6] The low substrate temperature employed (10-40 °C) allows for the coating also of delicate substrates. In these mild processing conditions, the full retention of delicate functional groups such as the adopted thermoresponsive species can be achieved upon deposition.

The chemical nature of monomer and cross-linker used in iCVD allows the further tailoring of the response behavior of the resulting smart polymer. For example, the most prominent thermoresponsive hydrogel, namely, poly-*N*-isopropylacrylamide (pNIPAAm), exhibits hydrophilic groups (i.e., amide) that are able to bind water and also the effective intrachain interactions causing the polymer to collapse.[7] The predominant behavior depends on temperature with the transition point being the lower critical solution temperature (LCST). Therefore, if in aqueous environment, the polymer accordingly undergoes a phase transition from a hydrated swollen state below to a dehydrated shrunken state above the LCST. Other thermoresponsive polymers with different functional groups interact differently with water and, therefore, vary in thermoresponsive behavior compared to pNIPAAm. For example, poly(*N,N*-diethylacrylamide) (pDEAAm) hydrogels show a broader LCST transition in water compared to pNIPAAm hydrogels.[8] In humidity, a similar trend has been reported for pDEAAm-based thin films deposited by iCVD.[9] Besides that, cross-linking has been reported to affect the thermoresponsiveness and, thus, where the LCST transition takes place. More hydrophobic[10] or hydrophilic[11] cross-linking agents can be used to deliberately control the direction of the shift.

As polymer synthesis is concerned, the NIPAAm monomer is solid at room temperature and exhibits low vapor pressure even at elevated temperatures (e.g., 85 °C); hence, different thermoresponsive agents are sought allowing for easier handling and, hence, enabling to exploit the full spectrum of possibilities in thin-film deposition by iCVD. Lee et al. reported on synthesizing another thermoresponsive polymer, namely, poly(*N*-vinylcaprolactam) (pNVCL), for the first time by iCVD.[12] This polymer is known for its nontoxicity and biocompatibility.[13] In contrast to, for example, pNIPAAm, its specific chemical structure (with the caprolactam ring) results in a 'classical' Flory-Huggins miscibility behavior, for which increasing the polymer chain length leads to a downward shift of the critical point (LCST).[13,14] For different molecular weight samples, transition temperatures in the range of ~30-40 °C have been reported.[14] Lee et al. reported on the synthesis of pNVCL homopolymer thin films by iCVD.[12] Pretreatment of the substrates by an oxygen plasma was used for grafting the polymer onto the surface.[12] In the present contribution, we aim at circumventing this step by introducing a cross-

linking agent that allows for stabilization of the thermoresponsive polymer layer on the substrate without further synthesis efforts. Moreover, the cross-linker used, namely, di(ethylene glycol) divinyl ether (DEGDVE), has been previously shown to allow for tuning of the thermoresponsiveness in pNIPAAm-based copolymers by our group.[9,15] Thus, the amount of DEGDVE will be utilized to tailor the response also of this novel co-polymer. To further tune the response properties of the deposited systems, we seek to employ the filament temperature during iCVD synthesis to control the molecular weight of the resulting polymers. We aim at demonstrating that differences in molecular weight will eventuate in differences in the position of the LCST transition for the first time.

III.2.4 Experimental Section

Thin-Film Synthesis

pNVCL-based thin films were deposited in a custom-built iCVD reactor. The experimental setup has already been described elsewhere.[15] In the present contribution, single-sided polished silicon wafer substrates with a native oxide of 1.6 nm thickness on top (Siegert Wafer, Germany) were used as substrates. All the depositions were run at substrate temperatures of 35 °C at a working pressure of 250 mTorr. tert-Butyl peroxide (TBPO, 98%; Aldrich, Germany), kept at room temperature, was used as the initiator at a flow rate of 1 sccm. The filament temperature was used to control the number of initiator radicals formed, as described in more detail later. N-Vinylcaprolactam (NVCL, 98%; Aldrich, Germany) is used as monomer and DEGDVE (99%; Aldrich, Germany) as cross-linker. To achieve the desired flow rates, NVCL and DEGDVE are kept at elevated temperatures of 78 and 70 °C, respectively. The monomer flow rate is set to 0.2 sccm. A series of films was deposited at a filament temperature of 200 °C with varying amounts of cross-linking in consequence of changing the cross-linker flow rate in the range of 0-2 sccm. Another series of samples with constant nominal cross-linking of 20% was deposited at varied filament temperatures between 165 and 215 °C, with and without nitrogen as patch flow; N_2 does not participate to the chemical reactions but allows for a better gas/vapor flow distribution in the reactor and was used at a flow rate of 2 sccm. For this series, the monomer and cross-linker flow rates were both kept constant at 0.2 sccm. All the corresponding p_M/p_{sat} values (ratios of the vapor pressure of the monomer/cross-linker to the saturation vapor pressure) are below 0.2, where a linear relation to the surface concentration of the chemical species has been reported for iCVD.[16]

In the present work, all the investigated p(NVCL-co-DEGDVE) thin films were deposited with similar film thickness values of (50 ± 5) nm. The series of thin films prepared with varying amounts of cross-linking was deposited

with average deposition rates of around 2 nm/min, whereas the filament temperature series varied in terms of average deposition rate between 0.1 and 2 nm/min, as described in more detail later.

Thin Film Characterization

Infrared absorbance spectra of the thin-film samples (1000 scans) were collected in transmission mode on a MB-102 (Bomem, Canada) Fourier transform infrared (FTIR) spectrometer in the wavenumber range 400-4000 cm^{-1} at a resolution of 4 cm^{-1} in mid IR mode.

Spectroscopic ellipsometry (SE) in a wavelength range of 370-1000 nm (M-2000S, J.A. Woollam, USA) was applied to determine film thickness and optical properties of the thin films in various environments (room temperature in nitrogen atmosphere or heating ramps in water). The swelling experiments in deionized water were performed in a temperature-controlled liquid stage (J. A. Woollam, USA). The recorded data was evaluated with an optical model consisting of a c-Si semi-infinite layer on the bottom (temperature dependent), a 1.6 nm thick native SiO$_2$ layer in the middle and the polymer film on top, modeled as a Cauchy function with an Urbach tail accounting for adsorption in the low-wavelength region. H$_2$O with temperature-dependent optical properties was set as the surrounding medium. For the temperature-dependent swelling experiments, the liquid stage and the mounted sample (already exposed to deionized water) were precooled to ~15 °C. The respective signal was then recorded while applying a temperature ramp from 15 to 50 °C at a heating rate of 0.5 °C/min. Directly after deposition, the thin-film samples were rinsed for 30 s with deionized water for equilibration. For thermal equilibration reasons reported earlier,[15,17] the temperature- dependent swelling behavior and the LCST of the iCVD thin films were evaluated from the third heating experiment. The SE measurements in dry N$_2$ atmosphere were performed in a THMS600 temperature stage (Linkam, UK) at room temperature (~25 °C). The samples were measured after 30 min of nitrogen flow, so that the film thickness would not vary for more than 0.5 nm in 5 min. The same optical model as in the liquid case has been used to evaluate the recorded data, but with the ambient material being set to air (n ≈ 1). Water contact angle (WCA) measurements were performed on a CAM 200 optical contact meter (KSV Instruments Ltd., Finland) equipped with a THMS600 temperature stage (Linkam, UK). For each measurement, the sample temperature was set to the desired value, measured with a thermocouple on the surface of the sample and equilibrated for 5 min before the actual water drop was applied. Advancing and receding contact angles were measured via the volume changing method. Thus, 5 drops were used on each sample and 15 advancing and 5 receding contact angles were evaluated for each sample.

For the mechanical properties of the swollen films, nanoindentation measurements were performed using an atomic force microscope (FlexAFM with

a C3000 controller from Nanosurf, Switzerland). A contact mode ContAl-G cantilever (Budgetsensor, Bulgaria) with a nominal tip radius of 10 nm was used. The spring constant was determined using the Sader thermal vibration approach.[18] The samples were measured using deionized water. The temperature was controlled by a bioheater (Nanosurf, Switzerland) with a control unit of Warner Instruments Corporation (Hamden, CT, USA). Deflection-separation curves were recalculated to force-versus-separation curves using MATLAB scripts employing the approach described elsewhere.[19] The apparent elastic moduli were derived and evaluated via the AtomicJ software package from 16 force curves measured on each sample.[20] The individual measurements were taken at different positions of 1 μm lateral separation.

III.2.5 Results and Discussion

Chemical Composition

For the first time, p(NVCL-*co*-DEGDVE) thin films with varying amounts of DEGDVE cross-linker content have been successfully polymerized by iCVD. Different degrees of cross-linking have been achieved by changing the cross-linker flowrate during deposition. The p_M/p_{sat} values in the applied temperature and pressure conditions have been used to precalculate the composition of the films to be deposited (i.e., nominal cross-linking degree) with the following formula

$$\text{DEGDVE fraction [\%]} = \frac{(p_M/p_{sat})_{\text{DEGDVE}}}{(p_M/p_{sat})_{\text{NVCL}} + (p_M/p_{sat})_{\text{DEGDVE}}}$$

The nominal DEGDVE fraction has been varied between 0 and 75%. As reported also in the literature,[21] such nominal cross-linker fraction does not always correspond to the real cross-linking fraction in the polymer. This is attributable to the different reaction rates of the polymerizable vinyl groups in the monomer and in the cross-linker. In particular, in this case, DEGDVE does not self-polymerize. Considering that it can only directly react with NVCL, it can be assumed that the maximum amount of incorporable DEGDVE should be around 30 and not 75%. Thus, a large quantity of DEGDVE adsorbed on the surface remains unreacted. While this behavior might be undesired, the dependency between nominal and real DEGDVE fraction is monotone; a higher nominal amount present on the surface during polymerization also gives a higher real amount of DEGDVE incorporated into the synthesized polymer, as confirmed by the experiments shown later.

To gain information about the chemical composition, the deposited films were investigated by FTIR absorbance spectroscopy. The FTIR data confirm the successful polymerization by all the recorded spectra not exhibiting characteristic vinyl group vibrations at 3150, 1620, and 1400 cm^{-1} as labeled

by Salzmann et al.[9] A representative spectrum of a nominally 75% cross-linked p(NVCL-*co*-DEGDVE) thin-film sample is shown in Figure III.2-1. The recorded absorption bands compare well to FTIR data of homopolymeric pNVCL films deposited by iCVD in the literature,[12] with all recorded peaks being successfully assigned to absorption bands within the chemical structure of pNVCL according to Lee et al.[12] The literature shows that DEGDVE is lacking strong characteristic FTIR absorption bands;[15,22] therefore, it is not possible to evaluate the cross-linker amounts from the FTIR data collected on nominally differently cross-linked samples.
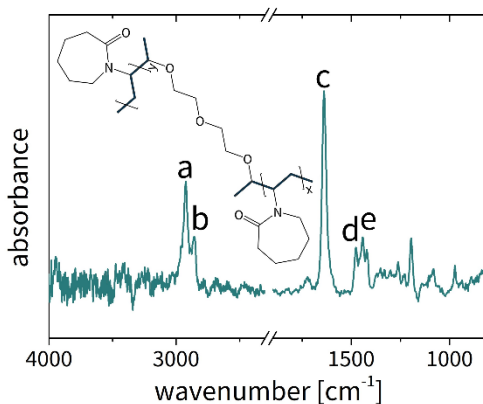
Label	Assignment	Position [cm^{-1}]
a	aliphatic C-H stretch (in ring)	2920
b	amine III (C-N)	2850
c	C=O stretch	1640
d	amide (C-N)	1480
e	aliphatic C-C (in ring)	1440

Figure III.2-1. FTIR absorption spectrum of a nominally 75% cross-linked p(NVCL-*co*-DEGDVE) 50 nm thin-film sample to indicate successful polymerization with the absence of characteristic vinyl group vibrations at 3150, 1620, and 1400 cm^{-1} as labeled by Salzmann et al.;[9] peaks of pNVCL assigned as labeled by Lee et al.[12]

Behavior in Water

Upon rinsing, samples exhibiting nominal degrees of cross-linking below 10% appear to swell (e.g., change in color) but are rather unstable in water and even delaminate from the substrate suggesting that an insufficient co-polymerization has taken place. In turn, the fact that stable films result for nominal cross-linking equal to or above 10% indicates that a successful co-polymerization of the monomer NVCL with the cross-linker DEGDVE was achieved. These samples allow then the swelling behavior to be investigated in more detail. Results of the temperature-dependent swelling experiments in water recorded by SE on the differently cross-linked polymers are shown in Figure III.2-2.

The swelling behavior changes with the cross-linker content. This tunability further proves the successful co-polymerization of NVCL and DEGDVE at different ratios.
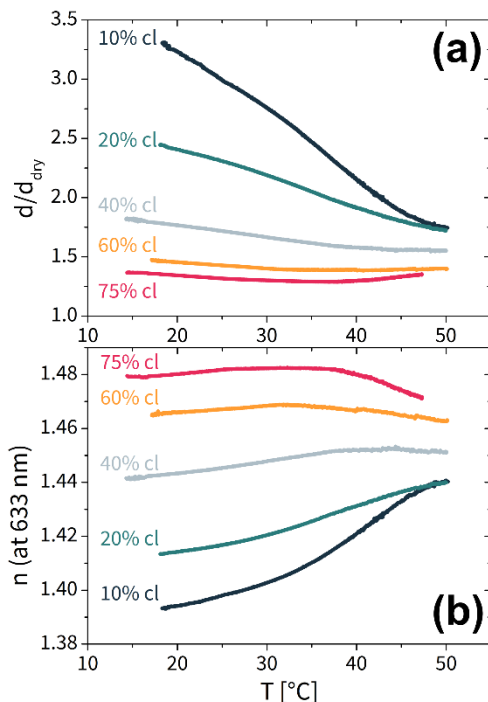

Figure III.2-2. Thickness of the swollen layers normalized by the dry thickness d/d_{dry} (a) and refractive index n (b) during swelling in water recorded by SE while applying heating ramps from ~15 to 50 °C for various differently cross-linked p(NVCL-*co*-DEGDVE) thin-film samples.

All samples presented in Figure III.2-2 show thermoresponsive swelling behavior by changing their film thickness and refractive index upon heating. The LCST values of the differently cross-linked p(NVCL-*co*-DEGDVE) samples have been evaluated as the mean values of the points of inflection of the respective swelling curves (exemplary data is shown in the Supporting Information). The LCST values are plotted in Figure III.2-3a as a function of the DEGDVE content. They vary from 40 to 23 °C. In the literature, an LCST of 31 °C was reported for a grafted pNVCL homopolymer thin film deposited by iCVD,[12] while we measure an LCST of 40 °C for the least cross-linked sample. We think such difference can be explained, hypothesizing that our samples exhibit lower molecular weight because they were deposited also at lower p_M/p_{sat}. The p_M/p_{sat} values employed during deposition and, as a consequence, the deposition rate, are known to influence the molecular weight of iCVD thin films, with increasing deposition rate yielding higher molecular weight polymers.[23] The LCST of pNVCL in water has been shown to strongly

depend on the molecular weight (i.e., chain length).[14] Meeussen et al. report on an increase of the viscosity-average molecular weight from 9 to 20 to 275 kg/mol lowering the transition temperature from 38 to 35 to below 30 °C, respectively.[14]
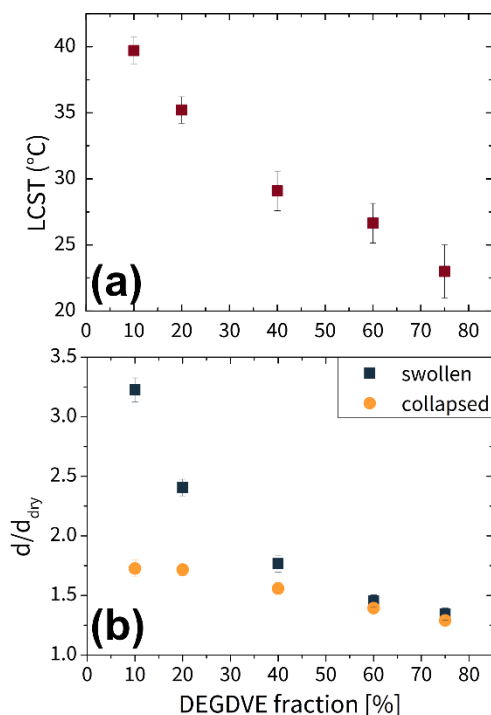

Figure III.2-3. (a) LCST and (b) thickness normalized by the dry thickness d/d_{dry} in the swollen (@20 °C) and in the collapsed state as a function of the nominal DEGDVE fraction of various differently cross-linked p(NVCL-*co*-DEGDVE) thin films.

Moreover, the results in Figure III.2-3a also show that the LCST decreases with adding DEGDVE to the polymeric structure, from 40 to 23 °C. This is in agreement with our previous work on DEGDVE, showing that the LCST of pNIPAAm-based thin films synthesized by iCVD also decreases with their DEGDVE content to a similar extent.[15] The hydrophobicity of the cross-linker has been deemed responsible for the downward shift of the LCST, allowing the polymer to push out water at lower temperatures.

Furthermore, the swollen and collapsed state were characterized by plotting the swelling ratio (measured thickness normalized by the respective thickness measured in dry N_2 atmosphere) in the swollen (@20 °C) as well as in the collapsed state in Figure III.2-3b.[*] Therefore, the more hydrophobic

---

[*] The collapsed state has been defined as the point, where the thickness is minimal from the curves recorded during temperature-dependent de-swelling upon heating (cf. Figure III.2-2). For the samples with 10 and 20% nominal DEGDVE fraction, the

nature of the thin films with higher amount of cross-linking can be seen in the degree of swelling at 20 °C (swollen) decreasing with the DEGDVE fraction. Please note, that for the more cross-linked samples 20 °C is also closer to the LCST (cf. Figure III.2-3a). However, in the collapsed state, the thickness normalized by the dry thickness also decreases with the DEGDVE content of the thin films (see Figure III.2-3b). This can be attributed to the fact that the mesh size of the more cross-linked thin films is smaller and, therefore, less water is retained in the polymeric system in the collapsed state.

Wettability

As the WCA probes a sample in terms of wettability and surface energy, the temperature-dependent swelling behavior of the differently cross-linked p(NVCL-*co*-DEGDVE) thin-film samples was also investigated by WCA measurements (Figure III.2-4). To avoid the kinetic effect of swelling interfering with the measurement, advancing and receding WCAs were determined. The advancing WCAs measured at several temperatures around the LCST transition of two differently cross-linked polymers (10 and 75%) are plotted in Figure III.2-4a. The advancing WCAs of the more cross-linked samples are lower than the values of the less cross-linked ones for all the substrate temperatures recorded. As the advancing WCA is viewed as a probe of the dry surface, these measurements hint at a more hydrophobic nature of the dry surface for the less cross-linked films. This can probably be attributed to the higher chain mobility compared to the more cross-linked sample, resulting in more surface rearrangement and more hydrophobic groups getting exposed to the polymer–air interface. The SE data showed that the less cross-linked samples take up significantly more water in the whole range of investigated temperatures (cf. Figure III.2-2). This is in agreement with the receding angle of the less cross-linked sample (10%) being lower than the receding angle of the more cross-linked one (75%). The corresponding receding WCAs are temperature-independent, exhibiting mean values of (21 ± 5)° and (29 ± 5)°, respectively. The ellipsometric data of Figure III.2-2 are taken in water and, therefore, they should be compared to the WCA measured after surface rearrangement at the polymer-water interface, that is, the receding angle. In addition, while SE records the consequences of the LCST transition averaged over the whole layer in depth (as film thickness and refractive index), WCA measurements are very surface-sensitive, probing only the outermost surface of the films. Therefore, SE shows a higher amount of water

---

values at 50 °C have been reported, as it is the upper limit of the measurement setup, although the LCST related de-swelling process is apparently not entirely finished at 50 °C in these cases (cf. respective curves in Figure III.2-2). In the collapsed state, for the more cross-linked samples, an increase in film thickness was observed after full de-swelling. We think that this can be attributed to thermal expansion of the polymer in water; this will be discussed in a following contribution.

taken up by a less cross-linked layer with the surface being more hydrophilic as evaluated from receding WCA measurements.
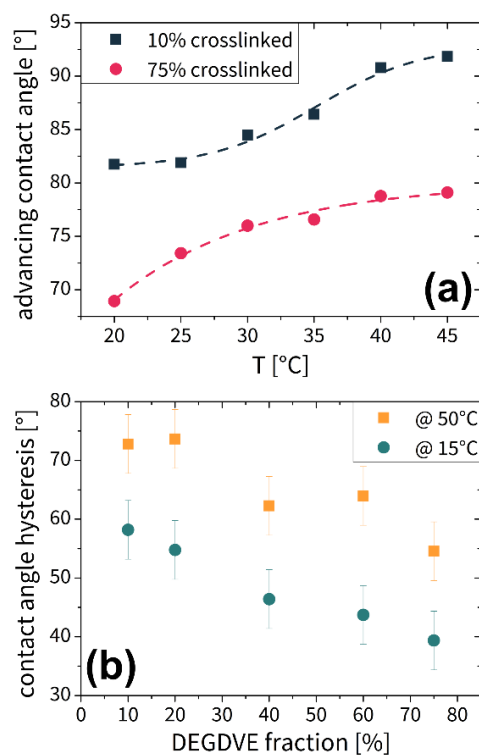

Figure III.2-4. (a) Advancing WCA of two differently cross-linked p(NVCL-*co*-DEGDVE) thin-film samples measured as a function of substrate temperature (dotted lines are for guidance of the eye; error bars are ±5° but have not been included in the plot for clarity) and (b) WCA hysteresis as a function of DEGDVE fraction for various differently cross-linked p(NVCL-*co*-DEGDVE) samples measured at 15 and 50 °C.

Moreover, the advancing WCA results (Figure III.2-4a) give evidence of a temperature-dependent transition of the surface from more hydrophilic at lower temperatures to more hydrophobic at higher temperatures. These results in temperature-dependent hydrophobicity/philicity of the surface also show the difference in transition temperature for the differently cross-linked samples, similar to the LCST values gained from SE measurements (cf. Figure III.2-3a).

Furthermore, WCA measurements reveal that the WCA hysteresis decreases with increasing the amount of cross-linking for the investigated series of p(NVCL-*co*-DEGDVE) thin-film samples (see Figure III.2-4b). The WCA hysteresis, as the difference between the advancing and receding WCAs, gives a measure about the ability of the surface for restructuring during water exposure. Hence, it is clear that cross-linking reduces this 'flexibility' of the

(surface) structure. Moreover, at higher temperatures, the more hydrophobic nature of the surface (in water) also makes for a higher hysteresis.

Mechanical Properties

To gain further understanding on the polymeric structures in the aqueous environment, the mechanical properties of the films have been probed by in situ force curve measurements. Force-separation profiles for the differently cross-linked samples were measured in water at 25 °C (Figure III.2-5a). Every measurement can be understood as the tip of the cantilever of the atomic force microscope (AFM) advancing toward the substrate surface from top (high apparent separation). Eventually, the tip gets in contact and starts to penetrate into the polymeric mesh (when the measured force starts to be larger than the noise). Upon further movement, the repulsion and the measured deflectional force increase and reach maximum values at 0 nm apparent separation; at this point, the mechanical properties of the cantilever used do not allow any further penetration. All the measured curves exhibit the described behavior; more cross-linked samples are less compressible than the ones with the lower cross-linker amount. The point where the tip starts to penetrate into the polymer mesh can be compared to the film thickness measured by SE at the respective temperature (cf. Figure III.2-2). For the least cross-linked samples (10 and 20%), the corresponding apparent separation is about 10-20 nm lower than the measured film thickness. Thus, the tip can penetrate most of the polymeric layer because of the mesh being large and/or the polymer being elastic enough. It should be noted that, in general, the true separation of the AFM tip from the substrate surface cannot be estimated using a setup like ours; the measured separation values just reflect the distance the tip is capable of compressing/penetrating the polymeric layer until the mechanical resistance of the layer gets too high. For the more cross-linked samples, the difference between the maximal apparent compression and the results from SE becomes more significant, meaning that the higher cross-linking results in a stronger resistance against the indentation of the tip, or its compression. For the sample with 75% cross-linking, hardly any compression can be observed, even though the sample has a nominal layer thickness of ~65 nm in water at 25 °C. In fact, at this temperature, the more cross-linked samples are closer to or even above their LCST (cf. Figure III.2-3a). The 75% cross-linked sample is, hence, in its 'collapsed state', hypothetically adding to the high stiffness observed (cf. Figure III.2-5b).

By modeling the data, the apparent elastic modulus (E) of the deposited systems could be extracted. To describe the force (F) as a function of the indentation depth (δ), we applied the Hertz equation for a parabolic shape AFM tip:[24]

$$F = \frac{4\sqrt{r_{tip}}}{3(1-\nu^2)} E\delta^{3/2}$$

As given by the manufacturer, the radius of the tip (r_{tip}) is 10 nm. The Poisson ratio ν was assumed as 0.5 and the spring constant of the cantilever used for all measurements was measured to be 0.24 N/m. The E values for the various samples are summarized in Figure III.2-5b. E increases from 5.8 MPa for 10% to 107.2 MPa for 75% nominal cross-linking measured at 25 °C in water, showing that with cross-linking, it is also possible to tune the mechanical properties. In comparison, for various end-grafted and highly extended polymer brushes, E values between 0.2 and 0.3 MPa have been reported,[24] while polymer brushes with 10 times higher grafting density show values in the range 30-80 MPa.[25] Furthermore, pNVCL has been previously employed to increase the elastic modulus of silicone rubber films from 1 MPa up to above 100 MPa.[26] In the present study, more cross-linking allowed for reaching high values of E in pNVCL-based thin films at a given temperature; this can be advantageous in actuator setups, where higher stiffness is in demand.
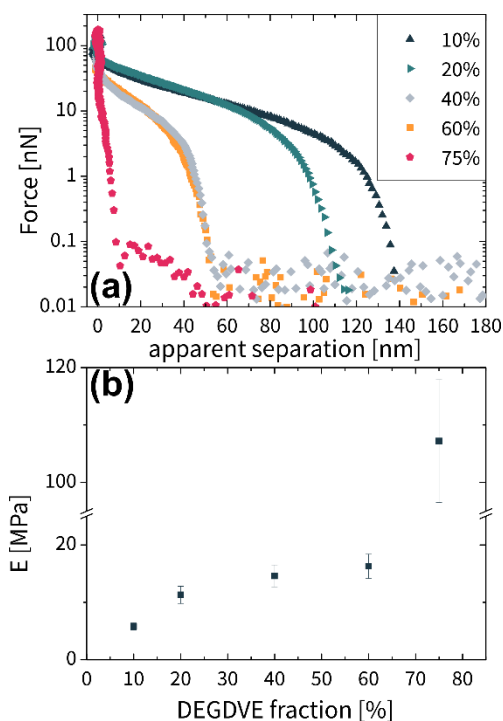

Figure III.2-5. Exemplary force-separation curves as measured by AFM for differently cross-linked p(NVCL-*co*-DEGDVE) samples (a) and their respective apparent elastic modulus E, as determined from the Hertz equation (b). The measurements were taken in water at 25 °C.

To investigate how the elasticity changes as the swelling is responding to a change in temperature, exemplary force curves for the sample of 10% cross-linking at different temperatures above and below its LCST of ~40 °C are shown in Figure III.2-6. At low temperatures, the layer can be compressed by about 140 nm. Increasing the temperature leads to a significant reduction of compression because of the collapse of the mesh. The calculation of the apparent elasticity reveals that the initial value of E at 25 °C (5.8 MPa) increases to 8.4 MPa at 36 °C and 12.2 MPa at 46 °C. The lower amount of swelling and the corresponding increased repulsion of adjacent meshes results in a reduction of the flexibility upon indentation.
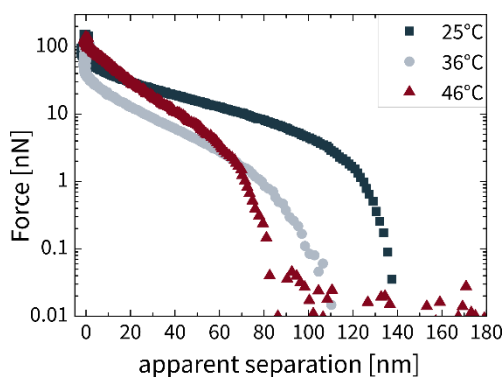
Figure III.2-6. Force-separation curves as measured by AFM on a 10% cross-linked p(NVCL-*co*-DEGDVE) sample at various temperatures above and below the LCST of ~40 °C in water.

Filament Temperature and Thermoresponsiveness

To investigate the effect of molecular weight on the LCST transition of p(NVCL-*co*-DEGDVE) thin films, the filament temperature (T_{fil}) was used to control the concentration of initiator radicals during polymerization. At ~150 °C, T_{fil} is sufficient to break the peroxide bond in the initiator molecules, leading to the formation radicals that initiate polymerization. Above 150 °C, Ozaydin-Ince et al. showed that the deposition rate increases proportionally to T_{fil}; hence, the filament temperature is proportional to the concentration of initiator radicals formed.[27] This relation makes it possible to distinguish between the initiation and the propagation step during polymerization, as only the first depends on the concentration of initiator radicals.[16] A lower filament temperature causes fewer radicals to be formed; while the initiation of new polymer chains should be decreased, the propagation of chains already existing remains unchanged, as this process does not require the presence of initiator radicals. Besides that, fewer termination events of polymer chains by initiator radicals will occur. Thus, the resulting smart polymer thin film should exhibit a polymeric structure with a larger molecular weight (i.e., longer chains). From the literature, it is known that for low filament temperatures (<270 °C), TBPO dominantly decomposes by cleavage

94

of the peroxide bond; in this case, primarily, the tert-butoxy radical is formed.[27] To ensure this (for reasons of simplicity), a series of samples has been deposited at filament temperatures between 165 and 215 °C with a constant nominal cross-linker amount of 20% with and without a patch flow of N_2. The flow rates of monomer, cross-linker, and initiator remained unchanged throughout the series. The low amounts (nm film thickness) of material deposited and the low solubility in common solvents due to cross-linking, make the experimental determination of the molecular weight not possible. However, the thermoresponsive swelling curves for samples deposited with N_2 (see Figure III.2-7a) indicate a strong difference in response behavior depending on the filament temperature in terms of transition temperature. The LCST decreases by 16 °C when T_{fil} is reduced from 200 down to 165 °C. Such change in LCST is twice as large as the one obtained by Meeussen et al. when the molecular weight of a pNVCL homopolymer was increased from 9 to 275 kg/mol.[14] This behavior can be attributed to the presence of DEGDVE as a cross-linking agent, being reported to lower the transition temperature also in NIPAAm-based co-polymers.[15]

Interestingly, the degrees of swelling of these samples (nominally 20% cross-linked, with N_2 patch flow) are more comparable to the one of the nominally 10% cross-linked sample of the previous cross-linker series (Figure III.2-7b). However, the LCST at ~33 °C still remains in the range of the nominally 20% cross-linked sample of that very series. Here, it has to be noted that introducing nitrogen as a carrier gas also reduces the p_M/p_{sat} values of the monomer and cross-linker used during iCVD. For example, deposition at a filament temperature of 200 °C and 2 sccm N_2 patch flow results in an average growth rate of 0.7 nm/min; lowering T_{fil} to 165 °C even yields 0.1 nm/min. Furthermore, a comprehensive review of pNVCL-based polymers showed that polymerization kinetics are challenging and controlling the co-polymerization of NVCL with other monomers is difficult because of the low vapor pressure of the NVCL monomer.[13] Growth kinetics seem to play an important role also in the co-polymerization process of NVCL with DEGDVE, but will be addressed in a future work, as this would go beyond the scope of the current contribution. Hypothetically, with changing the p_M/p_{sat}, the propagation kinetics are altered for NVCL and DEGDVE in a different way. The slower growth at lower p_M/p_{sat} (i.e., N_2 carrier gas) appears to alter the polymeric structure toward a more open mesh only being apparent when swollen. As the depositions are run in dry conditions (in vacuum), the polymer mesh grows in a collapsed state (as a reference state, cf. Harmon et al.[28]). Hence, also in water, the thickness fraction at elevated temperatures (i.e., collapsed state) is comparable to the one of the 20% cross-linked sample deposited without N_2 patch flow (see Figure III.2-7b).
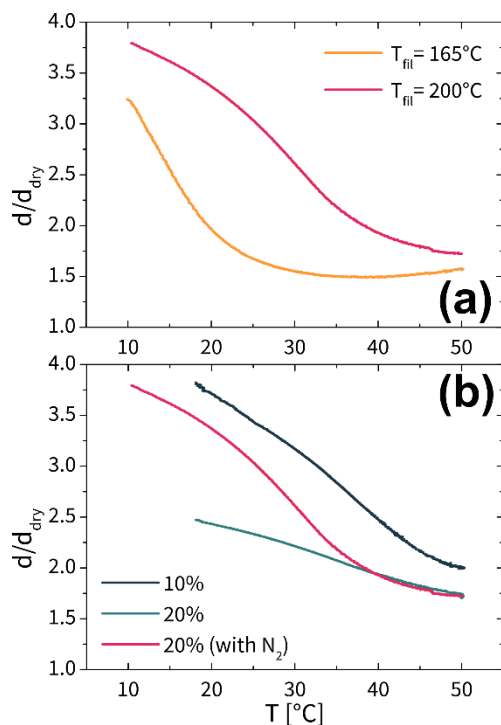
Figure III.2-7. Thickness of the swollen layers normalized by the dry thickness d/d_{dry} recorded by SE in water, while applying heating ramps from ~10 to 50 °C, for two nominally 20% cross-linked p(NVCL-*co*-DEGDVE) thin-film samples deposited (a) at different filament temperatures (T_{fil}) with N_2 patch flow; (b) measurement curves of samples deposited at T_{fil} = 200 °C without N_2 with nominal cross-linking of 10 and 20% (cf. Figure III.2-2) plotted together with the respective sample deposited with N_2 [see. (a)] for comparison of the degrees of swelling.

Nevertheless, with N_2 patch flow, by lowering the filament temperature from 200 to 165 °C, the degree of swelling stays comparable, whereas at the same time, the transition temperature decreases significantly, to ~16 °C. The longer polymer chains (i.e., lower filament temperature) appear to result in a similar mesh size, but a larger overall cross-linked structure making it possible to repel out water at lower temperatures. In the described way, the response of the newly developed thermoresponsive polymeric thin films can be tuned in transition temperature and toward very high degrees of swelling. Together with the resulting sharper transition (cf. Figure III.2-7), this tunability is crucial for the application in smart sensor setups.

A similar series of samples, deposited at different T_{fil} but without N_2, also resulted in sharper transitions for samples deposited at lower filament temperature, but constant transition temperature (see Supporting Information). The reason for such a behavior (e.g., unchanged molecular weight) could be

the fact that the used working conditions result in a mass transfer-limited process during iCVD synthesis of the polymer thin films. In these conditions, it has been reported that the filament temperature does not affect the deposition as it does in the reaction-kinetic regime (i.e., at higher flow rates).[27]

III.2.6 Conclusions

Novel pNVCL-based co-polymer thin films exhibiting promising thermoresponsive properties for sensor and actuator setups have been synthesized via iCVD for the first time. This study sheds light onto the swelling behavior of these p(NVCL-*co*-DEGDVE) systems and aims to reveal connections between deposition parameters, material properties, and the thermoresponsiveness of the deposited polymeric structures. Stable hydrogel thin films with different amounts of cross-linking were synthesized. The cross-linker amount was shown to change the amount of water uptake, with less cross-linked samples exhibiting higher swelling ratios. However, samples exhibiting nominal cross-linking below 10% are not stable in water. Furthermore, with increasing the amount of cross-linking, the transition temperature was shown to decrease because of the hydrophobicity of the cross-linker used.

The LCST transition has been observed to be present as a transition in wettability in WCA experiments. Furthermore, the WCA hysteresis showed that the surfaces are keener to rearrange in less cross-linked polymers. A force-separation study on the mechanical properties of the thin films by an AFM tip also revealed a denser polymeric mesh for more cross-linked samples with the apparent elastic modulus changing as a function of the cross-linker amount from 5.8 to 107.2 MPa at a constant temperature of 25 °C. During deswelling from temperatures below to above the LCST, the apparent elastic modulus of a 10% cross-linked sample is observed to double.

Moreover, the filament temperature affecting the chain length of the polymer has successfully been used to alter the thermoresponsiveness of p(NVCL-*co*-DEGDVE) thin films in a large range of transition temperatures (16-33 °C for similar cross-linking). Further investigations on the complex growth kinetics that lead to changes in the swelling behavior need to be addressed in future contributions.

Overall, we report on the successful synthesis of polymer thin films that swell up to 250% when compared to their thickness in the dry state (N_2 environment) with tunable transition temperatures in the range 16-40 °C, which is interesting for various applications in sensor and actuator setups.

III.2.7 Associated Content

Thickness and index as a function of temperature of a 40% cross-linked p(NVCL-*co*-DEGDVE) thin-film sample with their respective first and second derivatives to exemplarily show the evaluation of the LCST value from the data and swelling as a function of temperature in water of various 20% cross-linked p(NVCL-*co*-DEGDVE) thin-film samples deposited at filament temperatures between 185 and 215 °C without N_2 patch flow (PDF)
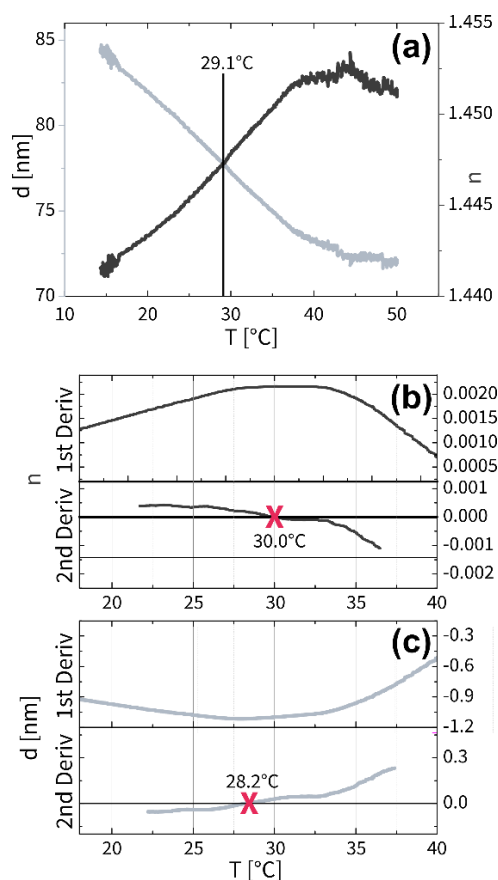

Figure III.2-S1. (a) Thickness d as recorded by spectroscopic ellipsometry during swelling in water while applying heating ramps from ~15 to 50 °C for a nominally 40% cross-linked p(NVCL-*co*-DEGDVE) thin film sample; (b) and (c) are the corresponding 1st and 2nd derivatives of the data in (a) for the evaluation of the LCST as the mean values of the respective points of inflection.
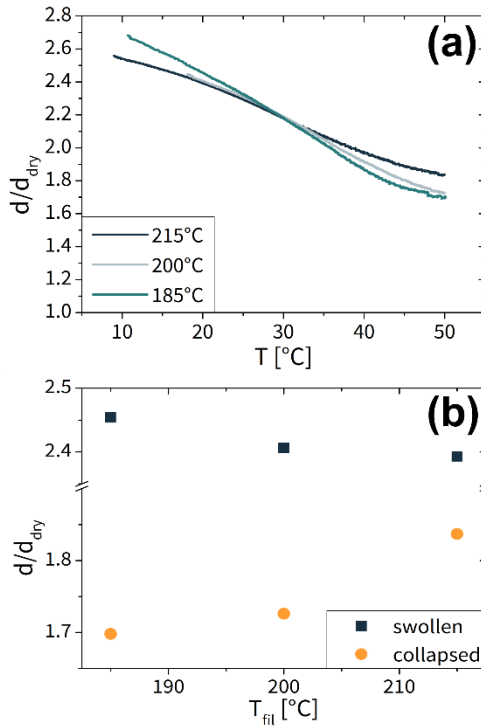
Figure III.2-S2. (a) Thickness normalized by the dry thickness d/d_{dry} during swelling in water recorded by spectroscopic ellipsometry while applying heating ramps from ~15 to 50 °C for various nominally 20% cross-linked p(NVCL-*co*-DEGDVE) thin film samples deposited at different filament temperatures (T_{fil}) between 185 °C and 215 °C without N_2 patch flow and (b) d/d_{dry} of the respective samples in the swollen (at 20 °C) and collapsed (at 50 °C) state plotted as a function of T_{fil}.

Figure III.2-2 shows that the swelling degrees remain similar and the transition temperature remains unchanged (in the range of ~33-35 °C) for 20% cross-linked p(NVCL-*co*-DEGDVE) thin film samples deposited at various filament temperatures (T_{fil}) between 185 and 215 °C. However, the degree of swelling below (at 20 °C) and above (at 50 °C) the LCST appear further apart for lower T_{fil}, corresponding to a sharper transition for samples deposited at lower filament temperature. We hypothesize that the mean value of the resulting molecular weight distribution does not change; however, the distribution seems to change slightly, as the transition gets sharper for samples deposited at lower filament temperature.

The reason for the LCST and, thus, the molecular weight remaining similar despite changing T_{fil} could be the fact that the used working conditions (see experimental section) result in a mass transfer limited process during iCVD synthesis of the polymer thin films. There, the filament temperature has

been reported to not affect the deposition as it does in the reaction-kinetic regime (i.e., at higher flow rates).[i]

(i)   Ozaydin-Ince, G.; Gleason, K. K. Transition between Kinetic and Mass Transfer Regimes in the Initiated Chemical Vapor Deposition from Ethylene Glycol Diacrylate. *J. Vac. Sci. Technol. A Vacuum, Surfaces, Film.* **2009**, *27* (5), 1135–1143. https://doi.org/10.1116/1.3168553.

III.2.8 Acknowledgments

III.2.9 References

(1) Palagi, S.; Mark, A. G.; Reigh, S. Y.; Melde, K.; Qiu, T.; Zeng, H.; Parmeggiani, C.; Martella, D.; Sanchez-Castillo, A.; Kapernaum, N.; Giesselmann, F.; Wiersma, D. S.; Lauga, E.; Fischer, P. Structured Light Enables Biomimetic Swimming and Versatile Locomotion of Photoresponsive Soft Microrobots. *Nat. Mater.* **2016**, *15* (6), 647–653. https://doi.org/10.1038/nmat4569.

(2) Ramakrishnan, N.; Vamsi, T.; Khan, A.; Nemade, H. B.; Palathinkal, R. P. Humidity Sensor Using NIPAAm Nanogel as Sensing Medium in SAW Devices. *Int. J. Nanosci.* **2011**, *10* (01n02), 259–262. https://doi.org/10.1142/S0219581X11007880.

(3) Chu, L. Y.; Xie, R.; Ju, X. J.; Wang, W. Smart Hydrogel Functional Materials. In *Smart Hydrogel Functional Materials*; Springer-Verlag: Berlin, Heidelberg, 2013; pp V–VII. https://doi.org/10.1007/978-3-642-39538-3.

(4) Beebe, D. J.; Moore, J.; Bauer, J. M.; Yu, Q.; Liu, R. H.; Devadoss, C.; Jo, B. H. Functional Hydrogel Structures for Autonomous Flow Control inside Micro-Fluidic Channels. *Nature* **2000**, *404* (6778), 588–590. https://doi.org/10.1038/35007047.

(5) Canal, T.; Peppas, N. A. Correlation between Mesh Size and Equilibrium Degree of Swelling of Polymeric Networks. *J. Biomed. Mater. Res.* **1989**, *23* (10), 1183–1193. https://doi.org/10.1002/jbm.820231007.

(6) Lau, K. K. S.; Gleason, K. K. Initiated Chemical Vapor Deposition (ICVD) of Poly(Alkyl Acrylates): An Experimental Study. *Macromolecules* **2006**, *39* (10), 3688–3694. https://doi.org/10.1021/ma0601619.

(7) Liu, R.; Fraylich, M.; Saunders, B. R. Thermoresponsive Copolymers: From Fundamental Studies to Applications. *Colloid Polym. Sci.* **2009**, *287* (6), 627–643. https://doi.org/10.1007/s00396-009-2028-x.

(8) Panayiotou, M.; Freitag, R. Influence of the Synthesis Conditions and Ionic Additives on the Swelling Behaviour of Thermo-Responsive Polyalkylacrylamide Hydrogels. *Polymer* **2005**, *46* (18), 6777–6785. https://doi.org/10.1016/j.polymer.2005.06.060.

(9) Salzmann, P.; Perrotta, A.; Coclite, A. M. Different Response Kinetics to Temperature and Water Vapor of Acrylamide Polymers Obtained by Initiated Chemical Vapor Deposition. *ACS Appl. Mater. Interfaces* **2018**, *10* (7), 6636–6645. https://doi.org/10.1021/acsami.7b18878.

(10) Alf, M. E.; Hatton, T. A.; Gleason, K. K. Novel N-Isopropylacrylamide Based Polymer Architecture for Faster LCST Transition Kinetics. *Polymer* **2011**, *52* (20), 4429–4434. https://doi.org/10.1016/j.polymer.2011.07.051.

(11) Pena-Francesch, A.; Montero, L.; Borrós, S. Tailoring the LCST of Thermosensitive Hydrogel Thin Films Deposited by ICVD. *Langmuir* **2014**, *30* (24), 7162–7167. https://doi.org/10.1021/la5003594.

(12) Lee, B.; Jiao, A.; Yu, S.; You, J. B.; Kim, D. H.; Im, S. G. Initiated Chemical Vapor Deposition of Thermoresponsive Poly (N-Vinylcaprolactam) Thin Films for Cell Sheet Engineering. *Acta Biomater.* **2013**, *9* (8), 7691–7698. https://doi.org/10.1016/j.actbio.2013.04.049.

(13) Cortez-Lemus, N. A.; Licea-Claverie, A. Poly(N-Vinylcaprolactam), a Comprehensive Review on a Thermoresponsive Polymer Becoming Popular. *Prog. Polym. Sci.* **2016**, *53*, 1–51. https://doi.org/10.1016/j.progpolymsci.2015.08.001.

(14) Meeussen, F.; Nies, E.; Berghmans, H.; Verbrugghe, S.; Goethals, E.; Du Prez, F. Phase Behaviour of Poly(N-Vinyl Caprolactam) in Water. *Polymer (Guildf).* **2000**, *41* (24), 8597–8602. https://doi.org/10.1016/S0032-3861(00)00255-X.

(15) Muralter, F.; Perrotta, A.; Coclite, A. M. Thickness-Dependent Swelling Behavior of

Vapor-Deposited Smart Polymer Thin Films. *Macromolecules* **2018**, *51* (23), 9692–9699. https://doi.org/10.1021/acs.macromol.8b02120.

(16) Lau, K. K. S.; Gleason, K. K. Initiated Chemical Vapor Deposition (ICVD) of Poly(Alkyl Acrylates): A Kinetic Model. *Macromolecules* **2006**, *39* (10), 3695–3703. https://doi.org/10.1021/ma0601621.

(17) Christian, P.; Coclite, A. M. Vapor-Phase-Synthesized Fluoroacrylate Polymer Thin Films: Thermal Stability and Structural Properties. *Beilstein J. Nanotechnol.* **2017**, *8* (1), 933–942. https://doi.org/10.3762/bjnano.8.95.

(18) Sader, J. E.; Chon, J. W. M.; Mulvaney, P. Calibration of Rectangular Atomic Force Microscope Cantilevers. *Rev. Sci. Instrum.* **1999**. https://doi.org/10.1063/1.1150021.

(19) Butt, H.-J.; Cappella, B.; Kappl, M. Force Measurements with the Atomic Force Microscope: Technique, Interpretation and Applications. *Surf. Sci. Rep.* **2005**, *59* (1–6), 1–152. https://doi.org/10.1016/J.SURFREP.2005.08.003.

(20) Hermanowicz, P.; Sarna, M.; Burda, K.; Gabryś, H. AtomicJ: An Open Source Software for Analysis of Force Curves. *Rev. Sci. Instrum.* **2014**, *85* (6), 063703. https://doi.org/10.1063/1.4881683.

(21) Coclite, A. M.; Lund, P.; Di Mundo, R.; Palumbo, F. Novel Hybrid Fluoro-Carboxylated Copolymers Deposited by Initiated Chemical Vapor Deposition as Protonic Membranes. *Polymer* **2013**. https://doi.org/10.1016/j.polymer.2012.11.004.

(22) Alf, M. E.; Hatton, T. A.; Gleason, K. K. Initiated Chemical Vapor Deposition of Responsive Polymeric Surfaces. *Thin Solid Films* **2011**, *519* (14), 4412–4414. https://doi.org/10.1016/j.tsf.2011.01.286.

(23) Lau, K. K. S.; Gleason, K. K. Initiated Chemical Vapor Deposition (ICVD) of Poly(Alkyl Acrylates): An Experimental Study. *Macromolecules* **2006**, *39* (10), 3688–3694. https://doi.org/10.1021/ma0601619.

(24) Kutnyanszky, E.; Vancso, G. J. Nanomechanical Properties of Polymer Brushes by Colloidal AFM Probes. *Eur. Polym. J.* **2012**, *48* (1), 8–15. https://doi.org/10.1016/J.EURPOLYMJ.2011.09.008.

(25) Julthongpiput, D.; LeMieux, M.; Tsukruk, V. . Micromechanical Properties of Glassy and Rubbery Polymer Brush Layers as Probed by Atomic Force Microscopy. *Polymer* **2003**, *44* (16), 4557–4562. https://doi.org/10.1016/S0032-3861(03)00404-X.

(26) Pino-Ramos, V. H.; Flores-Rojas, G. G.; Alvarez-Lorenzo, C.; Concheiro, A.; Bucio, E. Graft Copolymerization by Ionization Radiation, Characterization, and Enzymatic Activity of Temperature-Responsive SR-g-PNVCL Loaded with Lysozyme. *React. Funct. Polym.* **2018**, *126*, 74–82. https://doi.org/10.1016/J.REACTFUNCTPOLYM.2018.03.002.

(27) Ozaydin-Ince, G.; Gleason, K. K. Transition between Kinetic and Mass Transfer Regimes in the Initiated Chemical Vapor Deposition from Ethylene Glycol Diacrylate. *J. Vac. Sci. Technol. A Vacuum, Surfaces, Film.* **2009**, *27* (5), 1135–1143. https://doi.org/10.1116/1.3168553.

(28) Harmon, M. E.; Kuckling, D.; Pareek, P.; Frank, C. W. Photo-Cross-Linkable PNIPAAm Copolymers. 4. Effects of Copolymerization and Cross-Linking on the Volume-Phase Transition in Constrained Hydrogel Layers. *Langmuir* **2003**, *19* (26), 10947–10956. https://doi.org/10.1021/la030217h.

III.3 Wrinkling of an Enteric Coating Induced by Vapor-Deposited Stimuli-Responsive Hydrogel Thin Films

Wrinkling of an Enteric Coating Induced by Vapor-Deposited Stimuli-Responsive Hydrogel Thin Films

Fabian Muralter,*,† Anna Maria Coclite,† and Oliver Werzer‡

†Institute for Solid State Physics, NAWI Graz, Graz University of Technology, 8010 Graz, Austria
‡Institute of Pharmaceutical Science, Department of Pharmaceutical Technology, University of Graz, 8010 Graz, Austria
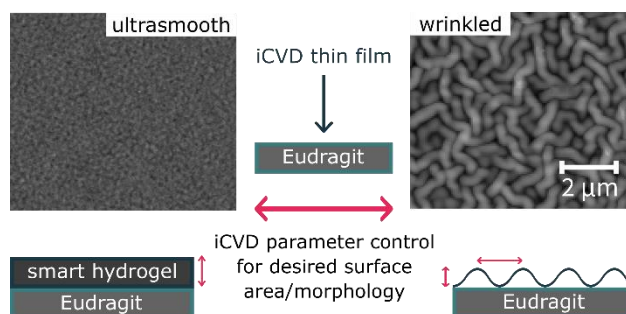
Reference: Muralter, F.; Coclite, A. M.; Werzer, O. Wrinkling of an Enteric Coating Induced by Vapor-Deposited Stimuli-Responsive Hydrogel Thin Films. *J. Phys. Chem. C* **2019**, *123* (39), 24165−24171. https://doi.org/10.1021/acs.jpcc.9b07340.

III.3.1 Preface

The work for this publication was conducted jointly at the University of Graz and the Graz University of Technology. Oliver Werzer (co)supervised the project, performed the atomic force microscopy measurements and provided support in preparing the manuscript. This thesis' author performed the sample preparation, all the remaining characterization, data evaluation and wrote the manuscript. Anna Maria Coclite advised the project and helped in the manuscript preparation process. The contribution as it is presented in the following sections is reproduced from the published article (text and illustrations identical) with permission from the publisher.

III.3.2 Abstract

In this contribution, we report on the thin-film synthesis of a thermoresponsive polymer onto another polymer used as an enteric coating in drug applications. In particular, we deposit cross-linked poly(*N*-vinylcaprolactam) (pNVCL) thin films by initiated chemical vapor deposition (iCVD) onto spincoated Eudragit (EUD) layers. Already upon iCVD synthesis, the layered structure starts to form wrinkles at a minimum iCVD thickness of 30 nm. By changing the EUD layer thickness and the amount of cross-linking used during iCVD, the morphology of the wrinkles is demonstrated to be readily tunable. Laterally, the double-layer structures vary in morphology from being ultrasmooth to exhibiting up to a 3.5 μm wrinkle wavelength. The surface roughness and, thus, the wrinkles' height can be tailored from below 1 nm up to 100 nm. From the resulting wavelength of wrinkles, an estimation of the elastic modulus of pNVCL proves its tunability over a wide range of values thanks to the iCVD process. This study elucidates an uncomplicated way to tune the wrinkles' morphology and, thus, the surface area of a system that can be employed in drug delivery applications. Hence, an enteric coating of EUD together with an iCVD-synthesized thermoresponsive thin film is proposed as a promising composite encapsulation layer to outperform established systems in terms of tunability of the response to multiple external stimuli.

III.3.3 Introduction

Besides fundamental interest in wrinkling, wrinkled structures are used in applications, where an enhancement of the surface area yields superior device performance. In photovoltaics, a larger contact area in pn-junctions allows for accessing higher currents, while structures used for light scattering would also enhance energy harvesting.[1,2] In biomedical applications, the larger areas produced by wrinkles are, according to Noyes-Whitney, responsible for higher dissolution rates and, thus, enable faster drug release.[3]

Wrinkling occurs in many situations in nature[4] or can be artificially employed.[5] While the former might display its consequences meeting the needs of specific purposes, the manmade induction of wrinkles allows for studying the fundamental mechanisms in more detail. Very often, a substrate is coated by another substance so that both form a strong connection.[6] Upon changing some environmental parameters such as temperature or pressure, the response of both will be distinct; differences in expansion might result in cracks,[7] while compression of some flexible material, eventually, induces wrinkling.[8] Typical examples are metal layers on compliant substrates.[9] For polymeric samples, such behavior is often observed on prestrained substrates; depositing a coating onto the strained substrate and, subsequently,

releasing the strain causes the structure to wrinkle. Employing anisotropic strain and release might even result in the formation of directed wrinkles.[10] Recently, isotropic wrinkle formation was also found to occur during the preparation of drug encapsulation layers employing a chemical vapor deposition (CVD) technique; the results showed that wrinkling occurs even without prestraining the substrate and, thus, directly upon coating an amorphous drug.[11] While the direction of the wrinkles is not adjustable, the wrinkles' size (height and wavelength) were clearly dependent on the thickness of the encapsulated layer. Further, the nature of the solid state of the encapsulated drug layer directly influenced the capability of wrinkle formation; while crystalline drug layers prevented the formation of wrinkles, an amorphous state was observed to induce wrinkled structures. Also, the chemical composition of the CVD coating had an impact not only on the wrinkle formation[12] but also on the stabilization of the amorphous state of the drug in general.[13]

Employing initiated chemical vapor deposition (iCVD) as a solvent-free process allows for the coating also of delicate substrates, which might even be liquid. The underlying mechanism is similar to free-radical polymerization processes,[14] where an initiator (typically, a peroxide) is decomposed into radicals at a heated filament, which interact with a monomer so that polymer synthesis is initiated, propagated by further monomer units until terminated by another radical. With the possibility of employing a plethora of chemical structures of the monomer, vast amounts of distinct polymers can be synthesized and conformally deposited onto three-dimensional (3D)-nanostructured substrates. For applications, the synthesis of smart polymer thin films is particularly interesting. Numerous polymers responding to variations in humidity, pH, salt, or solutes present in a solution have been developed.[15,16] For instance, temperature-responsive hydrogel encapsulations (e.g., poly(N-isopropylacrylamide)-based polymers, pNIPAAm) were reported to allow for the control of the release of drugs as a function of temperature; the release could even be slowed down at higher temperatures.[12] Cross-linking of the polymeric structures, for instance, by copolymerizing di(ethylene glycol) divinyl ether (DEGDVE) together with the monomer exhibiting the desired functionalities, enables the variation of the polymers' swelling behavior.[16,17] Recently, another interesting polymer, namely, poly(N-vinylcaprolactam) (pNVCL), has been synthesized by iCVD allowing for further tunability of the polymeric thermoresponsiveness. Importantly, this polymer is biocompatible, making it a promising candidate also for other medical applications, where coating might assist some purpose, i.e., abrasion or cell adhesion.

In this contribution, we study the wrinkle formation upon iCVD synthesis of a thermoresponsive polymer thin film (i.e., p(NVCL-co-DEGDVE)) directly

onto another polymer, being Eudragit E100 (EUD). EUD is typically employed as a drug coating itself, adopting solution-based techniques; it is soluble at low pH and only swells at larger pH, typically above 5, making it usable as an enteric coating. On addition of the thermoresponsive pNVCL-based thin film, the temperature response can be tuned in potential applications. On the one hand, a superior coating might be achieved by the tunability in the thermoresponsiveness of pNVCL and the enteric properties of EUD. On the other hand, the larger surface area due to wrinkling might be used to alter the release behavior of the resulting structures, when used for encapsulation purposes.

III.3.4 Experimental Section

Single crystal silicon wafers (Siegert Wafers, Germany) with a native oxide layer were used as substrates. Substrates were prepared by cutting the wafers into 2×2 cm^2 pieces, sonicating them in EtOH and acetone baths, and, finally, drying under a nitrogen stream. An amino methacrylate copolymer with the tradename Eudgagit E100 from Evonik (Germany) is a coating material typically used in pharmaceutical applications. The material was used as delivered. For the sample preparation, the material was dissolved in toluene (Sigma-Aldrich, Germany) at different concentrations. Using a standard spin coater employing a spin speed of 17 rps for 60 s, this allowed to deposit homogeneous layers of EUD ranging in thickness between a couple of nm up to nearly 1 µm. The thickness of these layers was determined using a spectroscopic ellipsometer (M-2000S, J.A. Woollam). The measurements were performed in a wavelength range of 370-1000 nm at three angles (65/70/75°). The experimental data was fitted within the CompleteEASE software package by an optical model consisting of a Si semi-infinite layer on the bottom, a 1.6 nm thick native SiO$_2$ layer in the middle, and the EUD film on top. The substrate materials were modeled by the corresponding material files available within the software, and the EUD layer was modeled as a Cauchy function with an Urbach tail accounting for adsorption in the low-wavelength region.

Poly(*N*-vinylcaprolactam-*co*-di(ethylene glycol) divinyl ether) thin films were synthesized by initiated chemical vapor deposition. The depositions were run in a custom-built iCVD reactor described elsewhere.[17] *N*-Vinylcaprolactam (NVCL, 98%; Sigma-Aldrich, Germany) is used as the monomer and di(ethylene glycol) divinyl ether (DEGDVE, 99%; Sigma-Aldrich, Germany) as the cross-linker. NVCL and DEGDVE are delivered to the reactor from their individual glass jars held at elevated temperatures: 78 and 70 °C, respectively. The monomer flow rate (NVCL) is set to 0.2 sccm; the DEGDVE flow rate is varied to employ different amounts of cross-linking.

The corresponding ratios of vapor pressures of the monomer and initiator to their saturation vapor pressures (p_M/p_{sat}) in the employed temperature and pressure conditions are considered for estimating the resulting compositions. All of the corresponding p_M/p_{sat} values are below 0.2 and, thus, lie in a range, where a linear relation to the surface concentration of the chemical species has been reported.[18] The applied flow rates yield polymer layers of p(NVCL-*co*-DEGDVE) with a nominal cross-linking of 20-85%, as evaluated from the ratio of employed p_M/p_{sat} values at a working pressure of 250 mTorr and a substrate temperature of 35 °C. A filament temperature of 200 °C was used for all presented depositions. To monitor the deposited thickness, in situ laser interferometry with a He-Ne laser (λ = 633 nm; Thorlabs) is performed through a removable quartz glass lid. All samples of the cross-linker series exhibit film thickness values of 100 ± 5 nm; moreover, a film thickness series with 45% of nominal cross-linking has been deposited with 10, 30, and 50 nm layer thicknesses.

Atomic force microscopy (AFM) measurements were performed using a FlexAFM (Nanosurf, Switzerland) equipped with a C3000 controller. The tapping mode measurements were performed using a Tap300-Al from Budget-Seonsors (Bulgaria). Data processing and analysis were performed using the software package Gwyddion.[19] For the extraction of the roughness, the implemented statistic evaluation was used, from which its uncertainty was also estimated. As the wrinkles are randomly oriented in a lateral dimension, a simple line-scan analysis cannot be performed. Therefore, we used a two-dimensional (2D) fast Fourier transform of the AFM height data. From this calculation, we evaluated the radial information by summing over distances from zero and fitting a Lorentzian function to it to extract the peak position that corresponds to the wrinkle wavelength. The uncertainty of fitting yields the uncertainty for the wavelength extracted.

III.3.5 Results and Discussion

Spacer Thickness Dependence

Eudragit (EUD) is readily soluble in various solvents up to high amounts. This makes it possible to use techniques like spin coating for the deposition of homogeneous thin films, e.g., on silicon wafer substrates. By applying different polymer concentrations, fully closed EUD thin films with thicknesses ranging from 20 to 800 nm, as determined by spectroscopic ellipsometry, were prepared. The resulting layers are amorphous and, if touched, sticky; the films are very smooth so that AFM analysis did not reveal any structural features.

On top of such an amorphous EUD layer, an additional polymer layer can be directly synthesized by iCVD. For a first set of samples, we deposited 100 nm

p(NVCL-*co*-DEGDVE) with a cross-linker content of 35%. Thin EUD films (up to 40 nm) coated by the iCVD layer show a rather smooth and homogeneous morphology (see Figure III.3-1, top left). Small spots of 5 nm in height exhibiting radii of about 100 nm are also observable but appear less frequent. In fact, these kinds of structures are only present when the EUD layers are thin. In a recent study using iCVD-deposited poly(2-hydroxyethyl methacrylat) (pHEMA) as an encapsulation for drug layers, a very similar behavior has been observed, i.e., particle-like structures concomitantly being present with rather smooth areas.[11] Using thicker EUD layers of 100 nm, the onset of wrinkle formation on the sample surface can be observed, while the mentioned spots are hardly noticeable anymore (see Figure III.3-1, top right).
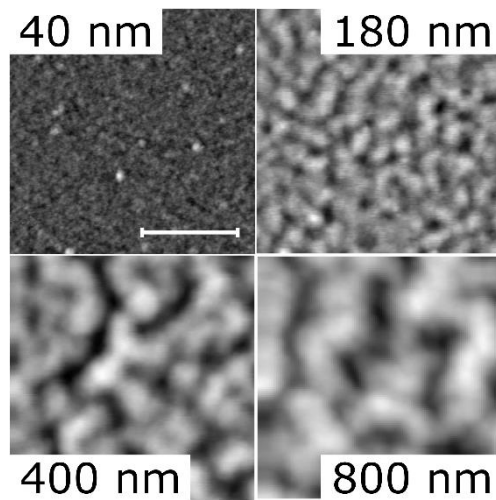

Figure III.3-1. Exemplary atomic force microscope images of wrinkle formation of various EUD-iCVD double layers; the thickness of the EUD film was varied (as indicated in the pictures), while the thickness of the 35% cross-linked iCVD thin film was kept constant at 100 nm (the scale bar indicates 2 μm and applies for all images; individual gray scales for heights).

The evaluation of such surfaces can be performed in various ways. Here, the root-mean-square roughness σ_{rms} and the lateral wavelength of the structures λ, both calculated directly from the AFM height data, are plotted in Figure III.3-2. For statistical reasons, these data were determined from scans of larger size (up to 50×50 μm^2), while the data in Figure III.3-1 elucidate more details on a smaller scale. For samples of a 100 nm EUD thickness or less, the small structures reflected in the roughness value remain comparably small; a root-mean-square roughness of $\sigma_{rms} = 2$ nm or below was identified. For these samples of low EUD thickness, the evaluation of the lateral wavelength from the AFM data was not unambiguously possible due to the low roughness and the random statistical nature of the surface structure.
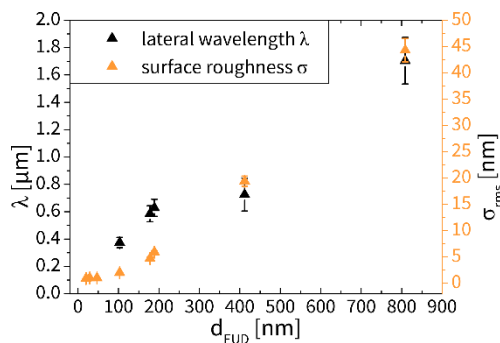
Figure III.3-2. Development of the root-mean-square roughness σ_{rms} of an EUD-iCVD double-layer system (35% cross-linked) as evaluated by AFM as a function of the EUD layer thickness d_{EUD}; the lateral wavelength of the structures λ was evaluated for the same samples from a 2D fast Fourier transform and is plotted on the right y-axis.

At a 180 nm EUD thickness, the morphology appears to be different and the formation of pronounced wrinkles is observed. The evaluation of the surface roughness shows an increase to around σ_{rms} = 6 nm. For these samples, the evaluation of the wrinkle wavelength reveals more precise and regular information and an average lateral size of about 600 nm could be extracted. It can be noted that, to a certain extent, σ_{rms}, determined here by the software, represents the amplitude of the structures (i.e., a measure for the deviation up and down from an average height).

For samples prepared from even thicker EUD layers, the situation remains similar, with homogeneous wrinkles being present on the entire surface; the surface roughness and lateral size of the apparent structures increase proportionally to the film thickness of the EUD layer (see Figure III.3-2). For an EUD layer of 800 nm, the roughness increases to a maximum value of 45 nm. On the same sample, a lateral structure with a wavelength of about 1.6 μm developed. The shallowness of these structures, apparent when comparing the thickness of the layer of about 900 nm (EUD and iCVD) to the relatively low roughness of 45 nm, suggests that the character of the wrinkles is more two-dimensional rather than fully 3D down to the substrate surface.

Cross-Linker Density

Besides the spacer thickness dependence, the observed wrinkle formation has also been studied as a function of cross-linking of the p(NVCL-*co*-DEGDVE) coating. By employing the iCVD technique for the synthesis of thin films, one can easily adjust the amount of cross-linking by changing the cross-linker flow rate during synthesis. This can have various effects on the film's performance. For instance, a cross-linking agent prevents the thin film from delaminating from the substrate when in contact with water.

p(NVCL-*co*-DEGDVE) thin films deposited by iCVD were reported to be stable above 10% cross-linking.[20] Further, cross-linking alters the swelling response of the hydrogel layer drastically when in contact with water or just specifically humid environments.[17,20] In medical or drug applications, this enables the tunability of release profiles of a drug out from an iCVD encapsulation with the dissolution rate being adjustable by orders of magnitude.[12] In the present contribution, we study the impact of the cross-linker amount used in iCVD synthesis on the film morphology, when deposited onto EUD films. In Figure III.3-3, exemplary AFM images of samples with about 400 nm EUD spacers coated by 100 nm p(NVCL-*co*-DEGDVE) thin films with varying cross-linker amounts are summarized.

For the sake of direct comparability, the average dark/brightness of the images in Figure III.3-3 gives an indication on the roughness of the structures using the exact same height scale of 250 nm for all images. Upon inspection, the overall roughness appears to increase with increasing the amount of cross-linking from 20% (top left) to 85% (bottom right). The low surface roughness (σ_{rms} = 4 nm) of the 20% cross-linked sample indicates a rather flat homogeneous surface. When a part of the image of the 20% cross-linked sample (top left) is adjusted in the height scale (see the inset), additional features appear, which are very similar to those observed when the onset of wrinkling is not entirely reached yet (cf. Figure III.3-1). For the same EUD layer thickness of about 400 nm, a sample coated with a cross-linking density of 35% clearly shows the presence of wrinkles; a roughness of about 20 nm was found, which is about 5 times higher than the 20% cross-linked system was able to induce. At cross-linking contents of 60 and 85%, large wrinkles develop, with the roughness increasing to 30 and 36 nm, respectively. In general, a change in morphology is often observed in different stages of wrinkling.[5,21] For instance, in the present contribution, the morphology of the wrinkles appears to be more round/hexagonal and very shallow for low amounts of cross-linking. When the cross-linker amount is increased, the situation changes toward more elongated wrinkles also exhibiting more pronounced height variations.

The surface roughness (σ_{rms}) as evaluated from the AFM data as a function of the spacer thickness (EUD coating) for various differently cross-linked p(NVCL-*co*-DEGDVE) systems can be found in Figure III.3-4. For low EUD spacer thickness (below 30 nm), similar surface roughness values (below 2 nm) were evaluated for all deposited cross-linker amounts. The surface morphology does not indicate wrinkle formation in that film thickness regime.
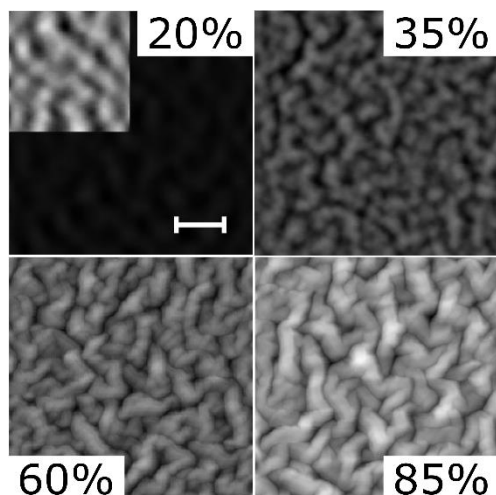
Figure III.3-3. AFM height images of samples with 400 nm EUD layers coated with various differently cross-linked 100 nm p(NVCL-*co*-DEGDVE) thin films (20-85% as indicated in the images). The scale bar represents 2 μm and applies for all images; the same gray scale for heights ranging from 0 to 250 nm (black to weight). For a region of the image of a 20% cross-linked sample (top left), the maximum of the gray scale/white was ad justed to 25 nm enhancing the visibility of surface structures.

Above 30 nm of EUD, the differently cross-linked polymer thin films lead to a strong dependence of the surface roughness on the spacer layer thickness, but each cross-linker amount results in distinct behavior. As already shown for the samples with a 400 nm spacer layer thickness (see Figure III.3-3), the data in Figure III.3-4 reveals that the surface roughness increases with increasing the cross-linker amount of the hydrogel in all of the range of investigated spacer layer thicknesses. From the respective AFM data, also the onsets (minimum spacer thickness values) of wrinkle formation as a function of cross-linking were evaluated. As an indication, one can see the significant change in morphology (from homogeneous to wrinkled) observable in the AFM height images. Nevertheless, for statistical reasons, another approach is used: at small spacer thickness, the samples appear to have a rather similar and homogeneous morphology exhibiting surface roughness values around 1 nm. At higher thickness, the surface roughness appears to depend linearly on the spacer layer thickness with increasing slopes for increasing cross-linker amounts. Using this second regime, extrapolation to zero surface roughness by linear regression fits shows that the onset of wrinkling is taking place at around 320 nm spacer thickness when the cross-linker is just 20%. Increasing the cross-linker amount, the onset shifts to 100 nm (at 35% cross-linker), 50 nm (at 60% cross-linker), and down to about 40 nm for the largest density of cross-linking (85%).
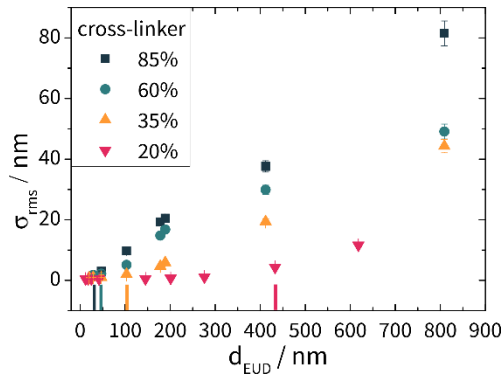
Figure III.3-4. Root-mean-square surface roughness (σ_{rms}) as a function of the spacer thickness (EUD) for various samples coated with 100 nm p(NVCL-*co*-DEGDVE) thin films with varying amounts of cross-linking as given in the legend; the onset thickness of wrinkle formation as evaluated by the morphology of the films is indicated at the x-axis as dashes for the respectively cross-linked systems (matching colors).

Again, the lateral wavelength of the wrinkles (λ) was determined from a 2D fast Fourier transform of the AFM data and plotted in Figure III.3-5a for the differently cross-linked samples. Thin spacer layers and low amounts of cross-linking do not result in significant wrinkling and, thus, unambiguous wavelength determination. Hence, the relatively small roughness of the samples with 20% nominal cross-linking did not allow for a determination of the wrinkle wavelength. For all of the other investigated samples, λ steadily increases with increasing the spacer thicknesses.

In the literature, there are several great examples of how the size of such wrinkles can be explained. For our previous work, when the iCVD layer was deposited on an amorphous drug layer made from clotrimazole, we used a model assuming a stiff film on a compliant substrate of similar thickness. For the case of an incompressible substrate (i.e., here EUD), an analytical expression can be derived, which relates the wrinkle wavelengths (λ), the thicknesses (d), and the elastic moduli (E) of the components

$$\frac{\lambda}{2\pi \times d_{iCVD}} = \sqrt{\frac{d_{EUD}}{d_{iCVD}}\left(\frac{E_{iCVD}}{18 \times E_{EUD}}\right)^{1/6}}$$

From a double-logarithmic plot of the normalized experimental data[11] (i.e., $\frac{\lambda}{d_{iCVD}}$ over $\frac{d_{EUD}}{d_{iCVD}}$), the ratio of the elastic moduli of the iCVD layer (E_{iCVD}) and the EUD layer (E_{EUD}) was determined from the intercept of the linear fit of the respective data with slope 0.5 with the y-axis (y_{int}, see Figure III.3-5b).
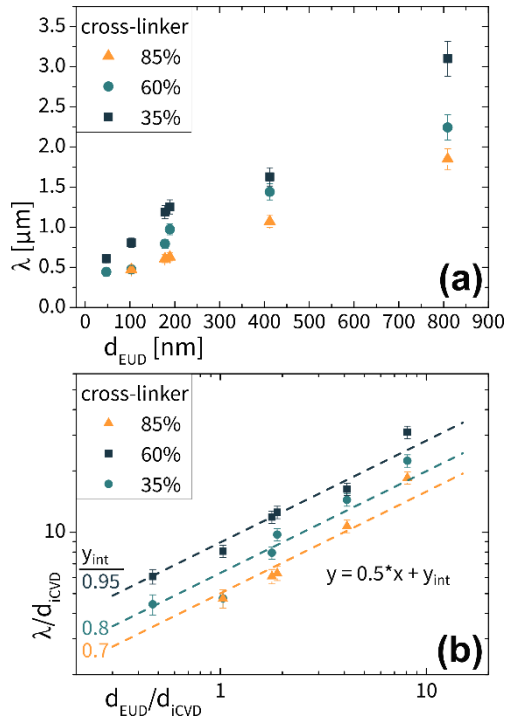
Figure III.3-5. (a) Wavelength λ as evaluated from the AFM height images of differently cross-linked (35, 60, and 85%) p(NVCL-*co*-DEGDVE) layers of 100 nm thickness (d_{iCVD}) deposited on EUD layers of different thickness (d_{EUD}); (b) plot for the evaluation of the ratio of iCVD to EUD elastic modulus for the differently cross-linked systems from linear fits of the plotted data (respective intercept with the y-axis, y_{int}).

The respective ratios are calculated by the following formula

$$\frac{E_{iCVD}}{E_{EUD}} = 18 \times \left(\frac{10^{y_{int}}}{2\pi}\right)^{1/6}$$

Performing the evaluation of the samples with 85% nominal cross-linking reveals that the elastic modulus of the iCVD layer is about 128 times larger than the one of the underlying EUD layers. In a previous contribution, we estimated the apparent elastic moduli of differently cross-linked p(NVCL-*co*-DEGDVE) thin films swollen in water to lay between 5 and 120 MPa, with E increasing with cross-linking.[20] The elastic modulus in air is expected to be at least 1 order of magnitude higher and should, thus, be in a range as for most polymers (e.g., polystyrene about 3.8 GPa within films).[22] The elastic modulus of EUD is unknown, but 128 times higher elasticity would suggest that the material is in a rubbery state with a rather low E-value. As the substrate temperature was held at 35 °C during iCVD synthesis and the EUD possesses a T_g of around 45 °C[23] with a typical layer thickness dependence of the T_g,[24] this might support this estimation.

For the samples with 60 and 35% cross-linker amounts, the elastic modulus ratios were determined to be 18 and 5, respectively. The magnitude of the range of values appears to be consistent with the assumption that the amount of cross-linking is directly related to the elastic modulus. This assumption has been proven to be present in the swollen state of differently cross-linked p(NVCL-*co*-DEGDVE) thin films.[20]

In general, for the wrinkling to take place, at least two slabs of materials with deviating properties need to be in contact. Strain in the system or differences in the mechanical properties can induce wrinkling. In the case of the investigated EUD-iCVD double layers, it can be assumed that the EUD is rather relaxed with minimum or even absent strain after the spin-coating process in its amorphous state. Upon iCVD synthesis, the monomers and the initiator radicals arrive at the substrate and adsorb at the EUD-air interface. Eventually, initiator radicals attack the vinyl bonds of the adsorbed species, which leads to polymerization of these monomer units. As the components are highly reactive, the synthesis is a rather fast process and just limited by the amount of material being present on the substrate in the applied conditions. As such, the time for adapting to low energetic steric sites is limited, causing the material to evolve in a strained state. With the strain exceeding the mechanical strength of the underlying EUD layer, wrinkling will be induced. The amount of wrinkling is then dependent on the amount of strain and the difference in the elastic moduli of the materials involved. High cross-linking of the iCVD polymer causes a higher rigidity, resulting in a reduced capability of adapting to steric limitations and, thus, more strain might be introduced by applying more cross-linked polymers. In a similar manner, having differences in the amount of cross-linking changes the chemical appearance, which, for instance, alters the surface energy of the deposited material. This is reflected in the (advancing) water contact angle changing from below 70° for 75% cross-linked p(NVCL-*co*-DEGDVE) thin films up to more than 80° for lower cross-linker amounts, as just recently determined.[20] Thus, the hydrophilic cross-linker reduces the hydrophobicity. As there was no change in the EUD layer surface, this change can result in a different energetic contribution (difference in surface energies) and superimpose the strain developing during deposition.[25]

iCVD Thickness Dependence

Intuitively, one follow-up question arises: is the induced strain already present at the beginning of the deposition, i.e., in the first nanometers, or does it vary with layer thickness of the iCVD film? To evaluate these considerations, several depositions (all being 45% cross-linked) exhibiting different iCVD thicknesses were carried out on similar EUD layers with varying thicknesses. Again, an AFM analysis has been carried out on the different systems; AFM height images are shown in Figure III.3-6. As described earlier,

wrinkle formation appears to yield more pronounced wrinkles with larger morphology and, hence, no wrinkle formation could be identified (see Figure III.3-6 bottom); the surface roughness remains at the value of the underlying layer of around 1 nm. At a 30 nm top layer thickness, wrinkles start to appear. They are similarly pronounced in height when compared to the 50 nm thick films as the surface roughness (σ_{rms}) is around 7 nm for the 30 and 50 nm films deposited on top of the 100 nm EUD layer. Correspondingly, σ_{rms} remains at around 13 nm, no matter if 30 or 50 nm of iCVD film is deposited on the 200 nm EUD layers. However, the wrinkles seem to grow in the lateral dimension between 30 and 50 nm of the deposited iCVD polymer. For the deposition on top of the 100 nm EUD layers, the lateral wavelength of the wrinkles (λ) increases from 0.3 µm for 30 nm of deposition to 0.6 µm for 50 nm. For the 200 nm EUD layers, the situation is similar, whereas λ was determined to be 0.5 µm for 30 nm of the iCVD polymer and 1 µm for 50 nm.
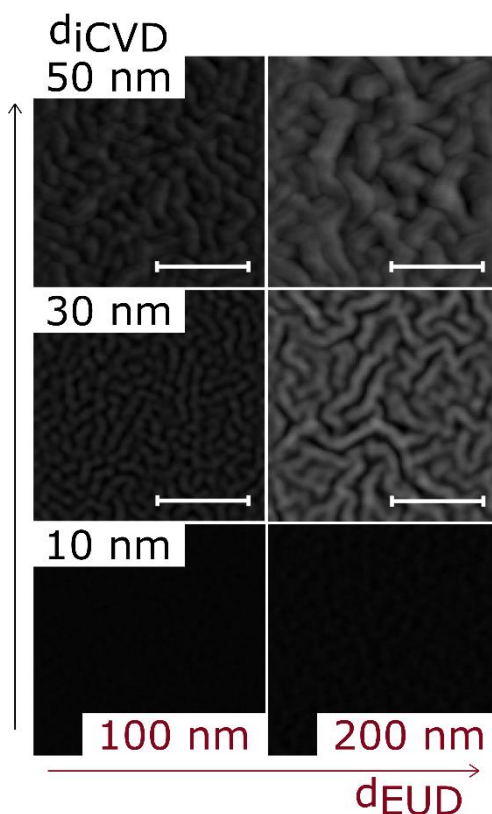

Figure III.3-6. AFM height images of samples with 100 and 200 nm EUD layers coated with various differently thick p(NVCL-*co*-DEGDVE) thin films (10, 30, and 50 nm); the scale bars indicate 2 µm and apply for all images; the gray scale corresponding to heights is defined in the range of 0-200 nm (black to white).

As can be seen by comparing the AFM height images in the middle and top of Figure III.3-6, the top layer thickness can also be used to alter the resulting wrinkle morphology. As for 30 nm of iCVD layer thickness, rather homogeneous wrinkled structures can be observed; the 50 nm samples appear to be more chaotic/inhomogeneous in terms of morphological diversity.

III.3.6 Conclusions

Wrinkling phenomena might be used in a variety of different fields. For the induction, often, prestrain is required. Wrinkling can directly be observed when the iCVD polymer is synthesized on top of another polymer layer, here made from EUD. For such a purpose, the lack of solvents used in iCVD is particularly advantageous. Changing the thickness of the underlying layer results in the ability to adjust the wrinkles induced in terms of morphology. Both the surface roughness (as a measure of the amplitude) and the wrinkle wavelength increase with increasing the spacer thickness, whereas the absolute value of the wavelength is always much larger than that of the amplitude. While this suggests that this is an effect, especially altering the surface of the layers, the variation in spacer thickness changing the surface structure over a large range of employed thicknesses hints toward a more general rearrangement of the entire layers. The iCVD technique is very versatile so that parameters like the flow rates can be used to tailor the properties of the deposited iCVD layers in a wide range of directions. The results here show that variation in cross-linker amount affects the onset of wrinkling and the wrinkle morphology. It can be expected that further variation in the iCVD process would also result in the further tunability of the resulting wrinkles in the investigated systems; among others, deposition rate, substrate temperature, or filament temperature might be varied easily, resulting in altered polymer properties. In a similar manner, different substrates can be employed to alter the wrinkling. While not shown here, stiff materials like PS or PMMA did not allow for the development of wrinkles upon applying p(NVCL-*co*-DEGDVE) thin films on top, while EUD even facilitates their extensive tunability. The addition of a material into the EUD polymeric film matrix (like a plasticizer) enables even further possibilities to change the wrinkling behavior. Having such possibilities, applications like light diffusion in solar cells or even surface enlargement in medication might be re-engineered to outperform established systems.

III.3.7 Acknowledgments

III.3.8 Note Added after ASAP Publication

This paper was published ASAP on August 30, 2019, and due to a production error the Figure III.3-2 graphic was incorrect. The corrected version was reposted on September 18, 2019.

III.3.9 References

(1)   Kim, J. B.; Kim, P.; Pégard, N. C.; Oh, S. J.; Kagan, C. R.; Fleischer, J. W.; Stone, H. A.; Loo, Y.-L. Wrinkles and Deep Folds as Photonic Structures in Photovoltaics. *Nat. Photonics* **2012**, *6* (5), 327–332. https://doi.org/10.1038/nphoton.2012.70.

(2)   Ryu, S. Y.; Seo, J. H.; Hafeez, H.; Song, M.; Shin, J. Y.; Kim, D. H.; Jung, Y. C.; Kim, C. S. Effects of the Wrinkle Structure and Flat Structure Formed During Static Low-Temperature Annealing of ZnO on the Performance of Inverted Polymer Solar Cells. *J. Phys. Chem. C* **2017**, *121* (17), 9191–9201. https://doi.org/10.1021/acs.jpcc.7b02149.

(3)   Chaieb, S.; Natrajan, V. K.; El-rahman, A. A. Glassy Conformations in Wrinkled Membranes. *Phys. Rev. Lett.* **2006**, *96* (7), 078101. https://doi.org/10.1103/PhysRevLett.96.078101.

(4)   Cerda, E.; Mahadevan, L. Geometry and Physics of Wrinkling. *Phys. Rev. Lett.* **2003**, *90* (7), 074302. https://doi.org/10.1103/PhysRevLett.90.074302.

(5)   González-Henríquez, C. M.; Sarabia Vallejos, M. A.; Rodríguez-Hernández, J. Strategies for the Fabrication of Wrinkled Polymer Surfaces. In *Wrinkled Polymer Surfaces*; Springer International Publishing: Cham, 2019; pp 19–59. https://doi.org/10.1007/978-3-030-05123-5_2.

(6)   Kato, M.; Tsuboi, Y.; Kikuchi, A.; Asoh, T.-A. Hydrogel Adhesion with Wrinkle Formation by Spatial Control of Polymer Networks. *J. Phys. Chem. B* **2016**, *120* (22), 5042–5046. https://doi.org/10.1021/acs.jpcb.6b01449.

(7)   Awaja, F.; Zhang, S.; Tripathi, M.; Nikiforov, A.; Pugno, N. Cracks, Microcracks and Fracture in Polymer Structures: Formation, Detection, Autonomic Repair. *Prog. Mater. Sci.* **2016**, *83*, 536–573. https://doi.org/10.1016/J.PMATSCI.2016.07.007.

(8)   Chung, J. Y.; Douglas, J. F.; Stafford, C. M. A Wrinkling-Based Method for Investigating Glassy Polymer Film Relaxation as a Function of Film Thickness and Temperature. *J. Chem. Phys.* **2017**, *147* (15), 154902. https://doi.org/10.1063/1.5006949.

(9)   Gao, N.; Zhang, X.; Liao, S.; Jia, H.; Wang, Y. Polymer Swelling Induced Conductive Wrinkles for an Ultrasensitive Pressure Sensor. *ACS Macro Lett.* **2016**, *5* (7), 823–827. https://doi.org/10.1021/acsmacrolett.6b00338.

(10)   Gu, J.; Li, X.; Ma, H.; Guan, Y.; Zhang, Y. One-Step Synthesis of PHEMA Hydrogel Films Capable of Generating Highly Ordered Wrinkling Patterns. *Polymer* **2017**, *110*, 114–123. https://doi.org/10.1016/J.POLYMER.2016.12.076.

(11)   Christian, P.; Ehmann, H. M. A.; Werzer, O.; Coclite, A. M. Wrinkle Formation in a Polymeric Drug Coating Deposited via Initiated Chemical Vapor Deposition. *Soft Matter* **2016**, *12* (47), 9501–9508. https://doi.org/10.1039/C6SM01919F.

(12)   Christian, P.; Tumphart, S.; Ehmann, H. M. A.; Riegler, H.; Coclite, A. M.; Werzer, O. Controlling Indomethacin Release through Vapor-Phase Deposited Hydrogel Films by Adjusting the Cross-Linker Density. *Sci. Rep.* **2018**, *8* (1), 7134. https://doi.org/10.1038/s41598-018-24238-w.

(13)   Christian, P.; Ehmann, H. M. A.; Coclite, A. M.; Werzer, O. Polymer Encapsulation of an Amorphous Pharmaceutical by Initiated Chemical Vapor Deposition for Enhanced Stability. *ACS Appl. Mater. Interfaces* **2016**, *8* (33), 21177–21184. https://doi.org/10.1021/acsami.6b06015.

(14)   Lau, K. K. S.; Gleason, K. K. Initiated Chemical Vapor Deposition (ICVD) of Poly(Alkyl Acrylates): An Experimental Study. *Macromolecules* **2006**, *39* (10), 3688–3694. https://doi.org/10.1021/ma0601619.

(15)   Chu, L.-Y.; Xie, R.; Ju, X.-J.; Wang, W. Smart Hydrogel Functional Materials. In *Smart

Hydrogel Functional Materials; Springer-Verlag: Berlin, Heidelberg, 2013; pp V–VII. https://doi.org/10.1007/978-3-642-39538-3.

(16)   Pena-Francesch, A.; Montero, L.; Borrós, S. Tailoring the LCST of Thermosensitive Hydrogel Thin Films Deposited by ICVD. *Langmuir* **2014**, *30* (24), 7162–7167. https://doi.org/10.1021/la5003594.

(17)   Muralter, F.; Perrotta, A.; Coclite, A. M. Thickness-Dependent Swelling Behavior of Vapor-Deposited Smart Polymer Thin Films. *Macromolecules* **2018**, *51* (23), 9692–9699. https://doi.org/10.1021/acs.macromol.8b02120.

(18)   Lau, K. K. S.; Gleason, K. K. Initiated Chemical Vapor Deposition (ICVD) of Poly(Alkyl Acrylates): A Kinetic Model. *Macromolecules* **2006**, *39* (10), 3695–3703. https://doi.org/10.1021/ma0601621.

(19)   Nečas, D.; Klapetek, P. Gwyddion: An Open-Source Software for SPM Data Analysis. *Cent. Eur. J. Phys.* **2012**, *10* (1), 181–188. https://doi.org/10.2478/s11534-011-0096-2.

(20)   Muralter, F.; Perrotta, A.; Werzer, O.; Coclite, A. M. Interlink between Tunable Material Properties and Thermo-Responsiveness of Cross-Linked Poly(N-Vinylcaprolactam) Thin Films Deposited by Initiated Chemical Vapor Deposition. *Macromolecules* **2019**, *in press*. https://doi.org/10.1021/acs.macromol.9b01364.

(21)   Guvendiren, M.; Burdick, J. A. The Control of Stem Cell Morphology and Differentiation by Hydrogel Surface Wrinkles. *Biomaterials* **2010**, *31* (25), 6511–6518. https://doi.org/10.1016/J.BIOMATERIALS.2010.05.037.

(22)   Miyake, K.; Satomi, N.; Sasaki, S. Elastic Modulus of Polystyrene Film from near Surface to Bulk Measured by Nanoindentation Using Atomic Force Microscopy. *Appl. Phys. Lett.* **2006**, *89* (3), 031925. https://doi.org/10.1063/1.2234648.

(23)   Jadhav, N. R.; Gaikwad, V. L.; Nair, K. J.; Kadam, H. M. Glass Transition Temperature: Basics and Application in Pharmaceutical Sector. *Asian J. Pharm. Free full text Artic. from Asian J Pharm* **2014**, *3* (2), 82–89. https://doi.org/10.22377/AJP.V3I2.246.

(24)   David S. Fryer; Richard D. Peters; Eui Jun Kim; Jeanne E. Tomaszewski; Juan J. de Pablo, A.; Nealey*, P. F.; And, C. C. W.; Wu, W. Dependence of the Glass Transition Temperature of Polymer Films on Interfacial Energy and Thickness. *Macromolecules* **2001**, *34* (16), 5627–5634. https://doi.org/10.1021/MA001932Q.

(25)   Huang, R.; Stafford, C. M.; Vogt, B. D. Wrinkling of Ultrathin Polymer Films. *MRS Proc.* **2006**, *924*, 0924-Z04-10. https://doi.org/10.1557/PROC-0924-Z04-10.

III.4 Applicability of Vapor-Deposited Thermoresponsive Hydrogel Thin Films in Ultrafast Humidity Sensors/Actuators

Applicability of Vapor-Deposited Thermoresponsive Hydrogel Thin Films in Ultrafast Humidity Sensors/Actuators
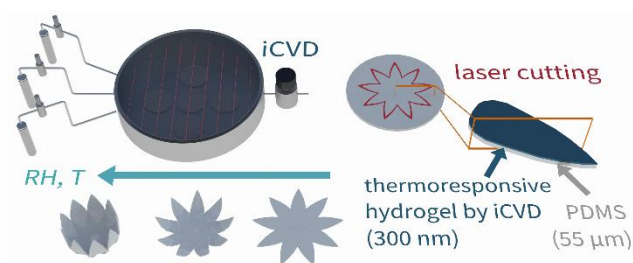
Fabian Muralter,* Francesco Greco, and Anna Maria Coclite

Institute of Solid State Physics, NAWI Graz, Graz University of Technology, Petersgasse 16, 8010 Graz, Austria

Corresponding Author
*(F.M.) E-mail: fmuralter@tugraz.at.

Reference: Muralter, F.; Greco, F.; Coclite, A. M. Applicability of Vapor-Deposited Thermoresponsive Hydrogel Thin Films in Ultrafast Humidity Sensors/Actuators. *ACS Appl. Polym. Mater.* **2020**, *2* (3), 1160-1168. https://doi.org/10.1021/acsapm.9b00957.

III.4.1 Preface

The work presented in this article was conducted at the Graz University of Technology. The author of this thesis performed the sample preparation, characterization, data evaluation and wrote the manuscript. Hannah Kaspret, an FIT intern (Frauen in die Technik program) at the Institute of Solid State Physics of TU Graz, helped building the flower-like devices. Francesco Greco supported the preparation and characterization of these devices and supported the manuscript preparation. Anna Maria Coclite supervised the project and helped in the manuscript preparation process. The published article is reproduced in the following sections with their text and illustrations being identical to the ones in the scientific publication.

III.4.2 Abstract

Thermoresponsive polymers reversibly react to changes in temperature and water content of their environment (i.e., relative humidity, RH). In the present contribution, the thermoresponsiveness of poly(*N*-vinylcaprolactam) thin films cross-linked by di(ethylene glycol) divinyl ether deposited by initiated chemical vapor deposition are investigated to assess their applicability to sensor and actuator setups. A lower critical solution temperature (LCST) is observed at around 16 °C in aqueous environment, associated with a dramatic change in film thickness (e.g., 200% increase at low temperatures) and refractive index, while only thermal expansion of the polymeric system is found, when ramping the temperature in dry atmosphere. In humid environment, we observed a significant response occurring in low RH (already below 5% RH), with the moisture swelling the thin film (up to 4%), but mainly replacing air in the polymeric structure up to ~40% RH. Non-temperature-dependent swelling is observed up to 80% RH. Above that, thermoresponsive behavior is also demonstrated to be present in humid environment for the first time, whereas toward 100% RH, film thickness and index appear to approach the values obtained in water at the respective temperatures. The response times are similar in a large range of RH and are faster than the ones of the reference humidity sensor used (i.e., seconds). A sensor/actuator hygromorphic device was built by coating a thin flower-shaped poly(dimethylsiloxane) (PDMS) substrate with the thermoresponsive polymer. The large swelling due to water uptake upon exposure to humid environment at temperatures below the LCST caused the petals to bend, mimicking the capability of plants to respond to environmental stimuli via reversible mechanical motion.

III.4.3 Introduction

Stimuli-responsive swelling is a property of smart hydrogel materials, which makes them suitable for a plethora of sensor[1] and actuator[2] setups. A variety of materials have been developed exhibiting a specific water uptake behavior depending on external stimuli including temperature, pH, magnetic/electric fields, or concentrations of specific chemical species (e.g., glucose).[3] Such hydrogels, as networks of hydrophilic polymer chains, can swell to up to a multiple of their dry size; they react reversibly by taking up or repelling out water upon changing the environment (i.e., the magnitude of the external stimulus).

This water exchange occurs diffusion-based and is, hence, time-limited by water diffusivity.[4] To achieve fast response times and, as a result, optimal device performance, thin polymeric films are employed. Furthermore, device setups often require the coating of delicate surfaces (e.g., drugs,[5] flexible substrates), exhibiting sophisticated nanostructure. In this contribution, initiated chemical vapor deposition (iCVD) was adopted to meet these specific requirements. This solvent-free technique enables the conformal thin film deposition of a plethora of chemical species and compositions from the vapor-phase similar to free radical polymerization processes.[6] The mild processing conditions employed allow for full retention of delicate functional groups, such as the adopted thermoresponsive units, upon deposition. A variety of process parameters (e.g., flow rates, pressure, filament temperature) can be utilized to tune the properties of the deposited thin films in a large range of directions (e.g., composition, morphology, molecular weight).

During swelling, the resulting smart hydrogel thin films undergo rearrangements of polymer chains that impose stress on the thin films, possibly eventuating in poor adhesion or mechanical failure. To increase the thin films' mechanical stability, a second monomer, working as a cross-linker, can be copolymerized. As the cross-linking agent binds two separate polymer chains, the cross-linked hydrogel can be viewed as a polymer network (with a certain mesh size), able to take up a specific maximum amount of water.[7]

The responsiveness to water and to the other external stimuli can be tailored via the chemical nature of monomer and cross-linker. In case of thermoresponsive hydrogels, e.g., the most prominent example poly(*N*-isopropylacrylamide) (pNIPAAm) exhibits hydrophilic groups (i.e., amide) that are able to bind water molecules via hydrogen-bonds; antagonistically, the polymeric mesh shows the potential for attractive intrachain interactions leading to polymer collapse at higher temperatures.[8] The combination of such specific properties result in the material exhibiting a lower critical solution temperature (LCST).[8] In aqueous environment, below the LCST, the polymer exhibits a hydrated swollen state and a transition to a dehydrated shrunken state, when the temperature is increased. Recently, another temperature-responsive polymer, namely poly(*N*-vinylcaprolactam) (pNVCL), was synthesized by iCVD for the first time.[9] Its nontoxicity and biocompatibility make it promising for biomedical applications.[10] Its specific chemical structure facilitates a typical Flory-Huggins demixing behavior with water, which is, for example, different from the miscibility of pNIPAAm.[11] Our group provided further evidence of such behavior by showcasing the tunability of the thermoresponsiveness of pNVCL-based copolymer thin films via molecular weight (i.e., chain length) by varying the filament temperature during iCVD.[12] Mechanical stabilization and further tailoring of the LCST were demonstrated by copolymerizing a cross-linking agent, namely di(ethylene

glycol) divinyl ether (DEGDVE), together with pNVCL, as described elsewhere.[12] DEGDVE has been previously shown to allow for tuning of the temperature-responsiveness in pNIPAAm- and pNVCL-based copolymers by our group.[12–14]

In this contribution, besides studying the swelling behavior of the p(NVCL-*co*-DEGDVE) thin films in water in situ, we aim at shedding light onto the thermoresponsive behavior of the polymer in humid environment. Kinetic swelling data is collected to gain information about the applicability of these systems as fast-responding thin films in sensor and actuator setups in humid environment as well as when water-immersed. The swelling behavior of simple polymeric systems in humidity has been investigated within few studies previously. For instance, Secrist and Nolte measured the response of single-component polyelectrolyte thin films in controlled humid environment by reflectometry.[15] They report on swelling curves of these thin films similar to results of our group published in previous contributions.[14,16] However, the literature is lacking clear, systematic studies. Furthermore, the swelling behavior of more complex systems like temperature- responsive hydrogels is not very well documented. Thijs et al., for instance, measured the weight change of two macroscopic temperature-responsive hydrogel powders (pNIPAAm, poly((dimethylamino)ethyl methacrylate) – pDMAEMA), while introducing water vapor into these systems up to 90% RH.[17] They report on the weight gain being a function of temperature in the whole range of investigated humidity values (up to 90% RH). Preliminary measurements on cross-linked pNIPAAm thin films contradict this observation. For such thin films, our group reported on the temperature-responsive transition not being present as a change in film thickness in nitrogen environment, but being tunable by cross-linking, when immersing the samples in liquid water.[14] In humid environment now, we employed cross-linked pNVCL thin films due to their great tunability in thermoresponsiveness, as demonstrated by us recently.[12] Instead of weight gain, we aim at measuring the change in film thickness in situ by spectroscopic ellipsometry (SE), upon introducing water vapor into the system, while it is held at certain temperatures below and above the LCST. The sharp temperature-dependent transition observed in pNVCL-based systems in water facilitates the described experimental determination of the thermoresponsiveness in RH-dependent swelling. Furthermore, it yields great potential for the applicability of the investigated systems in device setups.

To provide a proof-of-concept sensor/actuator device based on the fast and large swelling response and thermoresponsiveness of the pNVCL thin films, we fabricated a bilayer hygromorphic system, inspired by Taccola et al.[18] A pNVCL-based polymer layer was deposited onto a thin polydimethylsiloxane (PDMS) substrate and subsequently laser-cut into flower shapes. In such

124

double-layered structure, the PDMS acted as an elastic, mechanically passive layer, not being swollen by humidity. The swelling of the pNVCL layer caused a macroscopic, fast and reversible bending of the petals upon changes in the environment (i.e., temperature, RH). While previous studies focused on actuation of responsive hydrogels immersed in water,[19–21] we provide a first demonstration of macroscopic humidity-driven actuation with temperature-responsive tuning/switching.

III.4.4 Experimental Section

Thin Film Synthesis

Poly(*N*-vinylcaprolactam-*co*-di(ethylene glycol) divinyl ether) thin films were synthesized by initiated chemical vapor deposition. The depositions were run in a custom-built iCVD reactor, as described elsewhere.[14] *N*-Vinylcaprolactam (NVCL, 98%; Aldrich, Germany) is used as monomer and di(ethylene glycol) divinyl ether (DEGDVE, 99%; Aldrich, Germany) as cross-linker. NVCL and DEGDVE are kept in their individual glass jars at 78 and 70 °C, respectively. The monomer and cross-linker flow rates are both set to 0.2 sccm. Nitrogen is used as a carrier gas at a flow rate of 1.8 sccm. The corresponding values of the ratio between the monomer partial pressure and the saturation pressure at the substrate temperature (p_M/p_{sat}) are 0.063 and 0.018, for monomer and cross-linker, respectively. In this range of p_M/p_{sat} values, a linear relation to the surface concentration of the chemical species has been reported.[22] The applied flow rates yield polymer layers of p(NVCL-co-DEGDVE) with nominal cross-linking of 20%. To monitor the deposited thickness, in situ laser interferometry with a He-Ne laser ($\lambda = 633$ nm; Thorlabs, USA) is performed through a removable quartz glass lid. Several samples exhibiting film thickness values of (50 ± 5) nm have been synthesized and investigated in terms of their swelling behavior in different environmental conditions. Directly after deposition, the thin film samples were rinsed for 30 s with deionized water for equilibration reasons, as reported earlier.[14,23]

Characterization and Investigation

Spectroscopic ellipsometry (SE) in a wavelength range of 370-1000 nm (M-2000S, J. A. Woollam, USA) was applied to determine film thickness and optical properties of the thin films in the different environmental conditions. Swelling experiments in deionized water were performed in a temperature controlled liquid stage (J. A. Woollam, USA). The recorded data was evaluated with an optical model consisting of a c-Si semi-infinite layer on the bottom (temperature dependent), a 1.6 nm thick native SiO_2 layer in the middle and the polymer film on top, modeled as a Cauchy function with an Urbach tail accounting for adsorption in the low wavelength region. H_2O with

temperature-dependent optical properties was set as the surrounding medium. For the temperature-dependent swelling experiments, the liquid stage and the mounted sample (already exposed to deionized water) were precooled to 10 °C. The respective signal was then recorded while applying a temperature ramp from 10 to 50 °C (also the limitations of the temperature stage) at a heating rate of 0.5 °C/min. Similar heating rates have previously been shown to allow the temperature-responsive material to equilibrate during deswelling and hence yield an 'equilibrium swelling behavior'.[14] For thermal equilibration reasons reported earlier,[14,23] the temperature-dependent swelling behavior and the LCST of the iCVD thin films in water were evaluated from the third heating experiment. All subsequent measurements yielded similar curves and consistent results.

The spectroscopic ellipsometry measurements in controlled humid environment were performed in a THMS600 temperature stage (Linkam, U.K.) at different substrate temperatures (10-24 °C). Closing the lid constrains the volume within the cell to about 70 cm³. A custom-built setup has been used to provide controlled relative humidity (RH) with mixing N_2 bubbled through water (100% RH) and pure N_2 via needle valves. The relative humidity has been monitored in situ inside the temperature stage (2 cm from the substrate) with an SHT15 humidity sensor (Sensirion, Switzerland). To measure the response of the film as a function of RH at a constant substrate temperature, the humidity was increased from 0% RH up to the point where condensation occurs on the sample surface. With the temperature and RH value measured at the humidity sensor, the saturation vapor pressure values (p_{sat}) at the temperature measured by the humidity sensor (T_{sensor}) and at the substrate temperature (T_{sub}) were calculated with the help of the Arden-Buck equation (eq 1):[24]

$$p_{sat} = 0.61121 \times \exp\left(\frac{17.368 \times T}{T + 238.88}\right) \qquad (1)$$

The relative humidity at the substrate level (RH_{sub}), that the sample is effectively exposed to, was then calculated as the product of the relative humidity measured at the sensor (RH_{sensor}) and the ratio of the saturation vapor pressure values at the sensor temperature and at the substrate temperature (Equation 2):

$$RH_{sub} = \frac{RH_{sensor} \times p_{sat,sensor}}{p_{sat,sub}} \qquad (2)$$

The point of condensation could be taken as a reference for the validity of this calculation and could successfully be estimated by ±2% RH, which is within the uncertainty of the RH sensor used. To evaluate the film thickness and refractive index of the sample, the same optical model as in the liquid case has been used to fit the recorded data, but with the ambient material

126

being set to air (n ≈ 1). Thickness and refractive index were monitored at each humidity step and read out after several minutes of equilibration, so that the observed film thickness would not vary for more than 1% in 2 min. The transition temperature of the deposited systems has been evaluated from the optical thin film properties recorded by spectroscopic ellipsometry during swelling experiments in water while increasing the temperature from 10 to 50 °C.

Additionally, kinetic measurements were performed in situ while applying water or a certain amount of humidity onto the thin film samples. The same optical models as in the temperature-dependent measurements (liquid and humid environment, respectively) were employed for fitting the data.

Fabrication and Testing of Hygromorphic Devices

To fabricate hygromorphic actuator/sensor devices that respond to changes in the environment (i.e., temperature, RH), thin polydimethylsiloxane (PDMS) substrates were prepared. PDMS (10:1 ratio of base elastomer to curing agent; Sylgard 184 silicone elastomer base and curing agent, Dow Corning Corp.) was spin coated onto polystyrene (PS) disks for 60 s at a speed of 650 rpm and then cured at T = 80 °C for 3 h in an oven. The PDMS film had a thickness of t_{PDMS} = (55 ± 4) μm, as determined by stylus pofilometry (Alpha Step D-500 Profiler, KLA Tencor, USA). PDMS substrates, still supported by PS, were then coated with 300 nm of the 20% cross-linked p(NVCL-*co*-DEGDVE) thin film with the iCVD process as described above. After iCVD, the bilayer system was laser-cut into a flower shape (see design and schematics of bilayered actuators in Figure III.4-S1, Supporting Information), with a direct-write CO_2 laser (VLS 2.30, Universal Laser Systems, Inc., USA) equipped with a 30 W source. Power, speed, and resolution were tuned to optimize sharp cutting of PDMS with negligible damage to the underlying PS support.

For investigating the response to RH, a flower-shaped device was peeled off from the PS support and placed on a paper rod support, with the thermoresponsive layer pointing upward. After placing it in a cuboid (8 × 8 × 8 cm³) to constrain the gas exchange with the environment, the different levels of humidity were supplied at 25 °C by a gas stream flowing in from top, using the same mixing setup as described above. To investigate the response to temperature, the device was placed onto the temperature stage with the thermoresponsive layer being in direct contact with the sample table (i.e., pointing downward). The RH of the environment was measured to be 35% at 25 °C.

III.4.5 Results and Discussion

Thermoresponsiveness in Water and Dry Atmosphere

Effective sensors are characterized by a fast and large amplitude response. In a previous contribution, we demonstrated that the cross-linker amount largely affects the amplitude of the response in thermoresponsive films deposited by iCVD; together with employing distinct amounts of cross-linking, utilizing the knob of the filament temperature makes it possible to tune the LCST in the range 16-40 °C.[12] For the present study, we synthesized p(NVCL-*co*-DEGDVE) thin films by initiated chemical vapor deposition with a minimal nominal amount of cross-linking of 20% to ensure the films' stability in water. We use a model system with an LCST of about 16 °C (cf. Figure III.4-1). From ellipsometric measurements, the thickness and refractive index of the thin films in water have been evaluated via fitting the measurement data; they are plotted in Figure III.4-1a as a function of temperature.

From the measurement data represented in Figure III.4-1a, the transition temperature could be determined as the mean value of the points of inflection of the temperature-dependent thickness and refractive index curves, as already described elsewhere.[14] This gives an LCST value of 16.1 °C. The temperature-dependent swelling curves show an increase of the film thickness compared to the dry one of more than 250% at temperatures below the LCST. A strong transition between a swollen state with large film thickness and low refractive index below the LCST, and a collapsed state with smaller film thickness and higher refractive index above the LCST is observed. At temperatures above the LCST, the film thickness reaches values of ~1.5 times the dry film thickness, hinting toward a significant amount of water being retained in the polymeric structure also above the transition temperature, as already reported before.[12,14] Furthermore, at temperatures above ~40 °C, the refractive index appears to decrease, while the film thickness increases again. From 35 to 50 °C, the hydrogel film thickness increases by ~8%, while the refractive index decreases by ~0.012. Hypothetically, this can be attributed to thermal expansion at temperatures above the LCST, at which the transition is completely finished and the polymeric system appears in the collapsed state. However, the increase in film thickness and the decrease in refractive index seem unusually large.

To investigate this effect further, the thermal expansion of the hydrogel thin films in a dry environment (i.e., N_2 atmosphere) has been investigated by ramping the temperature from 10 to 50 °C and vice versa; ramping times of 10 min and wait times of 5 min were used, while recording the optical response of the material by spectroscopic ellipsometry. The film thickness normalized by the thickness obtained at 10 °C and the refractive index gained from the respective experiment are plotted in Figure III.4-1b as a function of

temperature. Interestingly, the hydrogel thin film does not exhibit a temperature-responsive behavior without the presence of water (in N_2 atmosphere).
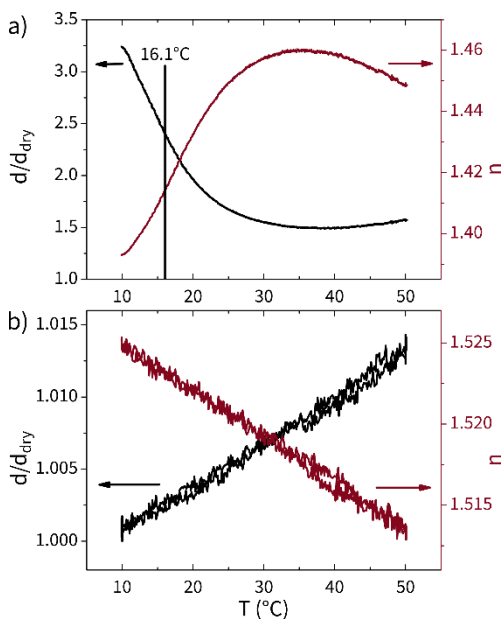

Figure III.4-1. (a) Film thickness normalized by the dry thickness (d/d_{dry}) and refractive index (n) measured during swelling of a nominally 20% cross-linked 50 nm p(NVCL-*co*-DEGDVE) thin film in water while heating from 10 to 50 °C, with dry thickness measured in N_2 atmosphere at 10 °C and transition temperature between swollen and collapsed state (as mean value of points of inflection of thickness and index curves) indicated with a vertical line at 16.1 °C. (b) d/d_{dry} and n measured during temperature ramps between 10 and 50 °C (10 min ramp; 5 min wait at max/min T) of the thin film in nitrogen atmosphere.

Hence, the (linear) thermal expansion of the polymeric material can be estimated. For comparison, from 35 to 50 °C, the film thickness is observed to increase by ~0.5% and the refractive index is observed to decrease by ~0.005. At the respective temperatures (above the LCST), the increase in film thickness in water appears to be larger than the one observed in N_2 atmosphere by 1 order of magnitude. Hypothetically, the water retained in the polymeric system in the collapsed state decreases the attractive interaction of polymeric structures. This promotes the entire polymeric system to expand more easily and would explain the higher thermal expansion in water.

Swelling in Humid Environment

Overall, the magnitude of the observed swelling and temperature-dependent response in water make the material promising for sensor and actuator systems. To investigate the applicability of the synthesized hydrogel thin films

also in humid environment, we probed the thermoresponsive thin films in terms of swelling in RH below and above the transition temperature of 16.1 °C by SE. For that, we monitored the film thickness and the refractive index, while introducing controlled amounts of water vapor into the nitrogen filled system. As described before, these experiments were performed at various substrate temperatures between 10 and 24 °C, measuring the response of the thin films at temperatures below and above the LCST, respectively (Figure III.4-2). As shown later, the response of the thin films investigated is in the order of seconds. To ensure measuring a reliable thickness value, the values were read out after several minutes of equilibration, so that the observed film thickness would not vary for more than 1% in 2 min.
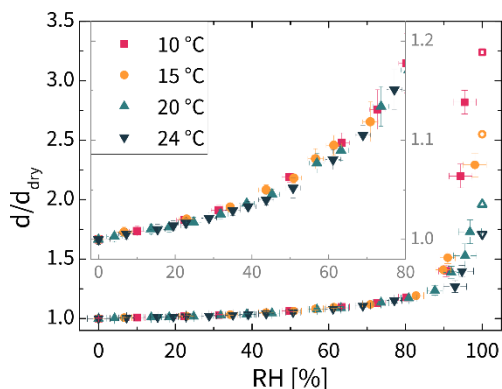

Figure III.4-2. Film thickness normalized by the dry film thickness (d/d_{dry}) of 50 nm p(NVCL-*co*-DEGDVE) thin films evaluated from spectroscopic ellipsometry measurements at various substrate temperatures between 10 and 24 °C measured in pure nitrogen environment and while introducing controlled amounts of water vapor (i.e., relative humidity, RH) into a nitrogen-filled system up to condensation; full symbols represent the described measurement points; empty symbols (at 100% RH) are taken from measurements in water (cf. Figure III.4-1); the inset shows a zoom-in of the region below 80% RH.

The SE measurements of p(NVCL-*co*-DEGDVE) thin films in humid environment at different temperatures (see Figure III.4-2) show swelling of the thin films already occurring at humidity levels of below 5% RH for all the investigated substrate temperatures. The measurements performed at different substrate temperatures yield similar swelling-vs-RH curves up to a humidity level of approximately 80% RH (see inset of Figure III.4-2). Above 80% RH, the thermoresponsiveness of the thin film samples, apparent when studied immersed in water, can also be observed in humid environment. In this region, the degree of swelling is a function of the substrate temperature and approaches the values observed in water at humidity levels close to 100% RH.

Even though the uncertainty of fitting the optical measurement data increases at humidity levels above 90% RH, the difference between the recorded measurement points at the different temperatures is clear and distinct.

Secrist and Nolte's measurements[15] of the response of non-thermoresponsive single-component polyelectrolyte thin films in controlled humid environment by reflectometry yield comparable results to the swelling-vs-RH-curves presented in Figure III.4-2. Thijs et al.[17] also report on the weight change of macroscopic hydrogel powders, exposing non-thermoresponsive hydrogels (pHEMA) to up to 90% RH; they observed similar swelling behavior as well. However, for thermoresponsive hydrogels investigated in the mentioned study,[17] only the trends of water uptake reported for temperatures below the LCST appear to be comparable to the ones reported in the present contribution. As described earlier, the cited publication reports on the weight gain being a function of temperature in the whole range of investigated humidity levels (measured up to 90% RH). Counterintuitively, even a negative weight change was reported for the measurements performed at elevated temperatures (above the LCST) as a function of RH.

The different results either arise from the different sample morphologies (macroscopic pNIPAAm powder vs cross-linked pNVCL-based thin film) or stem from the different measurement setups. In either way, temperature gradients are nearly unavoidable to measure thermoresponsive properties, but can be problematic in studying and interpreting the response of such a material in humid environment. In a more recent case, further pNIPAAm-based hydrogels were investigated in terms of moisture uptake from a humid environment.[25] Again, the weight change was reported to be a function of temperature in the whole range of investigated humidity levels; however, the resulting swelling-curves are different from the ones reported by Thijs et al.[17] gained from similar measurements. The results at temperatures below the LCST, again, appear to be comparable to the trends reported in Figure III.4-2. However, the data suggest that the systems have not been investigated at temperatures above the LCST at the same humidity levels as below the LCST. For example, the amount of adsorbed moisture reported for a temperature of 20 °C at 30% RH compares well to the one reported for 90% RH at 40 °C;[25] as a matter of fact, generating a humidity of 90% RH at 20 °C translates to a humidity of ~30% at 40 °C (cf. eqs 2 and 1 and Figure III.4-3). Figure III.4-3 should serve as an illustration for the relative humidity changing with temperature.

Overall, several studies report on data at a specific relative humidity, varying the temperature. However, they appear to disregard that changing the temperature also changes the relative humidity drastically; for example, a

humidity of 90% RH generated at 20 °C increases by ~5.6% for an object that is exposed to this very humidity, but is held at 1 °C lower (i.e., 19 °C) (cf. eqs 2 and 1). To avoid such problems in the experiments performed for the present contribution, the humidity was varied while keeping the temperature constant.
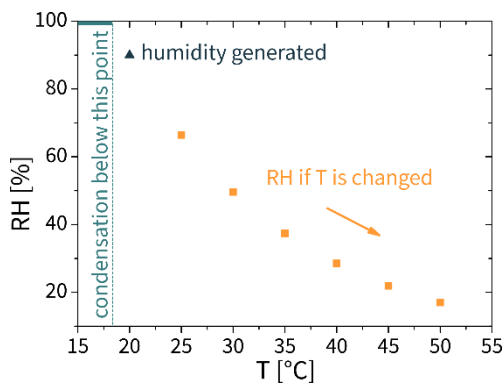

Figure III.4-3. Exemplary illustration of the relative humidity (RH) as a function of temperature (T), if an RH of 90% is generated at 20 °C (and kept constant) and T is varied. Condensation occurs below ~18.3 °C, as indicated by a dashed line and a bar at 100% RH; calculations according to eqs 2 and 1.

To give further insight into the experimental setup, the humidity (up to 100% RH) is generated by bubbling nitrogen through water (at 70 °C), air filtering and mixing it with pure nitrogen to be able to control the humidity level. This mixture is then flown into the measurement chamber via a 1-m tube to avoid fluctuations in temperature. In the chamber, a humidity sensor measures the RH approximately at room temperature. Only the substrate is cooled to temperatures below room temperature to prevent condensation happening anywhere else before 100% RH are reached at the substrate level. From the RH measured at room temperature right next to the substrate, as described earlier, the real RH that the sample is exposed to at the substrate temperature can be calculated via eqs 2 and 1. As stated above, temperature gradients need to be addressed with care. However, we believe this procedure leads to reliable RH values, as supported by the fact that the point of condensation could be estimated by ±2% RH, so within the error of the humidity sensor used in all the investigated temperatures.

A more systematic and detailed view on the swelling behavior of the hydrogel thin films investigated in humid environment is given in Figure III.4-4; there, the normalized film thickness (d/d_{dry} in part a)) and the refractive index (n in part b)) are plotted as a function of the relative humidity as obtained from SE measurements, while increasing the RH from 0 to almost 100% at 20 °C substrate temperature. From this data, the response behavior of the

132

hydrogel thin film to relative humidity can be divided into three different regions (boxes in Figure III.4-4): First, after starting off in dry atmosphere (0% RH), up to ~40% RH, the film thickness increases only slightly (by ~4%), whereas the refractive index also increases with respect to the dry state. This phenomenon occurred in all the temperatures investigated. The peak in refractive index appears at very similar values within the ~5% resolution arising from the RH increase steps (data not shown). This can be viewed, primarily, as filling of voids in the polymeric structure with water, as the refractive index of water (~1.33) is higher than that of air (~1.0). For comparison, the investigated polymer exhibits a refractive index of ~1.52 in the dry state (see Figure III.4-4). Second, from 40% up to ~80% RH, the film thickness increases fairly linearly to ~15% when compared to the dry state. In this region, the thin film starts to incorporate water into its polymeric structure, which can be observed as a decrease of the system's refractive index. However, the response is still small compared to the swelling in water at the specific temperature. Third, above 80% RH, the film thickness increases in a highly nonlinear manner, approaching the film thickness of the system ob-
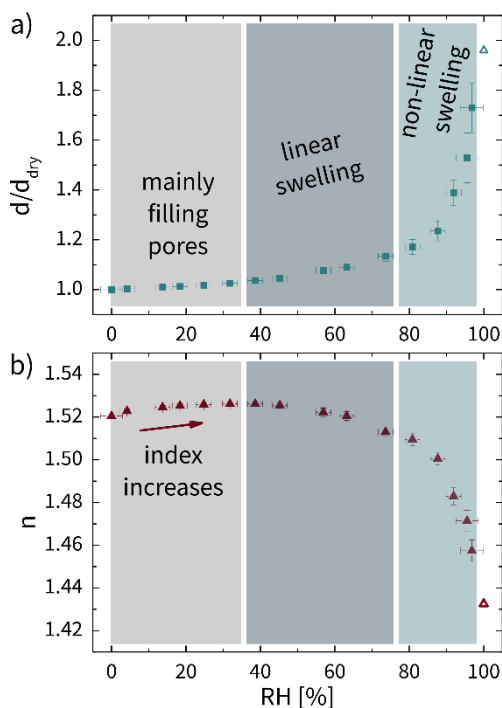

Figure III.4-4. (a) Film thickness normalized by the dry thickness measured in pure nitrogen atmosphere (d/d_{dry}) and (b) refractive index (n) as obtained from spectroscopic ellipsometry measurements of 50 nm p(NVCL-*co*-DEGDVE) thin film samples while ramping the relative humidity from 0 to ~100% at 20 °C substrate temperature; data in part a, also part of Figure III.4-2.

served in water at the corresponding temperature. The observed refractive index trend in the mentioned region above 80% RH exhibits the corresponding behavior.

The monotonous proportionality of the film thickness to the relative humidity at a certain temperature can directly be used in sensor and actuator setups (as shown below). The refractive index cannot be utilized in the whole range of RH due to its non-monotonous behavior. However, two regions can be identified with respect to n: Up to 40% RH, the response is small, but monotone; above 40%, the response is larger and also monotone. For example, in optical systems for RH determination, the refractive index can, thus, be employed in applications, where the environment remains within one of these mentioned ranges.

Kinetics in Water

As, especially, the response characteristics of the film thickness of the presented system to various environmental conditions are promising, to test its applicability to sensors and actuators, also the kinetic response behavior was experimentally probed. First of all, the kinetic swelling of the synthesized layers when flooded with water after being in dry atmosphere has been investigated by in situ SE measurements (see Figure III.4-5). The fast response of the film was shown, as the film thickness did not change for more than 1% already ~30s after the water exposure had been started. Anyhow, the behavior cannot be further resolved by SE because it takes time to fill the entire measurement chamber (5 mL) with water and align the sample, during which it is not possible to record meaningful data due to multiple gas-liquid
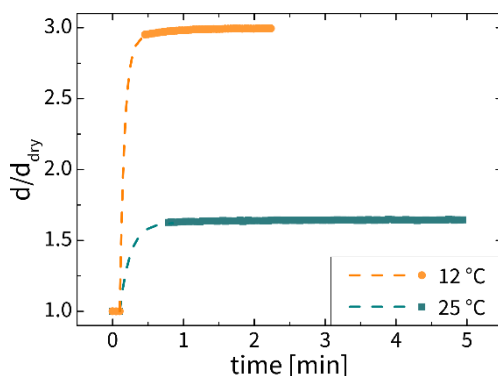

Figure III.4-5. Thickness normalized by the dry thickness measured in nitrogen atmosphere (d/d_{dry}) obtained from spectroscopic ellipsometry measurements as a function of time while exposing a p(NVCL-*co*-DEGDVE) sample (50 nm dry thickness) to water after starting off the measurement in dry atmosphere; the dashed lines give interpolated data during flooding and aligning of the liquid cell of the ellipsometer.

interfaces interfering with the measurement. However, these measurements appear to yield stable thickness values already within seconds of water exposure, perfectly in agreement with the values obtained from the temperature-dependent SE measurements in water (cf. Figure III.4-1a).

Kinetics in Humid Environment

As the response to water appears to be promisingly fast, also the kinetic behavior of the hydrogel thin film in humid environment was investigated. At a constant temperature (24 °C), the humid environment in the measurement chamber of the ellipsometer was changed by controlling the flow rates of humid and dry nitrogen vapors; the RH was measured in situ in the chamber. Relative humidity levels of below 20%, around 50% and above 80% were introduced to investigate the applicability in differently humid environments. The evident response in thickness was utilized to calculate directly back to an RH value via the d/d_{dry}-vs-RH plots measured for the respective temperature (cf. Figure III.4-2). For that, a triple-exponential function was used to interpolate the data. The respective responses of the investigated layers in RH together with the measurements of the reference sensor can be found in Figure III.4-6.
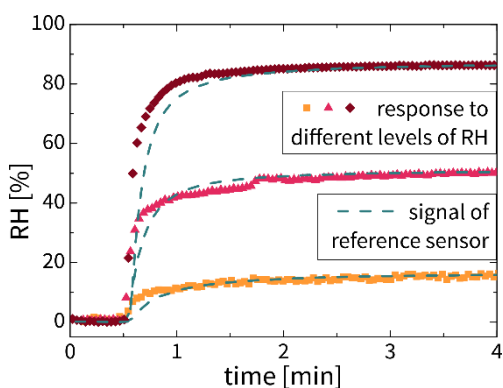

Figure III.4-6. Relative humidity (RH) as evaluated from the response of the sensor layers (cf. Figure III.4-2) and from the reference sensor during RH exposure at different levels over time at 25 °C.

The film thickness and, hence, the calculated RH follow the signal of the relative humidity as measured by the reference sensor and also stabilize, when a constant humidity is reached. The data suggest a faster response of the investigated layer compared to the signal of the reference sensor for all humidity levels employed. From the response curves over time, the respective time constants (τ) could be extracted from fitting double-exponential functions to the measured data. The time constants of the p(NVCL-*co*-DEGDVE) were evaluated to be $\tau_{iCVD,20\%}$ = (5.3 ± 0.6) s, $\tau_{iCVD,50\%}$ = (5.1 ± 0.3) s, and $\tau_{iCVD,80\%}$ = (4.9 ± 0.2) s. It should be noted that the measurement time of the ellipsometer was set to 2 s. The time constants determined from the

response of the reference sensor are $\tau_{ref,20\%} = (14.4 \pm 0.4)$, $\tau_{ref,50\%} = (8.8 \pm 0.1)$ s, and $\tau_{ref,80\%} = (7.6 \pm 0.1)$ s. A secondary time constant of about 1 min was evaluated to be present for all the data sets for both the responses of the investigated layer and the reference sensor, suggesting that the corresponding 'long-term' response stems from the experimental setup. Hence, the primary time constants evaluated from all the measurements yield information about the kinetics of the response of the investigated systems. Also for these primary time constants, the kinetics of the visible/extracted responses of both the investigated layer and the reference sensor (τ, as given above) are, most probably, a convolution of the real response of the sensing system (i.e., water uptake behavior, τ_{real}) and the time it takes to fill the measurement chamber experimentally with a certain relative humidity (τ_{setup}); thus, $\tau = \tau_{real} + \tau_{setup}$.

Overall, the response of the 50 nm p(NVCL-*co*-DEGDVE) layer determined from the increase in thickness upon humidity exposure appears to be about twice as fast as the response of the reference sensor. For decreasing the RH toward dry N_2 atmosphere, similar results were obtained; also when investigating the response at 10 °C, the p(NVCL-*co*-DEGDVE) film was observed to respond faster than the reference sensor, but the experimental setup at lower temperatures appears to stabilize slower as temperature gradients are involved (data not shown). In the data sheet of the reference sensor, a response time of 8 s is given; the response of the sensor to RH levels above 50% is comparable. At lower RH, the apparent larger time constant determined from the response of the sensor suggests a strong contribution from the experimental setup. For the reference sensor and the investigated polymer layer, the time constants appear to be lower (and, thus, the responses faster) for higher RH. Intuitively, the opposite would be expected, as it takes more time to experimentally reach a higher level of RH after starting out in dry nitrogen environment. However, the different flow rates of dry N_2 and a certain level of humidity (as controlled by the needle valves experimentally) could interfere with this consideration. As a consequence, it is not certain how much the experimental filling process (τ_{setup}) contributes to the evaluated time constants; in general, it seems to be plausible to assume a filling time in the order of seconds. Regardless, the developed sensing layer is at least as fast as evident from the derived response times or, most probably, faster.

The similar time constants at different levels of RH are, especially, promising for applications of the layers in humidity sensors, where operation over a wide range of humidity is needed. The observed fast responses make the layers appealing for applications, where changes in the RH need to be resolved in the order of seconds or below. An example of a fast sensor device based on such stimuli-responsive hydrogels is presented in Buchberger et al.[26]

Testing of the Sensor/Actuator Hygromorphic Device

The thermoresponsive swelling at high RH could be interesting for actuator setups, where two stimuli, T and RH, are used to obtain a mechanical deformation of the system. Hygromorphs, as objects responding to environmental humidity by changing their shape, show striking examples in nature (especially in plants, such as in pine cones)[27] and they have recently gained much interest for the development of biomimetic artificial structures for sensing and soft robotics.[18,28] To the author's knowledge, this is one of the first examples of a fast, humidity-driven and temperature-controlled actuator with a bilayered structure involving hydrogel thin films.

To investigate this potential application and provide a first proof of concept, a flower-shaped hygromorphic sensor/actuator system was fabricated (the schematics/design are provided in Figure III.4-S1, Supporting Information) based on a bilayer of PDMS/p(NVCL-*co*-DEGDVE). In such bilayer, the PDMS substrate (55 µm thick) is acting as a mechanically passive and elastic foundation, while the pVNCL coating (just 300 nm thick) is providing the capability to be swollen upon water uptake and thermoresponsiveness. Each petal of the flower structure can thus act as a simple unimorph actuator (bending beam geometry) upon uptake/release of water from the environment, as schematized in Figure III.4-S1. The double-layered device setup was tested upon changing the relative humidity and the substrate temperature. Movies (see Supporting Information) and pictures (see Figure III.4-7) were taken during these tests. The flower-shaped devices reacted to the stimuli by bending of their petals due to swelling/deswelling of the p(NVCL-*co*-DEGDVE). As can be appreciated in the pictures and videos, the device is able to act against gravity upon deswelling (RH-response, Figure III.4-7a) and upon swelling (in the experiment to probe its temperature-response, Figure III.4-7b). The (unbent) reference state of the flower was retrieved by lowering the RH (Figure III.4-7a). Alternatively, the humidity-driven swelling/deswelling could be triggered by temperature, given the thermoresponsiveness of the active layer (Figure III.4-7b). Again, the kinetics of the mechanical response appear to be very fast (i.e., in the order of seconds) and mostly limited by the kinetics of the external stimuli applied: The temperature ramp was applied with cooling/heating rates of 60 °C/min. In case of RH, with the flows supplied, it takes about 10 s to reach the respective maximal/minimal values. The bending radius of the petals is unequivocally set by a specific couple of temperature/humidity values; this fact makes the system interesting for further investigation to obtain reliable and fully reversible actuation.

Remarkably, the bending motion is obtained despite the low thickness of the pNVCL layer (i.e., 300 nm) compared to the PDMS foundation (around 150 times thinner) and compared to similar test devices (e.g., millimeters in
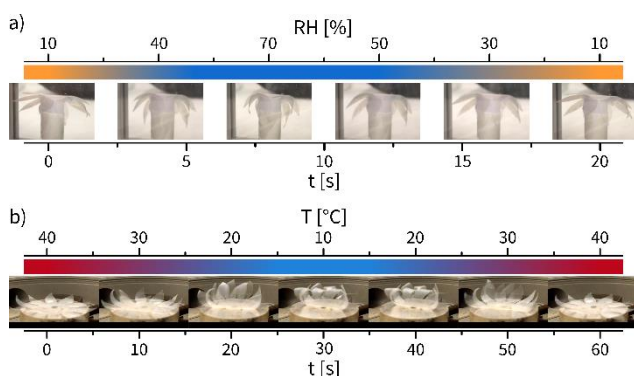
Figure III.4-7. Series of pictures of flower-shaped PDMS/pNVCL-based double-layer hygromorphic devices taken during ramping the (a) RH in a chamber between 10 and 70% at 25 °C (active pNVCL layer pointing upward) and (b) plate temperature T between 40 and 10 °C in a humid environment of 35% RH (measured at room temperature, i.e., 25 °C) (active layer of pNVCL pointing downward). Bending of petals due to differential swelling of the thermoresponsive polymer film as a function T/RH and time t.

thickness,[19,21] or hydrogel films of tens of micrometers thickness[20]). Such results support our hypothesis that the large and fast response of the pNVCL layers can be used for fast and integrated humidity-temperature actuators and sensors.

III.4.6 Conclusions

Thermoresponsive p(NVCL-*co*-DEGDVE) thin films were successfully synthesized via iCVD and probed in terms of response behavior to temperature and different environments (i.e., water, humidity, N_2). This study revealed that in water, the layer swells to up to 250% of its dry thickness below the transition temperature and repels out water upon undergoing a phase transition toward a shrunken state at elevated temperatures. In nitrogen atmosphere, only thermal expansion (~1.5% thickness increase) is observed upon heating the samples in a similar temperature range as in water (10 to 50 °C). In humid environment, a first detailed study on the swelling behavior of hydrogel thin films shows that the layer monotonously swells with increasing the RH. To the author's knowledge, with the described measurement setup, this is also the first contribution in which thermoresponsive hydrogel thin films are investigated at humidity levels above 80% RH below and above their LCST. This is why this is also the first contribution in which the thermoresponsiveness of hydrogel thin films is genuinely proved to occur as a change in film thickness and refractive index at different temperatures

138

(also) in humid environment. We show that the thermoresponsive transition (in film thickness and refractive index) only occurs at humidity levels above 80% RH for the investigated system. Toward 100% RH, the film thickness approaches the values observed in water at the respective temperatures. We also observed a significant response in low RH (already below 5% RH), with the moisture swelling the thin film (up to 4%), but mainly replacing air in the polymeric structure up to ~40% RH.

Kinetically, the investigated p(NVCL-*co*-DEGDVE) thin films were found to respond quickly to changes in the environment (i.e., water and different levels of humidity). With the help of calibrating the system by measuring a thickness-vs-RH curve, in subsequent measurements, the RH was directly evaluated from these curves after measuring the thickness at a certain temperature. The response in differently humid environments was about twice as fast as the one of the market-available reference sensor used.

The fast response together with the similar time constants measured for differently humid environments make the investigated system particularly interesting for its application in sensor and actuator setups. Such applicability was successfully demonstrated in flower-shaped double-layered hygromorphic devices. The artificial petals bend due to a humidity-driven and temperature-tunable actuation mechanism, showcasing also a fast mechanical response against gravity in both swelling and deswelling.
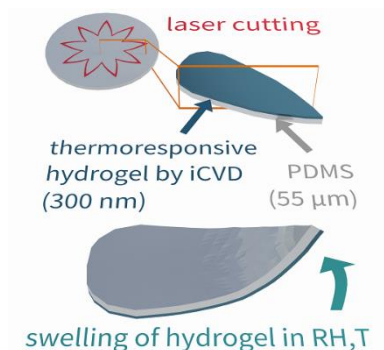
III.4.7 Associated Content

Figure III.4-S1. Schematics of the flower-shaped hygromorphic device used for demonstration of the applicability of the hydrogel thin film in sensor/actuator devices with petals that bend as a function of relative humidity (RH) and temperature (T).

Video III.4-S1. Bilayer flower-shaped hygromorphic actuator bending its petals due to swelling of the thermoresponsive hydrogel thin film (on top) as a function of relative humidity (bottom left of video) at a temperature of 25 °C.

Video III.4-S2. Bilayer flower-shaped hygromorphic actuator bending its petals due to swelling of the thermoresponsive hydrogel thin film (on the bottom) as a function of temperature (top left of video) at a relative humidity of the environment of 35% RH (measured at 25 °C).

III.4.8 Acknowledgments

III.4.9 References

(1)   Palagi, S.; Mark, A. G.; Reigh, S. Y.; Melde, K.; Qiu, T.; Zeng, H.; Parmeggiani, C.; Martella, D.; Sanchez-Castillo, A.; Kapernaum, N.; Giesselmann, F.; Wiersma, D. S.; Lauga, E.; Fischer, P. Structured Light Enables Biomimetic Swimming and Versatile Locomotion of Photoresponsive Soft Microrobots. *Nat. Mater.* **2016**, *15* (6), 647–653. https://doi.org/10.1038/nmat4569.

(2)   Ramakrishnan, N.; Vamsi, T.; Khan, A.; Nemade, H. B.; Palathinkal, R. P. Humidity Sensor Using NIPAAm Nanogel as Sensing Medium in SAW Devices. *Int. J. Nanosci.* **2011**, *10* (01n02), 259–262. https://doi.org/10.1142/S0219581X11007880.

(3)   Chu, L.-Y.; Xie, R.; Ju, X.-J.; Wang, W. Smart Hydrogel Functional Materials. In *Smart Hydrogel Functional Materials*; Springer-Verlag: Berlin, Heidelberg, 2013; pp V–VII. https://doi.org/10.1007/978-3-642-39538-3.

(4)   Beebe, D. J.; Moore, J.; Bauer, J. M.; Yu, Q.; Liu, R. H.; Devadoss, C.; Jo, B. H. Functional Hydrogel Structures for Autonomous Flow Control inside Micro-Fluidic Channels. *Nature* **2000**, *404* (6778), 588–590. https://doi.org/10.1038/35007047.

(5)   Christian, P.; Keimel, R.; Coclite, A. M.; Tumphart, S.; Werzer, O. Drug Release from Thin Films Encapsulated by a Temperature-Responsive Hydrogel. *Soft Matter* **2019**, *15* (8), 1853–1859. https://doi.org/10.1039/c8sm02529k.

(6)   Lau, K. K. S.; Gleason, K. K. Initiated Chemical Vapor Deposition (ICVD) of Poly(Alkyl Acrylates): An Experimental Study. *Macromolecules* **2006**, *39* (10), 3688–3694. https://doi.org/10.1021/ma0601619.

(7)   Canal, T.; Peppas, N. A. Correlation between Mesh Size and Equilibrium Degree of Swelling of Polymeric Networks. *J. Biomed. Mater. Res.* **1989**, *23* (10), 1183–1193. https://doi.org/10.1002/jbm.820231007.

(8)   Liu, R.; Fraylich, M.; Saunders, B. R. Thermoresponsive Copolymers: From Fundamental Studies to Applications. *Colloid Polym. Sci.* **2009**, *287* (6), 627–643. https://doi.org/10.1007/s00396-009-2028-x.

(9)   Lee, B.; Jiao, A.; Yu, S.; You, J. B.; Kim, D. H.; Im, S. G. Initiated Chemical Vapor Deposition of Thermoresponsive Poly (N-Vinylcaprolactam) Thin Films for Cell Sheet Engineering. *Acta Biomater.* **2013**, *9* (8), 7691–7698. https://doi.org/10.1016/j.actbio.2013.04.049.

(10) Cortez-Lemus, N. A.; Licea-Claverie, A. Poly(N-Vinylcaprolactam), a Comprehensive Review on a Thermoresponsive Polymer Becoming Popular. *Prog. Polym. Sci.* **2016**, *53*, 1–51. https://doi.org/10.1016/j.progpolymsci.2015.08.001.

(11) Meeussen, F.; Nies, E.; Berghmans, H.; Verbrugghe, S.; Goethals, E.; Du Prez, F. Phase Behaviour of Poly(N-Vinyl Caprolactam) in Water. *Polymer* **2000**, *41* (24), 8597–8602. https://doi.org/10.1016/S0032-3861(00)00255-X.

(12) Muralter, F.; Perrotta, A.; Werzer, O.; Coclite, A. M. Interlink between Tunable Material Properties and Thermo-Responsiveness of Cross-Linked Poly(N-Vinylcaprolactam) Thin Films Deposited by Initiated Chemical Vapor Deposition. *Macromolecules* **2019**, *in press*. https://doi.org/10.1021/acs.macromol.9b01364.

(13) Salzmann, P.; Perrotta, A.; Coclite, A. M. Different Response Kinetics to Temperature and Water Vapor of Acrylamide Polymers Obtained by Initiated Chemical Vapor Deposition. *ACS Appl. Mater. Interfaces* **2018**, *10* (7), 6636–6645. https://doi.org/10.1021/acsami.7b18878.

(14) Muralter, F.; Perrotta, A.; Coclite, A. M. Thickness-Dependent Swelling Behavior of Vapor-Deposited Smart Polymer Thin Films. *Macromolecules* **2018**, *51* (23), 9692–9699. https://doi.org/10.1021/acs.macromol.8b02120.

(15)   Secrist, K. E.; Nolte, A. J. Humidity Swelling/Deswelling Hysteresis in a Polyelectrolyte Multilayer Film. *Macromolecules* **2011**, *44* (8), 2859–2865. https://doi.org/10.1021/ma101983s.

(16)   Unger, K.; Resel, R.; Coclite, A. M. Dynamic Studies on the Response to Humidity of Poly (2-Hydroxyethyl Methacrylate) Hydrogels Produced by Initiated Chemical Vapor Deposition. *Macromol. Chem. Phys.* **2016**, *217* (21), 2372–2379. https://doi.org/10.1002/macp.201600271.

(17)   Thijs, H. M. L.; Becer, C. R.; Guerrero-Sanchez, C.; Fournier, D.; Hoogenboom, R.; Schubert, U. S. Water Uptake of Hydrophilic Polymers Determined by a Thermal Gravimetric Analyzer with a Controlled Humidity Chamber. *J. Mater. Chem.* **2007**, *17* (46), 4864. https://doi.org/10.1039/b711990a.

(18)   Taccola, S.; Greco, F.; Sinibaldi, E.; Mondini, A.; Mazzolai, B.; Mattoli, V. Toward a New Generation of Electrically Controllable Hygromorphic Soft Actuators. *Adv. Mater.* **2015**, *27* (10), 1668–1675. https://doi.org/10.1002/adma.201404772.

(19)   Thérien-Aubin, H.; Wu, Z. L.; Nie, Z.; Kumacheva, E. Multiple Shape Transformations of Composite Hydrogel Sheets. *J. Am. Chem. Soc.* **2013**, *135* (12), 4834–4839. https://doi.org/10.1021/ja400518c.

(20)   Liu, L.; Jiang, S.; Sun, Y.; Agarwal, S. Giving Direction to Motion and Surface with Ultra-Fast Speed Using Oriented Hydrogel Fibers. *Adv. Funct. Mater.* **2016**, *26* (7), 1021–1027. https://doi.org/10.1002/adfm.201503612.

(21)   Kim, T. H.; Choi, J. G.; Byun, J. Y.; Jang, Y.; Kim, S. M.; Spinks, G. M.; Kim, S. J. Biomimetic Thermal-Sensitive Multi-Transform Actuator. *Sci. Rep.* **2019**, *9* (1), 7905. https://doi.org/10.1038/s41598-019-44394-x.

(22)   Lau, K. K. S.; Gleason, K. K. Initiated Chemical Vapor Deposition (ICVD) of Poly(Alkyl Acrylates): A Kinetic Model. *Macromolecules* **2006**, *39* (10), 3695–3703. https://doi.org/10.1021/ma0601621.

(23)   Christian, P.; Coclite, A. M. Vapor-Phase-Synthesized Fluoroacrylate Polymer Thin Films: Thermal Stability and Structural Properties. *Beilstein J. Nanotechnol.* **2017**, *8* (1), 933–942. https://doi.org/10.3762/bjnano.8.95.

(24)   Buck, A. L. New Equations for Computing Vapor Pressure and Enhancement Factor. *J. Appl. Meteorol.* **1981**, *20* (12), 1527–1532. https://doi.org/10.1175/1520-0450(1981)020<1527:NEFCVP>2.0.CO;2.

(25)   Matsumoto, K.; Sakikawa, N.; Miyata, T. Thermo-Responsive Gels That Absorb Moisture and Ooze Water. *Nat. Commun.* **2018**, *9* (1), 2315. https://doi.org/10.1038/s41467-018-04810-8.

(26)   Buchberger, A.; Peterka, S.; Coclite, A.; Bergmann, A. Fast Optical Humidity Sensor Based on Hydrogel Thin Film Expansion for Harsh Environment. *Sensors* **2019**, *19* (5), 999. https://doi.org/10.3390/s19050999.

(27)   Reyssat, E.; Mahadevan, L. Hygromorphs: From Pine Cones to Biomimetic Bilayers. *J. R. Soc. Interface* **2009**, *6* (39), 951–957. https://doi.org/10.1098/rsif.2009.0184.

(28)   Abdullah, A. M.; Li, X.; Braun, P. V.; Rogers, J. A.; Hsia, K. J. Self-Folded Gripper-Like Architectures from Stimuli-Responsive Bilayers. *Adv. Mater.* **2018**, *30* (31), 1801669. https://doi.org/10.1002/adma.201801669.

IV Contextualized Conclusions

In this section, the conclusions drawn in the scientific articles presented in Chapter III are summarized. Furthermore, the individual conclusions are contextualized with respect to each other and all the background information provided in the remainder of this thesis.

The work presented in this thesis provides a variety of information on thermoresponsive hydrogel thin films and their applicability to device setups. In general, such smart polymers find application in sensor, actuator and biomedical setups. Being fragile compounds themselves, they also need to be fabricated on delicate substrates with complex nanostructures (e.g., nanotemplates, pharmaceuticals), onto which, oftentimes, they are required to be deposited as conformal coatings. Initiated chemical vapor deposition (iCVD) as a solvent-free synthesis technique meets these requirements and allows for the precise tailoring and tuning of material properties via controlling the deposition conditions.

Two polymeric (model) systems were synthesized by iCVD and investigated subsequently: *N*-isopropylacrylamide (NIPAAm) and *N*-vinylcaprolactam (NVCL) cross-linked by di(ethylene glycol) divinyl ether (DEGDVE). While cross-linked pNIPAAm systems are extensively described in the literature, as far as polymer synthesis is concerned, the NIPAAm monomer with its low vapor pressure is not ideal for iCVD. Therefore, novel pNVCL-based copolymer thin films were developed, characterized and applied to device setups for the first time. Studies demonstrating the nontoxicity and biocompatibility of both polymers make them particularly interesting for bio-applications; however, tests in the actual conditions are required to be performed for the specific biomedical applications in question. The successful polymerization and deposition of the respective smart polymer thin films was confirmed by Fourier-transform infrared spectroscopy (FTIR).

IV.1 Thermoresponsiveness in iCVD-Polymers

First of all, the presented work focuses on the fundamental understanding of the temperature-dependent swelling behavior of smart polymer thin films deposited by iCVD and how it can be controlled through their synthesis process. In such thin-film setups, the thermoresponsive behavior of smart polymers can be observed as a distinct change in film thickness upon ramping the temperature in aqueous environment. Therefore, the transition between a swollen state at lower temperatures and a shrunken state at elevated T and the corresponding lower critical solution temperature (LCST) were, mainly, investigated by spectroscopic ellipsometry performed in various environments (dry, humid and liquid at different T). While dramatic changes in refractive index and film thickness (up to >200% increase at low temperatures) could be observed in water, the response of the samples to ramping the temperature in dry atmosphere is limited to thermal expansion of the polymeric system (a few percent increase in film thickness at elevated T). At temperatures well above the LCST, where the thermoresponsive transition is already completed, enhanced thermal expansion can be observed upon further heating in water.

In humid environments, the samples were shown to already respond to low levels of relative humidity (RH below 5%) by swelling up to several percent in film thickness. However, the water uptake was shown to mainly occur as by replacing air/voids in the polymeric structure up to ~40% RH. Until 80% RH, the swelling was observed to be approximately linear, but temperature independent. Above 80% RH, the thin film samples were demonstrated to exhibit a thermoresponsive behavior (also) in humid environment for the first time by observing a distinct behavior/change in film thickness and refractive index as a function of temperature. The film thickness and refractive index appeared to converge with the values obtained in water at the respective temperatures, when approaching 100% RH. Overall, to the authors' knowledge, the respective article comprises the first detailed and comprehensive study on the thermoresponsive swelling behavior of hydrogel thin films in humid environments.

Furthermore, water contact angle (WCA) measurements showed that the thermoresponsive transition is accompanied by a change in wettability, according to a transition in hydrophilicity/-phobicity of the polymeric mesh. Upon investigating the thermoresponsive transition via nano-indentation experiments in water, the apparent elastic modulus was observed to approximately double, when ramping the temperature from ~10 °C below to ~10 °C above the LCST.

Characteristics Linked to Deposition Conditions

In the scientific articles presented in Chapter III, the thermoresponsive behavior/transition was shown to depend on parameters controllable in the synthesis process, i.e., the amount of cross-linking, the film thickness and the concentration of initiator radicals being delivered to the polymerization reactions.

Thus, hydrogel thin films exhibiting different amounts of cross-linking were synthesized. The cross-linker amount was demonstrated to alter the water uptake; less cross-linked samples swell more. However, samples without cross-linking were not stable in water. Hypothetically, the mechanical integrity and adhesion to the substrate cannot be preserved by 'only' physical bonding and cross-linking (the entanglement of polymer chains). Additionally, with increasing the amount of cross-linking, the transition temperature was observed to decrease due to the hydrophobicity of the cross-linker employed. In WCA studies, the surfaces of less cross-linked polymers were observed to be keener to rearrange. Correspondingly, nano-indentation experiments revealed that the polymeric mesh is less dense and less rigid in less cross-linked samples. At 25 °C, the apparent elastic modulus ranges from several to dozens of MPa depending on the amount of cross-linking.

Furthermore, the transition temperature was found to be thickness dependent in thermoresponsive iCVD films, as also observed in other hydrogel systems cross-linked in the dry state (photo-cross-linked). The films were shown to exhibit a minimum LCST at a film thickness of ~70 nm. At higher (and lower) film thickness, the transition temperature was found to increase; the magnitude of this increase depended on the cross-linker amount employed. This behavior could be correlated to a corresponding change in the films' (mass) density (in their dry states) as observed in X-ray reflectivity and spectroscopic ellipsometry measurements. Thus, a higher density of the polymeric matrix correlates with a decrease in transition temperature; naturally, the density in the dry state was higher for more cross-linked samples.

Moreover, the filament temperature (T_{fil}) set during iCVD synthesis is known to affect the chain length of the resulting polymer. As the thermoresponsive transition of pNVCL is molar-mass dependent, T_{fil} was successfully utilized to alter the LCST in a large range of temperatures (16-33 °C for similar cross-linking). To the authors' knowledge, such an approach was applied for the first time to tune the thermoresponsive behavior of vapor-phase-synthesized smart polymer thin films. In contrast to changing the amount cross-linking, it has the advantage that the degree of swelling remains comparable, while the transition temperature can be readily altered.

Even though parts of the interlink between material properties, characteristics of the samples and the employed deposition conditions were examined and elucidated, there is, definitely, further potential and the need for investigating and tailoring the complex growth, properties and swelling behavior of thermoresponsive hydrogel systems in future studies. Regardless, the work and insights presented in this thesis deepen the understanding of smart polymer thin films and, simultaneously, should raise awareness about the delicate influence of growth conditions and behavior on relevant material properties and, in turn, mechanisms during swelling of such structures.

Ultimately, smart polymer thin films that are able to swell up to 250% compared to their dry thickness (in N_2 environment) were successfully synthesized by iCVD. Their wettability, macromolecular structure, promising mechanical properties and interesting behavior in various environments (dry, humid and liquid) were examined. Furthermore, the thermoresponsive characteristics of these films could be tuned with distinct transition temperatures ranging between 16-40 °C being achievable.

IV.2 Smart Polymers for Device Applications

In a further step, the scientific articles presented in chapter III assess the applicability of the investigated systems to various device setups: for sensing of the humidity, humidity-driven and temperature-controlled actuating and in an encapsulation layer for pharmaceuticals.

Together with the biocompatibility of the investigated systems, the tunability and position of the LCST around human body temperature enables their application to biomedical setups such as for on-demand drug administration. Therefore, a system for a drug coating consisting of a thermoresponsive polymer deposited onto an enteric coating by iCVD was developed and investigated. Here, the solvent-free character of the iCVD process is advantageous as the underlying layer remains unfazed. Upon iCVD, the layered structure forms wrinkles. With the thickness of the iCVD film, the thickness of the underlying enteric coating and the cross-linker amount employed in iCVD, the morphology of the wrinkles was demonstrated to be readily controllable. In that way, tailored surface morphologies could be achieved ranging from ultrasmooth to strongly wrinkled; the wrinkles exhibited wavelengths of up to several µm and heights of up to dozens of nm.

In summary, an enteric coating together with a thermoresponsive thin film synthesized by iCVD was proposed as a promising encapsulation layer for pharmaceuticals being responsive to multiple external stimuli. Ultimately, an uncomplicated way to tune wrinkling and, thus, the surface area of such a system applicable to drug delivery applications was developed. With the possibility of employing different materials and the further tunability of the morphology with various parameters in the synthesis process, also other applications (e.g., light diffusion in solar cells) might become accessible to be re-engineered and, in that way, to outperform established systems.

As thermoresponsive polymers react to temperature and changes in the H_2O content of their environment, their applicability to the respective sensor and actuator setups is evident. For this purpose, fast kinetics and, consequently, short response times to such changes in the environment are essential. Time constants evaluated for the response to changes in RH were found to be particularly low for the investigated systems (seconds); the films were observed to respond to changes in RH approximately twice as fast as a market-available humidity sensor used for reference measurements. Furthermore, the response times were similar in all investigated levels of RH. A calibration curve (thickness-vs-RH) can be used to directly evaluate the RH from the film thickness at a certain temperature in subsequent measurements. Moreover, a sophisticated setup (e.g., multilayers) of various polymers exhibiting different transition temperatures could potentially be used to directly evaluate the relative humidity (with its temperature-dependence) from a single

(thickness) measurement. Together, these features make the investigated systems particularly interesting for the proposed device setups.

Finally, a sensor/actuator hygromorphic device was developed by coating a flexible substrate (poly(dimethylsiloxane) – PDMS; 55 μm thick) with a thermoresponsive polymer thin film (300 nm thick) by iCVD. This bilayered structure was laser-cut into flower-shapes, in which each petal acts as a unimorph actuator. By changing the substrate temperature and the humidity in the environment, the thermoresponsive polymer film selectively takes up or repels out water and, thus, causes the synthetic petals to bend. The (fast) mechanical response was demonstrated to be feasible against gravity both in swelling and de-swelling. Such a hygromorphic actuation mechanism mimics the capability of plants to respond to environmental stimuli. Conclusively, to the authors' knowledge, this was the first reported demonstration of macroscopic humidity-driven actuation with temperature-responsive tuning/switching in such synthetic setups.

In summary, several possibilities for the application of smart polymer thin films to device setups were examined. For instance, these hydrogel layers can serve as a matrix for applications, for which a specific aqueous environment is required (e.g., cell encapsulation). The response to environmental stimuli such as temperate or RH can be utilized to employ these materials as switches that change their properties as a function of an external parameter (e.g., on-demand drug delivery). The biocompatibility of such materials appears to be promising but needs to be tested in the actual applications. Furthermore, their applicability to sensor setups is interesting due to their fast response and the possibility of directly evaluating the RH (with temperature) from a single passive response. Besides being a distinct passive response, the mechanical motion of a thermoresponsive polymer thin film upon swelling is highly promising for future applications in soft robotics (e.g., soft gripping); actuation of such a 'soft' setup can, likely, aid the development of a new generation of smart devices.

A Appendix

This section provides further documents that were prepared within the framework of the doctoral program. In Appendix I, a list of scientific contributions with publications and oral as well as poster presentations at international conferences is presented. In Appendix II, a cover art prepared for a supplementary journal cover published in volume 2, issue 3 of the journal 'ACS Applied Polymer Materials' in March 2020 together with the article presented in section III.4 is depicted. In Appendix III, a report of the work and project conducted at Drexel University in Philadelphia, USA, during a research stay from September 2019 to March 2020 funded by the Marshall Plan Foundation, is provided.

AI List of Scientific Contributions

AI.1 Publications

(i) Perrotta, A.; Christian, P.; Jones, A. O. F.; Muralter, F.; Coclite, A. M. Growth Regimes of Poly(Perfluorodecyl Acrylate) Thin Films by Initiated Chemical Vapor Deposition. *Macromolecules* **2018**, *51* (15), 5694–5703. https://doi.org/10.1021/acs.macromol.8b00904.

(ii) Muralter, F.; Perrotta, A.; Coclite, A. M. Thickness-Dependent Swelling Behavior of Vapor-Deposited Smart Polymer Thin Films. *Macromolecules* **2018**, *51* (23), 9692–9699. https://doi.org/10.1021/acs.macromol.8b02120.

(iii) Muralter, F.; Perrotta, A.; Werzer, O.; Coclite, A. M. Interlink between Tunable Material Properties and Thermoresponsiveness of Cross-Linked Poly(N-Vinylcaprolactam) Thin Films Deposited by Initiated Chemical Vapor Deposition. *Macromolecules* **2019**, *52* (18), 6817–6824. https://doi.org/10.1021/acs.macromol.9b01364.

(iv) Muralter, F.; Coclite, A. M.; Werzer, O. Wrinkling of an Enteric Coating Induced by Vapor-Deposited Stimuli-Responsive Hydrogel Thin Films. *J. Phys. Chem. C* **2019**, *123* (39), 24165–24171. https://doi.org/10.1021/acs.jpcc.9b07340.

(v) Perrotta, A.; Berger, R.; Muralter, F.; Coclite, A. M. Mesoporous ZnO Thin Films Obtained from Molecular Layer Deposited "Zincones." *Dalt. Trans.* **2019**, *48* (37), 14178–14188. https://doi.org/10.1039/C9DT02824B.

(vi) Muralter, F.; Greco, F.; Coclite, A. M. Applicability of Vapor-Deposited Thermoresponsive Hydrogel Thin Films in Ultrafast Humidity Sensors/Actuators. *ACS Appl. Polym. Mater.* **2020**, *2* (3), 1160–1168. https://doi.org/10.1021/acsapm.9b00957.

(vii) Muralter, F.; Coclite, A. M.; Lau, K. K. S. Oxidative Chemical Vapor Deposition of a Conducting Polymer Film on Nanostructured Surfaces for Piezoresistive Sensor Applications. *Marshall Plan Scholarship Papers* **2020**, (submitted).

AI.2 Oral Presentations

(i)   Swelling Behavior of Thin Hydrogel Films in Humidity and when Water-immersed. *DPG Spring Meeting*, March **2018**, Berlin, Germany

(ii)   In-situ Swelling Studies in Humidity and Water of Hydrogel Thin Films deposited by initiated Chemical Vapor Deposition. *E-MRS Spring Meeting*, June **2018**,   Strasbourg, France

(iii) Tunable Swelling Behavior of Hydrogel Thin Films deposited by initiated Chemical Vapor Deposition. *OEPG Meeting*, September **2018**, Graz, Austria

(iv)   On Vapor-deposited Smart Hydrogel Thin Films and their possible Applications. *Advanced Materials Day*, September **2019**, Graz, Austria

(v)   Initiated Chemical Vapor Deposition of poly(N-vinylcaprolactam)-based Cross-linked Smart Hydrogel Thin Films with Tunable Temperature-responsive Swelling Behavior. *AVS Fall Meeting*, October **2019**, Columbus, OH, USA

(vi)   Thermo-Responsiveness Linked to Deposition Conditions in Initiated Chemical Vapor Deposition of Smart Hydrogel Thin Films for Sensor Applications. *MRS Fall Meeting*, December **2019**, Boston, MA, USA

AI.3 Poster Presentations

(i)   In-situ Swelling Studies in Humidity and Water of Hydrogel Thin Films deposited by initiated Chemical Vapor Deposition. *Eurosensors Conference*, September **2018**, Graz, Austria

(ii)   Thickness-dependent Swelling Behavior of Hydrogel Thin Films deposited by initiated Chemical Vapor Deposition. *Advanced Materials Day*, September **2018**, Graz, Austria

(iii) Cross-linked poly(N-vinylcaprolactam) Thin Films with Tunable Swelling Behavior by initiated Chemical Vapor Deposition. *E-MRS Spring Meeting*, May **2019**, Nice, France
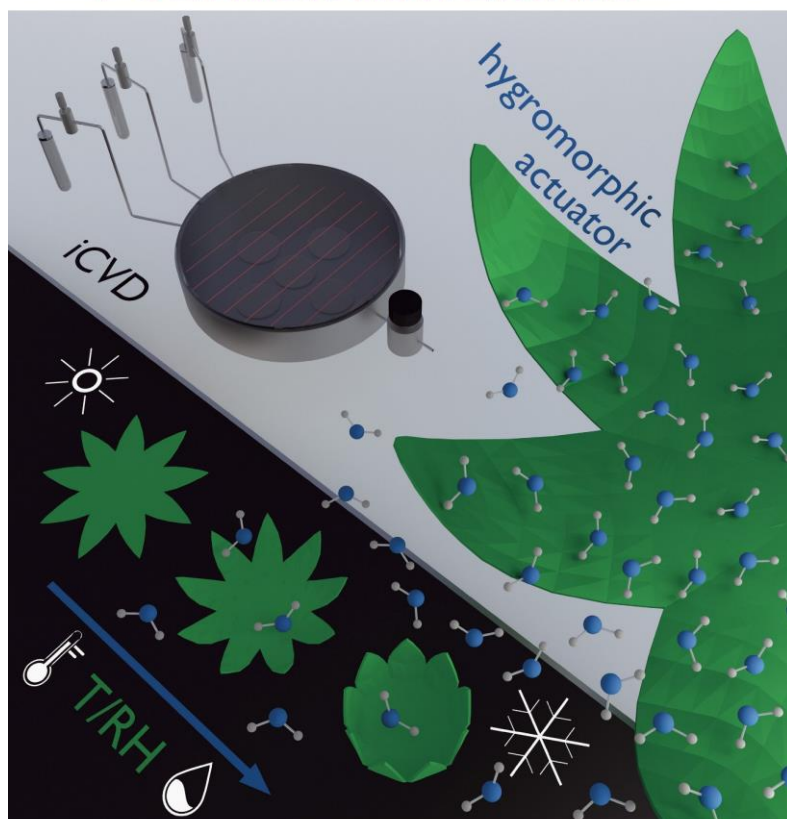
AIII Marshall Plan Scholarship Paper

AIII.1 Preface

The following sections were reproduced from the Marshall Plan Scholarship Paper submitted to the Marshall Plan Foundation, which will be published online on the foundation's website. The work presented in this paper was conducted at the Department of Chemical and Biological Engineering at Drexel University, Philadelphia, PA, USA, in the laboratory of Prof. Kenneth K. S. Lau during a research stay funded through a Marshall Plan Scholarship awarded to the author of this thesis by the Marshall Plan Foundation. The author of this thesis developed the idea of the project, prepared and characterized the samples, evaluated the data and wrote the research paper. Kenneth K. S. Lau supervised the project, supported the data interpretation and the manuscript preparation. Anna Maria Coclite aided in the development of the project, the data interpretation and the manuscript preparation. The results presented herein will be summarized in an article to be published in an international peer-reviewed journal. The text and illustrations are identical to the published research paper and are reproduced to fit the format and style of the thesis.

FABIAN MURALTER

Oxidative Chemical Vapor Deposition of a Conducting Polymer Film on Nanostructured Surfaces for Piezoresistive Sensor Applications

From Vapor Deposition to Piezoresistivity

Host Institution: Drexel University

Home Institution: Graz University of Technology

Supervisors:

PROF. KENNETH K. LAU, PHD
Department of Chemical and Biological Engineering
Drexel University

ASSOC.-PROF. DR. ANNA MARIA COCLITE
Institute of Solid State Physics
Graz University of Technology

Graz, April 30, 2020

AIII.2 Contents

AIII.3 Abstract

In this study, a novel, fully polymeric setup for piezoresistive sensing was prepared and tested. For this setup, a monolayer of polystyrene (PS) nanospheres (with a diameter of ~580 nm) was assembled on a flexible polyethylene naphthalate (PEN) substrate. Subsequently, a thin layer (~50-100 nm) of poly(3,4-ethylenedioxythiophene) (PEDOT) was deposited conformally around the spheres via oxidative chemical vapor deposition (oCVD). Two nickel top-contacts with a separation of 0.5 mm were used to characterize the individual samples. Voltage-current characteristics and direct resistance measurements were performed to test the electrical properties of the samples in their unstrained state and their piezoresistive response during bending. The substrate temperature and deposited thickness during oCVD were used as parameters to alter the properties of the PEDOT thin film, with increased substrate temperature and thickness leading to samples exhibiting lower intrinsic resistance. An estimation of the conductivity of the samples prepared yielded values of up to tens of S cm^{-1}. Intrinsically, with the setup used, the oCVD-PEDOT layer is chlorine-doped. Subsequent dopant exchange by putting the samples in 0.5 M sulfuric acid decreased their resistance by ~1/3. Regarding the piezoresistive properties of the devices prepared, lower intrinsic resistance and the acid treatment performed enhanced the response of the samples. Thus, in the range of parameters investigated, acid treatment, higher substrate temperatures and thickness yielded samples with increased response. As a result, gauge factors as high as 11.4 could be achieved. These results offer a promising basis for further investigations in a novel approach.

AIII.4 Introduction

The piezoresistive effect is broadly used in various devices such as transducers, accelerometers, piezo-FETs, etc. and most prominently in sensors.[1] Its basis is a change in resistance caused by a deformation of a material (i.e., strain). Thus, bending, pressure or stress acting on a piezoresistive material can be measured as a change in resistance as a function of strain. In this work, the objective of strain sensing with a novel, fully polymeric setup is proposed to serve as a basis, from which further possible applications can be derived in the future. Up to now, such materials are mostly silicon-based or involve other inorganic rigid solids. Their rigidity, however, is disadvantageous, if large strains and/or small pressures are of interest. To overcome this limitation, hybrid setups mainly consisting of inorganic nanostructures supported by flexible polymers have been investigated. In the last decade, strain sensors based on solution-processed piezoresistive polymer films

(e.g., PEDOT:polystyrene sulfonate or PSS) have also been developed.[2–4] However, these setups exhibit lower sensitivity than their inorganic counterparts do. Recently, the integration of nanostructures into the polymers towards a new generation of strain sensors has been reported.[1,4,5] This was reported to enhance the sensitivity by orders of magnitude. Moreover, the high mechanical flexibility typical for polymers is crucial for the application in various groundbreaking and growing fields such as wearable electronics. As the size of the nanostructures used is in the order of tens to hundreds of nanometers, the prospect in the present project is to use polymeric nanostructures of similar sizes. Furthermore, the piezoresistivity of PEDOT:PSS was reported to depend on the sizes of PEDOT- and PSS-rich domains, when PEDOT is doped with solid state PSS.[3,4] The present project aims to investigate and utilize this fact by conformal deposition of PEDOT thin films of different thicknesses around PS nanospheres assembled on the surface of a flexible substrate. Monolayers of PS nanospheres deposited onto flexible substrates serve as a basis for the proposed structure. The data in the literature suggests that the quality of and even the ability to deposit such PS monolayers strongly depends on the quality and impurities in the PS nanosphere suspension that is used.[6] The goal is to reproducibly deposit such uniform monolayers over large areas. Simple drop casting, spin coating and doctor blading were proposed, fulfilling this task to a varying extent. However, deposition of the PS beads onto the air-water interface and subsequent pick-up onto a substrate appears to yield the most convincing and reproducible results.[6,7]

Onto the monolayer of PS nanospheres, a PEDOT thin film will be deposited conformally around the nanostructure. Oxidative chemical vapor deposition (oCVD) specifically meets this need for conformality without damaging the substrate and with the advantage of vapor-phase processing (i.e., no swelling of PS during deposition in solutions). Acid treatment post-oCVD was shown to lead to a dopant exchange and, thus, altered film properties.[8] The described acid treatment of the entire structure also leads to a sulfonation/doping of the surfaces of the PS nanospheres.[9] Therefore, such acid treatment can be utilized to further understand the role of the PEDOT-PS interfaces on the piezoresistive effect of the resulting structure. A contribution of the doped aromatic units on the surfaces of the PS spheres to the conduction mechanisms in the material is assumed. Furthermore, parameters such as the substrate temperature during oCVD, or the flow rates of the individual chemical precursors used were shown to lead to different properties (e.g., conductivity) of the resulting PEDOT thin films.[10]

The piezoresistive response of such samples, when strained, can be estimated by measuring voltage-current characteristics during bending (e.g., cf. Latessa et al.[3]). By choosing the right electrode material (i.e., matching work

functions; ohmic contact), resistance measurements between two top-contacts deposited at a well-defined spacing suffice. Therefore, from calculating the strain via bending radii, the response of the samples is estimated as the percentage of the resistance change during bending and normalizing the value by the resistance value measured in the unstrained state. The response of the individual samples is investigated as a function of substrate temperature during oCVD, PEDOT thickness and acid treatment.

AIII.5 Methods

Sample Preparation

Silicon wafers (University Wafer) were used as test substrates for the deposition of polystyrene (PS) nanospheres and poly(3,4-ethylenedioxythiophene) (PEDOT) thin films. Polyethylene naphthalate (PEN) films (thickness 0.125 µm, Goodfellow) were used as substrates for the final test devices.

Various PEDOT thin films were synthesized by oxidative chemical vapor deposition (oCVD) in a custom-built reactor described by Smolin & Lau et al.[11,12] 3,4-Ethylenedioxythiophene (EDOT, 97%, Sigma-Aldrich) and vanadium oxytrichloride ($VOCl_3$, 99%, Sigma-Aldrich) were used as-received, and placed in separate glass jars as the liquid monomer and oxidant sources, respectively. The glass jar of EDOT was heated to 90°C, whereas $VOCl_3$ was kept at room temperature. For all the depositions described, both flow rates were set to 1 sccm (standard cubic centimeter per min) via individual low-flow precision metering valves (Swagelok). Nitrogen (1 sccm each) was used as an inert carrier gas to promote transport of the monomer and oxidant into the reaction chamber through individual gas lines. The pressure in the reaction chamber was monitored and controlled by a pressure controller in a feedback loop with a downstream throttle valve and a pressure transducer (MKS Instruments). During the depositions, the pressure was kept constant in the range of 100-400 mTorr. For the described depositions, the substrate stage was held at constant temperatures between 40 and 80 °C. The depositions were carried out for 30 or 60 min to achieve samples of different film thickness at a certain substrate temperature and pressure.

Polystyrene (PS) nanospheres are deposited onto the respective substrates from various suspensions. Commercially available dispersions of PS beads in water were purchased from Polysciences, Inc. (1 µm; 2.5 wt.-%, carboxylate-functionalized and plain) and from Microparticles GmbH (0.757 µm; 5 wt.-%). Suspensions in ethanol (EtOH), methanol (MeOH) with and without addition of a surfactant (Triton X-100, Sigma-Aldrich) were prepared from the commercial dispersions (cf. Hulteen et al.[13], Trujillo et al.[14]). The methods of drop casting, spin coating and doctor blading were tested for the deposition of monolayers of PS beads from such suspensions. Furthermore, the

assembly of a monolayer at an air-water interface was tested with suspensions of 1:1 volume ratio of EtOH and the as-received H_2O-dispersions of PS beads (cf. Vogel et al.[7]). Another dispersion of PS beads in water (580 nm; 5 wt.-%) prepared by surfactant-free emulsion polymerization was kindly provided by Prof. Vogel's group in Erlangen, Germany. This dispersion was used for the assembly of monolayers at the air-water interface as reported in Vogel et al.[7] The PS beads were added to the air-water interface in a glass beaker (8 cm diameter, 4.5 cm height) by dropping several microliters of the PS-H_2O:EtOH dispersion onto the dry end of a plasma-cleaned microscopy glass slide partially immersed in the water and tilted to ~45°. All the water used in these experiments was provided by a Milli-Q water purification station yielding deionized H_2O with a resistance value of 18.2 MΩ cm. The EtOH used (200 Proof, Decon Laboratories, Inc.) had a purity of 99.2%. All the substrates were plasma-cleaned under an air-atmosphere in a Harrick PDS-001 plasma cleaner for 10 min at 30 W.

Acid treatment was performed by placing the samples (PEDOT on PS on PEN) in a H_2SO_4 solution. For this purpose, concentrated H_2SO_4 (Sigma-Aldrich) was diluted to a 0.5 M solution with MiliQ-water.

The deposition of Ni top-contacts was performed in a Thermionics VE 90 thermal evaporator with a contact mask creating a spacing of 0.5 mm between the two contacts. A quartz crystal microbalance (QMB) was used to monitor the Ni growth rate to achieve a target film thickness of (50 ± 2) nm.

Investigation

The individual substeps in the experimental procedure are monitored by investigating the molecular nature of the thin films by Fourier-transform infrared spectroscopy (FTIR) and the structure of the assembled setup by optical and scanning electron microscopy (SEM).

Fourier-transform infrared spectroscopy (FTIR) measurements were performed on a Thermo Nicolet 6700 spectrometer in transmission mode. The spectra were collected in the wavenumber range 400–4000 cm^{-1} at a resolution of 4 cm^{-1} using a DTGS detector.

Scanning electron microscopy (SEM) was performed on a Zeiss Supra 50VP scanning electron microscope with an accelerating voltage of 5 kV. All the presented images were recorded at a working distance of ~11 mm. The samples were sputtered with Pt for 40 s before SEM analysis.

Voltage-current characteristics were measured on a Gamry Reference 600 system in the linear sweep voltammetry mode. The ohmic behavior of all the samples investigated was confirmed by the linear voltage-current characteristics and utilized so that further measurements could be performed on a Fluke 112 multimeter, directly evaluating the corresponding resistance

values. Two different methods were used to connect the Ni contacts to the measurement device: crocodile clips or test leads. Both are used with a piece of aluminum foil in between to prevent the ultrathin nickel contact film from being scratched. Strain was exerted on the devices via bending (longitudinal to the separation of the contacts). The corresponding strain ε (defined as the change in length normalized by the length of the unstrained device $\Delta l/l$) can be calculated via the bending radii r_b utilized and the substrate thickness t_{sub} (for $r_b \gg t_{sub}$). Tensile strain is given as a positive value, compressive strain as a negative one.

$$\varepsilon = \frac{\Delta l}{l} = \frac{t_{sub}/2}{r_b + t_{sub}/2} \approx \frac{t_{sub}/2}{r_b}$$
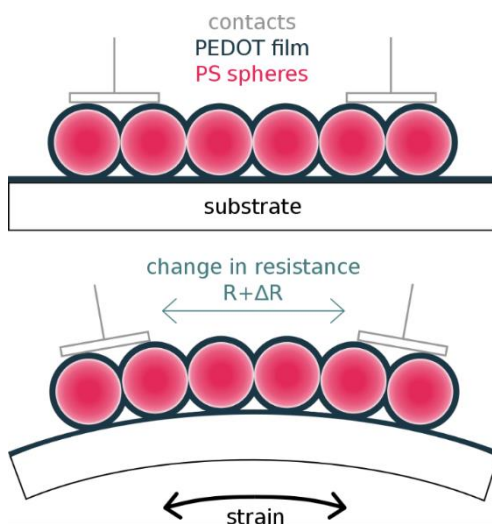

Figure AIII-1. Sketch of the device structure proposed and tested for strain sensing, exhibiting a resistance value R as assembled/unstrained (top) and changing its resistance by ΔR when strained via bending (bottom)

The bending experiments were performed at constant temperature (22°C) and relative humidity (40%). The final device setup, as assembled and when strained, is sketched in Figure AIII-1.

AIII.6 Experimental, Results and Discussion

Assembly of Monolayers of PS Nanospheres

In the first step, various methods were tested for the deposition of a monolayer of polystyrene nanospheres on various surfaces, including silicon wafers and polyethylene naphthalate (PEN) substrates. The aim was to achieve monolayers over adequate areas (~cm^2) prepared with reasonable reproducibility. First, this should serve as a basis for the architecture used for testing

and, subsequently, can ensure the potential for upscaling of the proposed methods.

At first, commercially available PS beads from Polysciences, Inc. were *drop casted* onto silicon wafers, as reported in Trujillo et al.[15]. Carboxylate-functionalized and plain beads (from Polysciences, Inc.) behaved similarly in the experiments described in the following. The as-received PS beads (2.5 wt% in water) were mixed 1:1 in volume with a solution of methanol and Triton X-100 (500:1 by volume). This solution was applied to the surface in drops of 1-10 µl and left to dry at ambient conditions until no liquid could be observed with the naked eye (~5 min). Subsequently, the substrates were dried for 30 min at 80 °C to remove any residual liquid. The drops smallest in volume (~1-2 µl) lead to the most promising results. However, optical and scanning electron microscopy revealed only very small areas (up to ~2 mm^2) of real monolayer coverage. Moreover, small regions showed coverages lower than a monolayer (i.e., de-wetted). The rest of the area covered by the applied drop (~1 cm in diameter in total) consisted of multilayers of PS nanospheres at the outermost parts (i.e., coffee ring effect) and in the middle of the drop. The SEM images shown in Figure AIII-2 depict the structure of regions covered by a monolayer in such a way. Overall (see Figure AIII-2 (a)), they exhibit a large number of lattice defects and dislocations with areas of hexagonally close-packed (hcp) nanospheres not larger than 10×10 spheres, areas of chaotic assembly of the beads (b) and regions of de-wetted structures with large areas (up to hundreds of micrometers) of bare substrate being visible between the deposited beads (c). The applied drops spread more effectively on plasma-cleaned substrates yielding regions of monolayer coverage of up to ~10 mm^2, still lower compared to other reports in the literature (e.g., 0.3 cm^2)[15]. The plasma-cleaning procedure applied (air, 30 W, 10 min) lowers the water contact angle on a silicon wafer from ~45° (uncleaned) to below 5° and, thus, also leads to better wetting of the applied drop. To promote spreading, different amounts of MeOH were added to the suspension prior to drop casting. However, more MeOH leads to immediate flow away from the center of the applied drop towards the edges of the substrate. Once the edges were reached, the liquid flowed back towards the center of the applied drop causing very inhomogeneous PS layers. If the substrate was big enough (no flow back to the center of the applied drop), the coverage of PS spheres remained well below a monolayer, with large areas exhibiting no nanospheres at all. Similar results were obtained by using EtOH instead of MeOH with and without addition of the surfactant Triton X-100. As-received PEN substrates were observed to exhibit a water contact angle of ~60°, whereas it could be lowered to ~10° by plasma-cleaning. Thus, using the PEN substrates as received for the described experiments mostly lead to

multilayer coverage. However, with the plasma-cleaned substrates, similar results as in the case of silicon wafers (described above) could be achieved.
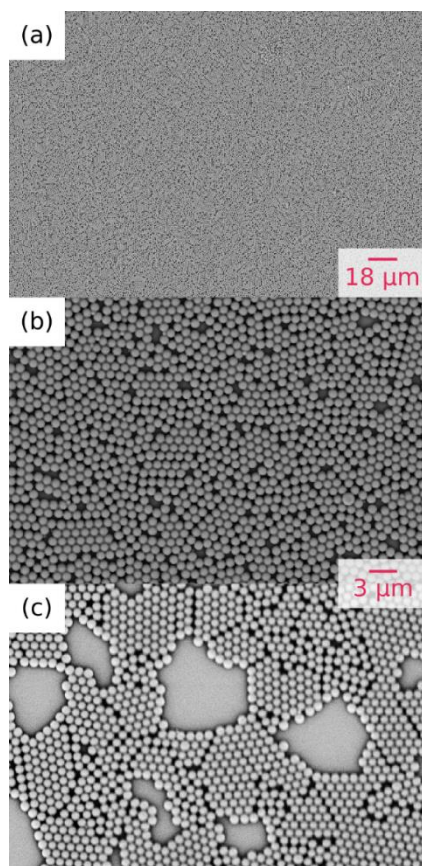

Figure AIII-2. Scanning electron microscopy images of regions of monolayers of polystyrene nanospheres assembled on a silicon substrate by drop casting: (a) overview image of such an area, (b) area showing large numbers of defects, and (c) area showing de-wetted structures with voids between deposited spheres.

As a second technique, *spin coating* was applied to deposit a monolayer of PS beads onto the substrates from the suspensions previously described. Two cases were tested: High spin speeds (>200 rpm) that lead to the quick spreading/removal of the drop from the substrate and low spin speeds (<100 rpm) that move the drop on the wetted surface. Similar to the drop-casted samples, they were dried for 30 min at 80°C after spin coating to remove any residual liquid. In the first case, high spin speeds resulted in very low coverage. By waiting longer before starting spinning, the coverage could be increased, however, not to the extent of avoiding blank spots in the tens of micrometers in size. In the second case at low spin speeds, results similar to the best results obtained by drop casting could be obtained with regions of monolayer coverage in the order of 10 mm². An approach similar to

Arutinov et al.[16] was applied to achieve regions with monolayer coverage over such areas. Specifically, increasing the spin speed from 80 rpm up to 1000 rpm by 100 rpm steps ca. every 2 min yielded the most promising results. The resulting PS monolayers exhibited similar structure (i.e., amounts of defects) as the ones prepared by drop casting, however, with a higher effort to obtain such results (e.g., need of a spin coater, setting up a routine).

In a further trial, *doctor blading* was evaluated as a technique to deposit a monolayer of PS beads on a substrate from the suspensions described above similar to Yang & Jiang[17]. A piece of silicon wafer was pinned down by two stripes of tape at either side of the substrate, also serving as a guard for the doctor blade. The drop was applied on one end of the bare region of the substrate and spread by pushing the blade across the substrate at a constant tilt angle and speed. Metal and plastic blades applying tilts between 10 and 90° were tested. Furthermore, different speeds (~0.1-10 cm/s) were tested, but with the disadvantage/unreliability of moving the blade manually. Slower speeds lead to more reproducible results. However, in all the conditions applied, inhomogeneous residues of solution remained on the substrate, leading to a greatly inhomogeneous distribution of PS spheres on the substrate after drying. Again, the samples were dried for 30 minutes at 80°C after the point where no residual solvent could be observed on the substrate by eye. However, all the resulting samples did not meet the requirements stated above. In the literature, very slow coating speeds (down to 1 µm/s) were reported to yield uniform results; but still, with the parameters and system applied by Yang & Jiang[17], monolayer coverage could not be achieved (a minimum of 12 layers of PS spheres were reported).

For all the previously described methods, the substrate plays an important role as the monolayer is assembled directly on its surface. For both silicon wafers (for test/investigative purposes) and PEN substrates (for the final devices) to be coated equally, the method described in the following seemed to be more suitable: namely, the assembly of a monolayer of polystyrene spheres at the air-water interface and subsequent pick-up on any desired substrate. Furthermore, large areas (tens of cm^2) were reported to be readily coverable by monolayers of PS nanospheres of different sizes with little effort (no need for special equipment).[7] An experimental routine similar to the one reported by Vogel et al.[7] was adopted. First, the commercially available dispersions from Polysciences, Inc. and Microparticles GmbH were each mixed with ethanol (1:1 in volume). A glass beaker (8 cm diameter, 4.5 cm height) was half filled with deionized water and a plasma-cleaned microscopy glass slide (diamond glass) was partially immersed at a tilt angle of ~45°. Drops (microliters in volume) of the PS:H$_2$O:EtOH solution were added to the dry side of the glass slide above the water. The liquid flowed towards the water surface, where the PS spheres spread immediately. However, with the

commercially available spheres tested, no monolayer could be observed on the surface of the water. Immediately after addition of the spheres to the water, the solution turned blurry, indicating the sinking of the spheres below the surface. Changing the amount of ethanol in the suspension with the PS beads was reported to aid spreading of the colloids at the air-water interface.[6] Also the pH of the subphase in the beaker was altered by adding specific amounts of acetic acid (~pH 2.5) or sodium hydroxide (~pH 12). Especially for functionalized colloids, increasing the pH was reported to aid ordering of the resulting monolayers.[7] However, neither of these approaches aided the formation of a monolayer in case of the commercially available beads used. Rey et al.[6] report that part of the reason for such a behavior are impurities and different chemical residues (e.g., initiator) altering the properties of the suspension and the surface of the commercially available colloids, mainly being a consequence of the preparation/polymerization process. Cleaning the beads by multiple centrifugation steps can help to get rid of some impurities; in case of the beads from Polysciences, Inc., Rey et al.[6] reported that even such a procedure did not aid in yielding monolayers of a satisfactory quality.

On the contrary, as described by Vogel et al.[7], the PS spheres obtained by initiator-free emulsion polymerization (provided by Prof. Vogel's group) formed a monolayer readily after adding drops of the corresponding solution to the air-water interface in the described way. Due to the different preparation method, these colloidal solutions exhibit less impurities interfering with the formation of a monolayer on the air-water interface.[6] After adding several drops, a closed monolayer was formed, visible as a continuous interference pattern covering the entire surface of the water (i.e., different colors visible at different angles of incidence). The transfer of this monolayer onto plasma-cleaned PEN substrates and silicon wafers was performed by taking the substrate with tweezers, immersing it into the water, moving it to an area at which an unaltered monolayer can be seen and picking it up slowly at shallow angles with respect to the water surface. Plasma-cleaning was crucial for the PEN substrates, for without it, no pick-up of large monolayers (areas of cm^2) was possible. The silicon wafers could be used with and without pre-cleaning them by the plasma treatment described. The results on a piece of PEN (a) and on a piece of a silicon wafer (b) are shown in the images in Figure AIII-3.

The structure of monolayers deposited in such a way is shown in the SEM images in Figure AIII-3 (c) and (d). Almost no double-layer formation/spheres on top of the monolayer were observed. The crystallite size of
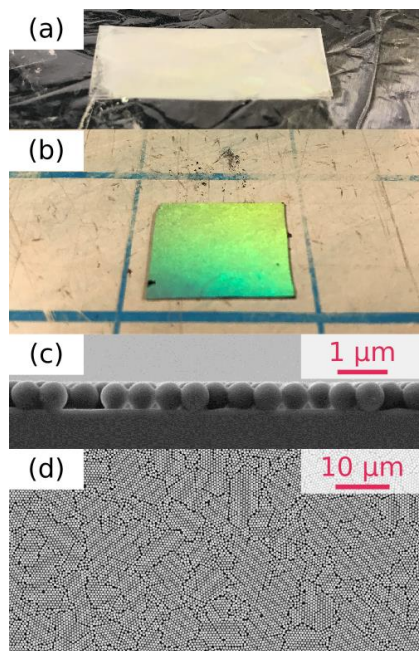
Figure AIII-3. Pictures of a ~3x1 cm piece of PEN (a) and a ~2x2 piece of silicon wafer (b) covered by monolayers of PS spheres (580 nm in diameter) via pick-up after assembly at the air-water interface; side (c) and top view (d) image of a corresponding sample recorded by SEM (on silicon substrate).

hexagonal close-packing within the monolayer (defect-free) is in the order of 20×20 spheres. As shown by Rey et al.[6], this value can be greatly increased by cleaning the beads (i.e., centrifuging), fine-tuning the ethanol content in the solution of the PS beads or changing the pH of the subphase used for the assembly of the colloids in the beaker. In the present project, a process yielding reproducible monolayer coverage with a comparable structure was sufficient. Thus, further efforts for tuning the structure and amount of defects of the monolayers were not pursued.

PEDOT Thin Film Deposition by oCVD

In the second step, the deposition of PEDOT films by oxidative chemical vapor deposition (oCVD) was investigated for the task in question. Since a conformal deposition around 3D-nanostructures is needed, the reactions were run with $VOCl_3$ as the oxidant. $VOCl_3$ is liquid at room temperature and exhibits a vapor pressure high enough in the pressure conditions applied in oCVD for sufficient flow to the reaction chamber. The high volatility of $VOCl_3$ yields a low sticking coefficient and, thus, ensures a high conformality for the resulting coatings.[18] Only few, recent (2019) publications on the deposition of PEDOT films by oCVD with liquid oxidants are available (e.g., with $VOCl_3$ in Gleason's group[19], with $SbCl_5$ and $VOCl_3$ in Nejati's group[10]).

In the beginning, suitable reaction conditions were determined. Overall, the following parameters were varied in order to optimize the depositions in terms of properties of the resulting thin films (as discussed in the further parts of this report): 100-400 mTorr in working pressure, 40-80 °C in substrate temperature and deposition times of 30 or 60 min were adopted. The maximum flow rate of the monomer of 1 sccm (heated to 90°C) achievable with the setup at hand was kept constant for all the depositions. Correspondingly, an equal flow rate of 1 sccm for the oxidant was adopted (also in all depositions) to avoid over-oxidization as reported by Kaviani et al.[10]. The resulting thin films were characterized by Fourier-transform infrared spectroscopy (FTIR). All the spectra recorded on the different samples showed almost identical patterns in terms of peak positions and relative intensities. The absence of a peak at 754 cm^{-1} (attributed to C$_\alpha$-H) confirms the successful polymerization of EDOT into its polymeric form (PEDOT) during thin film deposition; the FTIR spectra of all the deposited films are in good agreement with data on PEDOT thin films deposited by oCVD with the same oxidant in the literature[10]. This confirms the successful polymerization for all the reaction conditions applied in the present work. Besides the work of Gleason's[19] and Nejati's[10] groups, the present contribution is one of the first reporting on the successful deposition of PEDOT thin films with VOCl$_3$ as the oxidant. Furthermore, the successful deposition of PEDOT thin films onto/around PS nanospheres was confirmed by measuring and comparing FTIR spectra recorded on samples with only PEDOT, only a PS monolayer and with both the PEDOT and the PS layer on top of each other (see Figure AIII-4); the individual absorption spectra recorded on a monolayer of PS nanospheres and on a PEDOT thin film add up and, thus, can be used to explain all the peaks in the absorption spectrum of a PEDOT thin film deposited onto/around a monolayer of PS nanospheres. A detailed list of peaks assigned to the corresponding molecular vibrations in the structure of PEDOT can be found in the supplementary information to the publication of Kaviani et al.[10]. Accordingly, three main peaks in the spectra of PEDOT recorded within the present work (cf. Figure AIII-4) can be assigned to C-O-C stretching and occur around 1100 cm^{-1} (1090, 1135, 1180 cm^{-1}, respectively).[10] Moreover, C-S-C stretching vibrations can be observed between 650 and 1000 cm^{-1} (685, 825, 970 cm^{-1}, respectively).[10] Peaks at 920 and 1050 cm^{-1} can be assigned to C-S and C-O stretching, respectively, whereas C-C inter-ring stretching bands can be observed at 1320 cm^{-1}.[10]

An estimation of the film thickness of the PEDOT layers resulting from oCVD was performed by SEM of the thin film cross-sections exposed by cleavage of PEDOT-coated silicon substrates after deposition (see Figure AIII-5 (a)). However, especially thin layers (below 100 nm) were at the limit of detection
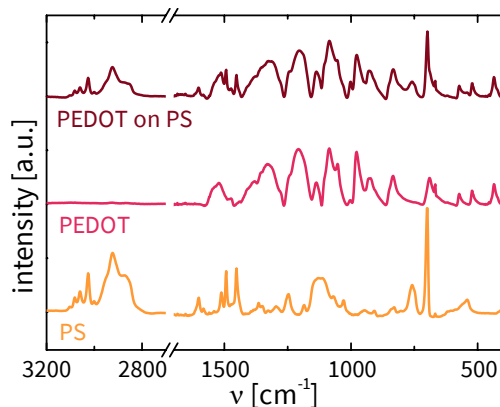
Figure AIII-4. Absorption spectra recorded by FTIR on a PEDOT thin film, a monolayer of PS nanospheres and a PEDOT film deposited onto/around a monolayer of the nanospheres (on silicon substrates).

for the SEM used, with charging (visible as a white shroud in Figure AIII-5 (a) at the top of the thin film) and lack of contrast blurring the images. However, the film thickness of thinner layers could be estimated by assuming constant deposition rate over time and back-calculating from the longer depositions. All the layers investigated exhibited thickness values between 50 nm and 1 μm, with lower pressure, higher substrate temperature and shorter reaction time leading to thinner films, as expected in most CVD processes. However, film thickness was not the most crucial parameter, as the main aim was to deposit uniform and conformal PEDOT layers onto/around PS nanospheres. Regardless, SEM helped to identify the most promising deposition conditions and resulting structures. The fastest depositions (i.e., highest working pressure) developed cracks when taking them out of the reactor, hinting towards a substantial strain in the films deposited in such a manner. Regardless, slower depositions yielded thin film samples with excellent uniformity, without the presence of any appreciable observable defects (cf. Figure AIII-5 (a)).

For the deposition onto substrates pre-covered by a monolayer of PS nanospheres, the following results can be summarized: the most conformal depositions around the PS nanostructures were achieved at relatively low pressures (i.e., slow depositions). For thicker depositions (>100 nm), a flat PEDOT layer on top of the nanostructures was observed to form, covering all the nanostructures. The thicker this top layer was, the less structured the film's surface looked from the top due to smoothening by the deposited PEDOT film with increasing deposited thickness.

The threshold in thickness observed (~100 nm) coincides with the thickness needed to be deposited for complete filling of the voids of the hcp-structure
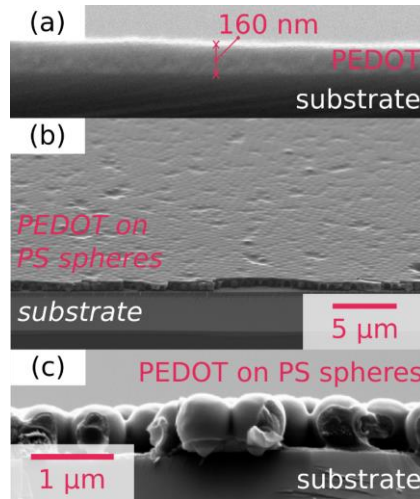
Figure AIII-5. Representative SEM images of (a) a 160-nm-thick PEDOT thin film on a silicon substrate (side view), (b) a PEDOT film deposited onto/around PS nanospheres (angled view) and (c) a close-up image (side view) of a sample with a thin PEDOT layer deposited onto/around PS nanospheres to demonstrate the conformality of the deposition.

between the flat substrate surface and the nanospheres. From geometrical considerations, the point last filled by a conformal and constant growth both from the substrate and the nanosphere surfaces can be estimated (see Figure AIII-6). Geometrically, this point must lie equidistant between the surfaces of the three surrounding spheres and the substrate surface. Therefore, as evident from a projection from top or bottom (see Figure AIII-6 (b)), this point has to lie exactly on the line perpendicular to the substrate that passes through the center of the triangle formed by the centers of the three surrounding spheres (marked as an orange line in (a) and an orange x in (b) of Figure AIII-6). The distance d_{sph} of each point on this line relative (perpendicular) to the surface of one of the spheres with radius r can be written as a function of the angle φ from the plane formed by the centers of the surrounding spheres, which reads as follows:

$$d_{sph} = r \left(\frac{2}{\sqrt{3} \cos \varphi} - 1 \right)$$

The distance d_{sub} on this line from the substrate surface can be written as a function of the same angle φ as follows:

$$d_{sub} = r \left(1 - \frac{2 \tan \varphi}{\sqrt{3}} \right)$$

By equating the distances from the surface of one of the spheres (d_{sph}) and from the substrate surface (d_{sub}), the exact thickness t can be calculated, at

173

which a conformal and equal growth from all the surrounding surfaces would meet last. Solving for the angle φ in the first quadrant yields $\varphi = \pi/6$. Inserting this value into one of the equations for d_{sph} or d_{sub} with $r = (580\text{ nm}/2)$ yields $t \approx 97$ nm. However, when including the fact that new molecules for film growth need to arrive at each spot on the surface from top, the path is blocked earlier; this happens exactly, when the smallest voids between the spheres (i.e., at half the height of the spheres) are closed. This point in thickness can be estimated by calculating the distance between the surface of a sphere at half the height of the sphere to the center of the triangle formed by the three centers of the surrounding spheres (see Figure AIII-6 (b)); it is visualized as the line labelled s in green. For spheres with a diameter of 580 nm, $s \approx 45$ nm. Furthermore, the fact that the growth is not perfectly conformal and effects such as capillary condensation, altering the growth in small voids, need to be considered. In the present work, we aim at minimizing the growth of PEDOT in a flat layer above the PS nanospheres
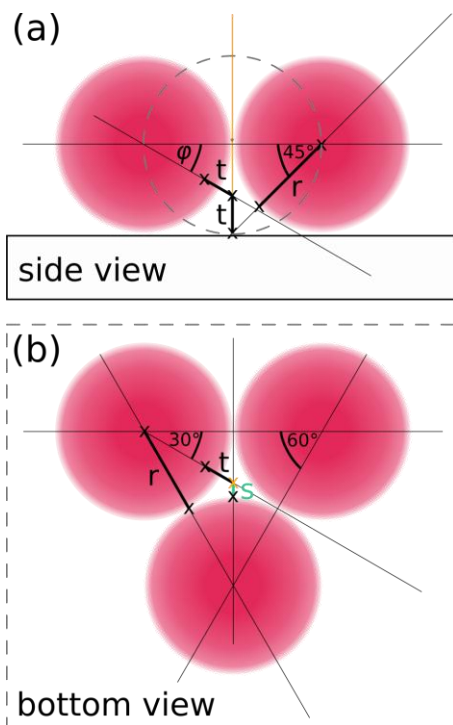

Figure AIII-6. Side view (a) and bottom view (b) sketches of 2D-projections of parts of the hcp-structure of nanospheres (with radius r) on a substrate surface aiding to explain the geometrical considerations behind the estimation of the point (at thickness t) last filled by a conformal growth of a film on the substrate and the nanosphere surfaces; dashed lines give shapes that need to be seen through to observe the sketched structures (nanosphere in (a) and substrate in (b)).

because the interfaces between PEDOT and PSS were reported to play an important role in the piezoresistive behavior. Therefore, slow depositions (i.e., low working pressure of 200 mTorr) between 50 and 100 nm in thickness (on a flat silicon substrate) were evaluated to yield the most promising results on the nanospheres by SEM (also in terms of uniformity (b) and conformality (c); see Figure AIII-5). Therefore, these conditions were adopted for the depositions on the PS spheres for the further device fabrication. Overall, this contribution is among the first to report on the conformal and uniform oCVD of conducting polymer thin films around nanospheres.

Regarding deposition conditions influencing material properties possibly altering the electrical and piezoresistive properties of the resulting thin films, the conductivity of oCVD-PEDOT films was reported to increase with increased substrate temperature during deposition.[10] To not damage the PS spheres thermally (i.e., glass transition temperature of polystyrene at ~100-107 °C)[20], substrate temperatures of 60 and 80 °C were applied for the deposition of PEDOT on the nanospheres. The two temperatures were also chosen to investigate the effect of the conductivity on the piezoresistive properties of the samples.

Assembly and Testing of Devices

For the fabrication of the actual piezoresistive devices, a monolayer of PS nanospheres was deposited onto PEN substrates (3x1 cm) via pick-up of the monolayer assembled at the air-water interface. Subsequently, PEDOT thin films were deposited onto the nanospheres at different substrate temperatures and thicknesses. Various samples were acid-treated by placing them in a 0.5 M H_2SO_4 solution for 10 min. This procedure is performed to achieve a dopant exchange process in the PEDOT layer such as described by Howden et al.[8] and a sulfonation of the surfaces of the PS spheres as reported by Nucara et al.[9]. Two 50-nm-thick nickel contacts were evaporated onto the PEDOT via physical vapor deposition (PVD). The two contacts were prepared with a separation of 0.5 mm via masking during deposition. Nickel was chosen due to its work function (4.9-5.2 eV in films)[21], matching the estimated work function of PEDOT (5.1-5.2 eV in oCVD films)[22], yielding ohmic behavior. The piezoresistive properties of these samples were investigated by determining their resistance as a function of straining. Initially, voltage-current measurements (see Figure AIII-7) were performed. All samples showed straight voltage-current characteristics, confirming the ohmic behavior of the devices (with nickel contacts). For the sake of usability, further measurements of the resistance were performed directly with a multimeter.

The resistance values of the unstrained devices (as-deposited and with 10 min H_2SO_4-treatment) measured directly with a multimeter are given in Table AIII-1. In accordance with literature (e.g., Kaviani et al.[10]), the
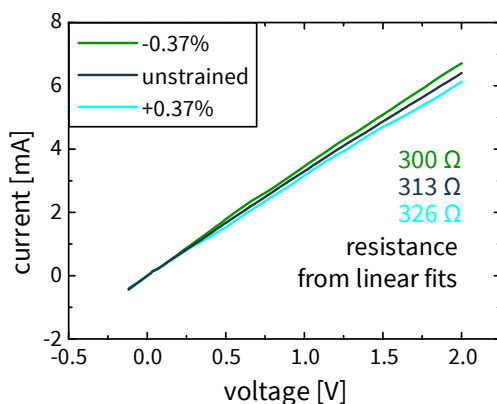
Figure AIII-7. Representative voltage-current characteristics (from -0.1 to 2 V) measured on a strained and unstrained device structure with the respective resistance values calculated from linear fits of the curves (reciprocal value of the slope); preparation conditions: $T_{sub} = 80$ °C, 60 min, H_2SO_4-treated.

conductivity appears to increase with substrate temperature and with deposited film thickness (i.e., deposition time), observable as a decreased resistance value. Furthermore, H_2SO_4-treatment decreases the resistance by ~1/3. For PEDOT films deposited with iron chloride as the oxidant, even larger increases in conductivity were observed (more than 100%), possibly due to different species and levels of doping. However, the present work is among or even the first to report on a dopant exchange in sulfuric acid enhancing the conductivity of oCVD-PEDOT films deposited with $VOCl_3$ as the oxidant by ~1/3.

The H_2SO_4-treated sample deposited at 80 °C substrate temperature with a deposition time of 60 minutes (cf. Figure AIII-7) shows a slightly lower resistance value when calculated from the slope of the voltage-current characteristics (~313 Ω) compared to the value obtained from a direct measurement with the multimeter (cf. Table AIII-1; 298 Ω) in its unstrained state. The measurement uncertainty and different wire and contact probe resistances might be possible sources for this difference. All the differences between the resistance values obtained from voltage-current characteristics and direct measurement lie within this range. For the remaining results of this contribution, the direct measurements are reported due to their ease in measurement (especially during bending). Regardless, both sets of data show the same trends.

With the geometry of the samples, their conductivity can be estimated to range in values of up to tens of S cm^{-1}, which is in the range of conductivity values reported in other studies on oCVD-PEDOT[15] and especially on films deposited at relatively low substrate temperatures.[10] For depositions carried

Table AIII-1. Resistance measured on device structures as-deposited and after 10 min of H_2SO_4-treatment for different deposition conditions.

Deposition conditions	Resistance [Ω]	
	as-deposited	H_2SO_4-treated
60 °C;30 min	1,711 ± 16	1,056 ± 11
60 °C;60 min	448 ± 6	320 ± 5
80 °C;30 min	1059 ± 11	717 ± 7
80 °C;60 min	397 ± 6	298 ± 5

out at even higher substrate temperatures (e.g., 145°C), conductivity values of up to several thousands of S cm^{-1} were reported.[10,19] Regarding the response to bending, Figure AIII-7 gives an idea about the amplitude of the change in resistance (~4% for an applied strain of 0.37% for the respective sample). Compressive and tensile strain yield shifts in the opposite direction but comparable in magnitude. A summary of the response of the different samples to 0.37% of tensile strain is given in Table AIII-2.

Table AIII-2. Response in change of resistance (percent compared to the unstrained state) to 0.37% of tensile strain (applied via bending) measured on device structures as-deposited and after 10 min of H_2SO_4-treatment for different deposition conditions.

Deposition conditions	Response [%]	
	as-deposited	H_2SO_4-treated
60 °C;30 min	0.2	0.4
60 °C;60 min	0.5	0.9
80 °C;30 min	0.8	1.6
80 °C;60 min	2.3	4.2

The data in Table AIII-2 shows that the response to 0.37% of tensile strain (applied via bending) is higher for samples prepared at higher substrate temperature (i.e., more conductive) and longer deposition time (i.e., greater deposited film thickness). Furthermore, an increase of the response by a factor of ~2 is observed after acid treatment, indicating an influence of the dopant species on the piezoresistive behavior. Howden et al.[8] hypothesize that acid rinsing has multiple potential effects on such vapor-deposited PEDOT films: It could help in removing residual oxidant from the film, in solvating the structure to allow for optimized morphology and in lowering the film roughness. Furthermore, the solvating effect was expected to allow for the

incorporation of further dopant ions, observable in a higher doping level and, thus, conductivity.[8] Furthermore, the sulfonated PEDOT-PSS interfaces are expected to contribute to the enhanced piezoresistive response, as reported and hypothesized in the literature on PEDOT:PSS-based piezoresistive devices.[3,4,23] Overall, a correlation between an increase in conductivity and an increase in gauge factor were found in the investigated samples.
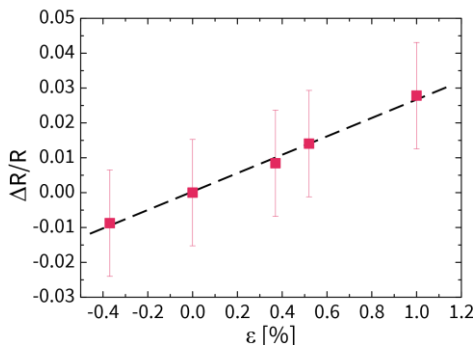

Figure AIII-8. Representative data on the change in resistance normalized by the resistance of the unstrained device ($\Delta R/R$) as a function of strain ε (in percent); preparation conditions: $T_{sub} = 60$ °C, 60 min, H_2SO_4-treated; the dashed line represents a linear fit to the measurement points.

With bending, different levels of strain (i.e., bending radii) can be applied on the devices. From such experiments (see Figure AIII-8), the relation between the change in resistance and the applied strain can be investigated. Successful fitting of the measured data with a linear function leads to the hypothesis of a linear relationship between these two parameters in the range of strains investigated. The uncertainties for the measured resistance values (cf. error bars in Figure AIII-8) arise from the measurement uncertainty of the multimeter. Despite the large uncertainty, as it is close to being constant for all the data points plotted, the linearity of the relation described can be assumed to be valid. Moreover, this relationship is confirmed by voltage-current measurements and by all the samples investigated in the present study exhibiting a similar relationship. This behavior is expected and reported widely in the literature.[2,3]

Furthermore, this relation is widely used to estimate the quality of a piezoresistive device. The quantity measuring this correlation is called gauge factor k. It relates the measured resistance change normalized by the resistance of the unstrained device ($\Delta R/R$) to the applied strain ε as the change in length normalized by the length in the unstrained state ($\Delta l/l$) as follows:

$$k = \frac{(\Delta R/R)}{(\Delta l/l)} = \frac{(\Delta R/R)}{\varepsilon}$$

Thus, with the values from Table AIII-2, the gauge factors can be calculated, yielding values of as high as 11.4. Furthermore, the Poisson's ratio of the polymer (ν), describing the transverse change in length resulting from longitudinal straining, can be estimated to be ~0.35.[2] This can be used to subtract the factor merely resulting from the geometrical change upon straining the device as follows:[1]

$$k = 1 + 2\nu + \frac{1}{\varepsilon}\frac{\Delta\rho}{\rho} = 1 + 2\nu + k_\rho$$

This yields an estimation of ~9.7 to be the value for the corresponding 'true' gauge factor (k_ρ) resulting from the change in conductivity (ρ) of the polymeric structure. Still, this value lies well above gauge factors of conventional metal strain gauges (k<5).[1] Considering the values of other polymer-based materials, the measured k value compares well to gauge factors determined on PEDOT:PSS-based structures measured in similar configurations (e.g., 0.48,[2] 17.8[3]). In conventional semiconductors (e.g., silicon, germanium), gauge factors of >100 have been reported.[24] However, these materials bear the disadvantage of a trade-off between their rigidity connected to the disability to sense large strains and/or small pressures and a high gauge factor. Furthermore, in a more sophisticated sandwich geometry (top-bottom contacting), very large responses to pressure (changes of the resistance of up to ~3 orders of magnitude) were reported for PEDOT:PSS films containing gold nanoparticles.[4] However, these devices exhibited a very large intrinsic resistance in their unstrained state (~10^{11} Ω). Furthermore, very high gauge factors (55-396), depending on the range of strains applied, were reported for an electrospun PEDOT:PSS-PVA nanofiber material; also for this material, low conductivities were reported (10^{-5}-10^{-8} Scm^{-1}).[5]

Regardless, it should be mentioned that the magnitude of the gauge factor is not the only parameter relevant for piezoresistive devices. For instance, the mechanical flexibility, elasticity, compatibility with biological systems and low-cost of fully polymeric setups makes them particularly interesting for future applications. Thus, structures like the proposed one here show great potential and exhibit a set of properties that is crucial for various different applications such as in biosystems or wearable electronics.

In the present work, a simple approach for testing a novel set of materials was adopted. It must be mentioned that the results published in this work should be regarded as preliminary. Herein, the materials and the measurement geometry have not been optimized to their full potential. For instance, different read-out geometries (e.g., sandwich) could be promising approaches. Optimizing the set of materials and structures used yields further opportunities of improving device performance. On the one hand, the possibility of changing the size of the polystyrene nanospheres represents a

knob to tune the interfacial contact area between PEDOT and PS(S). On the other hand, especially, the oCVD process yields great potential of tailoring and tuning material properties of the PEDOT layer such as conductivity and conjugation length,[10,19] directly influencing the piezoresistive behavior of the resulting material. As an increased conductivity was found to correlate with an increased gauge factor, a very promising outlook are the remarkably high conductivity values (thousands of S cm^{-1}) reported on oCVD PEDOT in the literature.[10,19] Besides substrate temperature and film thickness, the working pressure and the nature and flow rates of the individual chemicals used within the process were shown to alter the microstructure and the material properties of the resulting thin films further.[11,19] As the conductivity of the PEDOT film depends on doping, the oxidant species used within the oCVD process may be an interesting knob to play with (e.g., $SbCl_5$ as used by Nejati's group[10]). Moreover, the acid treatment (e.g., different acids) can be used to alter the resulting chemical nature of doping. Compared to regular PEDOT:PSS-based structures, the methods applied in the present work open up a vast number of tunable parameters, potentially enabling the structures to outperform conventional architectures. Moreover, the reported results broaden the impact and possibilities of applications of oCVD films.

AIII.7   Conclusions

In this work, a novel, fully polymeric composite material for piezoresistive devices was proposed, prepared and tested. The deposition of a monolayer of polystyrene nanospheres onto flexible polyethylene naphthalate (PEN) substrates over large areas (several cm^2) was achieved by the assembly of the monolayer at the air-water interface and subsequent pick-up with the plasma-cleaned PEN substrates. A thin layer (~50-100 nm) of PEDOT was deposited conformally around the PS nanospheres via oxidative chemical vapor deposition (oCVD). The successful polymerization and deposition were confirmed by scanning electron microscopy and Fourier-transform infrared spectroscopy. The intrinsically chlorine-doped nature of the oCVD-PEDOT layers was altered by a treatment in sulfuric acid post deposition. During deposition of the PEDOT thin film, the substrate temperature and deposited thickness were used as parameters to alter film properties in terms of conductivity and piezoresistive response.

Two nickel top-contacts were evaporated on top of the assembled PEN/PS/PEDOT-structure with a separation of 0.5 mm to allow for the electric characterization of the individual samples. The ohmic nature of the contacts and the entire device structure were confirmed by the linearity of their voltage-current characteristics (also when strained). Resistance measurements revealed that preparing the samples at higher substrate temperature

and increasing the deposited thickness yield structures exhibiting lower resistance. The dopant exchange performed by acid treatment in sulfuric acid decreased the samples' resistance by ~1/3. Conductivities were estimated to range as high as tens of S cm^{-1}. To test the piezoresistive properties of the samples, resistance measurements during defined bending (i.e., strain) were performed. All samples prepared were confirmed to exhibit piezoresistive behavior by changing their resistance as a function of applied strain. Lower intrinsic resistance (i.e., samples prepared at higher substrate temperature, samples with increased thickness) enhanced the piezoresistive response of the samples. Furthermore, the acid treatment applied increased the piezoresistive response of the samples by a factor of ~2. Besides performing dopant exchange, additional doping and optimizing the morphology of/in the PEDOT layer, this treatment is thought to sulfonate the surfaces of the PS spheres, contributing to the piezoresistive behavior of the final devices. From the relationship of the applied strain to the change in resistance measured, gauge factors as high as 11.4 were determined.

Overall, the results presented in this contribution serve as a promising basis for the optimization and development of the investigated structures for their application in piezoresistive devices. Further investigation on the performance of the proposed structures are needed and an optimized setup for the application of the investigated architectures is sought. Regardless, already the combination and substeps of the methods applied yielded novel insights into the capabilities of the investigated systems.

AIII.8 References

(1)   Fiorillo, A. S.; Critello, C. D.; Pullano, A. S. Theory, Technology and Applications of Piezoresistive Sensors: A Review. *Sensors Actuators, A Phys.* **2018**, *281*, 156–175. https://doi.org/10.1016/j.sna.2018.07.006.

(2)   Lang, U.; Rust, P.; Schoberle, B.; Dual, J. Piezoresistive Properties of PEDOT:PSS. *Microelectron. Eng.* **2009**, *86* (3), 330–334. https://doi.org/10.1016/j.mee.2008.10.024.

(3)   Latessa, G.; Brunetti, F.; Reale, A.; Saggio, G.; Di Carlo, A. Piezoresistive Behaviour of Flexible PEDOT:PSS Based Sensors. *Sensors Actuators, B Chem.* **2009**, *139* (2), 304–309. https://doi.org/10.1016/j.snb.2009.03.063.

(4)   Karmakar, R. S.; Lu, Y. J.; Fu, Y.; Wei, K. C.; Chan, S. H.; Wu, M. C.; Lee, J. W.; Lin, T. K.; Wang, J. C. Cross-Talk Immunity of PEDOT:PSS Pressure Sensing Arrays with Gold Nanoparticle Incorporation. *Sci. Rep.* **2017**, *7*, 12252. https://doi.org/10.1038/s41598-017-12420-5.

(5)   Liu, N.; Fang, G.; Wan, J.; Zhou, H.; Long, H.; Zhao, X. Electrospun PEDOT:PSS-PVA Nanofiber Based Ultrahigh-Strain Sensors with Controllable Electrical Conductivity. *J. Mater. Chem.* **2011**, *21*, 18962–18966. https://doi.org/10.1039/c1jm14491j.

(6)   Rey, M.; Yu, T.; Guenther, R.; Bley, K.; Vogel, N. A Dirty Story: Improving Colloidal Monolayer Formation by Understanding the Effect of Impurities at the Air/Water Interface. *Langmuir* **2019**, *35* (1), 95–103. https://doi.org/10.1021/acs.langmuir.8b02605.

(7)   Vogel, N.; Goerres, S.; Landfester, K.; Weiss, C. K. A Convenient Method to Produce Close- and Non-Close-Packed Monolayers Using Direct Assembly at the Air-Water Interface and Subsequent Plasma-Induced Size Reduction. *Macromol. Chem. Phys.* **2011**, *212* (16), 1719–1734. https://doi.org/10.1002/macp.201100187.

(8)   Howden, R. M.; McVay, E. D.; Gleason, K. K. OCVD Poly(3,4-Ethylenedioxythiophene) Conductivity and Lifetime Enhancement via Acid Rinse Dopant Exchange. *J. Mater. Chem. A* **2013**, *1*, 1334–1340. https://doi.org/10.1039/c2ta00321j.

(9)   Nucara, L.; Piazza, V.; Greco, F.; Robbiano, V.; Cappello, V.; Gemmi, M.; Cacialli, F.; Mattoli, V. Ionic Strength Responsive Sulfonated Polystyrene Opals. *ACS Appl. Mater. Interfaces* **2017**, *9* (5), 4818–4827. https://doi.org/10.1021/acsami.6b14455.

(10)   Kaviani, S.; Mohammadi Ghaleni, M.; Tavakoli, E.; Nejati, S. Electroactive and Conformal Coatings of Oxidative Chemical Vapor Deposition Polymers for Oxygen Electroreduction. *ACS Appl. Polym. Mater.* **2019**, *1* (3), 552–560. https://doi.org/10.1021/acsapm.8b00240.

(11)   Smolin, Y. Y.; Soroush, M.; Lau, K. K. S. Oxidative Chemical Vapor Deposition of Polyaniline Thin Films. *Beilstein J. Nanotechnol.* **2017**, *4* (8), 1601201. https://doi.org/10.3762/bjnano.8.128.

(12)   Smolin, Y. Y.; Soroush, M.; Lau, K. K. S. Influence of OCVD Polyaniline Film Chemistry in Carbon-Based Supercapacitors. *Ind. Eng. Chem. Res.* **2017**, *56* (21), 6221–6228. https://doi.org/10.1021/acs.iecr.7b00441.

(13)   Hulteen, J. C.; Treichel, D. A.; Smith, M. T.; Duval, M. L.; Jensen, T. R.; Van Duyne, R. P. Nanosphere Lithography: Size-Tunable Silver Nanoparticle and Surface Cluster Arrays. *J. Phys. Chem. B* **1999**, *103* (19), 3854–3863. https://doi.org/10.1021/jp9904771.

(14)   Trujillo, N. J.; Baxamusa, S. H.; Gleason, K. K. Grafted Functional Polymer Nanostructures Patterned Bottom-up by Colloidal Lithography and Initiated Chemical Vapor Deposition (ICVD). *Chem. Mater.* **2009**, *21* (4), 742–750. https://doi.org/10.1021/cm803008r.

(15)   Trujillo, N. J.; Barr, M. C.; Im, S. G.; Gleason, K. K. Oxidative Chemical Vapor Deposition (OCVD) of Patterned and Functional Grafted Conducting Polymer Nanostructures. *J. Mater. Chem.* **2010**. https://doi.org/10.1039/b925736e.

(16)   Arutinov, G.; Brichkin, S. B.; Razumov, V. F. Self-Assembling of Polystyrene Microsphere Monolayers by Spin-Coating. *Nanotechnologies Russ.* **2010**. https://doi.org/10.1134/S1995078010010064.

(17)   Yang, H.; Jiang, P. Large-Scale Colloidal Self-Assembly by Doctor Blade Coating. *Langmuir* **2010**, *26* (16), 13173–13182. https://doi.org/10.1021/la101721v.

(18)   Chelawat, H.; Vaddiraju, S.; Gleason, K. Conformal, Conducting Poly(3,4-Ethylenedioxythiophene) Thin Films Deposited Using Bromine as the Oxidant in a Completely Dry Oxidative Chemical Vapor Deposition Process. *Chem. Mater.* **2010**, *22* (9), 2864–2868. https://doi.org/10.1021/cm100092c.

(19)   Gharahcheshmeh, M. H.; Tavakoli, M. M.; Gleason, E. F.; Robinson, M. T.; Kong, J.; Gleason, K. K. Tuning, Optimization, and Perovskite Solar Cell Device Integration of Ultrathin Poly(3,4-Ethylene Dioxythiophene) Films via a Single-Step All-Dry Process. *Sci. Adv.* **2019**, *5* (11), eaay0414. https://doi.org/10.1126/sciadv.aay0414.

(20)   Rieger, J. The Glass Transition Temperature of Polystyrene. *J. Therm. Anal.* **1996**, *46*, 965–972. https://doi.org/10.1007/bf01983614.

(21)   Baker, B. G.; Johnson, B. B.; Maire, G. L. C. Photoelectric Work Function Measurements on Nickel Crystals and Films. *Surf. Sci.* **1971**, *24* (2), 572–586. https://doi.org/10.1016/0039-6028(71)90282-2.

(22)   Im, S. G.; Gleason, K. K.; Olivetti, E. A. Doping Level and Work Function Control in Oxidative Chemical Vapor Deposited Poly (3,4-Ethylenedioxythiophene). *Appl. Phys. Lett.* **2007**, *90*, 152112. https://doi.org/10.1063/1.2721376.

(23)   Wang, J. C.; Wang, J. C.; Subhra Karmakar, R.; Lu, Y. J.; Huang, C. Y.; Wei, K. C. Characterization of Piezoresistive PEDOT:PSS Pressure Sensors with Inter-Digitated and Cross-Point Electrode Structures. *Sensors* **2015**, *15* (1), 818–831. https://doi.org/10.3390/s150100818.

(24)   Yang, S.; Lu, N. Gauge Factor and Stretchability of Silicon-on-Polymer Strain Gauges. *Sensors* **2013**, *13* (7), 8577–8594. https://doi.org/10.3390/s130708577.